CONTRIBUTION OF MICROGLIAL REACTIVITY TO OLFACTORY ENSHEATHING CELL MIGRATION *IN VIVO*

A thesis submitted to the College of Graduate Studies and Research in partial
Fulfillment of the requirements for the degree of Doctor of Philosophy
in the

Department of Anatomy and Cell Biology
University of Saskatchewan
Saskatoon, Canada

By
Mohsen Basiri

PERMISSION TO USE

In presenting this thesis in partial fulfillment of the requirements for a Doctor of Philosophy degree from the University of Saskatchewan, I agree that the libraries of this university may make it freely available for inspection. I further agree that permission for copying of this thesis in any manner, in whole or in part, for scholarly purposes may be granted by professors who supervised my thesis work or, in their absence, by the Head of the Department or the Dean of the College in which my thesis work was done. It is also understood that any copying or publication or use of this thesis or parts thereof for financial gain shall not be allowed without my written permission. It is also understood that due recognition shall be given to me and to the University of Saskatchewan in any scholarly use which may be made of any materials in my thesis.

Requests for permission to copy or to make other use of material in this thesis in whole or part should be addressed to:

Head of the Department of Anatomy and Cell Biology

University of Saskatchewan, 107 Wiggins Road

Saskatoon, Saskatchewan S7N 5E5

CANADA

ABSTRACT

Olfactory ensheathing cells (OECs) are glial cells that are an attractive candidate for neural repair after spinal cord injury and for remyelination of axons in diseases such as multiple sclerosis. OECs appear to migrate within the adult mammalian central nervous system (CNS) in animal models of spinal cord injury, but until recently there has been no systematic examination of the factors inducing or guiding this migration. Previous work in our lab (V.Skihar) implicated microglial reactivity in the generation of a migratory signal(s) inducing OECs to migrate towards an ethidium bromide-induced focal demyelination in the adult rat spinal cord. The long-term objective of this research project was to test the hypothesis that reactive microglial provide a migratory signal(s) driving the migration of OECs within the spinal cord of adult rats.

The first set of experiments determined the time-frame in which Wallerian degeneration (WD) induced microglial reactivity occurs in the right dorsal corticospinal tract (dCST) of adult rats at the level of T11 following aspiration of the contralateral sensorimotor cortex. This timing data from this study demonstrated a prominent microglial activation in the right dCST of T11 eight weeks after sensorimotor cortex injury indicating the microglial response to WD of dCST axons was very slow to appear. The second set of experiments determined whether OECs were induced to migrate in response to WD-induced microglial reactivity in the dCST, which based on the first set of experiments was known to occur within 8 weeks of lesioning the left sensorimotor cortex. This second set of experiments also examined the migratory path taken by OECs with respect to the location of reactive microglia (i.e. inside vs outside the right dCST). For these experiments, the left sensorimotor cortex was damaged 8 weeks prior to grafting the OECs at T12.

The next group of experiments examined the contribution of TNF-α induced microglial reactivity to generation of a migratory signal. First we identified concentrations of TNF-α that when injected into the DF of the T11 spinal cord segment of an adult rat induced microglial reactivity either along at least a 5 mm distance from the injection site or confined to the immediate vicinity of the injection site. The result of this experiment identified a concentration of 1 ng/µl and 0.01 ng/µl TNF-α as appropriate concentrations to induce the appropriate amount of microglial reactivity,

respectively. The final set of experiments used these two concentrations to determine whether TNF-α induced microglial reactivity that is initiated 5 mm rostral to a DiI+ve OEC graft generates a migratory signal(s) inducing OECs to migrate towards the rostral part of T11 and whether the migratory signal(s) was present only if the microglial reactivity extended the full 5 mm distance between the TNF-α injection and the OEC graft.

The major findings were: i) there was a significantly higher density of DiI+ve OECs within the right dCST of rats in which there was WD-induced microglial reactivity as compared to the right dCST of rats in which there was no microglial reactivity; ii) the migratory path taken by DiI+ve OECs was preferentially within areas containing reactive microglia (i.e. dCST) and towards the site of TNF-α induced microglial reactivity (i.e. rostral to cell graft as opposed to caudal); iii) significantly more DiI+ve OECs migrated towards the site of a TNF-α injection when the microglia were reactive along the entire length of the migratory path between the cytokine injection and cell graft; and iv) minocycline treatment both dampened microglial reactivity and significantly reduced the number of migrating DiI+ve OECs. The major conclusions are that the migration of OECs within the adult rat spinal cord occurs in response to migratory signal(s) arising as a result of microglial activation and that this migration occurs preferentially along the path of microglial reactivity.

ACKNOWLEDGMENTS

I would like to express my heartfelt thanks to my supervisor Professor Ronald Doucette, who provided the necessary guidance and support in my Ph.D. research work.

I wish to express my sincere thanks to my committee members, Drs. Troy Harkness (Chair), David Schreyer (Graduate chair), Valerie Verge, Gillian Muir and Thomas Haas who found time in their busy schedules and provided me with their scientific insights and support throughout my study. I also thank the external examiner Dr. Kathryn Todd for coming to Saskatoon for my thesis defense.

I would also like to convey special thanks to colleagues in my supervisor's lab, Dr Victor Skihar, Anita Givens and Darren Nesbitt. Also I thank graduate students in the Department of Anatomy and Cell Biology: Rasheed bani Hammad, Sara Rigley (McDonald), and Suraj Abraham in providing me with technical information and equipment whenever I needed.

I would like to acknowledge other people who helped me in the Department of Anatomy and Cell Biology in many ways, including technical procedures and computer software programs that I needed to carry out my research. Especially I wish to thank Karen Yuen and Tonya McGowan. I also thank Mrs. Shirley West and Ms Corinne Howells for their kindness and help.

Lastly, great thanks to my family who provided the moral support to make my dreams come true.

I must thank Kerman University of Medical Sciences and the Ministry of Health and Medical Education, Government of IRAN, for financially supporting me in my Ph.D. studies.

TABLE OF CONTENTS

LIST OF TABLES Page

LIST OF FIGURES **page**

LIST OF ABBREVIATIONS

AP-1	activating protein 1
ATP	adenosine triphosphate
B7	peripheral membrane protein on activated antigen presenting cells
BBB	Blood brain barrier
bFGF	basic fibroblast growth factor
BCS	bovine calf serum
BDNF	brain-derived neurotrophic factor
BMCs	bone marrow cells
BSA	bovine serum albumen
Brdu	bromodeoxyuridine
cAMP	cyclic adenosine monophosphate
CD	Cluster of Differentiation
CG4	oligodendrocyte progenitor cell line
CNTF	Ciliary neurotrophic factor
CNPase	2',3'- cyclic nucleotide-3' phosphohydrolase
CNS	central nervous system
cIAP	cellular inhibitors of apoptosis

CST	corticospinal tract
CR-3	Complement receptor-3
CREB	cAMP Response element binding protein
CSF	cerebrospinal fluid
CSPGs	chrondroitin sulfate proteoglycans
CX32	connexin 32
DAB	diaminobenzidine tetrahydrochloride
DAT	dorsal ascending tract
DF	Dorsal funiculus
DiI	1,1'-dioctadecyl-3,3,3'3'- teramethylindocarbocyanine perchlorate
DIV	days *in vitro*
DMEM	Dulbecco's Modified Eagle's Medium
DMSO	dimethyl sulfoxide
DPBS	Dulbecco's phosphate buffered saline
DREZ	dorsal root entry zone
DRG	dorsal root ganglion
E18	18 days embryo
EAE	experimental autoimmune encephalomyelitis
ECM	Extracellular matrix

EDTA	ethylenediaminetetraacetic
ED1	monoclonal antibody recognizes a lysosomal membrane of myeloid cells
EGF	epidermal growth factor
FACS	fluorescence-activated cell sorter
FADD	Fas associated death domain
FBS	fetal bovine serum
FGF2	fibroblast growth factor 2
JAK/STAT	janus kinase-a cytoplasmic tyrosine kinase/ signal transducers and activators of transcription-a gene regulatory protein
JAM	junctional adhesion molecule
JNK	c-Jun N-terminal kinase; is one of the mitogen-activated protein kinases
GABA	Gamma-aminobutyric acid
Gal-C	galactocerebroside
GAP-43	43Kd growth associated protein
GDC	granular disintegration of the cytoskeleton
GDNF	Glial cell line-derived neurotrophic factor
GFAP	glial fibrillary acidic protein
GFP	green fluorescent protein
GLT-1	glutamate transporter

GLAST	glutamate–aspartate transporter
GPI	glycosyl phosphatidylinositol
H2O2	hydrogen peroxide
HBSS	Hank's balanced salt solution
HEPES	N-2- Hydroxyethylpiperazine-Ni-2 ethanesulfonic acid
HLA	human leukocyte antigen
HNK-1	human natural killer 1
HRP	horseradish peroxidase
HS	horse serum
ICAM -1	Intercellular adhesion molecule-1
Ig	immunoglobulin
IGF	insulin-like growth factor
ICAM	intercellular adhesion molecule
IL	interleukin
IFN-γ	interferon-gamma
IP	intraperitoneal
JNK	c- Jun N-terminal kinase
LP	lamina propria
LPS	lipopolysaccharide

LT	lymphotoxin
LIF	Leukemia inhibitory factor
LPS	Lipopolysaccharide
MAG	myelin-associated glycoprotein
MAPK	mitogen activated protein kinase
MAP	microtubule associated protein
MBP	myelin basic protein
MCP-1	monocyte chemotactic protein-1
M-CSF	Macrophage colony-stimulating factor
MIP-1	Macrophage inflammatory protein-1
mG5	modified G5 medium
mGluRs	metabotropic glutamate receptors
MHC	major histocompatibility complex
MMPs	matrix metalloprotease
MOG	myelin/oligodendrocyte glycoprotein
MS	multiple sclerosis
N-CAM	neural cell adhesion molecules
NF-*k*B	Nuclear factor kappa B
NGF	nerve growth factor

NMDA	N-methyl D- aspartate
NSCs	neuronal stem cells
NT3	Neurotrophin-3
NO	Nitric oxide
O-2A	oligodendrocyte type 2 astrocyte
NT-3	Neurotrophin-3
OB	Olfactory bulb
OECs	olfactory ensheathing cells
OMP	olfactory marker protein
ONL	olfactory nerve fiber layer
OX1	mouse monoclonal antibody, which recognizes CD45
OX6	monoclonal antibody, which recognizes the MHC class antigen II
OX18	monoclonal antibody, which recognizes the MHC class antigen I
OX35	monoclonal antibody, which recognizes the CD4 antigen
OX42	monoclonal antibody, which recognizes the complement type 3 receptor
p75	low-affinity neurotrophin receptor
PARP-1	Poly (ADP-ribose) polymerase-1
PBS	phosphate buffered saline
PBSS	Puck's balanced salt solution

PDGF	platelet derived growth factor
PF	paraformaldehyde
PKH26	lipophilic fluorescent dye
PKC	protein kinase C
PLP	proteolipid protein
PMP22	peripheral myelin protein 22
PNS	peripheral nervous system
PPG	picric acid/paraformaldehyde/glutaraldehyde
PSA-N-CAM	embryonic polysialic acid containing N-CAM
RIP	receptor-interacting protein
ROS	reactive oxygen species
SMA	Smooth muscle alpha actin
SMP	skim milk powder
SCI	spinal cord injury
SV 40	simian virus 40
TCR	T-cell receptor
TGF-ß	transforming growth factor-beta
Th	helper T cell
TMEV	Theiler's murine encephalomyelitis virus

TNF-α	tumour necrosis factor- alpha
TRADD	TNF-receptor associated death domain
TRAF2	TNF-R- associated factor 2
Trk	tropomyosin-related kinase
TX-100	Triton X-100
V-CAM	vascular cell adhesion molecule
VLA	very late antigen
WD	Wallerian degeneration

CHAPTER 1.0 INTRODUCTION

1.1 Primary Olfactory System

The primary olfactory pathway consists of olfactory receptor neurons in the nasal cavity whose unmyelinated axons project through the cribriform plate into the central nervous system (CNS) to synapse with mitral and tufted cells in the olfactory bulb (OB) (Barber and Lindsay, 1982). The olfactory receptor neurons have the ability to regenerate throughout life both in response to injury and as part of normal turnover (Calof and Chikaraiashi, 1989; Graziadei and Monti Graziadei, 1980; Tennent and Chuah, 1996). The growing axons of new olfactory receptor neurons form synaptic contacts with neurons of the olfactory bulb, with this regenerative cycle repeating itself every 30 to 60 days in rodents (reviewed in Farbman, 1990). This extraordinary ability of the olfactory receptor neurons to be regenerated in adult mammals has attracted the interest of many scientists interested in investigating the underlying mechanisms. In particular, attention has been directed towards the possible role of olfactory ensheathing cells (OECs), which are the glial cells that ensheath the olfactory axons (Doucette, 1983) and that may promote olfactory axonal elongation towards the OB (Tennet and Chuah, 1996).

1.2 Olfactory Ensheathing Cells (OECs)

Along the primary olfactory pathway, OECs are nonmyelinating glial cells that provide ensheathment for the small (0.1-0.5 μm in diameter in mammals) olfactory axons along their entire length, grouping them into fascicles of variable size in both the lamina propria and the olfactory nerve fiber layer (ONL) of the OB (Doucette et al., 1983; 1984). During embryonic development, OECs are thought to migrate ahead of the growing axons and are thought to guide and support this axonal growth both in the peripheral nervous system (PNS) and CNS portions of the primary olfactory pathway (Calof and Chikaraiashi, 1989; Doucette, 1983; Graziadei and Monti Graziadei, 1980; Tennet and Chuah, 1996).

In addition to the growth promoting properties that OECs appear to possess, an exceptional characteristic feature of the OEC is its highly malleable phenotype (Gong et al., 1994). OECs express a mixture of astrocyte-specific and Schwann cell-specific phenotypic features (Barber and Lindsay, 1982; Doucette 1984, 1990; Gong et al., 1994)

and perform the role of both astrocytes and Schwann cells (Doucette, 1990, 1993a; Doucette and Devon, 1993). In spite of these similarities OECs are referred to as a new class of glial cells (Barnett et al., 1993; Doucette and Devon, 1993). In recent years, *in vivo* (Lakatos et al., 2003) and *in vitro* (Lakatos et al., 2000) studies demonstrated clear differences between Schwann cells and OECs in terms of cellular interaction with astrocytes, thus reinforcing the notion of OECs as a distinct class of glia. Lakatos and coworkers (2003) showed that Schwann cell transplantation resulted in a greater area of increased glial fibrillary acidic protein (GFAP) expression compared to that associated with OEC transplantation in rat spinal cord. This was accompanied by a greater increase in the expression of axon growth inhibitory chrondroitin sulfate proteoglycans (CSPGs) following Schwann cell transplantation compared to OEC transplantation. In fact transplanted cells can exert an effect on the host tissue that will influence the extent to which regenerating axons can grow beyond the transplanted area and reenter the host environment.

Similar to Schwann cells in peripheral nerves; olfactory fascicles in the PNS are enclosed within a basal lamina that separates OECs from the surrounding connective tissue. However, in the OB OECs are only apposed to a basal lamina where they contribute to the formation of the glia limitans. Compared to other PNS-CNS transitional zones, the plasma membranes of ensheathing cells and astrocytes are not separated by a basal lamina (Barber and Lindsay, 1982; Doucette, 1991), because the OECs assist in forming the glia limitans, which elsewhere in the CNS is formed exclusively by astrocytes. OECs also form end-feet at blood vessels in a manner comparable to astrocytes (Doucette, 1984, 1990, 1991). The comparison is based exclusively on morphology and it is not clear whether OECs are functioning the same as astrocytes.

OECs are located within the lamina propria of the olfactory mucosa and in the first two layers of the OB (Doucette, 1993). It is well known that the olfactory epithelium originates from the olfactory placodes, which appear in the rostrolateral region of the embryonic head (Costanzo and Graziadei, 1983; Farbman and Squinto, 1985; Valverde et al., 1992). However, the OB originates from the rostral end of the cerebral vesicle (Doucette, 1989). Thus, OECs reside within two sets of tissues that arise in the embryo from components of the PNS and CNS, respectively, even though they are most likely

derived during embryonic development from the peripheral structure, namely the olfactory placode (Doucette, 1993b) OECs do not express the antigenic epitope recognized by the A4 monoclonal antibody (Miller et al., 1984), which immunostains all cells of neural tube origin.

1.2.1 Phenotype of OECs

OECs display several very distinct phenotypic features that are dependent on their immediate environment. These cells normally possess a mixture of astrocyte- and Schwann cell-specific phenotypic features *in vivo* (see Section 1.2). OECs can be distinguished from other cells migrating away from the olfactory placodes by their dark appearance, mode of association with axons, and their ultrastructural features (Doucette, 1989; Valverde and Lopez-Mascaraque, 1991). OECs contain a lobulated electron dense nucleus with irregular chromatin under the nuclear envelope and one or two nucleoli (Valverde et al., 1992).

There are several phenotypic markers known to be expressed by OECs. It was shown that OECs can be immunostained with antibodies to platelet-derived growth factor (PDGF) (Kott et al., 1994), neuropeptide Y (Ubink et al., 1994), and also with protein S100 (Gong et al., 1994), which is associated with growth and survival of cells in other systems (Van Eldik et al., 1991). In addition, OECs express low affinity nerve growth factor receptor (p75) (Barnett and Hutchins, 1993; Gong et al., 1994; Miwa et al., 1993; Turner and Perez-Polo, 1993, 1994; Vickland et al., 1991). Several studies showed that axotomy up-regulates the expression of p75 by OECs in the adult olfactory nerve (Gong et al., 1994; Miwa et al., 1993; Turner and Perez-Polo, 1993, 1994).

OECs also express membrane-associated molecules known to be involved in cell adhesion and axonal growth (Kleitmsn et al., 1988), such as L1 (Miragall et al., 1988), laminin (Doucette, 1996; Kafitz and Greer, 1997) and polysialic acid containing molecule (PSA-N-CAM) and adult forms of the neural cell adhesion molecule (N-CAM) (Miragall et al., 1988). L1, laminin and PSA-N-CAM are all expressed by OECs throughout development (Miragall et al., 1988). The O4 monoclonal antibody, which recognizes an antigenic epitope expressed on the surface of progenitor cells in the oligodendrocyte type 2 - astrocyte (O-2A) lineage as well as Schwann cells, also recognizes an epitope on the

surface of OECs at all development stages (Barnett and Hutchins, 1993; Franceschini and Barnett, 1996). However, OECs are HNK-1-ve and galactocerbroside-ve (Gal-C-ve), which are two markers expressed by oligodendrocytes (Jessen and Mirsky, 1991; McGary et al., 1983). In spite of OECs expressing cytoplasmic and membrane associated molecules in common with other known glial cell populations, the antigenic phenotype of OECs does not completely match any of these other glial cell types. Recent proteomic studies have revealed that OECs, but not Schwann cells, express calponin (Boyd et al., 2005) and smooth muscle alpha actin (SMA) (Jahed et al., 2007), thus demonstrating that these cells have a phenotype that is distinct from Schwann cells.

The first evidence of the myelinating capacity of OECs was demonstrated by Devon and Doucette (1992). They showed, at the light and electron microscopic level, that embryonic OECs co-cultured with dorsal root ganglion (DRG) neurons associated with both myelinated and unmyelinated axons in a manner virtually identical to the ensheathment normally provided by Schwann cells of the PNS. The authors explicitly stated that the myelinating cells are not contaminating Schwann cells since the negative controls were pure neuronal cultures that contained no glial cells and showed no ultrastructural evidence of myelination. In addition, it was observed that OECs expressed certain myelin-associated proteins under various culture conditions. O4+ve OECs isolated from neonatal rat OB were found to only weakly express the peripheral myelin protein P0 and Gal-C (Barnett et al., 1993). Noncompact myelin protein 2',3'-cyclic nucleotide 3'-phosphodiesterase (CNPase) was also reported to be weakly expressed by bipolar and/or multipolar OECs obtained from the adult OB (Santos-Silva and Cavalcante, 2001). However, Pixley (1996) failed to detect the CNPase in bipolar cells in explant cultures from neonatal OBs. A similar controversy exists over the expression of myelin basic protein (MBP) by OECs. In neuron-free cultures, neither unpurified embryonic OECs (Devon and Doucette, 1995) nor purified neonatal OECs (Barnett et al., 1993) expressed MBP *in vitro* even after intracellular up-regulation of cyclic adenosine monophosphate (cAMP), a strong stimulus for induction of MBP synthesis by Schwann cells (Devon and Doucette, 1995). In contrast, OECs isolated from the adult rat OB and purified on the basis of their expression of the p75 neurotrophin receptor (p75) displayed robust MBP immunoreactivity (Ramon-Cueto and Nieto- Sampedro, 1992).

1.2.2 Protocols for generating OEC cell cultures

Within the past decade, numerous studies have supported the idea that OECs are effective in promoting neural repair in several different animal models of CNS injury (Boyd et al., 2004; Chuah et al., 2004). The main aim of these experiments was to facilitate and support axonal growth across the lesion and into the tissue on the distal side through manipulation of the cellular environment of the lesion site in the brain or spinal cord. The OECs used in these cell grafting experiments were obtained from cell cultures set up using tissue from either the OB or lamina propria (LP); i.e. from either the CNS (Boyd et al., 2004, Chuah et al., 2004) or PNS (Au and Roskam., 2003) component of the primary olfactory pathway.

The two main tissue sources that have been used to initiate cell cultures of OECs are the PNS (i.e. lamina propria) and CNS (i.e. nerve fiber layer of OB) portions of the primary olfactory pathway. Since at day 18 of embryonic development all of the glial cells in the ONL of the rat OB are OECs (Doucette, 1989) no further purification steps are required when using this tissue for setting up OEC cultures, which is the main benefit of using embryonic tissue. However, the cell cultures obtained from the ONL of newborn and adult animals are usually contaminated with other cells (oligodendrocytes, astrocytes, and possibly even leptomeningeal Schwann cells); thus, further techniques such as immunopanning protocols using antibodies to p75 (Ramon-Cueto and Nieto-Sampedro, 1994; Takami et al., 2002) or using a cell sorter to choose O4+ve/Gal-C-ve cells (Pascual et al., 2002) are required to enrich the cell cultures for OECs. Barnett et al. (1993) used the O4 monoclonal antibody as a marker to recognize OECs since it was obsereved OECs *in vivo* in the OB are O4+ve. However, the O4 monoclonal antibody also immunostains Schwann cells, oligodendrocytes, and O-2A progenitors.

Establishing an OEC line is also another way to acquire OECs for transplantation. Goodman et al. (1993) successfully generated a p75 NGFR+ve OEC clonal cell line from Sprague-Dawley rat pups using the SV40 large T antigen. An advantage of engineering cell lines is to prevent cell contamination and provide a long constant supply of a purified cell population. However, more research needs to be done before any clinical approach is used to ensure the safety of the cell lines from developing tumors or from causing any

other disorders as a result of uncontrolled cellular growth after grafting. A majority of studies have used unpurified cell cultures of OECs. Mixtures of OECs with other cells, (i.e. meningeal cells) were used by Li et al., (1997, 1998) and Lakatos et al (2003) in their experiments. Recently, researchers used additional growth factors (i.e. bovine pituitary extract) in order to increase the number of OECs in cell cultures and/or after OEC transplantation (Chuan and Teague, 1999). In the absence of specific markers for OECs, these cells need to be prelabelled before grafting. There are several cell labeling techniques that have been used to prelabel OECs. Hoechst dye, a nuclear fluorochrome bisbenzimide (Imaizumi et al., 2000; Lu et al., 2002 ; Ramon-Cueto et al., 1998, 2000), DiI (1,1'-dioctadecyl-3,3,3',3'-tetramethylindocarbocyanine perchlorate), which is another fluorescent dye (Basiri and Doucette, 2007), and Cell-Tracker probes (Li et al., 1997) have all been used to label OECs before transplantation in different animal models. The disadvantage of using a fluorescent labeling dye might be its leakage to surrounding cells. Although there is no evidence of these dyes being transferred directly to surrounding cells, there is a possibility of phagocytosis of dying OECs at the implantation site by microglia, macrophages or astrocytes. Thus, false positives have been reported when Hoechst dye was used to prelabel OECs prior to transplantation (Ruitenberg et al., 2002), which may lead to overestimation of the survival and migration of Hoechst-prelabelled transplanted cells.

Molecular biological techniques for labeling OECs include adenoviral-mediated (Ruitenberg et al., 2002, 2003) or retroviral-mediated (Boyd et al., 2004; Lakatos et al., 2003) expression of *LacZ* or of the use of adenoviral vectors to induce expression of green fluorescent protein (GFP) (Li et al., 2003). These techniques have demonstrated at both the light and electron microscopic levels that implanted OECs can survive after grafting into a CNS lesion (Boyd et al., 2004, Lakatos et al., 2003; Li et al., 2003; Ruitenberg et al., 2002, 2003). The use of *LacZ* transfected OECs has provided information on the characterization of the interaction of these cells with their host environment at both the light and electron microscopic level. Boyd et al. (2004) demonstrated that the *LacZ*-expressing OECs had no direct contact with CNS axons that regenerated into a cystic cavity following spinal cord contusion and thus did not form myelin sheaths, but axon remyelination was a prominent feature due to the invasion of

the lesion by Schwann cells (Boyd et al., 2004). A proteomic comparison of OECs and Schwann cells by Boyd et al. (2005) revealed that OECs but not Schwann cells expressed calponin. A more recent study demonstrated the expression of smooth muscle actin (SMA) by OECs (Jahad et al., 2007). These two biomarkers will be most helpful in clarifying the fate of OECs following spinal cord implantation. Intracellular and cell surface receptor molecules expressed by OECs are summarized in Table 1.1.

1.2.3 Therapeutic potential of OECs for neural repair

The ultimate goal of grafting OECs into areas of CNS injury is to develop a therapeutic protocol that can be used to restore functional ability to patients with neurological injury. The first test of the therapeutic potential of OEC transplants in an animal model of neural injury was reported by Ramon-Cueto and Nieto-Sampedro (1994). In their experiment, the grafted OECs, which were obtained from the ONL of adult rats, promoted the regeneration of transected dorsal root axons. The grafted OECs accompanied the axons as they grew past the glial scar and into the dorsal horn. Li et al. (1997, 1998) showed that OEC transplants could promote the regeneration of spinal cord axons and restore behavior, and others have similarly observed improvement in coordinated locomotion, weight-bearing, touch, and proprioceptive functions following this treatment (Ramon-Cueto et al., 2000). Lu et al. (2002) also reported that OECs promoted axonal regeneration after delayed transplantation of up to four weeks after SCI. In addition to supporting axonal regeneration, OECs may be able to remyelinate spinal cord axons (Franklin et al., 1996b), thereby restoring action potential conduction (Imaizumi et al., 1998), although whether this occurs after grafting has been questioned (Boyd et al., 2004). In another CNS injury model, the cholinergic fibers of the fimbria/fornix pathway were destroyed by aspiration and then an OEC-containing collagen gel was placed into the cavity formed by the lesion. The data demonstrated that OECs promoted cholinergic fiber ingrowth into the lesion (Smale et al., 1996). Li et al. (1997, 1998) and Nash et al. (2002) lesioned the corticospinal tract in adult rats and showed that OEC grafts promoted the growth of corticospinal fibers. Ramon-Cueto et al. (1998) removed an entire spinal cord segment before grafting OECs into the proximal

Table 1.1 Molecules Expressed by OEC

Antigen	In vitro	In vivo	References
S100	+	OB, ON	Astic et al., (1998); Franceschini and Barnett(1996); Baber andLindsay (1982); Gong et al., (1994)
GFAP	+	OB, ON	Astic et al., (1998);Franceschini and Barnett (1996); Barber and Lindsay (1982)
P75	+	OB, ON	Barnett et al., 2000; Nash et al., (2002) Ramon-Cueto et al (1998, 2000)
O4	+	OB, ON	Barnett et al., (1993); Franceschini and Barnett (1996)
Neuropeptide Y	n.d	OB, ON	Ubink et al., (1994)
Nestin	+	n.d	Ubink et al., 1994; Sonigra et al., (1999)
Calponin	+	OB, ON	Boyd et al., 2006
SMA	+	OB, ON	Jahed et al., 2007

n.d= not determined; OB= Olfactory bulb; ON= olfactory nerve

and distal stumps of the transected cord and demonstrated significant long-distance regrowth of the damaged fibers with some axons appearing to have grown as far as 12-14 spinal cord segments.

Whether OECs have the ability to myelinate axons *in vivo* has received support in some research reports. Franklin et al. (1996) used an O4+ve clonal OEC cell line that was generated from the OB of rat pups and showed these cells would remyelinate spinal cord axons after transplantation into an ethidium bromide/X-irradiated demyelinated area of the adult rat spinal cord. Exposing the damaged spinal cord to high doses of X-irradiation causes a significant delay in the endogenous remyelination process. This animal model of CNS demyelination provides a microenvironment in which to test the remyelinating ability of transplanted cells. An idea that should be considered when using this animal model is the possibility that Schwann cells could migrate into the demyelinated zone and form peripheral myelin-like sheaths around the CNS axons. In the absence of a cell graft, a significant delay of more than eight weeks has been reported in the endogenous remyelination (Franklin et al., 1996; Imaizumi et al., 1998). However, implanted cells may provide an additional incentive (e.g. migratory signals) for Schwann cell migration into the demyelinated area, either via release of paracrine chemotactic factors or by providing a permissive substrate for Schwann cell migration into the CNS.

In a recent study, Akiyama et al. (2004) isolated OECs expressing the alkaline phosphatase gene from transgenic adult rats and transplanted these cells into the demyelinated dorsal columns of immunosuppressed rats. The authors described peripheral-type myelination in the dorsal columns after implantation of these transgenic OECs, but this pattern of alkaline phosphatase reactivity was diffuse, thus making it difficult to distinguish between axons that were myelinated by the transplanted OECs and axons that were myelinated by host Schwann cells. Subsequent investigation by Sasaki et al. (2004) addressed this concern by using OECs isolated from the ONL of the OB of adult transgenic Sprague-Dawley rats in which the OECs constitutively expressed GFP. The OECs were transplanted immediately after transection of the dorsal funiculus. The advantage of this strategy is that GFP could be detected immunohistochemically for ultrastructural identification of labeled cells. The results of this study showed that part of

the axons that displayed compact myelin were myelinated by GFP+ve cells (Sasaki et al., 2004).

However, in an *in vitro* study by Plant et al., (2002), using the technique of Ramon-Cueto and Nieto-Sampedro (1992) for generating OEC cultures, the myelinating ability of OECs were not verified as these cells failed to myelinate neurites when the cells were cocultured with DRG neurons. Boyd et al. (2004) used embryonic rat *LacZ*-expressing OECs for identification of the cells at the ultrastructural level. These *LacZ*-expressing OECs were grafted one week following a mild clip compression injury at the T10 spinal cord level. Evaluation of the injury and grafting site three weeks after cell transplantation revealed no *LacZ*-expressing OECs associated with either unmyelinated or myelinated axons. Instead, these *LacZ*-expressing OECs formed unique tunnel-like structures in the damaged spinal cord. Unlabeled cells were observed within these tunnels, and it was these cells that associated with single myelinated axons or with multiple unmyelinated axons. These unlabeled cells were morphologically identical to Schwann cells at the ultrastructural level, having small ovoid nuclei and a continuous basal lamina encircling a single cell and its associated axons. Thus, these cells within the tunnels created by the implanted *LacZ*-expressing OECs likely represent a population of host Schwann cells that had migrated into the cystic cavity. The number of axon-Schwann cell units inside the tunnels created by implanted OECs ranged from one to several dozen. Therefore, the myelination phenotype of OECs *in vivo* is still under debate.

OECs are also a potential source of a number of growth factors that could contribute to promotion of neuronal survival after transplantation (Ramon-Cueto and Avila, 1998). OECs express nerve growth factor (NGF), brain-derived neurotrophic factor (BDNF), and neutrophin 4/5, but there is no evidence they produce neurotrophin 3 (NT3) or ciliary neurotrophic factor (CNTF) (Boruch et al., 2001, Woodhall, et al., 2001). OECs also express glial cell line-derived neurotrophic factor (GDNF) and neurturin. OECs express the trkB and p75 low affinity NGF receptors and thus the BDNF they produce may have an autocrine action on the cells. In addition, OECs produce platelet-derived growth factor (PDGF) (Kott et al., 1994), neuropeptide Y (Ubink et al., 1994),

and S100 (Franceschini and Barnett, 1996), all of which are known to promote neuronal survival.

Upon survival, injured neurons should enter the regenerative mode and extend their axons, overcoming the inhibitory environment. OECs could favor axonal elongation by directly acting on axons through the expression of adhesion molecules, or indirectly by neutralizing the effects of the negative signals. OECs support neurite outgrowth from embryonic and adult neurons in culture (Kafitz and Greer, 1999; Ramon-Cueto et al., 1993; Sonigra et al., 1999). Neurites grew randomly with no particular orientation when the neurons were co-cultured with either astrocytes or fibroblasts; in contrast, neurons co-cultured with OECs oriented their neurites in parallel with the orientation of the OECs. In this study, the OECs had an elongated morphology, the neurite were aligned along the length of the cells, and the OECs ensheathed the neurites (Ramon-Cueto et al., 1993; Sonigra et al., 1999). In addition, OECs were found to be a better and more effective substrate for neurite elongation than Schwann cells (Sonigra et al., 1999). The expression of adhesion molecules on the surface of OECs could be responsible for this promotion of axonal elongation. These cells express molecules known to be involved in neurite extension such as L1, laminin, neural cell adhesion molecules (N-CAM), embryonic polysialic acid containing N-CAM (PSA-N-CAM), and fibronectin (Barnett et al., 2000, Doucette, 1996, Franceschini and Barnett, 1996, Kafitz and Greer, 1999; Pixley, 1992; Ramon-Cueto, and Nieto Sampedro 1992). OECs from the olfactory mucosa and OB also express the transmembrane adhesion molecule neuroglin 3 throughout life, and this expression is related to neuron-glia and glia-glia interaction (Gilbert et al., 2001). Similar to the tissue culture situation, after transplantation into injured spinal cords, OECs may be a good substrate for axonal elongation, and thus stimulate the growth of injured fibers. The expression of adhesion molecules by OECs could be, in part, responsible for this promotion of axonal regeneration.

In addition, OECs could also act as isolators, ensheathing regenerating fibers and preventing their exposure to chemorepellent molecules, as they do in the OB (Pasterkamp et al., 1998). Furthermore, OECs might be, somehow, changing the response of glial cells to damage and counteracting the effect of the growth inhibitors released at the lesion site. Strikingly, recent studies reported that in contrast to other cell types, OECs did not induce

changes in astrocytes associated with a reactive phenotype (Franklin and Barnett, 2000, Lakatos et al., 2000). The size and shape of astrocytes and the expression of CSPGs by these cells were not altered by contact with OECs.

One important consideration is that OECs have the potential to be directly harvested from the patient and then transplanted back into the same individual. Thus, the clinical issues of tissue rejection and immune suppression therapy can be avoided. The future of OEC research will require recording the properties and mechanisms by which OECs enhance regeneration and will require finding a reliable human source of these cells. The function of OECs and how they interact with axons includes their role in demyelinating situations, including spinal cord injury (SCI) and various types of demyelinating diseases. Although OECs do not normally myelinate axons in the olfactory system, they offer promise in the field of demyelinating diseases (Franklin, 2003). Franklin (2003) points out that OECs remyelinate more efficiently in combination with meningeal cells. The exact population of olfactory cells - whether pure or heterogeneous, neonatal or adult - that remyelinates axons needs to be defined, so that ultimately the most appropriate cell treatment can be applied to injury situations.

It was hypothesized that the presence of OECS would create a more favorable and supportive environment for axonal growth (Doucette, 1990, 1995; Franklin and Barnett, 1997; Ramon-Cueto and Valverde, 1995). OECs could freely migrate into white matter, gray matter, connective tissue, and glia to support axonal regeneration over long distances in the spinal cord (Ramon-Cueto et al., 1998), and this was an improvement over Schwann transplants. Schwann cells are also considered to be high-quality promoters of axonal growth (Ard et al., 1987, Bahr and Bunge, 1989). Also, under certain circumstances, astrocytes may promote axonal growth (Hatten et al., 1991; Smith et al., 1986). However, the treatment of SCI is more complex and promoting axonal growth through the injury site is not the only problem that must be overcome (Collins and West, 1989). It is unlikely that any glial cell type can correct all of these problems; however, it would be really interesting if a cell type can adopt several different roles as the need arises. OECs may be able to do that (Doucette and Devon, 1993) by switching their phenotype from an astrocyte-resembling phenotype to a myelinating Schwann cell-type one (Devon and Doucette, 1992, 1995). Thus, it is possible that OECs will be able to

combine the roles of Schwann cells and astrocytes when transplanted into a lesion cavity, due to their having such a phenotype (Doucette and Devon, 1993).

1.3 Microglia

1.3.1 Microglia in normal CNS

Microglia were first described by del Rio-Hortega as a third type of CNS glial cell that differed from macroglia (i.e., astrocytes and oligodendrocytes) in terms of their phenotype and function (Kim and de Vellis, 2005; Rezaie and Male, 2002), but were closely similar to tissue-resident macrophages in these aspects (Kim and Vellis, 2005). It was estimated microglia comprise 10% of all cells in the brain parenchyma (Yokoyama et al., 2004). Their main role is as a first line of defense against pathological insults and they are considered to be a kind of sensor in the brain, because they have receptors for CNS signalling molecules such as adenosine triphosphate (ATP), acetycholine and noradrenaline and can also react to changes in their extracellular ionic milieu (Kreutzberg, 1996). Microglia have at various times been described as mesodermal (Kitamura et al., 1984), hematomonocytic (Ashwell, 1990), or of ectodermal origin (Kaur et al*.,* 2001) but the current view is that monocytes in the bloodstream enter the CNS during embryonic development, differentiate into the brain resident microglia, and share many of the cell surface antigens found on macrophages (Guillemin and Brew, 2004).

Microglia exist in three distinct forms known as amoeboid, ramified and reactive microglia all of which serve different functions (Ladeby et al*.,* 2005). In rats it has been shown that amoeboid microglia appear late in gestation and disappear soon after birth (Dalmau et al*.,* 1997; Ling et al*.,* 1979). These cells exhibit a round cell body, possess pseudopodia and thin filopodia-like processes and contain numerous lysosomes, indicative of a motile phagocytic phenotype (Ladeby et al., 2005). During the postnatal period amoeboid microglia are believed to play a role in tissue histogenesis through the removal of inappropriate axons (Innocenti et al*.,* 1983) and through the promotion of axonal migration and growth (Polazzi & Contestabile 2002; Schwartz et al., 2006). Ultimately, amoeboid microglia grow long processes and transform into ramified microglia, which are the predominant cell type found in the adult CNS (Kaur and Ling 1991; Ling, 1979). These amoeboid microglia differentiate into ramified microglia

(postnatal days 9-15 in rats) that are characterized by long cytoplasmic processes and are found throughout the CNS of adult mammals (Ladeby et al., 2005; Ling 1991). Although ramified microglia were considered to be inactive as phagocytic cells, under normal conditions, Booth and Thomas (1991) showed that these microglia exhibited pinocytotic activity.

Microglial cytoplasmic processes make contact with neuronal cell bodies, astrocytes and the lamina propria of blood vessels (Nimmerjahn et al*.,* 2005). Thus, microglia are ideally situated to monitor the well-being of brain cells and also to function in cleaning up the extracellular fluid to maintain central homeostasis (Booth and Thomas, 1991; Fetler and Amigorena, 2005). In this respect, it has been suggested that ramified microglia contribute to metabolite removal and to the clearance of toxic factors released from injured neurons (Fetler and Amigorena, 2005). In case of CNS injury or disease (e.g., degenerative, infectious, or autoimmune diseases), the resident ramified microglia change their morphology and transform into cells having retracted cytoplasmic processes and enlarged cell bodies; these cells are generally referred to as "activated microglia" or "reactive microglia" (Kreutzberg, 1996). The term reactive microglia will be used in this thesis and these cells are described in more detail in Sections 1.3.2 and 1.3.3.

1.3.2 Microglial response to neural injury

Following CNS injury or pathogen invasion, quiescent ramified microglia transform into reactive microglia (Kreutzberg, 1996; Stence et al*.,* 2001). Proliferation and cell migration are two main factors contributing to the accumulation of reactive microglia at the site of injury (Dihne et al*.,* 2001; Giordana et al*.,* 1994) where they play a neuroprotective role in phagocytosing damaged cells and cellular debris. In acute lesions, usually 2-3 days after insult is the time when microglial activation reaches its peak (Banati, 2003). Although microglial activation is unrelated to the type of injury and is a rapid process that begins from minutes to a few hours after injury, in later stages of activation the morphological transformation is related to the type of lesion. For example, the "bushy" phenotype of microglia is observed in areas with Wallerian and terminal synaptic degeneration (Jensen et al., 1994). In contrast, rod cell-shaped reactive microglia are found where dense dendritic degeneration is occurring (Morioka et al., 1991) and

hyper-ramified perineuronal microglia are found around each degenerating neuron (Streit et al., 1999). In the presence of extensive neuronal degeneration, and especially in the later phase of the degenerative process, microglia may modify into round phagocytic cells that are indistinguishable from blood-borne macrophages (Guillemin and Brew, 2004). Throughout the remainder of this thesis these reactive cells will be referred to as microglia/macrophages if the morphology of the cells does not allow the two cell types to be distinguished or if the study being referenced has not clearly indicated which cell type is being described.

Reactive microglia express major histocompatibility complex (MHC) class I and II antigens as well as CD40, B7 and intercellular adhesion molecule-1 (ICAM-1), which are specific antigen presenting molecules (Benveniste et al., 2001; Finsen et al., 1993). Therefore, microglia are considered to be the most potent antigen presenting cell type in the CNS. Like macrophages, reactive microglia secrete a number of inflammatory mediators, which serve to organize the CNS immune response. Proinflammatory molecules secreted include various interleukins, monocyte chemotactic protein-1 (MCP-1) (Kim et al., 2005), and tumor necrosis factor alpha (TNF-α) (Taylor et al., 2005). Besides their morphology, reactive microglia/macrophages are identified based on their immunostaining with Mac-1, ED1, OX18, OX42, OX6 and OX1 antibodies (Ling et al., 1991).

Microglial/macrophage expansion in response to neural injury or to neuroinflammation can occur by: (1) proliferation of ramified resident microglia, (2) by their migration from adjacent intact brain areas, (3) by recruitment of monocytes from the blood, or (4) by a combination of each of these processes (reviewed Ladeby et al., 2005). Microglial cells are present in all regions of the mature CNS, but are at different cell densities in various areas of the parenchyma (Schwartz et al., 2006).

Following transection of the hippocampal perforant path projection, microglia located within the denervated outer part of the dentate molecular layer transformed into reactive microglia and began to display an activated morphology from 12 to 24 h after the axotomy (Jensen et al., 1994; Jensen et al., 1999), and they attained a typical bushy morphology by day 3. These morphological changes occurred in parallel to an increased intensity of microglial CD11b immunoreactivity (Jensen et al., 1999). At 24h after

perforant path transection, reactive microglia also began to accumulate at the border between the nondenervated inner commissural-associational zone and the denervated outer perforant path zone. The reactive microglia migrated into the denervated zone from day 1 to 3 after transection in parallel to their maximal rate of proliferation giving rise to a strongly increased cell density in the denervated zone (Jensen et al., 1994). The microglial response to perforant path transection reached maximum levels between 5 to 7 days after lesioning, with the reactive microglia having a bushy morphology and multiple partly retracted, cellular processes (Jensen et al., 1994; Jensen et al., 1997). Microglial activation measured as the density of Mac-1+ve cells within the denervated perforant path zone at day 5 after transection was correlated with the severity of the neuronal damage, as measured by the density of the anterogradely degenerating axons (Jensen et al., 1997). Estimates of the fold increase in the microglial cell population in the perforant path-denervated dentate gyrus at 3 days after injury vary from a 3-fold increase in mice (Lakeby et al., 2005) to a 6-fold increase in rats (Hailer et al., 1999). These estimates were obtained at a time point after injury at which microglial proliferation is just beginning (Hailer et al., 1999) so undoubtedly they are under estimates of the magnitude of the final increase in cell density. Microglial proliferation begins around postlesion days 2–3 and has been demonstrated by pulse labeling of mitotically active cells in perforant path lesioned rats using bromodeoxyuridine (Brdu) injected 1 h prior to sacrifice. Hailer et al. (1999) showed that 17–18% of microglia within the denervated zones in the dentate gyrus had incorporated Brdu at day 3 after transection, which decreased to 2% by day 7 and to 1% by 4 weeks (Hailer et al., 1999).

Microglial proliferation and expansion are under the control of several factors. Macrophage colony-stimulating factor (M-CSF) promotes microglial proliferation *in vitro* (Tomozawa et al., 1996) as well as *in vivo* (Raivich et al., 1994). In addition, upregulation of M-CSF receptors by reactive microglia further increases their responsivity to M-CSF during the acute phase 1–2 days after facial nerve axotomy at the onset of microglial proliferation (Raivich et al., 1998). In the osteopetrotic mice, which are deficient in M-CSF, there is a 30% and 39% reduction in microglial cell number per unit area in the neocortex and the pons, respectively (Sasaki et al., 2000). Other proinflammatory cytokines including interleukin- 6 (IL-6) (Klein et al., 1997), IL-1ß, and TNF-α (Kloss et al., 1997) have also

been shown to promote microglial proliferation and survival. However anti-inflammatory cytokines such as transforming growth factor-beta (TGFβ) are strong inhibitors of microglial proliferation (Jones et al., 1998).

1.3.3 Microglial response to neuroinflammation

For decades, the brain has been considered an immune privileged organ (Zipp and Aktas, 2006). Nowadays, biochemical studies of the nervous tissue in diverse physiological and pathological circumstances have revealed that inflammation in the CNS constitutes the principal host defense to CNS injury and infection. In contrast with the rapid and massive invasion of leukocytes and edema that are evident in peripheral tissues, it is the recruitment and rapid activation of locally resident microglia that occurs in the CNS.

Lipopolysaccharide, interferon-gamma (IFN-γ), HIV-related molecules, prion protein, ATP, and cytokines are among the best-documented activators of microglial cells (Nakamura, 2002). Within minutes or hours, resting ramified microglia transformed into motile amoeboid microglia (Kreutzberg, 1996). At the molecular level, a variety of genes show up-regulation, including the MHC and complement receptors (Liu and Hong, 2003) and the high affinity glutamate transporter-1 (GLT-1) (Lopez-Redondo et al., 2000; Persson et al., 2005). Finally, as a major issue in the neuroinflammatory process, activated microglia release a large variety of pro- and anti-inflammatory mediators, including cytokines, reactive oxygen species (ROS), nitric oxide (NO), prostanoids, and complement factors (Nakajima et al., 2001). Neuroinflammation in the CNS is a complex interplay of glial cells that begins with “reactive” microglial cells, which in turn activate astrocytes. Two major components of the reactive microglial response to CNS neuroinflammation are changes in cell immunophenotype including expression of MHC class I (OX18) (Graeber et al., 1992) and II (OX6) (Graeber et al., 1992) proteins, upregulation of CD11b (OX42 monoclonal antibody) (Nagai et al., 2001), CD4 (OX35 monoclonal antibody) (Ford et al., 1995), and ED1 (ED1 monoclonal antibody) (Lee et al., 2006) antigenic epitopes, as well as changes in cell secretory activity (Lee et al., 2006; Murphy et al., 1998; Puliti et al., 1999). In addition, there is consistent microglial

hyperplasia and hypertrophy, which have been documented in many animal models of acute CNS neuroinflammation (Ladeby et al., 2005).

1.4 Astrocytes

1.4.1 Astrocytes in normal CNS

Astrocytes are the most numerous non-neuronal cell type in the CNS that envelope all cellular components throughout the CNS with their fine branching processes (Bignami et al., 1972). Astrocytes make up around 50% of all glial cell types. Based on their morphology, they can be classified into two main groups; namely, the fibrillary astrocytes, which are located in white matter and have long slender cytoplasmic processes, and the protoplasmic astrocytes, which reside in gray matter and have numerous short, highly branched cytoplasmic processes (Tsacopoulos and Magistretti, 1996). The fibrillary astrocytes have more GFAP containing intermediate filaments in their cytoplasm, and thus stain more intensely with antibodies to GFAP than do protoplasmic astrocytes (Wagner et al., 1993). However, protoplasmic astrocytes are relatively poor in intermediate filaments, and consequently are only weakly immunostained with antibodies to GFAP (Wagner et al., 1993). Astrocytes exhibit a strong structural interrelationship with neurons in all regions of the CNS. Those somatic and dendritic surfaces that are not sites of synaptic terminals are invested by sheet-like processes from astrocytes. Astrocytes also provide the structural boundary to the blood vessels (perivascular endfeet), the pia mater (glia limitans), and the border between the CNS and PNS in sensory and motor roots of spinal and cranial nerves (Fraher, 1992). The expression of gap junctions by astrocytes and the use of these junctions to communicate with one another emphasizes the epithelial organization of astrocytes (Giaume and McCarthy, 1996), which also express transporter systems for several key molecules (Rothstein et al., 1994; Vannucci et al., 1997) as well as a wide variety of membrane receptors for neurotransmitters (Kimelberg, 1995) and growth factors (Raivich and Kreutzberg, 1994; Rudge et al., 1994). The astrocytic network thereby forms a syncytium, acting to optimize neural function by maintaining homeostasis in the extracellular environment (Montgomery, 1994).

Astrocytes provide many supportive activities that are essential for neuronal function in the normal CNS, including homeostatic maintenance of extracellular ionic concentrations, as well as the clearance and release of extracellular glutamate (Mazzanti et al., 2001). It has recently been appreciated that astrocytes also play an important role in regulating neuronal function through the release of neurotrophic factors, by guiding neuronal development, by contributing to the metabolism of neurotransmitters, and by regulating extracellular pH and K^+ levels (Haydon, 2000). Astrocytes also may actively participate in synaptic plasticity (Ullian et al. 2001). In addition, the formation and maintenance of the blood-brain barrier (BBB) are dependent on astrocytes *in vivo*; astrocytic perivascular endfeet are in close apposition to the basal lamina of endothelial cells lining the lumen of capillaries in the CNS, thus inducing the maintenance of a BBB. Soluble factors secreted by astrocytes appear to be involved in the maintenance of the BBB, possibly by inducing the formation of tight junctions between endothelial cells (Rubin and Staddon, 1999); thus, astrocytes contribute to both the structural and functional integrity of the BBB (Wolburg and Risau, 1995).

1.4.2 Astrocytic response to neural injury

Astroglia are known to play a key role in the tissue response to CNS injury (Fawcett and Asher, 1999; Hatten et al., 1991). In response to CNS injury, astrocytes proliferate, change their morphology, and increase their expression of GFAP; collectively, these changes are termed astrogliosis, which is an astrocytic response that is a common hallmark of neural injury and diseases in which neuroinflammation is a prominent component (reviewed in Hatten et al., 1991). Depending on the injury condition, astrogliosis may have beneficial effects for promotion of neuronal survival by the production of growth factors such as neurotrophins that support neuronal growth, or detrimental for neuronal functional recovery by the formation of a glial scar. After injury, these cells are involved in the uptake of potentially harmful substances, such as excitatory amino acids and K^+, and also in the release of certain cytokines (Norenberg, 1994, 1996). The basic process of reactive astrocytosis involves astrocyte proliferation and changes in gene expression (Fawcett and Asher, 1999). Nevertheless, the specific functions performed by reactive astrocytes are not well defined, although they are always present in

CNS tissue that has been damaged or that contains degenerating neurons. Some of the suggested functions of reactive astrocytes include contributing to the inflammatory response, secretion of cytotoxins that kill neurons, and forming scar tissue that inhibits axonal regeneration (Norenberg, 1996). Experimental investigations have demonstrated a heterogeneous reaction pattern of astrocytes depending on the proximity to and the type of injury. Lesions involving direct tissue damage and destruction of the BBB lead to an anisomorphic astrogliosis (Wolburg and Risau, 1995).

The astroglial response to injury is characterized by an increase in cell numbers (hyperplasia), cell size, and cytoplasmic processes (hypertrophy). These changes in cell number and morphology of reactive astrocytes are accompanied by an increased expression of GFAP by the cells contributing to the formation of a gliotic scar (Ridet et al., 1997). Within 3-5 days after motor axon injury, reactive astrocytes begin to wall-off the injured area by interdigitating their cytoplasmic processes (reviewed in Eddleston and Mucke, 1993; Hatten et al., 1991; Norenberg, 1994; Ridet et al., 1997). These astrocytic responses create a dense plexus, or wall, of astrocytes. The molecular profile of reactive astrocytes also includes high concentrations of S100ß (Tateishi et al., 2006) and of growth factors such as fibroblast growth factor 2 (FGF2), NGF, CNTF, and glia-derived nexin, which is a protease inhibitor with neurite promoting activity (Games et al., 1999; Markiewicz and Lukomska, 2006). Numerous aspects of astrocytosis point to reactive astrocytes as cells that phenotypically revert to a primitive, fetal state, re-acquiring factors that are present in the developmental state that had been lost upon differentiation into mature astrocytes (Markiewicz and Lukomska, 2006). The proteins expressed by reactive astrocytes that support this view include nestin (Brook et al., 1999), microtubule associated protein-2 (MAP-2), and gamma-aminobutyric acid (GABA) (Geisert et al., 1990).

Within less than one hour after motor axon injury, there is an increased immunoreactivity for connexin 43, the major component of astrocytic gap junctions (Rohlmann et al., 1994). Within 24 hr, astrocytes expressed increased immunoreactivity for GFAP (Graeber and Kreutzberg, 1986; Ruan et al., 1994) and upregulated both GFAP mRNA and protein (Tetzlaff et al., 1988). In a longer time frame, reactive astrocytes develop slender, sheet-like processes covering non-synaptic areas of the neuronal

membrane. In parallel with the increased expression of GFAP there is also increased expression of the multifunctional glycoprotein clusterin (Svensson et al., 1995). Clusterin inhibits complement-mediated cell lysis, but is also involved in cell adhesion, lipid transport, and processes associated with cell survival or cell degeneration (Rosenberg and Silkensen, 1995). Its role in the axotomy-induced astroglial response is unknown, however. Astrocytes upregulate PDGF and mRNA for the B-chain of the PDGF receptor during the injury response (Hermanson et al., 1995). However, a proportion of these cells also begin to express TGFβ-1 mRNA (Acarin et al., 2000). Since astrocytes respond to TGFβ-1 (Acarin et al., 2000), it is possible that this molecule is involved in autocrine or in paracrine interactions, influencing neighboring cells including other astrocytes (Lindholm., et al., 1992)

1.4.3 Astrocytic response to neuroinflammation

After neuroinflammation, astrocytes release large amounts of ATP into the extracellular environment (Zimmermann, 1994). Such ATP release may be important in triggering cellular responses to trauma and ischemia by initiating and maintaining reactive microglia and involves striking changes in astrocyte proliferation and morphology (Neary et al., 1999). ATP released as part of the astrocytic response to neuroinflammation may contribute to the pathophysiology initiated after trauma (Neary et al., 2006). For example, treatment of cultured astrocytes with cytokines such as IL-1ß enhanced the ATP-evoked release of arachidonic acid via P2Y2 receptors and cytosolic phospholipase A2 (Neary et al., 1999). This enhanced release from astrocytes may contribute to the neuronal loss associated with the neuroinflammation caused by cerebral ischemia or traumatic brain injury (Stella et al., 1997). Several experimental strategies designed to elucidate the roles of astrocytes and their interaction with extracellular matrix (ECM) molecules after CNS inflammation have identified these molecules as contributing to the formation of an astrocytic scar as well as establishing a favorable environment for neuronal repair (McGraw et al., 2001). Nevertheless, it is most likely that to obtain long distance axonal regeneration within the injured adult CNS will require different repair strategies, not limited solely to the modulation of astrogliosis.

Neuroinflammation as a result of brain damage causes the release of glutamate by neurons and astrocytes that may cause secondary excitotoxic neuronal and oligodendroglial progenitor cell death (Liberto et al., 2004). The level of glutamate may be regulated homeostatically by activated astrocytes that can remove it from the extracellular space and convert it to glutamine (Zelenaia et al., 2000). Therefore, the capacity of astrocytes to reduce extracellular levels of glutamate can dramatically impact the extent of neuronal and oligodendroglial damage after an insult. The expression levels of glutamate transporter and glutamine synthase both increase when astrocytes become activated (Ahlemeyer et al., 2002). GLT-1 and glutamate-aspartate transporter (GLAST) are two glutamate transporters that remove excess glutamate (Duan et al., 1999). Astrocytes *in vitro* that are exposed to epidermal growth factor (EGF) increase their expression of GLT-1 (Zelenaia et al., 2000). Likewise, the level of GLAST expression by astrocytes increases following treatment with FGF-2, EGF, and insulin-like growth factor 1 (IGF-1) (Suzuki et al., 2001). Neuroinflammation also affects GLT-1 and GLAST expression *in vivo*. GLT-1 levels increased 2.5 fold above control levels three days after trauma produced by transplanting E18 neocortical tissue into adult rat cerebral cortex (Krum et al., 2002). Similarly, GLT-1 and GLAST mRNA expression were induced after physical trauma to astrocytes *in vitro* (Faden et al., 1989; Eng et al., 1997). The levels of the glutamate transporters also may be indirectly regulated by cytokines (Aronica et al., 2003). *In vitro* studies have shown that astrocytic expression of metabotropic glutamate receptors (mGluRs) can be altered in response to FGF-2 and EGF (Balaz et al., 1997; Minoshima and Nakanishi 1999); as a consequence of the altered expression of mGluRs, the level of glutamate transporters on astrocytes increased (Ciccarelli et al., 1997; Bruno et al., 1998). Therefore increased expression of mGluRs, GLAST and GLT-1 following neuroinflammation better enables astrocytes to deal with the excess glutamate and provide some measure of neuroprotection.

1.5 Cytokines

Cytokines are polypeptides or glycoproteins with low molecular weight (<40 KDa) that regulate a variety of cellular functions including proliferation, survival and maturation (Aarli, 2003; Farina & Winkelman, 2005). One major function of cytokines is

as chemical messengers for regulating the activity of the innate and adaptive immune system (Vilcek & Feldmann, 2004). The major cytokine producers in the body are T helper cells (Th) and macrophages (Kielian, 2006), although all cells involved in innate and adaptive immunity can synthesize and secrete cytokines. The activation of cytokine-producing cells by UV light, heat-shock, hyperosmolarity, infection etc. triggers them to synthesize and secrete their cytokines (Dinarello, 2000).

Cytokines generally act over short distances (paracrine signaling), for short time spans (from minutes to hours) (Deehan et al., 1995), and at very low concentrations (2-20 pg/ml) (Farina & Winkelman, 2005). Cellular responses to cytokines include increasing or decreasing expression of membrane proteins (including cytokine receptors), cell proliferation, and secretion of effector molecules, free radicals, growth factors, enzymes etc. (Farina & Winkelman 2005; Popovich et al., 1997).

Cytokines are pleiotropic molecules, which means that a particular cytokine can act on a number of different cell types rather than a single cell type. They are also redundant, which refers to different cytokines regulating similar cellular functions**.** In addition, cytokines are also multifunctional since each cytokine is able to regulate a number of different cellular functions (Farina & Winkelman, 2005). Cytokines act by binding to specific membrane receptors on target cells, which then signal via second messengers (e.g. tyrosine kinases) inducing the cell to alter its behavior (for instance, gene expression) (Munoz-Fernandez & Fresno, 1998). Thus, what determines the response of a target cell to a specific cytokine is dependent on which signalling pathways are activated when the ligand binds its receptor.

1.5.1 Cytokines in CNS

Cytokines function as powerful regulators of astrocyte and microglial function in the CNS (Fawcett & Asher, 1999). The numerous cytokines that can affect cellular functions in the CNS have two possible cellular sites of synthesis: (1) from cells of peripheral immune organs (e.g. spleen, lymph node), with the cytokines crossing BBB; or (2) from astrocytes and microglia in the CNS (Segal, 2005). The expression of most cytokines is tightly regulated by negative feedback and these factors are usually only produced in quantities sufficient to reach physiologically relevant concentrations after

activation of peripheral immune cells, astrocytes, or microglia in response to an induction signal (John et al., 2003).

Following brain damage or infection, peripheral immune cells, such as macrophages, Th cells and neutrophils, can enter the brain due to the breakdown of the BBB and comprise the main sources of proinflammatory cytokines such as IL-1ß, IL-6, TNF-α, and IFN-γ (Hopkins and Rothwell, 1995). Astrocytes and microglia can also synthesize and secrete some of those cytokines (IL-1ß, IL-6 and TNF-α) as part of an inflammatory response as well as during neural development (Benveniste et al., 1990; Lechan et al., 1990). Each of these proinflammatory cytokines can, in turn, induce the synthesis and secretion of a variety of other cytokines by CNS glia, as well as regulate by autocrine mechanisms their own synthesis and secretion. *In situ* mRNA analyses have shown that proinflammatory cytokine synthesis occurs not only by astrocytes and microglia *in vitro* but also by these same cells *in vivo* (Benveniste et al., 1990; Lechan et al., 1990).

Damage to the CNS is probably the most profound activator of inflammatory cytokine expression (Hashizume et al., 2000). There is an increase in the concentration of several proinflammatory cytokines (e.g. IL-1ß, TNF-α, IL-6) in the cerebrospinal fluid (CSF) and in brain and spinal cord tissues after mechanical injury; for instance, by insertion of a microdialysis probe designed to induce mechanical trauma to the brain. There is also a remarkable upregulation of IL-1ß mRNA in the cerebral cortex, hippocampus, striatum, and thalamus after transient forebrain ischemia or infection (e.g., malaria, HIV, meningitis) (Hopkins and Rothwell, 1995; Merrill and Benveniste, 1996). The expression of IL-6 and TNF-α seem to be greatest in the hypothalamus and hippocampus after ischemia and infection, with lower levels of expression in the cerebral cortex and brainstem, and even lower but still detectable levels in other brain regions (Hopkins and Rothwell, 1995; Mehler and Kessle, 1997).

Certain proinflammatory cytokines in the CNS might function early to amplify the disease process, such as in the experimental autoimmune encephalomyelitis (EAE) animal model, and then later function to attenuate the pathophysiology. It was shown that IL-6 increased BBB permeability, induced gliosis, upregulated proinflammatory cytokine and antibody production, and yet might have accounted for the survival, migration and

differentiation of oligodendrocyte precursors that are required for the repair of damaged myelin. TGF-β is chemotactic for macrophages, microglia and astrocytes and therefore induces infiltration and gliosis and yet it is a potent inhibitor of the functions of astrocytes and microglial cells when these cells are in an activated state (Merrill and Zimmerman., 1991).

The major source of proinflammatory cytokines (e.g. IL-1ß, IL-6 and TNF-α) in the brain appears to be from activated microglia and astrocytes (Giulian et al., 1986; Sawada et al., 1989; Chung and Benveniste, 1990). Perivascular macrophages and brain endothelial cells are two additional potential sources of cytokines in CNS tissue, and each of these cell types have been shown to express IL-6 in response to other proinflammatory cytokines (Fabry et al., 1993). Proinflammatory cytokines can trigger the synthesis and secretion of a cascade of cytokines in the CNS, normally first acting on astrocytes and microglia, followed by glial-derived cytokines acting on neurons, although the initially produced proinflammatory cytokines may have a direct influence on neurons as well (Sawada et al., 1989; Chung and Benveniste, 1990). For example, TNF-α mostly induces IL-1ß and IL-6 expression. In contrast, growth factors such as neurotrophins are induced by IL-1ß, and IL-6 can block IL-1ß and TNF-α expression in target cells (Norris et al., 1994). It is interesting that proinflammatory cytokines can regulate the production and release of NGF and other neurotrophic molecules by astrocytes *in vitro* (Spranger et al., 1990; Sagoh et al., 1993) and by cells in the injured sciatic nerve (Lindholm et al., 1987) that are capable of promoting neuronal survival and repair of neural tissue.

1.5.2 Proinflammatory Cytokines: Signal Transduction

There is considerable evidence that the peripheral immune system can signal the CNS to elicit a response during CNS inflammation or infection (Hosoi et al., 2002). Proinflammatory cytokine expression such as IL-1ß, TNF-α and IL-6 is involved in response to a variety of animal models of CNS injury (Besedovsky et al., 1996; Hosoi et al., 2002). CNS injury may upregulate specific transcription factor-dependent cytokine production; for example, the activity of nuclear factor kappa B (NF-kB), an inflammatory-induced transcription factor (Haddad, 2002). Poly (ADP-ribose) polymerase-1 (PARP-1) is an abundant nuclear enzyme that is activated by DNA

damage. In response to proinflammatory cytokine up regulation, PARP-1 may play a key role in NF-kB-driven expression of inflammatory mediators by microglia and astrocytes during the neuroimmune response. PARP-1 promotes the DNA binding of NF-kB in microglia exposed to lipopolysaccharides, IFN-λ or β-amyloid (Chiarugi and Moskowitz, 2003). Excessive PARP-1 activation is implicated in a variety of pathologies, such as cerebral ischemia and traumatic SCI (Chiarugi and Moskowitz, 2003).

The JAK/STAT signal transduction pathway is one of the intracellular signaling pathways activated by cytokines and growth factors that was first studied in the hematopoietic system, but recent data demonstrate that pathway is also greatly utilized by other systems. The JAK/STAT pathway is a signaling cascade that links the activation of specific cell membrane receptors to nuclear gene expression (Licinio et al., 2000; Kim et al., 2002). Most cytokines act through cell surface receptors that have one transmembrane domain and transduce a signal through the JAK/STAT pathway. Signaling through its receptor, IL-3 has been shown to induce the activation of JAK/STAT and MAPK pathways in microglial cells, thereby upregulating the expression of CD40 and MHCII molecules (Natarajan et al., 2004).

1.5.3 Proinflamatory Cytokines: Neural Injury

The upregulation of several families of inflammatory molecules, including cytokines and chemokines, is a prominent consequence of SCI (Bethea, 2000; McTigue et al., 1998; Jones et al., 2005). The potential sources of these molecules are intrinsic CNS cells, including microglia, and extrinsic leukocytes that are recruited to the site of damage. Breakdown of the BBB, demyelination, and axonal injury are some detrimental consequences of rapid upregulation of inflammatory mediators (Allan and Rothwell, 2003). In correspondence with these undesirable actions, systemic treatment with the anti-inflammatory cytokine IL-10 limited the neuronal damage and improved the functional recovery in rats after SCI (Bethea et al., 1999). Furthermore, neutralization of the T cell chemoattractant CXCL10 reduced T cell infiltration and secondary degeneration in SCI (Gonzalez et al., 2003). Finally, depletion of peripheral macrophages resulted in improved hindlimb function after SCI in rats (Popovich et al., 1999). The temporal pattern of cytokine expression after clip compression-induced SCI in the mouse

revealed an elevation of IL-1ß mRNA levels by 30 minutes after injury. This rapid elevation of IL-1ß was transient and peaked between 90 minutes and 3 hours after injury; the levels had decreased to sham levels by 24 hours after injury (Rice et al., 2007). Molecules such as the IL-1 receptor antagonist (IL-1ra) and IL-6 were induced within the first 3 hours after SCI but were not readily apparent by 30 minutes after injury. TNF-α is a proinflammatory cytokine that has been implicated in the inflammatory reaction associated with SCI. The expression of TNF-α mRNA was elevated within 30 minutes of SCI, but the mRNA levels of cytokines such as IL-6, lymphotoxin-ß (LT-ß) and TGF-ß remained at normal levels at this time (Rice et al., 2007).

In situ hybridization and immunocytochemistry have demonstrated that microglia/macrophages are a source of the cytokines produced early in the inflammatory reaction to spinal cord injury. Rice et al. (2007) have shown that cells that expressed IL-1ß mRNA were seen around the lesion site by 3 hours after SCI in mice. These cells were Iba-1+ve, a microglia/macrophage marker. Not all Iba-1+ve cells, however, expressed the IL-1ß signal, but the cells that expressed this cytokine were all Iba-1+ve at the 3-hour time point. As blood-derived macrophages are known to infiltrate the parenchyma of the injured brain no earlier than 5 hours after traumatic brain injury (Giulian et al., 1989), Rice et al. (2007) hypothesized that microglia within the CNS are the main source of IL-1ß mRNA in the acute phase after SCI in mice. However, since staining with Iba-1 cannot discriminate between microglia and macrophages, the latter cell type cannot be excluded as a possible source of IL-1ß in the study by Rice et al. (2007). Recently, however, Pineau and Lacroix (2007) reported data from chimeric mice that had a SCI; in these mice, GFP-expressing hematopoietic stem cells had been transplanted 6 months prior to the SCI, with the transplantation occurring following bone marrow irradiation. At 1 hour after SCI in these chimeric mice the cells expressing IL-1ß were GFP-ve, thus supporting the hypothesis of Rice et al. (2007) that cells other than those derived from the blood must be the source of inflammatory molecules early after such an injury. Within 30 minutes of an impact injury to the rat spinal cord, the activation of NF-κB, which regulates the transcription of several cytokines and cytokine-responsive genes, was demonstrated in microglia and endothelial cells whereas neuronal expression of NF-κB was only evident after 24 hours (Bethea et al., 1998). After a contusion injury to the

mouse spinal cord, astrocytes and microglia were reported to express proinflammatory cytokines by 1 hour after injury (Pineau and Lacroix, 2007).

To further dissociate infiltrating macrophages from microglia as the early cellular sources of IL-1ß and other inflammatory molecules after SCI, it would be ideal to have a model of SCI in which no leukocytic infiltration occurs. In this regard, the spinal cord slice culture provides at least a partial solution (Pan et al., 2002). Obtaining a slice of the spinal cord to grow as an organotypic slice culture is a type of transection injury, and the time in culture is similar to the time after injury. Over the first 1, 3, and 6 hours, neurons in the spinal cord became pyknotic, the processes of neurons disappeared, and the neuronal density declined. Microglia in the slices transformed from a ramified morphology typical of resting microglia and acquired shorter thicker processes that are indicative of activated microglia (Pan et al., 2002). There was an upregulation of IL-1ß, IL-6, monocyte chemotactic protein-1 (MCP-1), macrophage inflammatory protein 1 alpha (MIP-1α), MIP-1ß, and MIP-2 in the slices as early as 3 hours *in vitro* (Rice et al., 2007). These results demonstrated that cells intrinsic to the spinal cord are sufficient to mount an inflammatory response, similar to that observed following the *in vivo* clip compression SCI, and in the absence of a blood source and potential infiltration of the lesion by leukocytes. A likely source of inflammatory molecules in the *in vitro* SCI model are the microglia, a conclusion supported by the morphological evidence of their activation. There is increasing recognition of the fact that there are different functional states of microglia/macrophages, such that one that is performing a phagocytic role or generating free radicals may not be playing a role in the production of inflammatory cytokines. In support of this suggestion, the treatment of microglia with GDNF increased nitric oxide production and phagocytic activity but had no effect on the secretion of IL-1ß and TNF-α (Chang et al., 2006). Disrupting the function of the Kv1.3 ion channel in microglia attenuated their neurotoxic property but did not affect their production of nitric oxide (Fordyce et al., 2005). Furthermore, the production of CCL3 and the phagocytic function by microglia are regulated through different signaling cascades (Song et al., 2004). Clearly, much remains to be understood of the functions of proinflammatory cytokines in the context of the neuroinflammation that occurs after a SCI. It is possible

that the type of SCI, such as contusion, transection, or ischemic damage, may differentially alter cytokine secretion and thus the intensity of the inflammatory reaction.

1.5.4 Proinflamatory Cytokines: Neuroinflammation

Cytokines have been implicated in oligodendrocyte cell death, axonal degeneration and neuronal dysfunction (Wujek et al., 2002). Proinflammatory cytokines are thought to be key players in the pathophysiology of MS (Lucchinetti et al., 2001). The cerebrospinal fluid (CSF) from patients with the primary progressive type of MS contains soluble mediators that have been shown to induce axonal damage and apoptosis of neurons *in vitro* (Alcazar et al., 2000). Therefore, understanding the mechanisms of cytokine-mediated neural injury is necessary to design therapies that promote oligodendrocyte and axon survival and prevent irreversible chronic disability as a consequence of CNS inflammation.

On the other hand, proinflammatory cytokines may have some beneficial roles to play in some aspects of neuroinflammation after SCI (Franzen et al., 1998; Prewitt et al., 1997). It was hypothesized that neuroinflammation also has an important role to play as a host defense mechanism after different types of SCI. In support of this hypothesis, the application of macrophages (Franzen et al., 1998; Rapalino et al., 1998) or microglia (Prewitt et al., 1997) into the lesion site after SCI promoted neural repair. Thus, the role of inflammation in tissue repair after SCI is complex. In addition, proinflammatory cytokines within the CNS have been suggested to provide neuroprotective benefits during the healing process of the brain and spinal cord that depends on the activation state of the cytokine-producing cells (Klusman and Schwab, 1997; Schwartz and Yoles, 2006). In addition to proinflammatory cytokines, macrophages can secrete factors that are growth promoting, such as NGF and NT-3 (Elkabes et al., 1996) and thrombospondin (Chamak et al., 1994). Even zymosan, which triggers a robust inflammatory reaction, when placed in the vitreous chamber of the eye can facilitate regeneration of injured optic nerve fibers (Leon et al., 2000). Injection of zymosan into a DRG prior to a crush injury of its dorsal root when combined with modification of the ECM in the CNS component of the pathway appear essential to the success of axon regeneration into the spinal cord (Steinmetz et al., 2005). Intense inflammatory states created just outside of the CNS

illustrate that in certain circumstances inflammation can facilitate axon regeneration, perhaps by triggering a conditioning-like effect within the neuron (Calvo et al., 2005).

The size, duration and location of the injury, as well as the predominant expression of specific cytokines and neurotrophic factors, are important determinants of whether neuroinflammation will be beneficial or detrimental. The time period after SCI may be another criterion, and there are data to support the suggestion that although the very early phase of neuroinflammation after SCI may be undesirable, at later times after injury it may have a useful role to play (Bethea, 2000). Klusman and Schwab (1997) noted that a mixture of IL-1ß, IL-6 and TNF-α delivered into the spinal cord 1 day after SCI exacerbated the injury-induced inflammatory reaction but it reduced tissue loss if the cytokine treatment was delivered 4 days after SCI. Microglia are a pivotal cell type in the regulation of the early neuroinflammatory response after SCI and the main source of the different type of cytokines produced in the injured spinal cord (Lotan and Schwartz, 1994; Schwartz and Yoles, 2006).

1.6 Cellular Therapeutic Strategies for Neural Repair

Cell-based therapeutic approaches are being considered for a number of neurological diseases. Remyelination and improvement in action potential conduction has been demonstrated following transplantation of oligodendroglial lineage cells (Utzchneider et al., 1994; Keirstead et al., 2005; Groves et al., 1993), Schwann cells (Honmou et al., 1996), OECs (Barnett et al., 2000; Kato et al., 2000; Franklin et al., 1996; Imaizumi et al., 2000) and various types of stem cells (Akiyama et al., 2001; Akiyama et al., 2002, Brustle et al., 1999; Nistor et al., 2005). Given the success of cell transplantation to form functional myelin in animal models, myelin-forming cell transplantation has been suggested as a potential repair strategy for demyelinated CNS axons (Kocsis, 1999; Groves et al., 1993, Honmou et al., 1996).

1.6.1 Transplantation of Oligodendrocytes

The studies on oligodendrocyte transplantation have great importance. Recently, it has become evident that axonal degeneration and/or SCI induces considerable oligodendrocyte apoptosis, thus reducing the number of glial cells that are able to remyelinate axons at the lesion site (Warden et al., 2001; Casha et al., 2001). The long fiber tracts situated in the white matter of the spinal cord provide an excellent model system for the study of migration and remyelination of grafted oligodendrocytes. Wild-type oligodendrocytes transplanted into the hypomyelinated brain of Shiverer mice were able to remyelinate the axons that were left unmyelinated as a result of the Shiverer mutation (Lachapelle et al., 1983). It appeared likely that demyelination and transplantation enhanced the remyelination capability of host oligodendrocytes but the host cells were not able to migrate over as long distances as did the transplanted oligodendrocyte progenitor cells (Wolswijk and Noble, 1989). Human oligodendrocyte progenitor cells have been shown to myelinate axons in lysolecithin-induced demyelinated lesions of the adult mouse brain (Windrem et al., 2002). *LacZ*-expressing oligodendrocyte progenitor cells obtained from rat optic nerve cell cultures and transplanted directly into an x-irradiated EtBr lesion remyelinated approximately 90% of the axons by 21 days after transplantation, which indicated the transplanted *LacZ*-expressiong progenitor cells were able to differentiate into myelinating oligodendrocytes (Groves et al., 1993). Remyelination of axons in an x-irradiated EtBr lesion can also be achieved using oligodendrocyte cell lines such as the CG4 cell line (Franklin et al. 1995). Transplanted CG4 cells were able to migrate within x-irradiated areas of the adult rat spinal cord and they could enter and contribute to the repair of areas of demyelination remotely located with respect to the point of transplantation. However, the transplanted CG4 cells failed to survive and did not migrate when transplanted into the spinal cord of control (i.e. no x-irradiation or EtBr injection) adult rats (Franklin et al., 1996). It is likely that oligodendrocyte progenitor cells would be the most suitable for cell transplantation for the repair of CNS demyelination in diseases such as MS, but because of the complexity of getting sufficient numbers of these cells from a therapeutically and ethically viable tissue source, these cells have yet to be tested in a clinical trial.

1.6.2 Schwann Cell Transplantation

Schwann cells from peripheral nerves have been used for transplantation into a variety of SCI models. After transection and implantation of Schwann cells, sensory and spinal axons whose cell bodies are located near the grafts and the site of injury grow into these bridging grafts and were myelinated (Xu et al., 1995). After a contusion injury and implantation of Schwann cells in adult rats, cavitation is reduced and spinal axons grow into the grafts, with many of these axons being remyelinated (Takami et al. 2002). After thoracic spinal cord transection in adult rats the transplantation of Schwann cells with concomitant delivery of neurotrophins enhances axon regeneration (Menei et al., 1998; Xu et al., 1995). The accessibility of Schwann cells from a patient's peripheral nerves for setting up cell cultures to obtain a sufficient number of cells for grafting makes autograft transplantation feasible, which in turn means there would be no need for immunosupressive procedures if Schwann cells from this tissue source were used. However, it is also known that Schwann cells migrate into areas of CNS injury and remyelinate axons only in the absence of astrocytes from the injury site (Franklin and Blakemore, 1993; Woodruff and Franklin, 1999).

1.6.3 OEC Transplantation

Embryonic or adult OECs (porcine, primate and human) obtained from the OB or olfactory mucosa have been tested in rodent and non-human primate models of SCI or demyelination (Barnett et al., 2000; Kato et al., 2000; Imaizumi et al., 2000) (see section 1.2.3). Functional recovery and/or CNS axon regeneration has been reported when OECs are transplanted immediately or as long as 2 months after SCI in adult rats (Li et al., 1997; Li et al., 1998; Li et al., 2003; Lu et al., 2001; Lu et al., 2003; Ramon-Cueto et al., 2000; Sasaki et al., 2006). After lateral cervical hemisection in adult rats, injection of OECs led to improvements in respiratory function and enhanced their performance on a climbing task (Li et al., 2003). It was suggested these OEC transplants might also have prevented injury-induced loss of neural tissue (Sasaki et al., 2006; Ruitenberg et al., 2005) and also appeared to have resulted in enhancement of the remyelination after SCI (Sasaki et al., 2004), although whether OECs directly remyelinated these regenerated axons or provided an environment conducive for the ingrowth of host remyelinating

Schwann cells is controversial (Boyd et al., 2005). The general consensus is that OEC grafts facilitate neural repair, although the mechanisms through which this is accomplished are under debate (Boyd et al., 2005; Ramon-Cueto et al., 1998). Important issues that remain to be resolved include the optimal source of cells (lamina propria versus OB), age of the animal for obtaining the cells (embryonic versus adult) and the graft strategy (for example, injection of suspensions or transfer within a cellular matrix). It will also be important to determine whether enriching cultures for specific phenotypes of OECs improves the structural and/or functional recovery (Li et al., 2003; Boyd et al., 2005; Lakatos et al., 2003).

1.6.4 Transplantation of Neuronal Stem Cells (NSCs)

After spinal cord transection in adult rats and transplantation of neural stem cells (NSCs) into the lesion site, a small number of host axons regenerated into the transplant but their growth terminated near the host transplant border (Bregman et al., 1997; Jakeman et al., 1991). A small but significant degree of functional recovery was observed in rats (Kunkel-Bagden and Bregman 1990) and cats (Reier et al., 1992) who had received such grafts. Mouse clonal NSCs that were injected into the brain ventricles of newborn Shiverer mice have also been shown to myelinate axons and result in improved function in the mutant strain (Yandava et al., 1999). In the latter study, it was found that most of the transplanted cells migrated through the brain and differentiated into oligodendrocytes. The injection of NSCs derived from wild type mice and injected either intravenously or into the cerebral ventricles of EAE mice resulted in a remarkable increase in the number of oligodendrocyte progenitors within demyelinated areas as well as of functional recovery in the mice receiving such transplants, along with a significant decrease in the extent of axonal loss (Pluchino et al., 2003).

Grafting of human NSCs into a demyelinated area of adult rat spinal cord showed extensive remyelination with a peripheral myelin pattern similar to that seen when Schwann cells remyelinate axons, characterized by large cytoplasmic and nuclear regions, a basal lamina, and P0 immunoreactivity; there was also an improvement of conduction velocities of the remyelinated axons (Akiyama et al., 2001). When mouse NSCs were transplanted into the embryonic and neonatal CNS of wild-type mice, they

differentiated into both neurons (Brustle et al., 1995; Stemple and Anderson, 1992) and oligodendrocytes (Hammang et al., 1997; Milward et al., 2000) but when grafted into the adult CNS they only differentiated into astrocytes (Lundberg and Bjorklund, 1996). Therefore, the differentiation of NSCs following grafting is indeed dependent on environmental signals. Grafts might also provide growth factors or improve conduction in spared axons (Reier et al., 1994; Bregman et al., 2002). When fetal spinal cord transplants are combined with neurotrophin delivery after complete spinal cord transection in adult rats, recovery of function was observed (Coumans et al., 2001), with some supraspinal and propriospinal axons growing into the caudal spinal cord (Bregman et al., 2002).

The best current tissue source for human NSCs is considered to be fetal tissue. However, a major concern in future clincal applications would be along the line of ethical issues with respect to using fetal tissue as a source for the cells. The other important issue that needs to be resolved is the highly proliferative nature of the progeny of stem cells, a feature that may contribute to the formation of tumors (Bjorklund et al., 2002).

CHAPTER 2.0 Specific Aims

In recent years, a number of studies have examined the potential beneficial effect of transplantation of OECs into, or adjacent to, a SCI in rats (Barnett and Chang, 2004; Coumans et al., 2001; Deumens et al., 2005; Koopmans et al., 2005; Li et al., 2005; Nash et al., 2002; Sasaki et al., 2004). Some of these studies have reported improvements in motor and sensory function (Chuah et al., 2004; Imaizumi et al., 2000; Nash et al., 2002, Raisman, 2001, Ramon-Cueto et al., 2000, Woodhouse et al., 2005). While these data provide support for the suggestion that OEC transplantation can be beneficial for neural repair after SCI, more experiments are needed in order to better understand the signals that induce transplanted OECs to migrate towards sites of injury. Although it has been reported that OECs possess the ability to migrate within the adult mammalian CNS in animal models of SCI (Li et al., 1998; Ramon-Cueto and Nieto-Sampedro, 1994; Ramon-Cueto et al., 1998), there has been no systematic examination of the factors inducing or guiding this migration. Migration of the OECs that accompany the axons that are regenerating is thought to be critical to promoting axonal growth. However, little is known about the extracellular and intracellular factors that regulate the migration of OECs. The migratory signals coming from a lesion and along the migratory path may participate in various aspects of neural repair. Microglia, which respond to CNS trauma both at the site of injury and along the length of degenerating fiber tracts, are extraordinarily sensitive to microenvironmental changes within the CNS, thus making them ideally suited to playing an important role in directing the repair of neural tissue.

My Ph.D. research project concentrated on the potential contribution of reactive microglia to the generation of a migratory signal for OECs by applying different injury paradigms to activate the microglia in different ways and in different fiber tracts within the white matter of the spinal cord, and to assess the effect of these experimental manipulations on the migration of OECs. There were four specific aims:

Specific Aim # 1 To determine the time-frame in which Wallerian degeneration induced glial reactivity occurs in the lower thoracic spinal cord of

adult rats following aspiration of the contralateral sensorimotor cortex. (Addressed in Chapter 4)

Specific Aim # 2 To determine whether OECs are induced to migrate in response to glial reactivity arising as a result of Wallerian degeneration following sensorimotor cortex aspiration in adult rats and whether the migratory signal(s) is dependent on microglial reactivity. (Addressed in Chapter 4).

Specific Aim # 3 To identify concentrations of TNF-α that when injected into the posterior funiculus of the T11 spinal cord segment of an adult rat will induce glial reactivity either along at least a 5 mm distance from the injection site or confined to the immediate vicinity of the injection site. (Addressed in Chapter 5)

Specific Aim # 4 To examine whether a focal injection of TNF-α gives rise to a migratory signal(s) that induces OECs to migrate and whether this migration occurs only if reactive microglia are present along the entire extent of the migratory path. (Addressed in Chapter 5)

CHAPTER 3.0 MATERIALS AND METHODS

3.1 OEC Cultures

3.1.1 Tissue Dissection

On day 18 (E18) of pregnancy female Wistar rats were killed by CO_2 inhalation, using sterile techniques the abdomen was opened, and the uterine horns were removed and placed into a 100 ml Petri dish containing Hank's balanced salt solution (HBSS). Embryos that were at Theiler stage 23 of development (Theiler, 1972) were selected for further dissection. Four phenotypic features were used to assign embryos to Theiler stage 23: A) the presence of hair follicles over all the skin of the embryos; B) the complete separation and divergence of the digit in both the forelimbs and the hind limbs; C) an ear pinna that covered more than half of the external auditory meatus; and D) the presence of an umbilical hernia. Under a dissecting microscope, the Theiler stage 23 embryos were decapitated, their heads transferred to a 1:1 mixture of Dulbecco's Modified Eagle's Medium (DMEM; 4.5 g/l of glucose; Sigma-Aldrich Canada Ltd.) and F12 containing 10% fetal bovine serum (FBS; Hyclone, Logan, UT).

The OBs were dissected from the heads of each Theiler stage 23 rat embryo using the technique described by Doucette (2001). The details are as follows. One at a time the heads were dissected inside a 60 mm Petri dish containing growth medium (DMEM/F12/10%FBS). Under a dissecting microscope, a pair of Dumont forceps was used to position each head upright by inserting the prongs of the forceps into the tissue lying to either side of the nose. Using a pair of spring scissors the cranium was cut along the midline between the right and left cerebral hemispheres, with the cut continuing caudally along the midline overlying the cerebellum. Using a #11 scalpel blade a midsagittal cut was then gently made through the thickness of the head to separate it into right and left halves. The exposed OBs were dissected out of their position in the anterior cranial fossa by cutting the olfactory peduncle. The OBs were collected in growth medium in a 60 mm Petri dish. The remainder of the head was then discarded. This procedure was then repeated for each head (Fig 3.1).

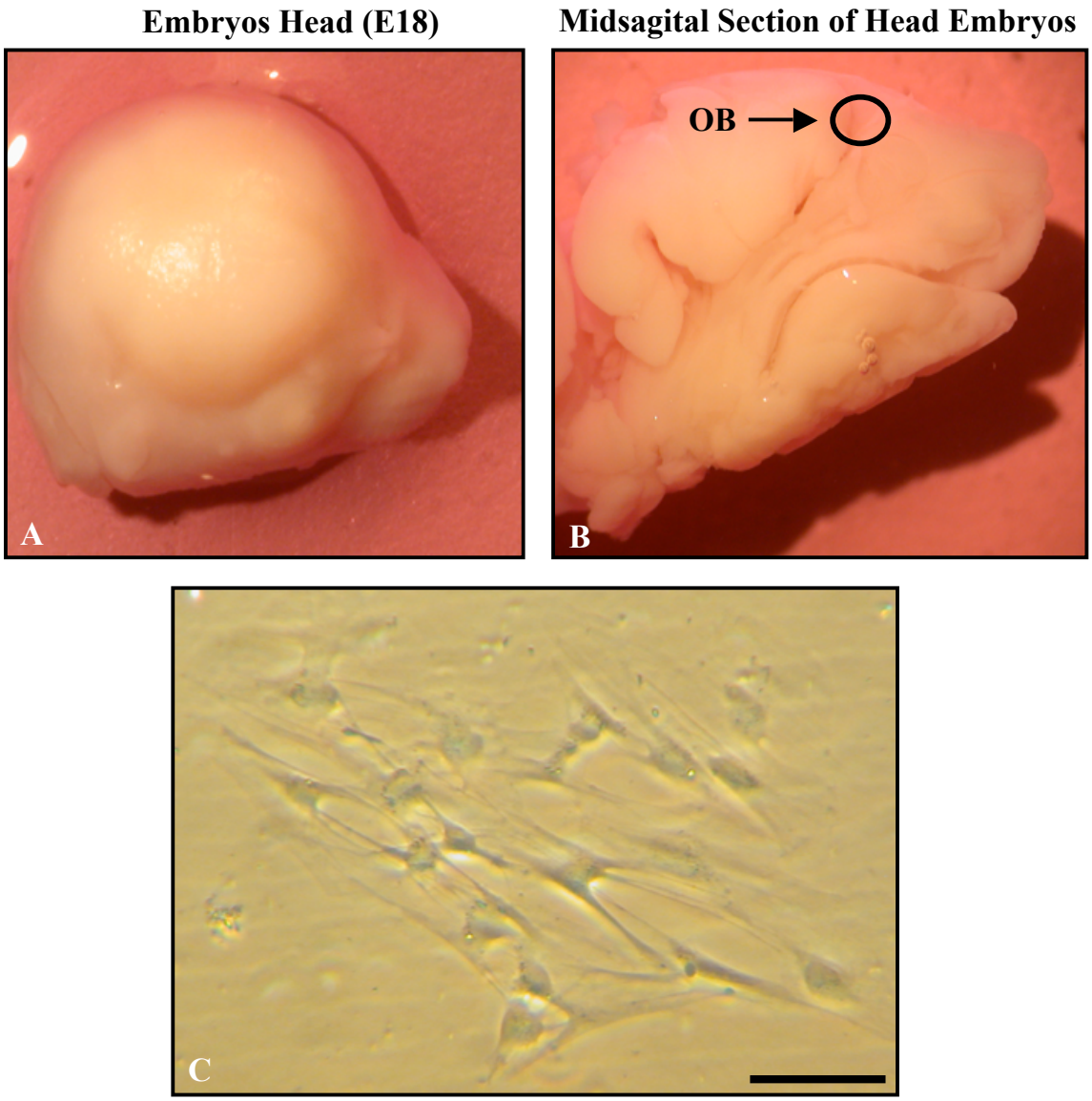

FIGURE 3.1: Dissection of embryos and setting up cell culture.

(**A**) The head of a rat embryo (E18) prior to beginning the dissection to obtain the OBs for setting up the OEC cultures. The view is from the superior surface, with the nose to the right side of the image. (**B**) The left-hand side of this embryo's head as seen after cutting the head in two by means of a midsagital cut. The circle shows the location of the OBs, which is dissected from both the left and right sides of the head. (**C**) A phase contrast micrograph of an OEC culture initiated from the nerve fiber layer that is stripped off the OBs dissected in the previous step. Scale bar in '**C**' = 100 µm.

3.1.2 Tissue Disaggregation and Expansion of Cell Cultures

Two pairs of sharp forceps were used to dissect the ONL off the OB. The prongs of one pair of forceps were placed in the tissue in the cut end of the OB in the area that previously had been attached to the olfactory peduncle. The second pair of forceps were used to grasp the free edge of the ONL at the cut end of the bulb; the ONL was then gently peeled off the deeper layers of the bulb. The ONLs were pooled together in growth medium (DMEM/F12/10%FBS) in a 35 mm Petri dish.

Once all the ONLs were dissected they were mechanically disaggregated using Nitex mesh (75µm pore size). The resulting cell suspension was diluted with DMEM/F12/10% FBS to a final volume of 40 ml. This cell suspension was plated into a total of eight 25 cm^2 Falcon tissue culture flasks by placing 5 ml of cell suspension into each flask. The cells from these flasks were used for DiI (1, 1', di-octadecyl-3, 3, 3'3'-tetramethylindocarbocyanine perchlorate) labeling and cell grafting. For immuno-staining, 2 ml of the cell suspension were plated into each of at least ten 35 mm Falcon dishes containing glass coverslips; the remainder of the cell suspension was plated into 25 cm^2 Falcon tissue culture flasks (5 ml per flask). All cell cultures were incubated at 37°C in a humidified atmosphere of 5% CO_2 in air.

After 3-4 days *in vitro*, the cell cultures in the flasks were switched to a modified G5 medium (mG5). The basal medium of mG5 consisted of DMEM (4.5 g/l of glucose), to which was added insulin (5 mg/ml), transferrin (50mg/ml), selenium (5.2ng/ml), hydrocortisone (3.63ng/ml), and biotin (10ng/ml); this growth medium was referred to as mG5 because in contrast to the G5 medium it contained neither epidermal growth factor nor fibroblast growth factor. In fact, this serum-free and mitogen-free growth medium is not a suitable medium for any contaminating meningeal fibroblasts that may have been carried into the primary cell culture along with the OECs. After 10-14 days in mG5, the growth medium was changed back to DMEM/F12/10% FBS and the cell cultures were fed with this medium twice per week until they approached confluence.

3.1.3 Harvesting and Long Term Storage of OECs

Once the cell cultures were approximately 80% confluent, the following harvesting procedure was used. The cell cultures were washed three times with Puck's balanced salt solution (PBSS) to remove all traces of serum. Then they were incubated in 0.025% trypsin/0.01% ethylenediaminetetraacetic (EDTA)/PBSS for 5 min at room temperature. The progress of the trypsinization was monitored with a phase contrast microscope. The flasks were gently tapped on the countertop several times to accelerate cell detachment from the substratum. Also, the trypsin solution was triturated to assist in dislodging the cells. The resulting cell suspension was transferred to a 50 ml sterile plastic centrifuge tube and was centrifuged at the centrifugal force of 160G (800 RPM) for 10 min and then resuspended in DMEM/F12/10% FBS. In order to determine the number of viable cells, 100µl of 0.3% Nigrosin dye was added to 400µl of cell suspension. With this technique, dead or dying cells are stained purple-black by the Nigrosin dye due to the leakiness of their plasma membranes, whereas living (i.e. viable) cells are left unstained. The number of viable (i.e. Nigrosin-excluding) cells was counted in four corners of an Improved Neubauerlevy Hemacytometer (Hausser Scientific Partnership, Horsham, PA, 19044). The number of viable cells per ml was calculated based on the following formula:

$$\frac{\text{Total \# Viable Cells}}{4} \times 10 \times 1000 \times \frac{5}{4} = \text{number of viable cells/ml.}$$

Based on the viable cell count, the original trypsinized cell suspension was diluted in DMEM/F12/10% FBS to the desired cell concentration of 1×10^6 cells per ml.

3.1.4 Prelabelling Cells with DiI

In order to label OECS with DiI, which is a fluorescent dye that becomes incorporated into the plasma membrane, the cells were harvested and viable cell counts done as described in Section 3.1.3. The resulting cell suspension was incubated in DMEM/F12/10% FBS containing 40 µg/ml of DiI for 1 hour at 37 °C in a humidified atmosphere of 5% CO_2 in air. Then the cell suspension was centrifuged at 160G (800 RPM) for 10 min and resuspended in DMEM/F12/10% FBS. After a second

centrifugation and resuspension in DMEM/F12/10% FBS, a cell count was performed to determine the number of viable cells that had survived the DiI prelabelling and the cell suspension was diluted once more to a viable cell count of 1 x 10^6 cells per ml. This cell suspension was frozen in 1 ml aliquots using Nalgene cryovials (1 x 10^6 cells per ml) with 110 µl of dimethyl sulfoxide (DMSO) being added to each vial prior to sealing them and placing them into a NALGENE Cryo 1°C Freezing Container (Nalge Company, Rochester, N.Y., USA) containing isopropyl alcohol. The NALGENE Cryo Container was stored overnight in a -80°C freezer. The next day, the cryovials were transferred to the vapor phase of liquid nitrogen in a Locator (JR Plus, Cryo Biological Storage System) for long term storage.

3.2 Surgery

All surgical procedures were performed using aseptic techniques. All experimental protocols in this research work were approved by the animal care committee of the University of Saskatchewan in accordance with policies established in the Guide to the Care and Use of Experimental Animals prepared by the Canadian Council of Animal Care. Rats were housed in conventional cages on a 12:12 hr light-dark cycle and had free access to food and water throughout the period of study.

3.2.1 Anesthesia and Analgesia

Female Wistar rats (3-4 months old) weighing 220-260 grams (U of S Laboratory Animal Service Unit) were anesthetized by inhalation of Halothane (MTC Pharmaceuticals, Ontario, Canada). A mixture of 3% halothane in 100% oxygen was applied by using a Boyle anesthetic machine (Ohmeda, Mississauga, ON) to induce anesthesia. After approximately 5 min the animal became immobile and unresponsive to a pinch test on their hind paws (pedal reflex). To minimize animal pain and distress a single intramuscular injection of Buprenex (0.05 mg/kg) was administered prior to making a skin incision along the midline of the rat's back. The concentration of 3% Halothane was maintained during the initial parts of the surgery and laminectomy. The Halothane concentration was reduced, however, to 2-2.5% during cell grafting and cytokine injection. When suturing the wound, the concentration of Halothane used was 1-

1.5%. Throughout the surgery, each animal was carefully monitored (every 3-5 min) for both physiological parameters and analgesia, including their respiration, heart rate, pedal reflexes, and the color of their paws (pink in color).

3.2.2 Laminectomy

A rectangular area of the skin (5 x 2 cm) was shaved on the back of each rat and sterilized with a 1:1 mixture of Betadine antiseptic solution (10% provide-iodine topical solution UPS) and 70% ethanol. A midline incision was made using a #23 Almedic stainless steel scalpel blade and the paravertebral muscles attached to each side of the vertebral column were reflected from the spinous processes. A laminectomy was performed on the T8 and T9 vertebrae in order to expose the thoracic spinal cord segments (i.e. T11 or T12) under visual guidance using a surgical microscope (Nikon-SMZ-1B) until only a very thin layer of bone remained. A small hole was then drilled in this thin layer of bone using a dental drill to expose the dura matter. Under higher magnification and with the aid of a surgical microscope the exposed dura matter was cut longitudinally by traversing the surface of the dura with the tip of a 22-gauge needle, a procedure that resulted in the leakage of a small amount of CSF. The T8 spinous process was rigidly clamped using forceps to fix the vertebral column, and hence the spinal cord, in position and prevent the slight movement that might occur, for example, during respiration.

3.2.3 Grafting DiI-Labeled OECs

The Cryovials containing DiI-labeled OECs were removed from storage in the liquid nitrogen locator and transferred to a bath of lukewarm water to thaw the cells. In order to dilute the DMSO, the 1.1 ml of thawed cell suspension was then gradually added to 5 ml of growth medium (DMEM-F12/10%FBS) in a 15 ml Falcon centrifuge tube. The cell suspension was centrifuged at 160G twice (10 min each), followed each time by resuspension in growth medium. Following the last wash in growth medium, a viable cell count was done (see Section 3.1.3) and the cell density adjusted to 50,000 cells/µl using a grafting solution containing 1µg/ml of $CaCl_2$, 1µg/ml of $MgCl_2$, and 0.1% glucose in 0.1M PBS. The cell viability after thawing averaged 74.5% (Table 3.1). A total of 5µl of

Table 3.1 Viability of Thawed OECs Used for Cell Grafting

Cell Culture	# of Viable Cells Frozen	# of Viable Cells After Thawing	% Viability After Thawing
K586	1,000,000	750,000	75.0
K586	1,000,000	820,000	82.0
K586	1,000,000	820,000	82.0
K586	1,000,000	740,000	74.0
K586	1,000,000	720,000	72.0
K577	1,000,000	710,000	71.0
K577	1,000,000	700,000	70.0
K577	1,000,000	740,000	74.0
K577	1,000,000	770,000	77.0
K594	1,000,000	660,000	66.0
K594	1,000,000	710,000	71.0
K56-13	1,000,000	650,000	65.0
K56-13	1,000,000	770,000	77.0
K56-13	1,000,000	810,000	81.0
K56-13	1,000,000	800,000	80.0
	Average =	**744,666.7**	**74.5**

this cell suspension was loaded into a 32 Gauge needle attached to a 5 µl Hamilton syringe. After zeroing the XYZ coordinates of the stereotaxic apparatus, the 32 Gauge needle was slowly lowered into the right dorsal funiculus of the spinal cord to a depth of 1 mm; the needle was inserted immediately to the right of the dorsal spinal artery. The needle was left in position for 2 min after which time 1 µl of DiI-labeled OECs was injected over 10 min with a flowrate of 0.01µl/min using the KDS 310 syringe pump. After completion of the injection, the needle was left in position in the spinal cord for 5 min prior to being slowly withdrawn. The syringe and needle were rinsed with dH_2O, followed by two washes with acetone, and a few final rinses with dH_2O at the completion of the cell grafting.

3.2.4 Wound Closure and Postoperative Care

Using Ethicon 4-0 surgical silk, the dorsal spinal muscles were sutured along the spine. For antiseptic purposes, the surgical area was washed with a 3% solution of hydrogen peroxide (diluted in dH_2O). Then the skin wound was sutured with 3-4 silk sutures and betadine solution diluted 1:1 with 70% ethanol was applied to the wound to prevent infection. A 2% Xylocaine local anesthetic gel was applied on top of the sutured skin wound (Lidocaine Hydrochloride Jelly, USP Sterile Topical Anesthetic, Astra Pharma Inc., ON, Canada).

During the first hour postoperatively the animal was monitored every 5 min for their respiration rate and for the color of their paws. Each rat was kept on a heated blanket for the first 15-30 min and then was transferred to their own cage once they started to move and once their respiration and paw color were normal. The rats were then checked every hour post-surgically for the next three hours and also the following morning to ensure they were drinking water and eating food. Subsequently, each rat was checked daily with particular attention being paid to the sutures and to the healing of the wound. None of the rats had any problem with the sutures and there were no complications with postoperative healing of the wounds, which typically occurred within 2-3 weeks. The postoperative scar was covered with new hairs by 4 weeks after the surgery. The rats were also checked for their general behavioral status including their mobility, alertness, and their food and water consumption. No noticeable mobility

problems were observed in any of the rats, including sensorimotor cortex aspirated and TNF-α injected animals, as a result of the surgical manipulations. Also, their activities and behaviors appeared to be normal.

3.3 Necropsy of Tissue

3.3.1 Perfusion of the Rats

The rats were deeply anesthetized by administering a lethal dose (90 mg/kg body weight) of sodium pentobarbital (Somnotol) injected intraperitoneally (i.p.). Once the rat failed to respond to either a tail or a paw pinch the animal was placed on its back in a dissection tray and a surgical cut was made with scissors along the midline of the chest to separate the rib cage into right and left halves, thus opening the thoracic cavity. The tip of the apex of the left ventricle was cut off with scissors and a large bore (18 gauge) blunt needle, which was connected to the tubing of a Variable Flow Tubing Pump (VMP Scientific Products, VWR Canlab), was inserted through the apex of the left ventricle and up into the ascending aorta. The needle was clamped in place with a pair of hemostat forceps. Using a pair of small sharp tipped scissors a slit was made in the right atrium to allow the blood and fixative to leave the body during perfusion. Perfusion was begun with approximately 300 ml of a 1% solution of sodium nitrite dissolved in 0.03 M PBS (pH 7.4) for the purpose of washing out the blood. When the fluid exiting the opening in the right atrium was clear, the perfusate was changed to the fixative solution and approximately 300 ml of a freshly made cold solution of 4% paraformaldehyde (PF) in 0.03 M PBS (pH 7.4) was perfused through the circulatory system over a period of 20-30 min.

3.3.2 Dissection of Brain and Spinal Cord

Following completion of the perfusion a #23 scalpel blade was used to make a longitudinal cut along the dorsal midline from the skull to the tail base. Using a bone rongeur, the spinous processes and vertebral laminae were removed beginning caudally and proceeding to the rostral end of the spinal cord. The rongeurs were also used to remove the cranium. The spinal cord with its short rootlets as well as the brain were gently dissected out, immersed in fresh fixative (4% PF), and stored overnight at 4^{o}C. On

the next day, the spinal cord and brain were immersed in a 30% solution of sucrose dissolved in 0.03 M PBS (pH 7.4). If the specimens were kept in 30% sucrose for more than 2 weeks, then they were transferred to fresh sucrose solution.

3.3.3 Cutting Free-Floating Frozen Tissue Sections

The short rootlets that were left attached to the spinal cord during dissection from the vertebral column were counted to identify the T11 spinal cord segment; the counting began at the cervical rootlets and proceeded caudally. A unilateral (left side) and narrow longitudinal cut was performed on the left site of the spinal cord segments using a #11 scalpel blade prior to cutting the segment out from the spinal cord. The idea was to use this longitudinal cut to distinguish the right and left sides of tissue sections used for cell counting and for immunohistochemical analysis of glial reactivity. The specimen holder of a sliding microtome (American Optical Company, Scientific Instrument Division, Buffalo, New York, USA) was kept enclosed within a Styrofoam box containing dry ice for approximately 15-20 min prior to application of Tissue-Tek O.C.T. 4583 compound (Sacura Finerek U.S.A., Inc., Torrance, CA 90504 USA) onto its surface. Then the specimen (i.e T11 spinal cord segment) was placed onto the specimen holder, covered with O.C.T. medium, and covered with dry ice to keep the tissue frozen for sectioning. Serial coronal tissue sections (40μm thick) were cut with a sliding microtome and collected in groups of 10 sections in the wells (10-12 wells) of a 96 well plate; the sections were stored in cryoprotectant (a solution of 0.11 M sodium phosphate monobasic and 0.38 M sodium phosphate dibasic in distilled water, containing 3% glycerin and 3% ethylene glycol). The plates were stored at -20 ºC until sections were removed for mounting onto slides for cell counting or for immunostaining.

3.4 Immunofluorescent and Immunohistochemical Staining

3.4.1 Single and Double Labeling of Cell Cultures

To assess the phenotype of the cells in the OEC cultures the OECs were grown on glass coverslips in 35 mm Petri dishes. Beginning with the first feed, these cell cultures were fed with mG5 medium for 10-14 days, following which they were fed with DMEM/F12/10%FBS for an additional 2-3 weeks. The cell cultures were then

immunostained with a select set of antibodies (see below) to determine the phenotype of the cells.

The following protocol was used for single immunostaining of intracellular antigens expressed by the OECs. The cells were first fixed for 15 min at room temperature in either 0.2% picric acid and 4% paraformaldehyde in 0.2M phosphate buffer, pH 7.4 (Zamboni's fixative) or 0.2% picric acid/4% paraformaldehyde/0.05% glutaraldehyde (PPG; in 0.2 M phosphate buffer, pH 7.4). The PPG fixative was used when the cells were to be immunostained with the rabbit polyclonal anti-S100; Zamboni's fixative was used for immunostaining with monoclonal mouse anti-nestin and mouse anti-smooth muscle alpha actin (SMA). Fixation was followed by two rinses in 0.03M PBS (30 sec each at room temperature), followed by a third PBS wash for 30 min at 4°C and a fourth PBS rinse for 1 min at room temperature. The next step was to permeabilize the cell membrane by incubation of the cells in 0.2% triton X-100 (TX-100) diluted in 0.03M PBS for 5 min, which was followed by a 10 min rinse in PBS. The cells were then incubated for 10 min in a blocking solution of 2% skim milk powder (SMP) dissolved in 0.2% TX-100 followed by a 30 min incubation at room temperature in a mixture of mouse anti-nestin (1:100, clone Rat 401, Developmental Studies Hybridoma Bank, Deptartment of Biological Sciences, University of Iowa, Iowa City, IA, USA) and rabbit anti-S100 (1:200, Dimension Labs, Dako A/S, Denmark) antibodies. These primary antibodies were diluted in 1% SMP/0.2% TX-100 in 0.03 M PBS. Control sections were incubated in diluent only. The cells were then rinsed in 0.03 M PBS for 10 min after which they were incubated in a cocktail mixture of secondary antibodies for 30 min at room temperature; the secondary antibodies used were swine anti-rabbit IgG FITC (1:100, Dimension Labs, Dako A/S, Denmark) and goat anti-mouse IgG Texas Red (1:100, Bio/Can Scientific, Misissauga, ON, Canada). At the end of this incubation period in the secondary antibodies, the coverslips were rinsed in 0.03 M PBS for 5 min. Following this rinse, the cells were incubated in a Hoechst solution (1μM) for 15 min at room temperature to stain the cell nuclei. The cells were then given a final rinse in 0.03 M PBS for 5 min, the coverslips were mounted onto slides using Citifluor (Marivac Ltd, Halifax, NS, Canada) mounting medium (a Glycerol/PBS solution), and the edges of the coverslips were sealed with clear nail polish. Controls for the specificity of the secondary

antibodies (by omitting the primary antibodies) yielded no specific immunofluorescence staining in any of the cell cultures.

The following protocol was used for single immunostaining of cell surface antigens expressed by OECs. The cells were first incubated for 5 min at room temperature in DMEM medium containing 5% horse serum (HS) and 15 mM 4-(2-hydroxyethyl)-1-piperazineethanesulfonic acid (HEPES). The cells were then incubated for one hour in rabbit anti mouse p75 NGFR (1:100, Chemicon International Inc., Temecula, CA 92590, USA) diluted in DMEM/5% HS/15 mM HEPES. The control sections were incubated in diluent only. Dulbecco's phosphate buffered saline (DPBS) was used as a rinse solution after incubation in the primary antibody; the coverslips were rinsed four times (5 min each at 4°C) in DPBS, which contained 2.68 mM potassium chloride, 1.47 mM potassium dihydrophosphate, 0.14 M sodium chloride, 8.1 mM di-sodium hydrophosphate, 0.49 mM magnesium chloride and 1.19 mM calcium chloride dissolved in distilled water. The cells were then fixed by immersion in Zamboni's fixative (0.2% picric acid/4% PF in 0.2 M phosphate buffer, pH 7.4) for 15 min at room temperature. Then the coverslips were washed three times in DPBS (30 sec each at room temperature), followed by a fourth wash in DPBS for 1 min. A swine anti-rabbit FITC-conjugated secondary antiserum (1:100, Dimension Labs, Dako A/S, Denmark) was applied to the coverslips for 30 min at room temperature. There then followed four rinses in DPBS over a 20 min time period (5 min each at 4 °C). After the final rinse, the cells were incubated in a Hoechst solution (2 μg/ml) for 15 min at room temperature to stain the cell nuclei. The cells were rinsed 4 additional times in DPBS (5 min each), after which the coverslips were mounted onto slides using Citifluor mounting medium (Marivac Ltd, Halifax, NS, Canada).

The following protocol was used for double immunostaining of an intracellular protein (nestin) and a cell surface protein (p75) expressed by OECs. The cells were first incubated for 5 min at room temperature in DMEM medium containing 5% HS and 15 mM HEPES. The cells were then incubated for one hour in rabbit anti mouse p75 NGFR (1:100, Chemicon International Inc., Temecula, CA 92590, USA) diluted in DMEM/5%/HS/15 mM HEPES. The control sections were incubated in diluent only. DPBS was used as a rinse solution after incubation in the primary antibody; the

coverslips were rinsed four times (5 min each at 4°C) in DPBS, as described in the previous paragraph. The cells were then fixed by immersion in Zamboni's fixative (see above) for 15 min at room temperature. Then the coverslips were washed three times in DPBS (30 sec each at room temperature), followed by a fourth wash in DPBS for 1 min. The cells were then incubated for 15 min in a solution of 0.2% TX-100, 5% HS and 0.1% BSA in 0.03M PBS (pH 7.4). The next step was to permeabilize the cell membrane by incubation of the cells in a solution of 0.2% TX-100, 5% HS and 0.1% bovine serum albumen (BSA) in 0.03 M PBS (Ph 7.4). A 30 min incubation in the mouse anti-nestin (1:100, Clone Rat 401, Developmental Studies Hybridoma Bank, Department of Biological Sciences, The University of Iowa, Iowa City, IA, USA) monoclonal antibody followed immediately after the TX-100 incubation. DPBS was used as a rinse solution after incubation in this primary antibody; the coverslips were rinsed four times (5 min each at 4°C) in DPBS. The cells were then incubated in a cocktail mixture of secondary antibodies for 30 min at room temperature; the secondary antibodies used were swine anti-rabbit IgG FITC (1:100, Dimension Labs, Dako A/S, Denmark) and goat anti-mouse IgG Texas Red (1:100, Bio/Can Scientific, Mississauga, ON, Canada). There then followed four rinses in DPBS over a 20 min time period (5 min each at 4 °C). After the final rinse, the cells were incubated in a Hoechst solution (2 μg/ml) for 15 min at room temperature to stain the cell nuclei. The cells were rinsed 4 additional times in DPBS (5 min each), after which the coverslips were mounted onto slides using Citifluor mounting medium (Marivac Ltd, Halifax, NS, Canada).

The following protocol was used for immunostaining of SMA, which is an intracellular protein that is expressed by OECs. The Zamboni-fixed cells were first incubated for 10 min at room temperature in a solution of proteinase K (0.05 mg/ml) in 0.1M TBS. The cells were then incubated for 1 hour in a blocking solution of 2% SMP diluted in 0.1M TBS plus 0.25% TX-100 for 1 hour at room temperature. After a rinse (10 min) with 0.1M TBS, the cells were incubated with mouse anti-SMA (1:1000) monoclonal antibody for 48 hours at room temperature. The cultures were then rinsed in 0.1M TBS (30 min) and incubated in an FITC-conjugated donkey anti mouse IgG (1:50; Medicorp, Montreal, QC, Canada) for 2 hours at room temperature in the dark. After the final rinse (10 min), the cells were incubated in a Hoechst solution (2 μg/ml) for 15 min

at room temperature to stain the cell nuclei. The cells were rinsed 1 additional time in 0.1M TBS (5 min), after which the coverslips were mounted onto slides using Citifluor mounting medium (Marivac Ltd, Halifax, NS, Canada)

The following protocol was used for immunostaining of calponin, which is an intracellular protein that is expressed by OECs. The Zamboni-fixed cells were first incubated for 10 min at room temperature in a solution of proteinase K (0.05 mg/ml) in 0.1M PBS. The cells were then incubated for 15 min in a blocking solution of 0.2% TX 100/5% HS/0.1% BSA at room temperature. After a rinse (10 min) with 0.03M PBS the cells were incubated with mouse anti-calponin (1:100 diluted in 0.2% TX 100/5% HS) monoclonal antibody for 1 hour at room temperature. The cells were then rinsed in 0.03M PBS (10 min) and then incubated in an FITC-conjugated goat anti-mouse IgG (1:100, Dimension Labs, Dako A/S, Denmark) for 30 min at room temperature in the dark. After a final rinse (10 min) in 0.03M PBS, the cells were incubated in a Hoechst solution (2 μg/ml) for 15 min at room temperature to stain the cell nuclei. The cells were rinsed 1 additional time in 0.03M PBS (5 min), after which the coverslips were mounted onto slides using Citifluor mounting medium (Marivac Ltd, Halifax, NS, Canada) (Fig 3.2).

3.4.2 Immunohistochemical Staining of Tissue Sections

The OX42 antibody recognizes complement receptor type 3 (CR3) on the surface of resting and phagocytic microglia (Kaur & Ling, 1992; Perry et al., 1993; Mander and Morris, 1995; Streit et al., 2004). In the normal CNS, resident (ramified) microglia constitutively express the CR3 receptor (Perry et al., 1993; Mander and Morris, 1995; Streit et al., 2004). In contrast to that of OX42 expression, many studies have shown that the MHC class I antigen, which is recognized by the OX18 antibody, is absent or present only at low levels in parenchymal microglia of normal spinal cord tissue (Ling et al., 1991, 1992; Mander and Morris, 1995; Streit et al., 2004). OX35 recognizes an antigenic epitope on the rat CD4 antigen (Brostoff and White, 1986; Wang et al., 1996; Wu et al., 1997), which is expressed by reactive microglia. The ED1 antibody recognizes a lysosomal membrane-associated antigenic epitope that is expressed by macrophages (Flariz et al., 1993; Graeber et al., 1990). In the brains of young animals, macrophages in the leptomeninges and choroid plexus, as well as perivascular macrophages, are ED1+ve;

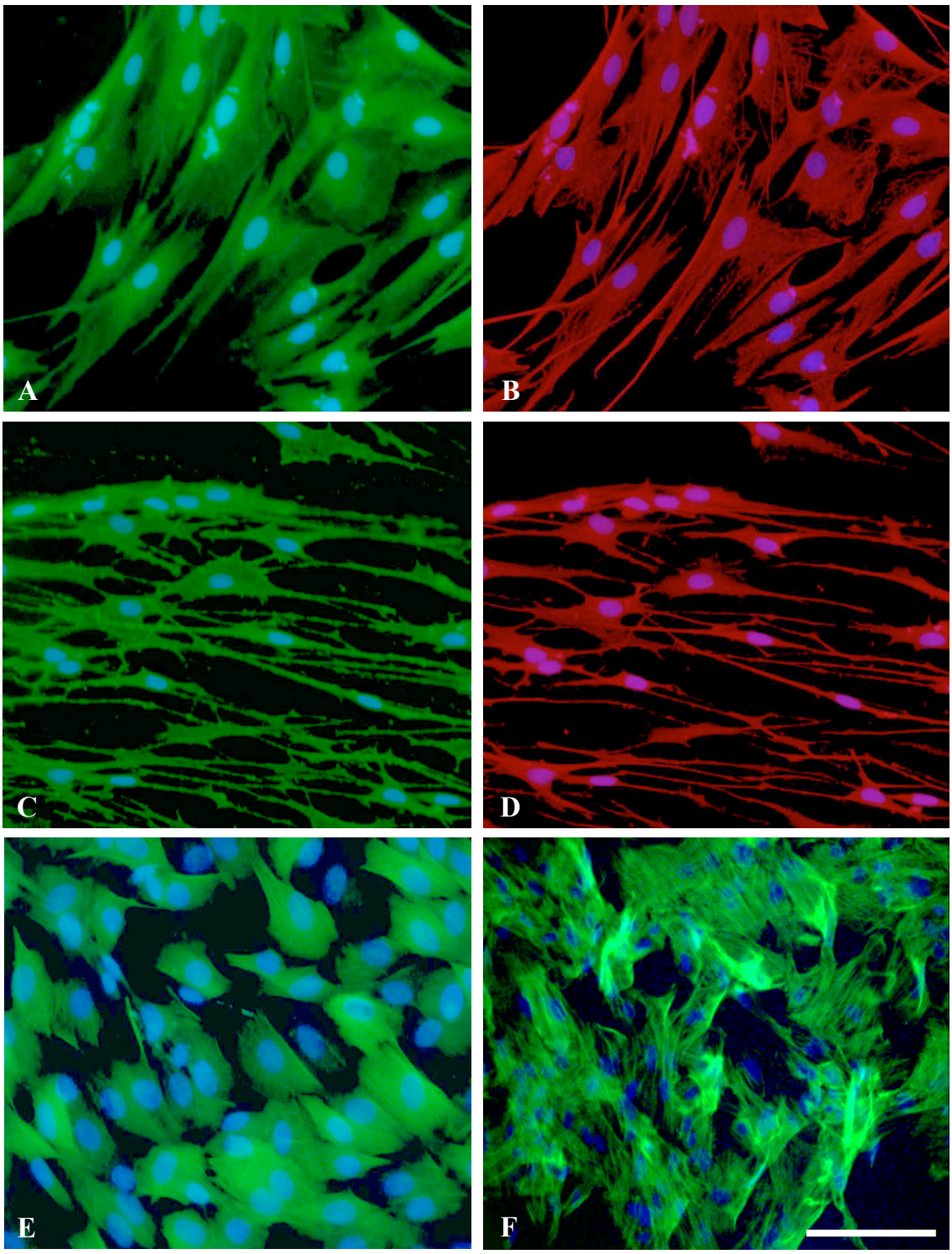

FIGURE 3.2: Phenotype of OECs *in vitro.*

Double immunostaining of OECs *in vitro* shows their co-expression of S-100 (**A**) and nestin (**B**), and of p75 NGFR (**C**) and nestin (**D**). The OECs are also calponin +ve (E) and SMA +ve (F). Hoecsht staining of the nucleus (blue) shown in (A-F). Scale bar in '**F**' = 50 μm.

an occasional cell within the young animal brain parenchyma also expresses the ED1 antogenic epitope. Based on small and heterochromatic nuclei, Perry et al. (1993) concluded the ED1+ve cells within the brain parenchyma were microglia. Microglia in adult rats greatly downregulate their expression of the ED1 antigenic epitope, in contrast to the developing brain where ED1+ve cells are abundant (Sminia et al., 1987). A striking feature of the aged rat brain is the large number of ED1+ve cells throughout the parenchyma, and although the intensity of the immunostaining varies from cell to cell it is nevertheless readily detectable (Sminia et al., 1987). Since the ED1 antigenic epitope is a cytoplasmic marker and primarily confined to the cell body, immunostaining with the ED1 monoclonal antibody does not stain the cell processes. However, the density, distribution, and small heterochromatic nuclei of ED1+ve cells strongly suggest they are microglia (Perry et al., 1993).

GFAP is expressed in mature and reactive astrocytes in the CNS of adult mammals (Martinez et al., 1998; Pekny and Pekna, 2004). Following brain or spinal cord injury, astrocytes become reactive, change their shape to become more fibrous in morphology, and also up-regulate their expression of GFAP (Martinez et al., 1998; Raivich et al., 1999). Vim is found in mesoderm-derived cells, including endothelial cells and pericytes (Takehana et al., 1992), as well as in neuroectodermal precursors of neurons and glial cells (Pixley and Vellis 1984; Schnitzer et al., 1981). In normal spinal cord tissue, Vim+ve cells are limited to just the ependymal cells of the central canal, the leptomeninges, and an occasional astrocyte (Farooque et al., 1995). Nestin is an intermediate filament protein expressed in dividing cells during the early stages of development in the CNS (Lendahl et al., 1990). Upon differentiation, nestin expression is downregulated and the cells express instead tissue-specific intermediate filament proteins (Lendahl et al., 1990; Moky and Nemeck, 1998). Interestingly, nestin expression is reinduced in the adult nervous system during pathological situations, such as the formation of the glial scar after CNS injury, with reactive astrocytes being the cells that re-express this protein (Ernst and Christie, 2006).

For each rat, tissue sections were chosen from wells corresponding to rostral, middle and caudal parts of T11. The chosen tissue sections were briefly rinsed in 0.03 M PBS and mounted on subbed coverslips; the subbing solution contained 1% gelatin and

0.5% chrome alum dissolved in distilled water. The tissue sections were left to air dry and to adhere to the coverslips for approximately 2-3 hours prior to initiating the immunostaining. The coverslips were then first washed three times in 0.03 M PBS (30 sec each at room temperature), followed by a fourth PBS rinse for 30 min at 4°C. An incubation for 30 min in a solution of 3% SMP and 0.1% TX-100 in 0.03 M PBS (pH 7.4) was then done in order to permeabilize cell membranes and block non-specific binding sites.

Each coverslip was covered with one primary antibody (approximately 500 µl per coverslip), with incubation in each antibody being done overnight (16-18 hours) at 4°C. The primary antibodies used on the tissue sections were for assessing the presence and location of microglial and astrocytic reactivity. These primary antibodies included: mouse anti-rat MHC class I (1:9600, Clone OX-18, Secotec, Kidlington Oxford, England), mouse anti-CD11b (1:3200, Clone MRC OX-42, Serotec, Kidlington Oxford, England), mouse anti-CD4 (1:3000, Clone OX-35, Serotec, Kidlington Oxford, England), mouse anti-rat CD68 (ED1) (1:2000, Serotec, Kidlington Oxford, England), mouse anti-GFAP (1:500, Clone G-A.5, Sigma, St. Louis, MO 63178, USA), mouse anti-vimentin (1:1000, Clone V9, Sigma, St. Louis, MO 63178, USA) and mouse anti-nestin (1:2000, Clone Rat 401, Developmental Studies Hybridoma Bank, Department of Biological Sciences, University of Iowa, Iowa City, IA, USA). All primary antibodies were diluted in 0.03 M PBS. The control sections were incubated in diluent only.

The next morning the tissue sections were rinsed twice in 0.03 M PBS and then were incubated in blocking solution (3% SMP/0.1% TX-100 in 0.03 M PBS) for 30 min. Horse anti-mouse biotinylated IgG was used as the secondary antiserum (1:150, Vector Laboratories, Burlingame, Ca 94010 USA) with the sections being incubated in the secondary antibody for 30 min at room temperature. The coverslips were then immersed in a 1% solution of hydrogen peroxide (H_2O_2) in 30% methanol for 15 min to quench endogenous peroxidase activity, followed by two rinses in 0.03 M PBS (pH 7.4), and a 30 min incubation in a 3% solution of SMP in 0.03 M PBS (pH 7.4). The Avidin DH (reagent A)/ biotinylated horseradish peroxidase (HRP) H (reagent B) cocktail was made by adding 8 µl of each reagent per ml of 0.03 M PBS (pH 7.4); this solution is referred to

as the Vectastain AB reagent (Vector Laboratories, Inc., Burlingame, CA 94010 USA) and was made at least 30 min prior to being used. Then the sections were covered with this Vectastain AB reagent for one hour at room temperature. The sections were then washed two times in 0.03 M PBS (pH 7.4) followed by a rinse in 0.175 M sodium acetate (pH 6.8) for 10 min. A solution of 0.0185 M diaminobenzidine tetrahydrochloride (DAB) and 0.1586 M nickel sulfate ($NiSO_4$) in 0.175 M sodium acetate (pH 6.8) was made one hour prior to use and kept in the dark until needed. Immediately prior to use, 63.75 µl of a 30% solution of H_2O_2 was added to each 75 ml volume of 0.0185 M DAB/0.1586 M $NiSo_4$ solution, and the sections were then immersed in this DAB/$NiSO_4$/H_2O_2 solution for 5 min in the dark. The sections were then rinsed once (for 10 min) in 0.175 sodium acetate (pH 6.8), rinsed in 0.03 M PBS (pH 7.4) for 10 min, and dehydrated in an ascending series of ethanols (70%, 95%, 100%). The sections were cleared in xylene for 2 min and then mounted onto slides using Shandon xylene substitute mountant (Shandon, Pittsburgh, PA15275, USA).

3.5 Data Collection and Statistical Analysis

3.5.1 Counting DiI-Labeled Cells

Approximately 120 tissue sections (40 µm thick) were obtained when cutting the T11 spinal cord segment from rostral to caudal. The tissue sections were pooled in groups of 10 and stored in cryoprotectant solution in approximately 12 wells of a 96 well plate (see Section 3.3.3). For cell counting, one section was randomly chosen from each well, stained with Hoechst dye (2 µg/ml), mounted onto a microscope slide, and coverslipped using Citifluor anti-quenching mounting medium (Marivac Ltd, Halifax, NS, Canada). Once mounted, each tissue section was assigned an alphanumeric code by a lab technician so that all cell counts could be done blindly.

For the purpose of the experiments reported in this thesis, tissue sections collected into the first four wells were considered to comprise the rostral one-third of T11; sections in the second four wells comprised the middle one-third, and the final four wells comprised the caudal one-third of T11. Each tissue section was examined to determine whether it contained any DiI+ve cells, to identify the specific location in which the cells

were found, and to count the total number of DiI+ve cells either within specific fiber tracts (see Section 4.2.6) or within the entire dorsal funiculus (see Section 5.2.6). For statistical analysis, the mean cell count for each group of 4 sections was computed. Only DiI+ve profiles that were associated with a nucleus were counted.

3.5.2 Reliability of Cell Counts

Seven 40 μm tissue sections from the T11 spinal cord segment of one rat in each of Groups 1 and 2 were randomly picked, stained with Hoechst dye (2 μg/ml), mounted onto a microscope slide, and coverslipped using Citifluor (Marivac Ltd, Halifax, NS, Canada) anti-quenching mounting medium. Once mounted, each tissue section was assigned an alphanumeric code by a lab technician so that all cell counts could be done blindly. The number of DiI+ve cells was counted in four separate quadrants of the white matter on the dorsal surface of the T11 spinal cord segment; these quadrants included the right corticospinal tract (dCST), left dCST, right dorsal ascending tract (DAT) and left DAT. The cell counts were done twice on each tissue section, with the time between cell counts being 10 days apart. The purpose of this study was to determine the repeatability of the cell counts. The data were analyzed for statistical significance using a t-test.

3.5.3 Statistical Analysis of Data

The initial data analysis showed there were differences among the data collected from the rostral, middle and caudal portions of each spinal cord segment. Therefore, for the statistical analysis of the data they were analyzed separately, rather than pooling the data to obtain average cell counts for the entire T11 segment. The T11 cell counts collected for Groups 1-10 were statistically compared using a two-factor analysis of variance (ANOVA) (Prism software program), with the data for the rostral, middle and caudal thirds of the right and left dorsal funiculi of this spinal cord segment being analyzed separately for statistical significance (Prism software program). The independent variables for the two sets of experiments are listed in Sections 4.2.6 and 5.2.6. The significance level was set at $p < 0.05$. Multiple post hoc comparisons were performed with Bonferonni's multiple comparison post-test (Prism software program) with the significance level being set at $p < 0.05$.

CHAPTER 4.0 OEC Migration in Response to Wallerian Degeneration-Induced Glial Reactivity

4.1 Introduction

4.1.1 Wallerian Degeneration

Waller in 1850 described axon degeneration in transected frog peripheral nerves distal to the site of injury, a process that was later referred to as Wallerian degeneration (WD). The usual cause of axonal degeneration has diverse underlying etiologies, including traumatic, metabolic and inflammatory causes (Raff et al., 2002). Degeneration of the distal segments of axons in the PNS is generally followed by their regeneration, whereas in the CNS axon regeneration is usually not successful (Franson and Ronnevi, 1984).

Nevertheless, there are some similarities in the molecular and cellular pattern of WD in the PNS and CNS including the breakdown of the lesioned axons and the degradation of the myelin sheaths (Franson and Ronnevi, 1984; George and Griffin, 1994a). An early step of WD is granular disintegration of the cytoskeleton (GDC), which is an event found in both the CNS and PNS. During GDC, the neurofilaments and microtubules of the cytoskeleton are rapidly degraded to granular and amorphous debris (Griffin et al., 1992; George and Griffin, 1994b)**.** GDC occurs in both central and peripheral nerve fiber tracts between 18 and 72 h after the lesion and progresses away from the site of initial injury (George and Griffin, 1994b)**.** GDC occurs mostly as a consequence of the activation of proteases such as calpains through an increase in the intra-axonal concentration of Ca^{2+} (Coleman and Perry, 2002; George et al., 1995). In the CNS, oligodendrocyte apoptosis is a noticeable event following WD; however, Schwann cells survive in the distal segments of lesioned peripheral nerves and form new myelin sheaths around the regenerating axons (Stoll and Muller, 1999).

A rapid invasion of macrophages from the peripheral blood has been reported following PNS axonal injury (Shamash et al., 2002). Endogenous endoneurial macrophages, and to a lesser extent Schwann cells, are responsible for the rapid phagocytosis of the injured axons and their myelin sheaths (Bruck, 1997). In contrast to peripheral nerves, invasion of degenerating CNS nerve fiber tracts by macrophages

occurs in much lower numbers (Aldskogius and Kozlova, 1998; Stoll and Jander, 1999). Instead, endogenous microglia are activated following CNS injury, including morphological alteration and the upregulation or *de novo* expression of several microglial activation markers; microglia are responsible for the phagocytosis of the axonal and myelin debris (Aldskogius and Kozlova, 1998; Stoll and Jander, 1999). The time course of the removal of the degenerated tissue is greatly delayed in the CNS as compared to the PNS (Griffin et al., 1992; George and Griffin, 1994). In the rodent, axonal degeneration is completed 3 days after nerve section in the PNS and CNS (George and Griffin, 1994). Despite this rapid axonal degeneration in both the CNS and PNS, the axonal debris is cleared within 14 days in the PNS (George and Griffin, 1994), but axonal debris can still be detected in the CNS 90 days post-axotomy (Bignami et al., 1981). Myelin degradation and removal are complete within 25 days in the rat sciatic nerve (Stoll et al., 1989). In the CNS, degraded myelin becomes apparent by 4 days after injury but myelin proteins can still be detected in the degenerating rat optic nerve up to 90 days after axotomy (Bignami and Eng, 1973).

It appears that macrophages are more important in the later stages of PNS myelin removal (Perry et al., 1995). In the CNS there is a significant rise in mononuclear phagocytes 2-3 days later than in the PNS, which is primarily due to the proliferation of microglia rather than to macrophage recruitment (Lawson et al., 1994). The phagocytic activity of microglia could possibly be incompetent or at least less competent than that of macrophages, although phagocytic and endocytic related molecules are promptly expressed by microglia activated during WD (Lawson et al., 1994). A small percentage of blood borne macrophages are present at the site of transection in the CNS where the BBB is disrupted. However, along the length of the degenerating distal part of the fiber tract the BBB remains intact (George and Griffin, 1994); in the PNS the blood-nerve barrier breaks down within 48 h along the whole length of the degenerating nerve (Bouldin et al., 1990). The inefficient breakdown of myelin and the slow removal of axonal and myelin debris in the CNS has been attributed to an inadequate response by microglia (Lawson et al., 1994), or to differences between oligodendrocytes and Schwann cells in terms of their capacity for differentiation and proliferation (Stoll et al., 1989; Perry et al., 1995). Shortly after axotomy, Schwann cells in the degenerating sciatic nerve

dedifferentiate, proliferate, and secrete molecules such as NGF and BDNF, both of which play important roles in the repair process (Martinni et al., 1988; Meyer et al., 1992). Schwann cells also actively initiate myelin degradation or phagocytosis during WD in the PNS (Stoll et al., 1989).

Proteolytic enzymes have been implicated in WD at several stages, including degradation of the axon itself (Schlaepfer, 1974) and myelin degradation (Hallpike and Adams, 1969). Proteolytic activity is elevated as early as 12 h after transection of a rodent sciatic nerve and continues to rise during the first week (Hallpike and Adams, 1969). Axonal neurofilament proteins in transected nerves undergo calcium-activated proteolysis (Schaepfer, 1974). Increased proteolytic activity could also facilitate macrophage invasion and contribute to the disruption of the blood nerve barrier (Hughes et al., 1998). Although proteolytic activity is elevated during WD in the PNS, the identities of the enzymes and their physiological roles have only been partially determined. The involvement of calpains in axonal degeneration was confirmed using cell permeable specific inhibitors, which preserved axons for up to 4 days following nerve transection in a DRG explant (George et al., 1995).

Rho GTPases are a family of highly related proteins best known for their effect on the actin cytoskeleton. It was reported (Yamagishi et al., 2005) that Rho, a small GTPase, is involved in WD *in vitro* and *in vivo.* The breakdown of neurofilaments depends on an influx of Ca^{2+} and the activation of the Ca^{2+}-dependent protease, calpain (Messier and Stewart., 1997). Inhibition of the ubiquitin proteosome system delays axon degeneration both *in vitro* and *in vivo* (Zhai et al., 2003). However, the molecular target of ubiquitin proteosome system-mediated proteolysis is unknown. It is noted that Rho-kinase inhibitor partially prevents WD. Rho/Rho-kinase is associated with the inability of CNS neurons to regenerate (Tanaka et al., 2004). Inactivation of Rho-kinase by Y-27632 significantly promotes the regeneration of corticospinal tract (CST) axons after SCI (Tanaka et al., 2004). Thus, Rho/Rho-kinase may play an important role in the pathogenesis of SCI, perhaps by delaying the clearance of myelin debris.

4.1.2 The Corticospinal Tract

In rats, the CST is the longest descending axonal pathway in the CNS and is mainly involved in skilled motor functions, such as grasping, handling and eating of food (Whishaw et al., 1998); it is less involved in simple locomotion (Matz et al., 1998; Muir and Whishaw, 1999). The neurons that give rise to the CST are located in layer V of the cerebral cortex. Most CST neurons are located in the primary motor cortex and in the forelimb and hindlimb parts of the primary somatosensory cortex. Neurons in the forelimb area of motor and somatosensory cortex project to the cervical enlargement, while those in the hindlimb area project to the lumbar enlargement (Li et al., 1990). CST neurons are not restricted to primary motor and somatosensory cortex, but are also found in the supplementary motor area and prefrontal cortex (Li et al., 1990; Miller, 1987), as well as in the posterior parietal cortex, visual association cortex, and anterior cingulate cortex (Miller, 1987).

Most CST axons (90%-95%) decussate in the caudal medulla in the pyramidal decussation (Schreyer and Jones, 1982; reviewed in Joosten and Bar, 1999) and in the rat all but a small number of these decussated axons run in the base of the dorsal columns (Armand, 1982). A small population of decussated axons descends within the lateral funiculus. As found in humans, rats also have a ventral uncrossed CST that descends within the ventral funiculus (Brosamle and Schwab, 1997). In the rat, as the CST axons travel through the brainstem they send collaterals to neurons of the red nucleus in the midbrain and to the trigeminal nuclei (Killackey et al., 1989). The CST is the last descending tract to enter the rat spinal cord white matter during development, doing so approximately at postnatal day 1 (Schreyer and Jones, 1982). Myelination of CST axons begins around day 10 postnatal in the rat spinal cord (Matthews and Duncan, 1971; Schreyer and Jones, 1982; Schwab and Schnell, 1989), with the number of myelinated axons in the CST increasing steadily during the third and fourth postnatal weeks. By four weeks postnatally, the majority of CST axons have also established their mature functional contacts with interneurons, with a much smaller number of synaptic contacts being made directly with motoneurons in the rat spinal gray matter (Karimi-Abdolrezaee et al., 2002).

Thereafter, during the second and third postnatal months, the total number of myelinated CST axons in rats increases more slowly than it did during the first month (Gorgels, 1990) and myelination may continue even beyond the third postnatal month (Leenen et al., 1989). Several studies have reported large numbers of thin unmyelinated CST fibers, which constitute approximately 45% of the total number of fibers located at the mid-thoracic level (Gorgels, 1990; Schreyer and Jones, 1988) within the CST in mature rats. It has been argued that, in monkeys at least, many of the cross-sectional profiles in the lateral CST that were presumed to be unmyelinated axons, in longitudinal sections were seen instead to be astroglial processes (Ralston et al., 1987). While this may be true in monkeys, a study at the electron microscopic level in six-month-old rats that had received injections of the anterograde tracer HRP into the entire sensorimotor and frontal cortex of the left hemisphere demonstrated that both unmyelinated and myelinated axons within the CST were labeled (Joosten and Gribnau, 1988). Thus the CST in adult rats does indeed contain a number of unmyelinated axons. During myelination of the CST, the larger diameter axons are the first to become myelinated (Gorgels et al., 1989; Gorgels 1990) and it appears that some axons may increase in diameter just prior to myelination (Gorgels, 1990). Later, while myelination of the large corticospinal axons continues, some smaller diameter axons become myelinated as well. The diameters of the HRP-labeled unmyelinated CST axons remained fairly constant at about 0.2μm, whereas myelinated CST axons had variable diameters between 0.5-3 μm (Joosten and Gribnau, 1988). Furthermore, as in the PNS and in other CNS pathways, there is a fairly strong correlation between the diameter of corticospinal axons and the thickness of their myelin sheath (Gorgels, 1990).

4.1.3 Microglial response to Wallerian degeneration

Microglia are important players in WD, with several of the steps, such as axonal breakdown and clearance of myelin debris, requiring a reactive microglial response (Ludwin and Bisby, 1992). Microglial numbers rise in response to WD 2–3 days later than does the number of macrophages in response to PNS injury (Lawson et al., 1994). After dorsal root rhizotomy, it takes almost two weeks for microglia inside the dorsal funiculus to express immunoreactivity for ED-1, which recognizes one of the antigenic

epitopes expressed by reactive microglia (see Section 1.4.2). Phagocytic microglia express MHC classes I and II during WD (Stoll et al., 1989). Nonetheless, microglia clear myelin extremely slowly (Aldskogius et al. 1974). The contribution of factors that regulate clearance of cellular debris in the CNS is incompletely understood. The very slow microglial clearance of axonal and myelin debris from degenerating CNS fiber tracts and the limited peripheral macrophage influx into the CNS during WD collectively contribute to the delayed clearance of debris in CNS fiber tracts undergoing WD.

One key difference between the response of the PNS and the CNS to injury is that the BBB is disrupted at the site of injury but not along the entire length of the distal nerve tract (George and Griffin, 1994), unlike what happens with the blood nerve barrier in the PNS (George and Griffin, 1994). The lack of BBB breakdown post injury may limit the infiltration of hematogenous macrophages into degenerating CNS tracks (George and Griffin, 1994), thus leaving the job of cleaning up the axonal and myelin debris primarily to microglia. Another difference between PNS and CNS injury is a slower rate of clearance of the debris by the reactive microglia; for example, the rate of myelin phagocytosis in optic nerve explants is far slower than in sciatic nerve explants due to decreased microglial activity measured using the fluorescence-activated cell sorter (FACS) technique (Kuhlmann et al., 2002).

Transmembrane molecules expressed by reactive microglia/macrophages have important roles in regulating the phagocytic response by these cells. Recognition of specific molecules on dead cells and on cellular debris, in particular phosphatidylserine, triggers phagocytosis by macrophages (Fadok and Henson, 2003). The expression of certain cell surface molecules including CD47 and CD200 inhibits phagocytosis of live cells by microglia/macrophages (Hoek et al., 2000). In CD200 knockout mice, microglia show faster activation. CD200 deficiency in the CNS was shown to affect microglial responsiveness to nerve damage, as demonstrated using the facial nerve transection model to induce localized microglial activation (Graeber et al., 1988). The course of microglial activation in the facial motor nucleus of wild-type mice is well documented (Graeber et al., 1988) and can first be detected 4 days after facial transection; the peak of activation is at day 7 after transection (Hoek et al., 2000). In $CD200^{-/-}$ mice the microglial response was accelerated dramatically, with a detectable microglial reaction seen after 2

days and maximal activation by 4 days after transection, as detected by quantifying the number of CD11b-expressing cells (Hoek et al., 2000). In healthy wild-type mice, microglia are quiescent cells expressing molecules such as MHC class I and II, CD11b, and CD45 at low or negligible levels and show an ordered, ramified appearance (Kreutzberg, 1996). In contrast, the microglia of $CD200^{-/-}$ mice spontaneously exhibited many features of activation, including less ramified, shorter cytoplasmic processes and increased CD11b and CD45 expression. Microglia in $CD200^{-/-}$ animals formed aggregates and strongly expressed CD11b and CD45, especially in the spinal cord (Hoek et al., 2000).

The abilities of microglia and macrophages to phagocytose debris are highly regulated by cellular and humoral immune responses, and the role of the immune system in regulating myelin phagocytosis is only just beginning to be explored. Following spinal transection, microglia/macrophages were identified immunohistochemically using antibodies to complement type 3 receptor, CD11b (OX-42 monoclonal antibody), the macrophage lysosomal antigen CD68 (ED1 monoclonal antibody), major histocompatibility complex class II (MHC II), and CD163 (ED2 monoclonal antibody). One week after spinal cord transection at T8 in adult rats, the density of OX-42+ve microglia/macrophages had nearly doubled (McKey et al., 2007). In the white matter, microglia/macrophages became enlarged, often having retracted cytoplasmic processes and exhibiting an amoeboid morphology. After 8 weeks, ED1+ve microglia/macrophages were prominent in fiber tracts undergoing WD, including within the dorsolateral, lateral and ventral funiculi (McKay et al., 2007). Notably, microglia in these tracts transformed into activated microglia/macrophages and began to phagocytose degenerating myelin. Prolonged activation of ramified microglia in the grey matter may reflect ongoing degenerative processes that are both retrograde (Streit et al., 1999) and transsynaptic (Banati, 2002).

Differences in the pattern and degree of inflammation were present between the segments controlling the hindlimbs (L4/5) and the pelvic organs (L6/S1) after mid thoracic spinal transaction (McKey et al., 2007). The focus on a region of the cord 9 to 12 spinal segments (4-5 cm) beyond the lesion has revealed inflammatory responses not only in the vicinity of the neuronal cell bodies of the axotomized axons but also a markedly

increased density of OX42+ve microglia throughout the lumbosacral spinal cord after spinal transection at T8 in adult female Wistar rats (McKey et al., 2007). Furthermore, the duration of microglial activation in the spinal cord was prolonged relative to that of other axotomized CNS pathways such as in the thalamocortical and corticothalamic pathways after a cortical aspiration lesion in male Wistar rats. The latter rats were killed 3, 7, 14 and 28 days after sensorimotor cortex aspiration. Histological analysis of the thalamus showed the presence of OX42+ve, OX18+ve and OX6+ve reactive microglia in the ventrolateral, posterior, and ventrobasal thalamic nuclei, along with ongoing retrograde and anterograde neuronal degeneration (Sorensen et al., 1996). Microglial proliferation has been demonstrated at other sites far from a lesion; for example, in the axotomized facial motor nucleus and in the spinal cord after cerebral infarction (Wu and Ling, 1998).

There was no evidence of vascular infiltration after perforant path axonal lesioning in adult female SJL/N and C57/BL6 mice. Using bone marrow chimeras, only a few bone marrow-derived microglia/macrophages appeared in the areas with anterograde axonal degeneration in the first few days after a lesion (Ladeby et al., 2005). The immediate triggers for the microglial response distal to a spinal cord transection are likely to be the degeneration of synaptic terminals in the spinal grey matter (Jensen et al., 1994) and the onset of WD in the descending fiber tracts (Koshinaga and Whittrmore, 1995). Furthermore, microglia accumulate rapidly in response to axotomy of nearby neurons (Kobbert and Thanos, 2000), likely in response to chemokine signals released from the damaged neurons (Flugel et al., 2001).

Activated microglia/macrophages appeared in the outer white matter of L4/5 and extended through the depth of the ventral columns in L6/S1 during WD. The likelihood is low that the additional microglia were hematogenous because WD occurs a distance away from a lesion and there is no break down in the BBB (Streit et al., 1999). In contrast, deep in the dorsal and ventral columns (i.e. in the 2 components of the CST where myelination is limited (Brosamle and Schwab, 1997), activated and ramified microglia showed both OX42 and MHC II expression.

In CNS regions undergoing WD the microglia are usually described as possessing a "bushy" morphology, with greatly enlarged somata and short thickened processes

(Sorensen et al., 1996). However, reactive microglia at the level of the spinal cord do not assume this morphology after spinal cord transection. Within grey matter in brain regions containing both anterograde and retrograde degeneration, microglia/macrophages cluster around dying neurons (Sorensen et al., 1996). Rapid expression of ED1+ve antigenic epitopes by reactive microglia in the spinal cord is prominent during transganglionic degeneration early after peripheral nerve injury (Ramer et al., 2001), tissue inflammation (Guo et al., 2005) and experimental neuritis (Beiter et al., 2005). Ramified microglia containing ED1+ve antigenic epitopes in their lysosomes also appeared throughout the brain during the relapse phase of EAE (Bauer et al., 1994). MHC II is also expressed by activated microglia/macrophages at the later stages of WD (Graeber et al., 1998). MHC II+ve ramified microglia were localized to a broad band through the medial cord, extending from the CST to the ventral columns in L4/5. These sites in lamina VII, VIII, and X in L4/5 give rise to the propriospinal and supraspinal projections (Dado and Giesler, 1990). MHC II+ve microglia were rare in the grey matter one week after spinal transection, consistent with terminal degeneration being largely complete by this time (Weaver et al., 1997).

Taken together, hematogenous macrophage entry into the CNS post injury is limited to the site of injury and is much slower than occurs at the site of injury in the PNS (Popovich and Hicky, 2001; Schnell et al., 1999). Currently there is little evidence for entry of large numbers of peripheral macrophages during WD in the CNS. This difference may be an important contributor to why myelin debris is robustly cleared in the PNS but not in the CNS.

4.1.4 Astrocytic Response to Wallerian degeneration

Although the relative contributions of hypertrophy and hyperplasia to the astrocytic response to WD is not clear, most studies report only a slight increase in astrocyte numbers in the degenerating fiber tracts (Hajos et al., 1993; Privat et al., 1981). In contrast, astrocyte hypertrophy is a more prominent event as a result of WD (Hajos et al., 1993; Murray et al., 1990). The astrocyte reaction to WD in the rat optic nerve entails a reduction in the number of cytoplasmic processes and a thickening of the remaining processes (Hajos et al., 1993). Astrocytes in the fiber tract undergoing WD express GFAP

and vimentin (Baldwin and Scheff, 1997; Butt and Kirvell, 1996). It has been suggested vimentin may label astrocytes only when they are reactive (Schiffer et al., 1986; Takamiya et al., 1988). During WD, reactive astrocytes express increased levels of clusterin (Liu et al., 1998). In addition, reactive astrocytes increase their expression of endothelin receptors along the pathway undergoing WD (Rogers et al., 1997). In human neurological disorders in which WD occurs as a result of CNS neurodegeneration or neural injury to the CNS, astrocytes display an isomorphic reaction in which they hypertrophy without proliferating. Accordingly, there is no formation of a dense, permanent astroglial scar (Reier et al., 1983; Fernaud-Espinosa et al., 1993; Ridet et al., 1997).

In contrast to the experimental data obtained from animals, some unexpected findings have been described in postmortem human brain tissue. A detailed investigation of fiber tracts undergoing WD in penetrating spinal cord injuries in humans has revealed a slow astrogliosis taking place around the lesion site (Buss et al., 2004). Astrocytes close to the lesion demonstrated an anisomorphic response, whereas astrocytes located further away from the primary lesion, particularly in the degenerating nerve fiber tracts, demonstrated an isomorphic response without the formation of a permanent glial scar or distortion of the local cytoarchitecture (Mansour et al., 1990; Fernaud-Espinosa et al., 1993; Ridet et al., 1997). There is also a centrifugal pattern of axonal degeneration away from the site of injury, a gradual loss of the major component of compact myelin (i.e. MBP) and a delayed astroglial reaction in the myelinated fiber tracts undergoing WD (Oberheim et al., 2006).

Tissue homeostasis is a balance between proliferation and apoptosis. Various lesions in the brain are accompanied by proliferation and subsequent death of glial cells. It was reported that Fas and FasL is strongly upregulated on astrocytes in the zone of WD after an entorhinal cortex lesion in adult rats (Bechmann et al., 2000). After such a lesion, the mitotic activity of astrocytes reached a peak 5 days postlesion, then returned to the control levels by 10 days postlesion (Bechmann et al., 2000). However, there was no evidence for astrocyte cell death either by TUNEL staining, or from immunohistochemical staining for c-Jun or the apoptosis specific protein (ASP). Thus,

increased expression of Fas and FasL by reactive astrocytes is not accompanied by their death during WD (Bechmann et al., 2000).

4.2 Material and Methods

4.2.1 Anesthesia, Laminectomy, Analgesia, Wound Closure and Postoperative Care

In the experiments comprising this portion of the research project the rats underwent either one or two surgeries; for rats receiving two surgeries they were 8 weeks apart. One of the surgeries was aspiration of the left sensorimotor cortex (Groups 1 and 2); in the pilot study reported in Section 4.3.1 the rats were subjected to only one surgery, namely for aspiration of the left sensorimotor cortex. The other surgery was a laminectomy done to graft OECs into the dorsal funiculus of the T12 spinal cord segment (Groups 1-4). Group 1 and 2 rats received both a sensorimotor cortex lesion and an OEC graft at T12, whereas Group 3 and 4 rats received only the OEC graft. The general surgical procedures related to anesthesia, analgesia, laminectomy, wound closure and postoperative care were as described in Sections 3.2.1, 3.2.2, and 3.2.4.

4.2.2 Sensorimotor Cortex Aspiration

Once the halothane inhalation had induced a sufficient level of anesthesia such that the rat was immobile and unresponsive to a pinch test on their hind paws (pedal reflex) (see Section 3.2.1), the scalp was shaved with an electric razor, the rat positioned in a stereotactic apparatus, and the incision site was swabbed with Betadine antiseptic solution (see Section 3.2.2). A single intramuscular injection of Buprenex (0.05 mg/kg body weight) was then administrated prior to making a midline incision in the scalp, with the incision beginning just caudal to the eyes and continuing caudally to approximately 10 mm behind the ears. The periostium was deflected and a rectangular craniotomy was done using a surgical drill; this craniotomy extended rostrocaudally from approximately 4 mm rostral to the coronal suture to approximately 2 mm rostral to the lambdoid suture, and medio laterally from approximately 1 mm lateral to the sagittal suture all the way to the temporal ridge. Upon completion of the craniotomy, the dura was carefully reflected out of the way. A Pasteur pipette was connected to a rubber tube, which in turn was connected to a vacuum pressure created from the tap running. With the aid of a surgical

microscope (Nikon-SMZ-1B) the cortical brain tissue (predominantly sensorimotor cortex) was aspirated by suction, with the brain tissue being removed from the area exposed by the carniotomy as deep as the cortical white matter (Fig 4.1).

4.2.3 Grafting DiI-Labeled OECs

For Groups 1 to 4, OECs from the K586 cell cultures (see Table 3.1) were used for the grafting of DiI-labelled OECs. A final cell concentration of 50,000 DiI-labelled OECs per µl was loaded into a 5 µl Hamilton syringe and the cells grafted into the right dorsal funiculus of T12 as described in Section 3.2.3.

4.2.4 Minocycline Treatment

Minocycline, a second generation tetracycline, is an antibiotic that possesses better penetration into the CNS via the BBB in comparison to other tetracycline drugs such as methacycline (Aronson, 1980). One critical CNS target of minocycline is inhibition of the proliferation and activation of microglia (Tikka and Koistinaho, 2001). *In vitro*, minocycline prevents the excitotoxicity of glutamate on neurons, presumably via the inhibition of N-methyl-D-aspartate-induced activation of microglia (Tikka and Koistinaho, 2001). *In vivo*, the protection afforded by minocycline in various models of CNS diseases is correlated with a lack of the activation of microglia (Yrjanheikki et al., 1998; Popovic et al., 2002). In the experimental design described in Section 4.3.4, minocycline was used to dampen the WD-induced microglial reactivity and thus to address the extent to which microglial reactivity contributed to the generation of a migratory signal(s). Minocycline was freshly prepared in saline each time before use and heated briefly in a water bath until completely dissolved. Then the minocycline solution was buffered to pH 7.2-7.4 using 0.1 N NaOH. Group 1 and 3 rats received daily intraperitoneal injections of minocycline (45 mg/ kg) whereas Group 2 and 4 rats received daily intraperitoneal injections of an equivalent volume of vehicle (i.e. 0.9% saline). The minocycline and saline injections were begun exactly 2 weeks prior to the grafting of OECs and continued for an additional 4 weeks after the cell grafting. Daily examination of each rat prior to performing the intraperitoneal injection did not show any observable evidence of adverse reactions to either the minocycline or saline injections.

4.2.5 Necropsy, Tissue Sectioning and Immunohistochemistry

Rats were deeply anesthetized by administering a lethal dose (90 mg/kg body weight) of sodium pentobarbital injected intraperitoneally (i.p.) 8 weeks after receiving the OEC graft. They were perfused through the heart with 1% sodium nitrite followed by 4% PF as described in Section 3.3.1. The brain and brainstem were dissected from the cranium and the spinal cord from the vertebral column, as described in Section 3.3.2. Serial, free-floating 40 µm tissue sections (see Section 3.3.3) were cut in the coronal plane from the forebrain of all rats that had received a sensorimotor cortex lesion to determine the size and location of this lesion. A small longitudinal cut was made on the left side of each piece of CNS tissue to distinguish the right from the left side after sectioning and staining. Serial, free-floating 40 µm tissue sections (see Section 3.3.3) were cut in the coronal plane from the medulla and from the C6 and T11 spinal cord segments of the sensorimotor cortex-lesioned rats used in the pilot study to determine the survival time (2-16 weeks) at which the microglial and/or astrocytic reactivity first appeared at these three rostral-caudal levels of the dCST. Finally, in the Group 1 and 2 rats, glial reactivity was assessed only at the T11 segment.

Every 10^{th} tissue section collected through the forebrain of left sensorimotor cortex lesioned rats was mounted onto 1% gelatin and 0.5% chrom alum-subbed coverslips (see Section 3.4.2); the tissue sections were left to air dry for 2-3 hours at room temperature to allow the tissue to adhere to the coverslip before starting the staining. The tissue sections were then rinsed for 10 min in 0.03M PBS followed by 10 min in distilled water. The tissues were dehydrated in an ascending series of ethanols (70%, 90% 95% and 100%) for 2 min in each concentration. The sections were then stained with 0.2% nuclear fast red (diluted in distilled water) for 3 min, followed by a quick rinse in distilled water. This was then followed by quick rinses (30 seconds each) in 70%, 90% and 100% ethanol. The sections were then rinsed in a 1:1 mixture of xylene and absolute alcohol for 1 min, were cleared in three changes of xylene, and were mounted on slides using Shandon xylene substitute mountant (Fig 4.6). Four different mouse monoclonal antibodies were used to assess microglial reactivity, including: mouse anti-rat MHC Class 1 (Clone OX-18, 1:9600, Serotec Product Datasheet, Kidlington Oxford, England),

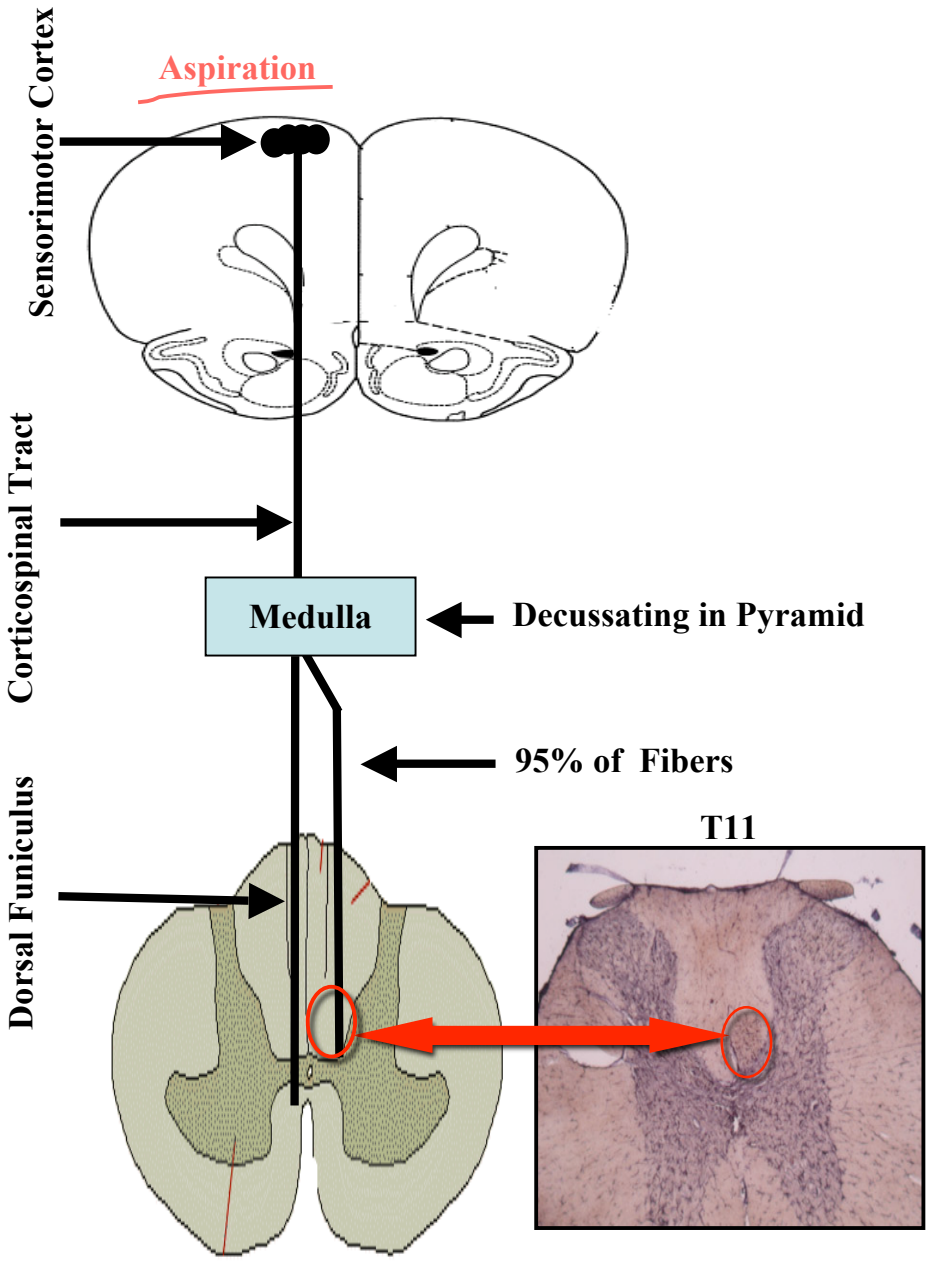

FIGURE 4.1: Schematic of dorsal corticospinal tract (dCST) pathway in the rat.

To induce Wallerian degeneration-induced glial reactivity in the dorsal corticospinal tract (d-CST), the neurons giving rise to this fiber tract were lesioned in the sensorimotor area of the contralateral cerebral cortex (blackened area in left cortex). The left sensorimotor cortex was lesioned by aspiration of cortical tissue. Neurons in the sensorimotor cortex send their axonal projections all the way down to the lower levels of the spinal cord. Decussation of the fiber tract occurs in the pyramidal decussation in the caudal medulla just prior to the fibers entering the spinal cord; approximately 95% of the axons decussate at this level and enter the dCST located in deepest portion of the dorsal funiculus. The dCST extends the entire length of the spinal cord. The histological section on the lower right shows microglial reactivity, as detected with the OX42 monoclonal antibody, confined to the right dCST (red circle) 16 weeks after aspiration of the left sensorimotor cortex.

mouse anti-CD11b (Clone MRC OX-42, 1:3200, Serotec Product Datasheet, Kidlington Oxford, England), mouse anti-CD4 (Clone OX-35, 1:3000, Serotec Product Datasheet, Kidlington Oxford, England) and mouse anti-rat ED1 (1:2000; Serotec, Oxford, England) (Section 3.4.4). Three different mouse monoclonal antibodies were used to assess astrocytic reactivity, including mouse anti-GFAP (1:1000 Dimension Labs, Dako A/S Denmark), mouse anti-vimentin (Clone V9, 1:1000, Sigma, St. Louis, MO 63178, USA), and mouse anti-nestin (1:2000, Clone Rat 401, Developmental Studies Hybridoma Bank, Department of Biological Sciences, University of Iowa, Iowa City, USA) (Section 3.4.2). All primary antibodies were diluted in 0.03 M PBS. The control sections were incubated in diluent only. See Section 3.4.2 for a description of the procedure used for the immunostaining of the tissue sections from the medulla, and from the C6 and T11 segments of the spinal cord.

4.2.6 Data Collection and Statistical Analysis

Assessment of the presence or absence of glial reactivity in the sensorimotor cortex lesioned rats used in the pilot study was done subjectively. For the purpose of the experiments reported in Sections 4.3.7- 4.3.8 of this chapter, tissue sections collected into the first four wells were considered to comprise the rostral one-third of T11, sections in the second four wells comprised the middle one-third, and the final four wells comprised the caudal one-third of T11. Each tissue section was examined to determine whether it contained any DiI+ve cells, to identify the specific location in which the cells were found, and to count the total number of labelled cells within the dCST and the dorsal ascending tract (DAT). The numbers of DiI-labelled cells within the dCST and the DAT on the right and left sides were computed separately. For statistical analysis, the mean cell count within each of the fiber tracts for each group of 4 sections was computed. Only DiI+ve profiles that were associated with a nucleus were counted.

To ensure consistent identification of the border between the dCST and the adjoining DAT when counting cells on the fluorescence microscope (40X objective), it was necessary to determine the dorsal-ventral height of the dCST. Tissue sections (24 sections) from the T11 segment of the spinal cord from saline-treated sensorimotor cortex

aspirated rats (i.e., Group 2) were immunostained with the OX18 monoclonal antibody. The immunostaining of the reactive microglia, which the pilot study had revealed was confined to the dCST, was used to measure the height of the right dCST with respect to the adjacent central grey matter. Using a rectangular eyepiece graticule that was 250 μm tall when using the 40X objective, it was determined the portion of the white matter of the dorsal funiculus that contained OX18+ve reactive microglia was approximately the height of the graticule (i.e. ~250 μm tall). Thus, for the purpose of counting the DiI+ve cells the entire white matter on the dorsal surface of the spinal cord was divided into four unequal sized quadrants, with the two deep, smaller quadrants comprising the right and left dCSTs each being 250 μm tall and the reminder of this area of white matter up to the pial surface comprising the right and left DATs. The eyepiece graticule and the 40X objective was used to view the Hoechst-stained tissue sections to count the number of DiI+ve cells in each of the four unequal sized quadrants; namely, the right and left dCSTs (the two smallest and deepest quadrants) and the right and left DATs (the two largest and most superficial quadrants). Due to unequal size of quadrants (dCST vs. DAT) the mean DiI+ve cell counts were converted to cell densities per 0.05 mm^2.

The T11 cell counts collected for Groups 1-4 were statistically compared using a two-factor analysis of variance (ANOVA), with the data for the rostral, middle and caudal thirds of the right and left dCST and DAT of this spinal cord segment being analyzed separately for statistical significance (see Section 3.5.3). The independent variables were lesion (i.e. sensorimotor cortex lesion vs. no lesion) and treatment (i.e. minocycline vs. vehicle).

4.2.7 Measuring the size of dCST and DAT using Northern Eclipse software

In order to measure the size of the dCST and DAT on tissue sections from the T11 spinal cord segment of rats in Group 1 (n=3 tissue sections) and Group 2 (n=9 tissue sections), the tissue sections were immunostained with the OX42 monoclonal antibody. Digital images of the dorsal part of the spinal cord were analysed using Northern Eclipse 5.0 software (Empix Imaging Inc. Mississauga, ON). The intensity of OX42 immunostaining within the deepest part of the dorsal funiculus (i.e. in the dCST) was used as a criterion for determining the border between the dCST and the DAT. For

calculating the density of DiI+ve OECs within the dCST vs the DAT, the area of the right and left dCST, as well as the area of right and left DAT, were measured on each tissue section that was used for counting the number of DiI+ve OECs.

4.3 Results

4.3.1 Timing of Wallerian Degeneration-Induced Glial Reactivity: Experimental Design

In order to address specific aim #1 a pilot study was conducted to determine the timing for the appearance of WD-induced microglial reactivity in the right dCST at the level of T11 following aspiration of the left sensorimotor cortex. This timing had to be determined before specific aim #2 (see Section 4.4.4) could be tested. Following destruction of the left sensorimotor cortex, WD would gradually progress down the entire length of the right dCST. In order to address the first hypothesis, grafting of OECs at T12 needed to be done at a time when microglial reactivity was present at T11. In the Pilot Study, immunohistochemistry was used to determine the time course of this WD-induced glial reactivity as it reached progressively more distal parts of the right dCST. Antibodies used included the OX42, OX18, OX35 and ED1 monoclonal antibodies for immunostaining of reactive microglia. Antibodies to GFAP, to Vim, and to nestin were used to determine the time course of the astrocytic response to the axonal degeneration. Since the axonal degeneration would be confined to the right dCST, it was predicted the glial reactivity (i.e. microglial and astrocytic) would also be restricted to this fiber tract.

Three distinct proximal-distal levels of the CST pathway were examined to determine the morphology, distribution and immunophenotype of microglia and astrocytes between 1 day and 16 weeks (Table 4.1) after sensorimotor cortex aspiration. Histological analysis of the cerebral hemispheres of each rat was done to determine the location and extent of the cortical lesion. Only rats with a lesion that removed tissue from sensorimotor cortical areas M1 and M2 over a distance of several mm were used for the immunohistochemical examination of glial reactivity in the medullary pyramid, C6 and T11 portions of the CST pathway (Paxinos and Watson, San Diego: Academic Press, 1998). The postlesion survival time at which microglial or astrocytic reactivity were first seen at each of these levels was noted for each of the microglial (OX42, OX18, OX35,

ED1) and astrocytic (GFAP, Vim, nestin) markers; the findings are summarized in Table 4.1 and in Figs. 4.2 and 4.3. As expected, there was a proximal to distal gradient in the appearance of glial reactivity along the length of the CST pathway, with the microglial reactivity being seen as early as 3 weeks in the left pyramid, by 4 weeks in the right dCST at C6, and by 6 weeks in the right dCST at T11 (Table 4.1 and Fig. 4.2). Astrocytic reactivity lagged behind that of the microglial response at each level of the CST pathway (Table 4.1 and Fig. 4.3). These data are described in more detail in Sections 4.4.2 and 4.4.3.

4.3.2 Wallerian Degeneration-Induced Glial Reactivity in Pyramid and at C6

In the pyramidal tract at the level of the medulla the intensity of immunostaining with OX42 was greater for microglia on the ipsilateral side by 3 weeks after left sensorimotor cortex aspiration; these reactive microglia had small cell bodies and short cytoplasmic processes. Furthermore, round-shaped ED1+ve reactive microglia were first seen at the same time point in the ipsilateral medullary pyramid, namely by 3 weeks after cortical injury. OX18+ve and OX35+ve reactive microglia, both having amoeboid cell bodies, were not seen in the ipsilateral pyramid until 4 weeks following sensorimotor cortex aspiration (Fig 4.2 and Table 4.1). The first intense GFAP+ve reactive astrocytes were seen in the ipsilateral pyramid by 4 weeks after cortical injury. These GFAP+ve astrocytes had star-shaped cell bodies and possessed numerous, short cytoplasmic processses. In contrast, Vim+ve reactive astrocytes, which had small cell bodies and a few long cytoplasmic processes, were not seen in the ipsilateral pyramid prior to 6 weeks after sensorimotor cortex aspiration. Furthermore, it was not until 12 weeks after cortical injury that even the first weakly-immunostained nestin+ve reactive astrocytes were seen in the ipsilateral pyramid of sensorimotor cortex lesioned rats; these weakly-immunostained nestin+ve reactive astrocytes were morphologically similar to the Vim+ve reactive astrocytes also present within the ipsilateral pyramid.

In the cervical level of the spinal cord (i.e. at C6) OX42+ve reactive microglia were first seen at 4 weeks after left sensorimotor cortex injury and were confined to the contralateral (i.e. right) dCST; with OX42 immunostaining, no detectable microglial reactivity was seen in any of the other CST tracts. The morphology of OX42+ve reactive

microglia in the right dCST at C6 was similar to that seen in the medullary pyramid 1 week earlier. OX18+ve reactive microglia with short cytoplasmic processes were also seen in the right dCST at C6 by 4 weeks after left sensorimotor cortex aspiration, while OX35+ve and ED1+ve reactive microglia were first seen only at 6 weeks. It also took 6 weeks for the first GFAP+ve reactive astrocytes to be seen in the right dCST at C6, whereas only very low numbers of Vim+ve reactive astrocytes were seen in the same fiber tract even by 8 weeks after cortical injury. Furthermore, even by 16 weeks after cortical injury, the astrocytes in the right dCST remained nestin-ve; however, nestin+ve cells were always seen around the central canal of the C6 spinal cord segment.

4.3.3 Wallerian Degeneration-Induced Glial Reactivity at T11

The OX42+ve microglia displayed shorter, thicker processes and stronger immunoreactivity in the right dCST of T11 at the 6 week time point after cortical injury, in comparison to the left dCST in which the corticospinal axons remained intact (Fig. 4.2C). In the present study, OX18+ve microglia, with sparse, short cytoplasmic processes, were localized to the right dCST and were found in this fiber tract only in sensorimotor cortex lesioned rats (Fig. 4.2F). OX42 and OX18 immunostaining revealed that the earliest microglial reactivity was seen in the right dCST at T11 only by 6 weeks after the cortical lesion. By 8 weeks after cortical injury microglia of the right dCST began to express the OX35 (Fig. 4.2I) and ED1 (Fig. 4.2L) antigenic epitopes, in addition to being OX42+ve and OX18+ve. No OX35+ve or ED1+ve cells were seen elsewhere in the parenchyma of the T11 spinal cord of sensorimotor cortex lesioned rats or anywhere in the parenchyma of the spinal cord of control rats. In the present study a more intense GFAP immunostaining, similar to what has been reported in other studies where astrocytes become reactive in response to injury (Martinez et al., 1998; Raivich et al., 1999), was seen at T11 only in sensorimotor cortex lesioned rats, only in the right dCST, and only by 8 weeks after the cortical lesion (Fig. 4.3C). It took approximately 12 weeks after the left-sided sensorimotor cortex lesion for Vim+ve reactive astrocytes to appear in the right dCST of T11 in response to degeneration of the CST axons (Fig. 4.3F).

Table 4.1 Pilot Study: WD-Induced Glial Reactivity

Survival time	Medulla (left pyramid)	C6 (Right CST)	T11 (Right CST)
1 day (n=1)			
3 day (n=2)			
1 week (n=2)			
2 week (n=4)			
3 week (n=3)	OX42, ED1		
4 week (n=4)	OX18, OX35, GFAP	OX42, OX18	
6 week (n=4)	Vim	OX35, ED1, GFAP	OX42, OX18
7 week (n=2)			
8 week (n=4)		Vim	OX35, ED1, GFAP
10 week (n=2)			
12 week (n=2)	Nestin (Rat 401)		Vim
16 week (n=2)			

n= numbers of rats for each survival time

Three distinct proximal-distal levels of the CST pathway (i.e. pyramid, C6 and T11) were examined to determine the immunophenotype of microglia and astrocytes between 1 day and 16 weeks after sensorimotor cortex aspiration.

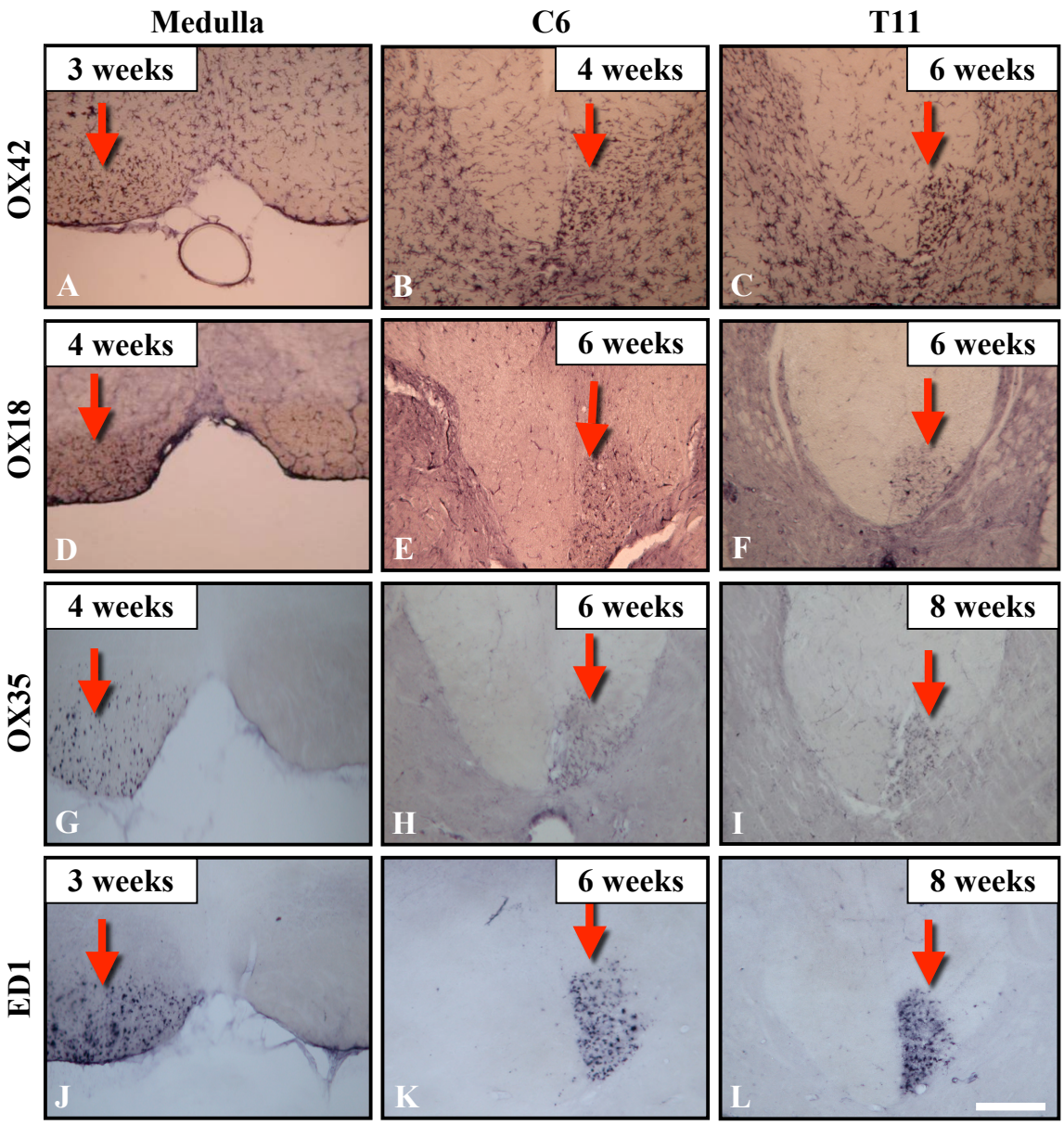

FIGURE 4.2: Time frame of microglial reactivity following sensorimotor cortex aspiration.

Wallerian degeneration-induced microglial reactivity was detected using OX-42 (**A-C**), OX-18 (**D-F**), OX-35 (**G-I**) and ED1 (**J-L**) monoclonal antibodies. The data show the microglial reactivity was first seen in the ipsilateral (i.e. left) medullary pyramid (**A**, **D**, **G**, **J**) by 3 (**A**, **J**) or 4 (**D**, **G**) weeks after cortical injury, depending on the antibody that was used to stain the tissue. In the contralateral dCST at the level of C6 (**B**, **E**, **H**, **K**) the first signs of microglia reactivity were seen using OX-42 antibody (**B**) at 3 weeks after cortical injury but only after 6 weeks using the other three microglial markers (**E**, **H**, **K**). At T11 (**C**, **F**, **I**, **L**). It took 6 (**C**, **F**) to 8 (**I**, **L**) weeks before microglial reactivity could be detected. The red arrows show the location of the left pyramid in the medulla (**A**, **D**, **G**, **J**), and of the right dCST at C6 (**B**, **E**, **H**, **K**) and T 11 (**C**, **F**, **I**, **L**). At all levels, the microglial reactvity was confined to the corticospinal pathway. Scale bar = 300 µm.

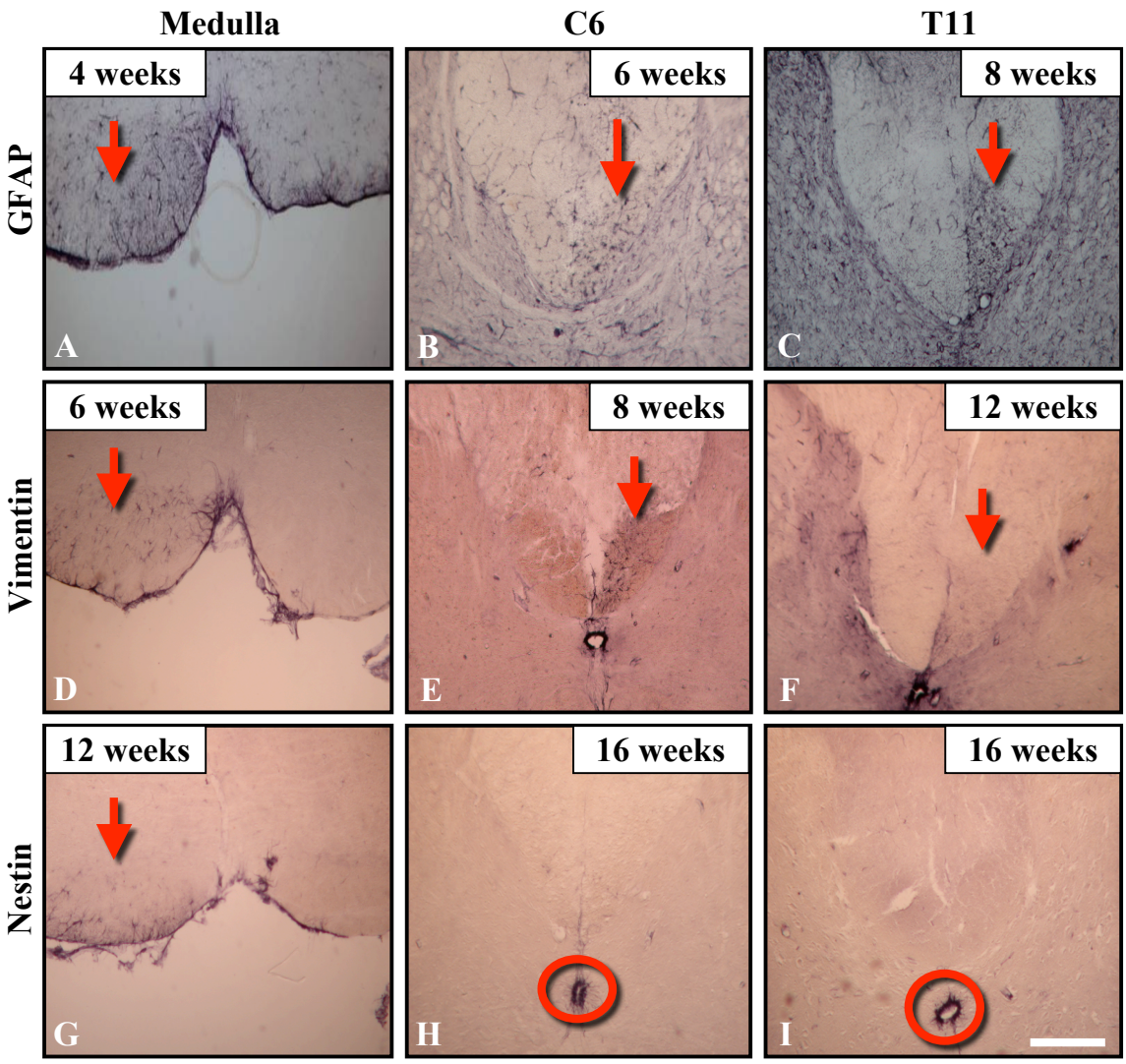

FIGURE 4.3: Time frame of astrocyte reactivity following sensorimotor cortex aspiration.

Wallerian degeneration-induced astrocytic reactivity was detected using GFAP (**A-C**), vimentin (**D-F**) and nestin (**G-I**) antibodies. The data show the astrocytic reactivity was first seen in the ipsilateral (i.e. left) medullary pyramid (**A**, **D**, **G**,) by 4 (**A**), 6 (**D**), or 12 (**G**) weeks after cortical injury, depending on the antibody that was used to stain the tissue. In the contralateral dCST at the level of C6 (**B**, **E**, **H**) the first signs of astrocytic reactivity were seen using the GFAP antibody (**B**) at 6 weeks after cortical injury but only after 8 weeks using the vimentin antibody (**E**). At T11 (**C**, **F**, **I**). it took 8 (**C**) to 12 (**F**) weeks before astrocytic reactivity could be detected. Even as late as 16 weeks after cortical injury, the reactive astrocytes of the dCST remained nestin-ve at both C6 (**H**) and T11 (**I**); red circles in '**H**' and '**I**' highlight nestin+ve staining around the ependymal lining of the central canal. The red arrows show the location of the left pyramid in the medulla (**A**, **D**, **G**), and of the right dCST at C6 (**B**, **E**) and T 11 (**C**, **F**). At all levels, the astrocytic reactvity was confined to the corticospinal pathway. Scale bar = 300 µm.

Although the intensity of the Vim immunostaining was usually very low (Fig. 4.3F), there was no staining of adjacent parts of the white or grey matter, except around the central canal. Reactive astrocytes in the right dCST of T11 of sensorimotor cortex lesioned rats were nestin-ve up to at least 16 weeks after injury, which was the longest survival time studied (Fig. 4.3H & I). However, nestin+ve cells were consistently seen surrounding the central canal of T11, even in control rats (Fig. 4.3H and I), thus serving as a positive control for the nestin immunostaining. As shown in Section 4.4.2, nestin+ve cells were seen in the medullary pyramid at both 12 and 16 weeks after cortical injury (Fig. 4.3G), thus indicating expression of nestin by reactive astrocytes in more rostral parts of the CST undergoing WD.

In summary, OX42+ve, OX18+ve, OX35+ve and ED1+ve microglia were detected only in the right dCST of T11 and only in rats that had received a sensorimotor cortex lesion at least six (OX42+ve and OX18+ve) or eight (OX35+ve and ED1+ve) weeks beforehand (Fig. 4.2 and Table 4.1). GFAP+ve and Vim+ve reactive astrocytes were also detected only in the right dCST of T11 and only in rats that had received the cortical injury at least 8 (GFAP+ve) and 12 (Vim+ve) weeks beforehand (Fig. 4.3 and Table 4.1). Based on the intensity of OX18+ve, OX42+ve and OX35+ve immunostaining of reactive microglia as well as GFAP+ve and Vim+ve reactive astrocytes in the right dCST of T11 there was no detectable difference in glial reactivity in rats killed 12-16 weeks after the cortical injury. Furthermore, there was no morphological variation in the reactive microglia or astrocytes between 12-16 weeks after the cortical injury. The timing data obtained in this Pilot Study revealed that at least a 6 week time interval is required after lesioning the left sensorimotor cortex before WD-induced microglial reactivity could be detected in the right dCST at T11. By 8 weeks after cortical injury the microglial reactivity was more prominent and astrocytic reactivity was now detected as well. Based on these data, the 8 week time point was chosen for injecting DiI+ve OECs into the right DAT of T12 for the purpose of addressing the second objective.

4.3.4 Sensorimotor Cortex Injury and OEC Migration: Experimental Design

On the basis of the findings of the pilot study (specific aim #1) (see Sections 4.4.1-4.4.3), 8 weeks after sensorimotor cortex injury was chosen as the time point at which to graft DiI+ve OECs into the right DAT of the T12 segment of the spinal cord. The rationale for choosing this time point was that although OX42+ve and OX18+ve reactive microglia were present in the right dCST at T11 by 6 weeks after left sensorimotor cortex aspiration, it was 8 weeks after cortical injury before OX35+ve and ED1+ve reactive microglia were seen inside the same fiber tract. At 8 weeks after cortical injury there was minimal astrocyte reactivity in the right dCST at T11, with GFAP being the only astrocytic marker used that showed any indication the astrocytes were even responding to the WD of axons in this fiber tract. It was at least 12 weeks before even a small number of Vim+ve reactive astrocytes were detected in the right dCST of sensorimotor cortex lesioned rats, with these reactive astrocytes being nestin-ve even up to 16 weeks after cortical injury. Furthermore, at survival times longer than 8 weeks there was no detectable change in the intensity of immunostaining, the distribution of the cells, or the morhology of OX18+ve, OX42+ve and OX35+ve and ED1+ve reactive microglia in the dCST of the T11 segment of the spinal cord.

Thus, in rats it takes at least 6 weeks after lesioning the left sensorimotor cortex before WD-induced microglial reactivity can first be detected in the right d-CST at T11. By 8 weeks after cortical injury the microglial reactivity was more prominent and by now the first sign of astrocytic reactivity was also seen. Based on these data, we chose to use the 8 week time point for injecting DiI+ve OECs into the right DAT of T12 for the purpose of addressing the second objective. In order to ensure the minocycline treatment would successfully dampen the WD-induced microglial reactivity, the daily injection of either minocycline or vehicle was begun 2 weeks prior to the OEC grafts and the injections were continued for an additional 4 weeks after the cell grafts (Fig. 4.4). Half of the rats received a left sensorimotor cortex injury and the other half comprised the no lesion controls. All rats were killed 8 weeks after the OECs were grafted at T12 and the brains processed for histological analysis of the lesion location and size, whereas the T11 segment of the spinal cord of each rat was processed for immunohistochemical analysis

of microglial and astrocytic reactivity and for quantification of the numbers of DiI+ve OECs in the right and left dCSTs and DATs (Fig. 4.4).

4.3.5 The Size and Location of the Cortical Lesion

The topographical extent of damage following aspiration lesion of the sensorimotor cortex was assessed in neutral fast red stained sections. Lesions produced by aspiration were similar in the anterior-posterior and medial-lateral directions in all lesioned animals. The lesion included all six layers of the cortex and most also involved the corpus callosum. The principle difference between the largest and smallest lesions was the extent to which the injury extended into subcortical areas (Fig 4.5). Based on comparisons of the location of the lesions with respect to coronal sections in a rat brain atlas (Paxinos and Watson, San Diego: Academic Press,, 1998) all rats had cortical lesions that extended from 3.70 mm rostral to bregma to 3.60 mm caudal to bregma; the lesion extended mediolaterally from 0-2 mm. The comparable location of cortical injury in all rats demonstrated the reproducibility of the sensorimotor cortex aspiration. Miller (1987) determined precisely the somatotopic distribution of CST neurons in the sensorimotor cortex of adult rats by injecting the retrograde tracer horseradish peroxidase (HRP) into the cervical (C5-C6), upper thoracic (T2-T3), lower thoracic (T8-T9), and lumbar (L2-L3) segments of the spinal cord. His study demonstrated that retrogradely labelled neurons were distributed throughout brodmann areas 3, 4, 6/8, 18b and 24b; however, the density of HRP rerogradely labelled neurons was greatest in area 4, which forms part of the motor cortex area and corresponds to the M1 and M2 motor areas (Paxinos and Watson, San Diego: Academic Press, 1998).

4.3.6 Minocycline Dampens Wallerian Degeneration-Induced Microglial Reactivity

To confirm that the minocycline treatment had been effective in dampening the intensity of the microglial response and in assessing the treatment's effect on astrogliosis, tissue sections from the rostral, middle and caudal levels of T11 of all groups of rats were stained with the same panel of antibodies as was used in the Pilot Study to identify reactive microglia (i.e., OX42, OX18, OX35 and ED1 monoclonal antibodies) and

reactive astrocytes (i.e., GFAP, Vim and nestin monoclonal antibodies). In the lesion saline-treated rats (Group 2), OX42+ve microglia were detected throughout the tissue sections, but the immunostaining was more intense in the right dCST (Fig 4.6). In contrast, in the lesion minocycline-treated rats (Group 1) the intensity of the immunostaining of microglia in the right dCST with the OX42 monoclonal antibody was not detectably different from elsewhere in the tissue section. In the no lesion saline-treated (Group 4) and minocycline-treated (Group 3) rats the OX42+ve microglia in right dCST were also indistinguishable from the OX42+ve microglia in the remainder of the same tissue section. Likewise, OX18+ve and OX35+ve reactive microglia, each with short cytoplasmic processes, as well as round ED1+ve reactive microglia were detected in the right dCST of saline-treated rats that had received a cortical lesion (Group 2). It was noted that the minocyline treatment in Group 1 rats had dramatically reduced the immunostaining intensity of OX18, OX35, and ED1 antibodies following aspiration of the left sensorimotor cortex (Fig 4.6). No cell counts of microglia or other tests to determine the level of OX42, OX18, OX35 and ED1 expression were performed on spinal cord tissue of rats in any of the 4 groups who were treated either with saline or with minocycline.

In the rats that had received the cortical injury (Groups 1 and 2), Vim+ve reactive astrocytes in the T11 spinal cord segment were primarily seen along the pial surface and within the right dCST, regardless of whether the rats had been treated with saline or minocycline (Fig 4.6). Also, GFAP+ve astrocytes were seen throughout both the grey and white matter of T11 of the Group 1 and 2 rats, with no detectable reduction in the intensity of immunostaining in rats treated with minocyline. In all four groups, nestin+ve cells were only seen around the central canal of T11, regardless of whether the rats had been treated with saline or minocycline. In summary, the minocycline treatment effectively dampened the WD-induced microglial reaction in the right dCST, as evidenced by immunostaining with the OX18, OX42, OX35 and ED1 antibodies. The daily minocycline injections were timed so they began at a time point at which microglial reactivity (OX42+ve and OX18+ve) was first detectable in the right dCST of T11 in rats

FIGURE 4.4: Summary of experimental design

Four groups of adult female rats (n=4 per group) received grafts of DiI labeled OECs in the right dorsal funiculus of T12. In Groups 1 and 2, the left sensorimotor cortex was aspirated 8 weeks previously to induce a glial reaction in the right dorsal corticospinal tract (dCST) as a result of the Wallerian degeneration of axons. Groups 3 and 4 rats served as unlesioned controls. As an additional experimental manipulation, each rat received a daily i.p. injection of either minocycline (Groups 1and 3) or vehicle (Groups 2 and 4) over a six week period beginning two weeks prior to and continuing for four weeks after the OECs were grafted at T12. All rats were killed eight weeks after cell grafting.

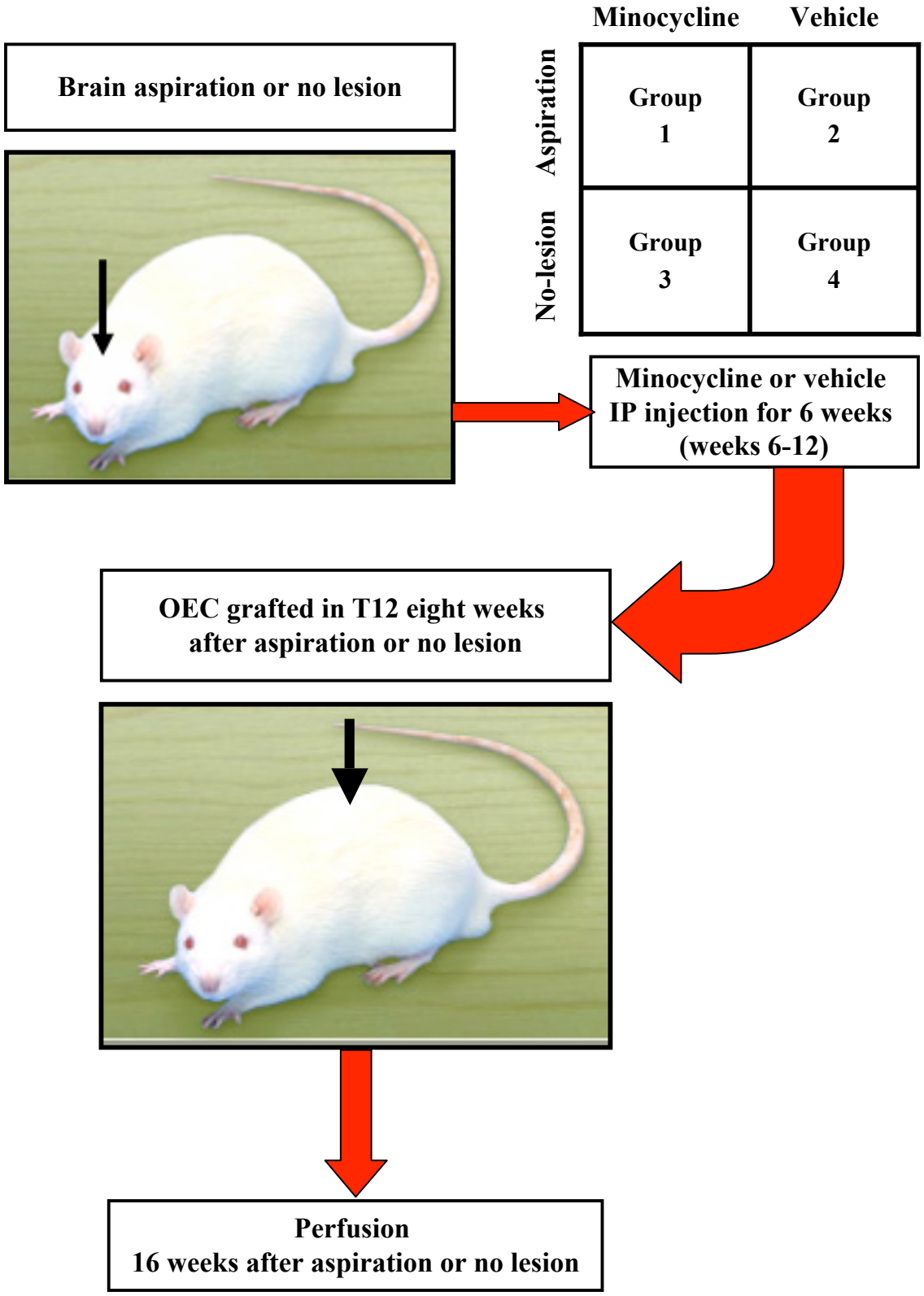
Minocycline
Vehicle
Aspiration
No-lesion
Group 1
Group 2
Group 3
Group 4
Brain aspiration or no lesion
Minocycline or vehicle IP injection for 6 weeks (weeks 6-12)
OEC grafted in T12 eight weeks after aspiration or no lesion
Perfusion 16 weeks after aspiration or no lesion

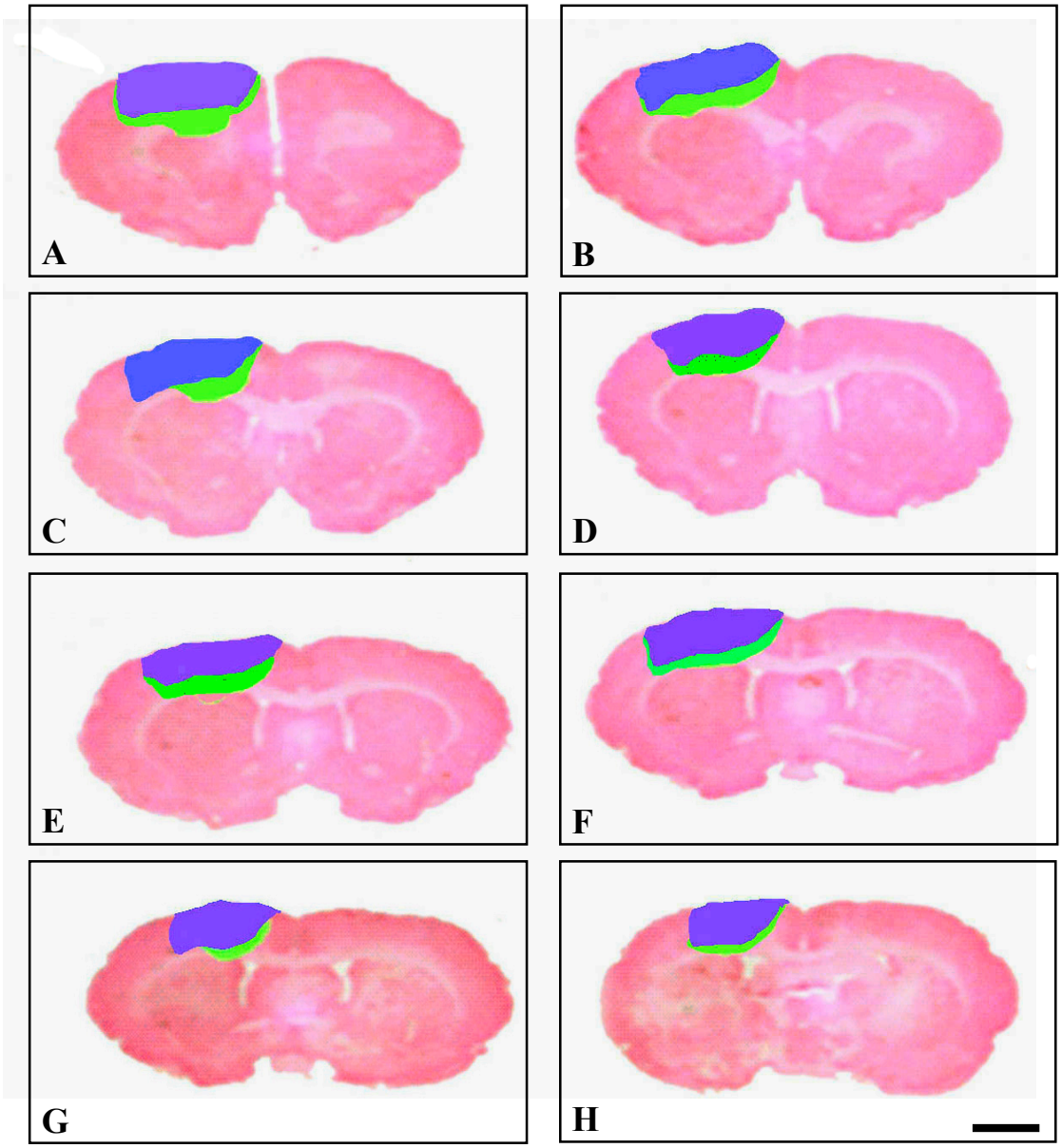

FIGURE 4.5: Size of the sensorimotor cortex lesion in rats of Groups 1 and 2.

Sections of the forebrain were cut in the coronal plane of all rats in Groups 1 and 2 to determine the size and location of the cortical lesion. The tissue sections in this figure, which were cut from an unoperated control rat and stained with neutral fast red, are arranged from most rostral (**A**) to most caudal (**H**). These images were used to compare directly the size and location of the cortical lesion in all rats of Groups 1 and 2. Of the 8 rats whose left sensorimotor cortex was lesioned, the rat who had the smallest lesion (depicted here in blue colored shading) belonged to Group 2 and the rat with the largest lesion (depicted here in green colored shading) belonged to Group 1. Scale bar =1000 µm.

receiving a sensorimotor cortex lesion; the daily injections continued over a total period of 6 weeks. The WD-induced astrocytic reactivity in the right dCST was less prominent than that of microglia and the minocycline treatment had no apparent effect on the astrocytic response to the degeneration of CST axons, at least as evidenced by immunostaining with GFAP and Vim antibodies.

4.3.7 Reproducibility of DiI+ve cell counts

A pilot study was performed to confirm the reproducibility of DiI+ve cell counts. This pilot study used a total of 14 tissue sections from the T11 spinal cord segment; these tissue sections were obtained from rats in Groups 1 (n=7 tissue sections) and 2 (n=7 tissue sections). To confirm the reproducibility of the cell counts, the number of DiI+ve cells in the right and left dCST (R-dCST and L-dCST) as well as in the right and left DAT (R-DAT and L-DAT) were counted twice, with the counts being done 10 days apart. The data obtained from the two cell counts were analyzed statistically using a t-test, which showed no significant differences between the first and second cell counts for any of the four fiber tracts.

The Northern Eclipse software was used to measure the area of the R-dCST, L-dCST, R-DAT, and L-DAT in tissue sections that were immunostained with the OX42 monoclonal antibody and in other tissue sections in which the nuclei had been stained using Hoechst dye. These measurements were made on tissue sections from the T11 spinal cord segment and were used to compare the size of these fiber tracts as measured using brightfield microscopy (n=12 OX42-immunostained sections) vs. using immunofluroescence (n=12 Hoechst-stained sections). The OX42 immunostaining of microglia as seen in light microscopy was used to identify the dCST, with the DAT being the remainder of the funiculus up to the pial surface. For the Hoechst-stained sections, the rectangular eyepiece graticule (~250 μm tall) used for cell counting was used to identify the approximate border between the dCST and DAT on the fluorescence microscope because we were not able to determine the border using Hoechst staining. This eyepiece graticule was the one used for cell counting, whereas the OX42 immunostained tissue sections were the ones used to measure the area of the dCST and of the DAT for computation of DiI+ve cell densities. Statistical analysis of these data by t-test showed

significantly larger areas of the R-dCST and L-dCST when they were measured on the OX42 immunostained tissue sections as compared to the Hoechst-stained sections. Conversely, the t-tests showed significantly smaller areas for the R-DAT and L-DAT when they were measured on the OX42 immunostained tissue sections as compared to the Hoechst-stained sections (Fig 4.12). The importance of these findings is that using the eyepiece graticule to identify the approximate border between the dCST and DAT on the fluorescence microscope for cell counting includes the entire DAT and a small part of the superficial component of the adjacent dCST.

4.3.8 Wallerian Degeneration-Induced OEC Migration in the dCST at T11

We found that WD-induced microglial reactivity was associated with increased OEC migration into the right dCST at T11 when DiI+ve OECs were injected into the right dorsal funiculus of T12 eight weeks after aspiration of the left sensorimotor cortex. Due to the much smaller size of the dCST (0.06 mm^2) with respect to the DAT (0.2 mm^2) (see Fig. 4.13), the cell counts of DiI+ve OECs were converted to the number of cells per 0.05 mm^2. A two-factor analysis of variance (ANOVA) was applied to these data, with the data for the rostral (A), middle (B) and caudal (C) thirds of the right (Fig. 4.13) and left (Fig. 4.15) dCST at T11 being analyzed separately for statistical significance. The independent variables were lesion vs. no lesion and minocycline vs. saline treatment. Multiple post hoc comparisons were performed with Bonferonni's multiple comparison post-test.

The two-factor ANOVA on the data for the right dCST, which being contralateral to the cortical lesion contained WD-induced glial reactivity, showed a significant main effect of the sensorimotor cortex aspiration at all levels of the right dCST in the T11 spinal cord segment; $F(1,10) = 13.48$, $p<0.0043$ (Fig. 4.13A; rostral), $F(1,10) = 28.70$, $p<0.0003$ (Fig. 4.14B; middle), and $F(1,10) = 143.0$, $p<0.0001$ (Fig. 4.14C; caudal). There was also a significant main effect of the minocycline treatment at all levels of the right dCST in the T11 segment of the spinal cord; $F(1,10) = 45.97$, $p<0.0001$ (rostral), $F(1,10) = 35.70$, $p<0.0001$ (middle), and $F(1,10) = 150.8$, $p<0.0001$ (caudal). The two-factor ANOVA revealed a significant interaction between the lesion/no lesion and minocycline/saline variables in the right dCST of the middle (Fig. 4.13B), $F(1,10) =$

7.131, $p<0.0235$) and caudal (Fig. 4.13C), $F(1,10) = 74.51$, $p<0.0001$) part of the T11 spinal cord segment. The average number of DiI+ve OECs per 0.05 mm^2 in the right dCST of the saline-treated cortical lesion group was 5.86 +/- 0.40 (rostral T11), 9.77 +/- 1.11 (middle T11), and 10.73 +/- 0.37 (caudal T11), which were all significantly higher ($p<0.05$; Bonferroni's post-test; Fig. 4.14) than the average cell density in the right dCST of the saline-treated no lesion group at the rostral (3.94 +/- 0.16), middle (4.19 +/- 0.01), and caudal (4.89 +/- 0.06) levels of T11. The density of DiI+ve OECs in the right dCST was also significantly higher at each level of T11 in the saline-treated cortical lesion group as compared to the minocycline-treated cortical lesion group, which had cell densities of 2.59 +/- 0.60, 3.77 +/- 0.35, and 4.80 +/- 0.24 DiI+ve OECs at the rostral, middle and caudal parts of T11, respectively ($p<0.05$; Bonferroni's post-test; Fig. 4.14). The post-test also revealed a significant reduction in the density of DiI+ve OECs in the right dCST of the no lesion group as a consequence of the minocycline treatment (1.31 +/- 0.19) in comparison to the saline-treated no lesion group (3.94 +/- 0.16), but this significant difference was only seen in the right dCST at the rostral level of T11 ($p<0.05$; Bonferroni's post-test; Fig. 4.13A).

A two-factor ANOVA was applied to the data for the left dCST, which being ipsilateral to the cortical lesion contained no WD-induced glial reactivity. The two-factor ANOVA showed a significant main effect of the sensorimotor cortex aspiration on cell densities in the left dCST at the middle level of T11 (Fig. 4.16B; $F(1\text{-}10) = 9.218$, $p<0.0125$), but not at the rostral (Fig. 4.15A) or caudal (Fig. 4.16A) levels of T11. There was, however, a significant main effect of the minocycline treatment in the left dCST at all levels of T11; $F(1,10)=9.928$, $p<0.0103$ (A), $F(1,10)=11.30$, $p<0072$ (B), and $F(1,10)=9.020$, $p<0.0133$ (C). The two-factor ANOVA revealed no significant interaction between the lesion/no lesion and minocycline/saline variables in the left dCST at any of the three levels of T11. Bonferonni's post-test revealed the density of DiI+ve OECs in the left dCST was significantly higher ($p<0.05$; Fig. 4.16, brackets) in the saline-treated cortical lesion group than in the minocycline-treated cortical lesion group at the rostral (2.21 +/- 0.69 vs. 0.48 +/- 0.22, respectively), middle (3.16 +/- 0.59 vs. 1.27 +/- 0.50, respectively) and caudal (2.85 +/- 0.52 vs. 1.42 +/- 0.10, respectively) levels of T11 (Fig. 4.16). Although these differences in cell densities in the left dCST were statistically

significant, the actual numerical differences between the cell densities ranged from 1.43 to 1.89 cells per 0.05 mm^2, which are small enough to make it questionable whether they are of any therapeutic interest.

4.3.9 OEC Migration in the Dorsal Ascending Tract (DAT) at T11

There was very little migration of DiI+ve OECs into the right DAT of T11 following injection of the cells into the right dorsal funiculus of T12 eight weeks after aspiration of the left sensorimotor cortex. It should be borne in mind that although the differences reported below were statistically significant, the actual numerical differences between the cell densities ranged from 0.80 to 1.65 cells per 0.05 mm^2, which are so small it is questionable whether they are of any therapeutic interest. A two-factor ANOVA was applied to the data for the right DAT, which although being contralateral to the cortical lesion contained no WD-induced glial reactivity since in the dorsal white matter of the spinal cord the CST axons are confined to the dCST. The two-factor ANOVA showed a significant main effect of the sensorimotor cortex aspiration at all levels of the T11 spinal cord segment; $F(1,10) = 10.54$, $p<0.0088$ (A), $F(1,10) = 16.58$, $p<0.0022$ (B), and $F(1,10) = 58.31$, $p<0.0001$ (C). There was also a significant main effect of the minocycline treatment at all levels of T11; $F(1,10) = 40.99$, $p<0.0001$ (A), $F(1,10) = 61.72$, $p<0.0001$ (B), and $F(1,10) = 250.6$, $p<0.0001$ (C). The two-factor ANOVA revealed a significant interaction between the lesion/no lesion and minocycline/saline variables in the right DAT of the middle portion of the T11 spinal cord segment (B); $F(1,10) = 5.064$, $P<0.0481$. The average number of DiI+ve OECs per 0.05 mm^2 in the right DAT was significantly higher in the saline-treated cortical lesion group (3.80 +/- 0.09) as compared to the saline treated no lesion group (2.92 +/- 0.03) only at the caudal level of T11 ($p<0.05$; Bonferroni's post-test; Fig. 4.13C). Bonferroni's post-test also revealed that the density of DiI+ve OECs in the right DAT of the saline-treated cortical lesion group was significantly higher than the average cell density in the right DAT of the minocycline-treated cortical lesion group at the rostral (2.79 +/- 0.12 vs. 1.81 +/- 0.24), middle (3.03 +/- 0.17 vs. 2.23 +/- 0.16), and caudal (3.80 +/- 0.09 vs. 2.15 +/- 0.12) levels of T11 ($p<0.05$; Fig. 4.14).

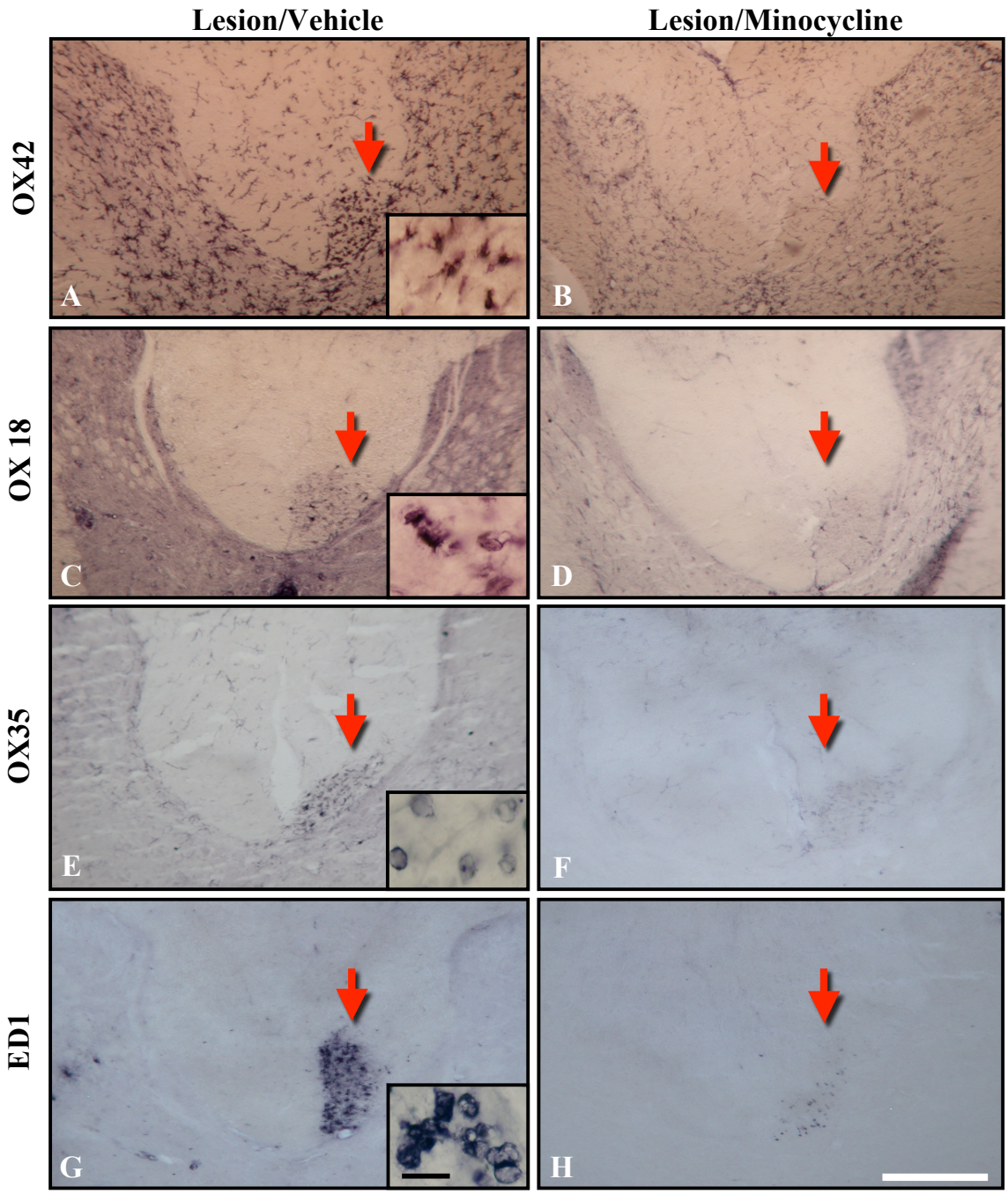

FIGURE 4.6: Microglial reactivity in the right dCST of T11 in Groups 1 and 2.

OX42+ve (**A**,**B**), OX18+ve (**C**,**D**), OX35+ve (**E**,**F**) and ED1+ve (**G**,**H**) microglia in the right dCST of T11 at 16 weeks after left sensorimotor cortex aspiration. The minocycline treatment dramatically reduced the microglial reactivity (**B**, **D**, **F**, and **H**) as compared to vehicle controls (**A**, **C**, **E**, and **G**). The red arrows denote the location of the right dCST. Scale bar = 400 µm. Insets in **A**, **C**, **E** and **G** show the morphology of reactive microglia. Scale bar insets in **G**=50 µm and applied to all insets.

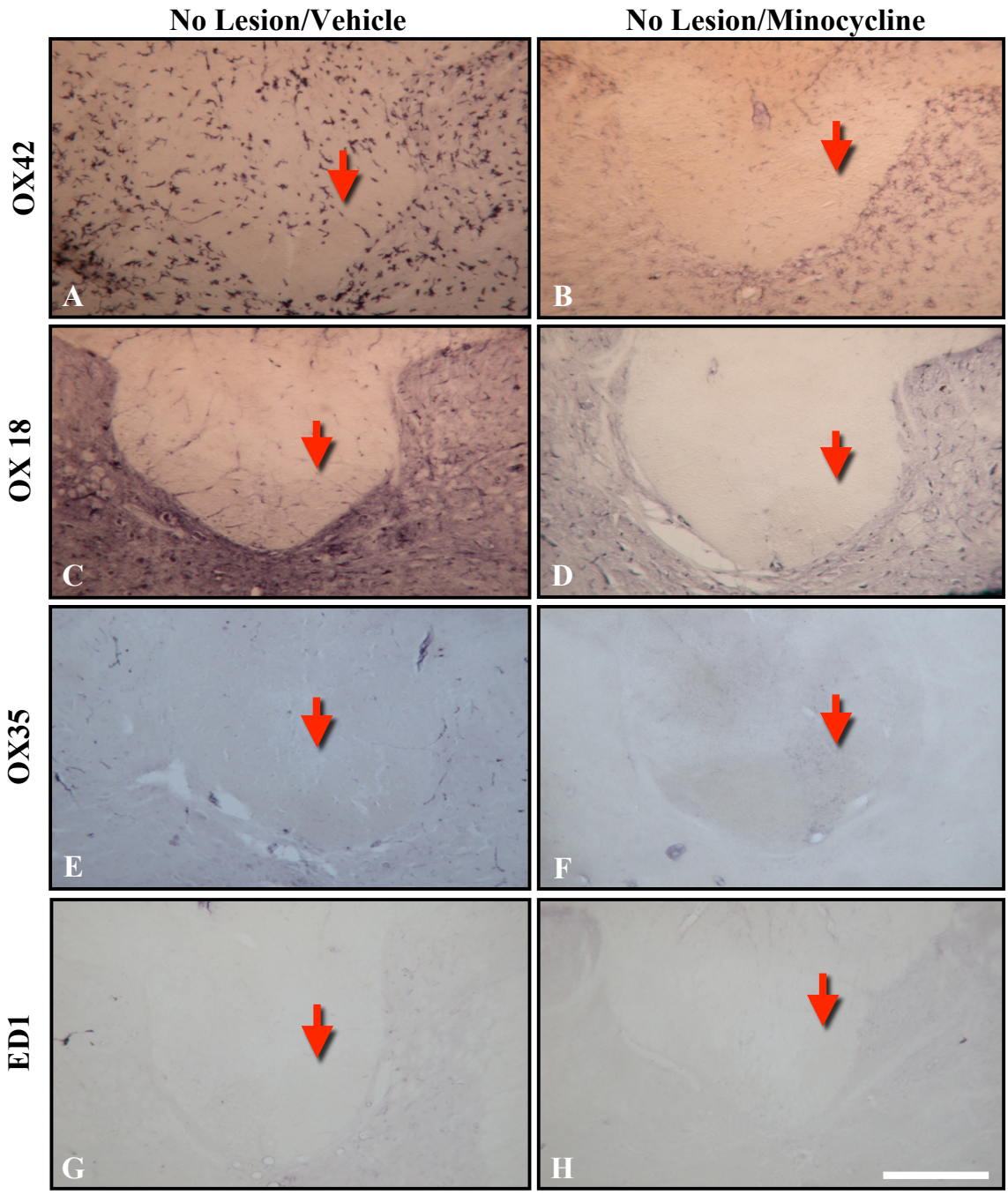

FIGURE 4.7: Microglia in the right dCST of T11 in Groups 3 and 4.

OX42 (**A**,**B**), OX18 (**C**,**D**), OX35 (**E**,**F**) and ED1 (**G**,**H**) immuno-staining showed no microglial reactivity in the right dCST of T11 in rats who received a DiI+ve OEC graft at T12 but who received no cortical lesion. Aside from a reduction in the intensity of the OX42 immunostaining (**B**), there was no apparent difference between tissue sections from rats treated with minocycline (**D**, **F**, and **H**) and those treated with vehicle (**C**, **E**, and **G**). The red arrows denote the location of the right dCST. Scale bar = 400 µm.

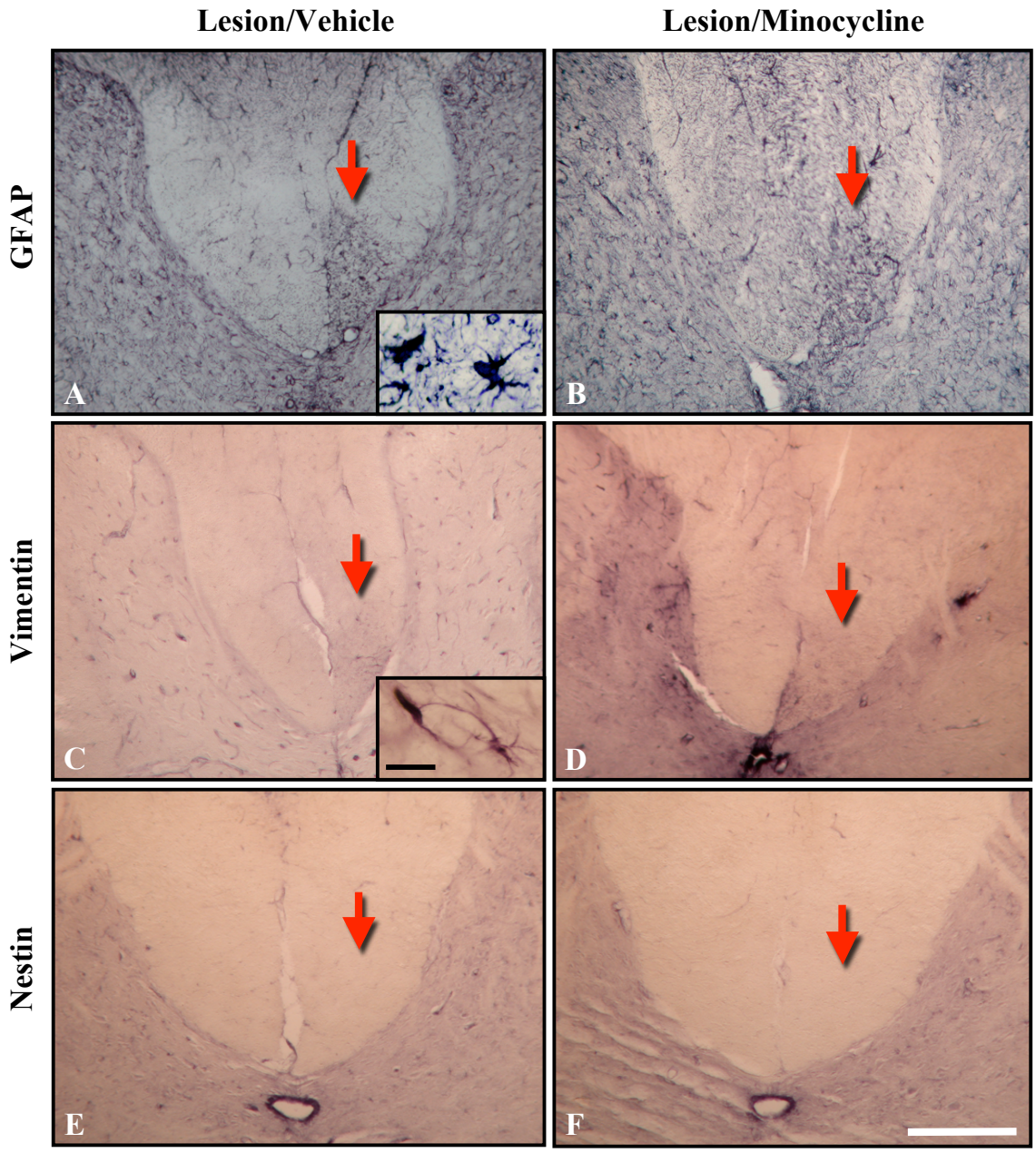

FIGURE 4.8: Astrocyte reactivity in the right dCST of T11 in Groups 1 and 2.

There was astrocyte reactivity in the right dCST of T11 at 16 weeks after left sensorimotor cortex aspiration. The presence of increased GFAP+ve (**A**,**B**) immunostaining and of light immunostaining for vimentin (**C**,**D**) in the right dCST are indicative of astrocytic reacitivity, but these reactive astrocytes were nestin-ve (**E**,**F**). The minocycline treatment had no detectable effect on the astrocytic reactivity (**B**, **D**) as compared to vehicle controls (**A, C**). Scale bar = 400 µm. Insets in **A** and **C** show the morphology of reactive astrocytes, scale bar insets in **C**=50 µm and applied to a **A**.

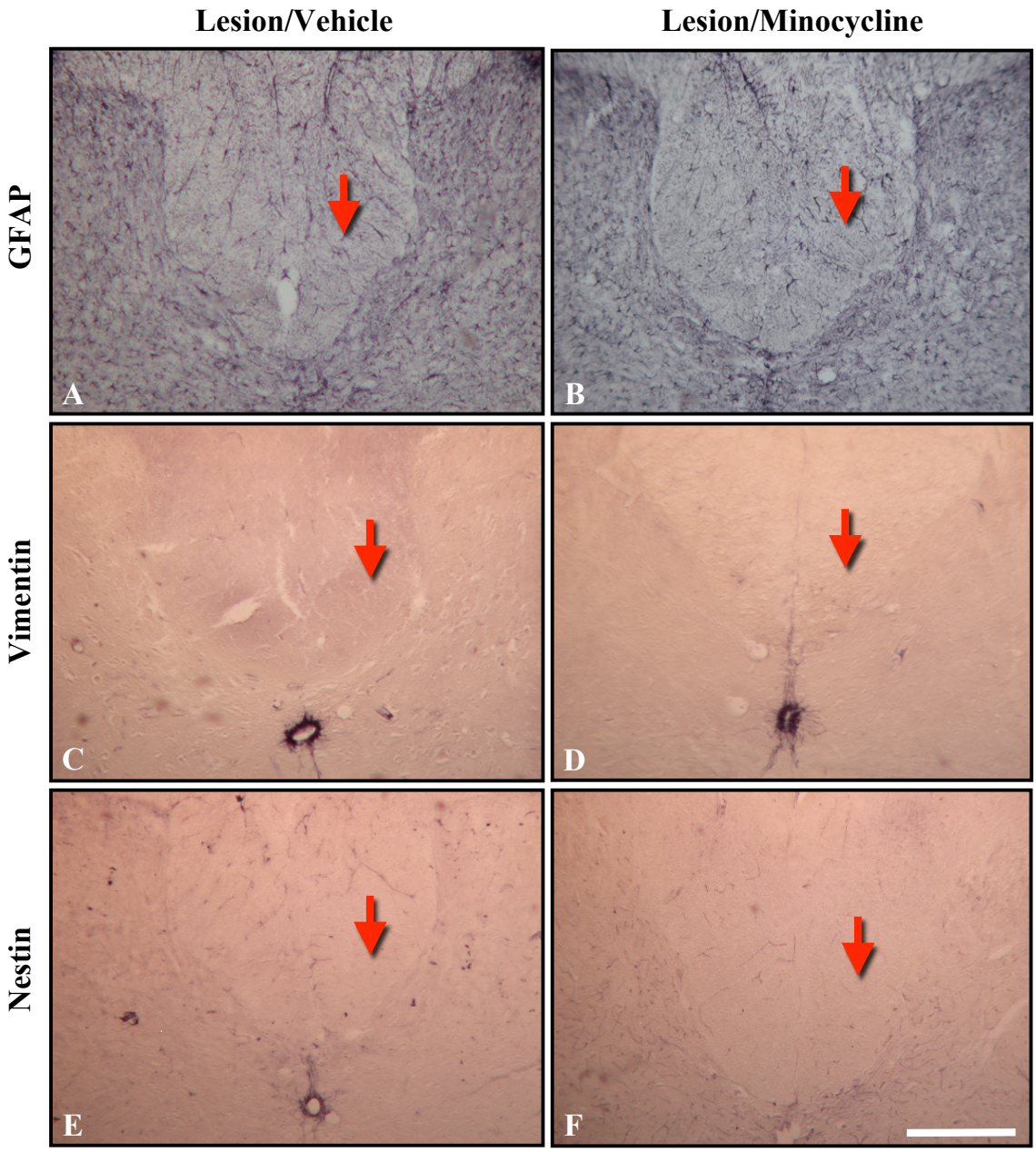

FIGURE 4.9: Absence of astrocyte reactivity in the right dCST of T11 in Groups 3 and 4.

GFAP (**A**,**B**), vimentin (**C**,**D**) and nestin (**E**,**F**) immunostaining showed no astrocyte reactivity in the right dCST of T11 in rats who received a DiI+ve OEC graft at T12 but who received no cortical lesion. There was no apparent difference between tissue sections from rats treated with minocycline (**B**, **D** and **F**) and those treated with vehicle (**A**, **C** and **E**). The red arrows denote the location of the right dCST. Scale bar = 400 µm.

The density of DiI+ve OECs in the right DAT was also significantly higher in the saline-treated no lesion group as compared to the minocycline-treated no lesion group at the rostral (2.31 +/- 0.04 vs. 1.27 +/- 0.02), middle (2.77 +/- 0.10 vs. 1.33 +/- 0.02) and caudal (2.92 +/- 0.03 vs. 1.59 +/- 0.07) parts of T11 ($p<0.05$; Bonferroni's post-test; Fig. 4.14).

There was also very little migration of DiI+ve OECs into the left DAT of T11 following injection of the cells into the right dorsal funiculus of T12 eight weeks after aspiration of the left sensorimotor cortex. As mentioned above with respect to the cell densities in the right DAT, although the differences reported below were statistically significant the actual numerical differences between the cell densities ranged from 0.46 to 0.86 cells per 0.05 mm^2, which are so small it is questionable whether they are of any therapeutic interest. A two-factor ANOVA was applied to the data for the left DAT, which also contained no WD-induced glial reactivity. The two-factor ANOVA revealed a significant main effect of the sensorimotor cortex aspiration only at the middle level of T11 (B); $F(1,10) = 14.10$, $p<0.0038$. There was also a significant main effect of the minocycline treatment at all levels of the T11 spinal cord segment; $F(1,10) = 21.42$ $p<0.0009$ (A), $F(1,10) = 26.95$, $p<0.0004$ (B), and $F(1,10) = 46.91$, $p<0.0001$ (C). The average number of DiI +ve cells per 0.05 mm^2 in the left DAT was significantly higher in the minocycline-treated cortical lesion group (1.29 +/- 0.10) as compared to the minocycline-treated no lesion group (0.76 +/- 0.05) only at the middle level of T11 ($p<0.05$; Bonferroni's post-test; Fig. 4.16B). Bonferroni's post-test also revealed that the density of DiI+ve OECs in the left DAT of the saline-treated cortical lesion group was significantly higher than the average cell density in the left DAT of the minocycline-treated cortical lesion group at the rostral (1.35 +/- 0.15 vs. 0.89 +/- 0.08), middle (1.78 +/- 1.31 vs. 1.29 +/- 0.10), and caudal (1.85 +/- 0.21 vs. 1.01 +/- 0.04) levels of T11 ($p<0.05$; Fig. 4.16). The density of OECs in the left DAT was also significantly higher in the saline-treated no lesion group as compared to the minocycline-treated no lesion group at the rostral (1.19 +/- 0.08 vs. 0.69 +/- 0.02), middle (1.46 +/- 0.14 vs. 0.76 +/- 0.05) and caudal (1.66 +/- 0.01 vs. 0.80 +/- 0.04) parts of T11 ($p<0.05$; Bonferroni's post-test; Fig. 4.16). As mentioned above with respect to the cell densities in the right DAT.

FIGURE 4.10: Quantification of DiI+ve OECs in the right and left dCST and DAT

A) A coronal section obtained from the T11 segment of the spinal cord of a rat from Group 2. The section has been stained with the OX18 monoclonal antibody to show the location of the right dCST (R-dCST), which is the only location containing Wallerian degeneration-induced microglial reactivity. The entire white matter on the dorsal surface of the spinal cord was divided into 4 quadrants, with the two deep, smaller quadrants comprising the right (R-dCST) and left (L-dCST) dorsal corticospinal tracts. The remainder of the white matter on the dorsal surface comprised the other two quadrants, the right (R-DAT) and left (L-DAT) dorsal funiculi. Using an eyepiece graticule on a microscope equipped with both brightfield and fluorescence optics it was determined the area containing OX18+ve reactive microglia was approximately 250 μm high. B) The 4 quadrants used for cell counting are indicated in this Hoechst-stained coronal section, which is representative of the tissue sections used for computing the cell counts. The cell counts were done using a 40X objective; at this magnification the dCST on each side filled the entire height of a rectangular eyepiece graticule (~250 μm high) on the fluorescence microscope. Cell counts for the right and left DAT were then computed for the remainder of the white matter up to the pial surface of the cord. C) and D) Higher power views of the L-dCST and R-dCST, respectively, showing single DiI+ve cells and their Hoechst-stained nuclei. Each DiI+ve cell with a red fluorescent cell body (red arrowhead) and a blue Hoechst stained nucleus (white arrow) was counted. Bar in 'A' = 400 μm and applies to both 'A' and 'B'; Bar in 'C' = 100 μm and applies to both 'C' and 'D'.

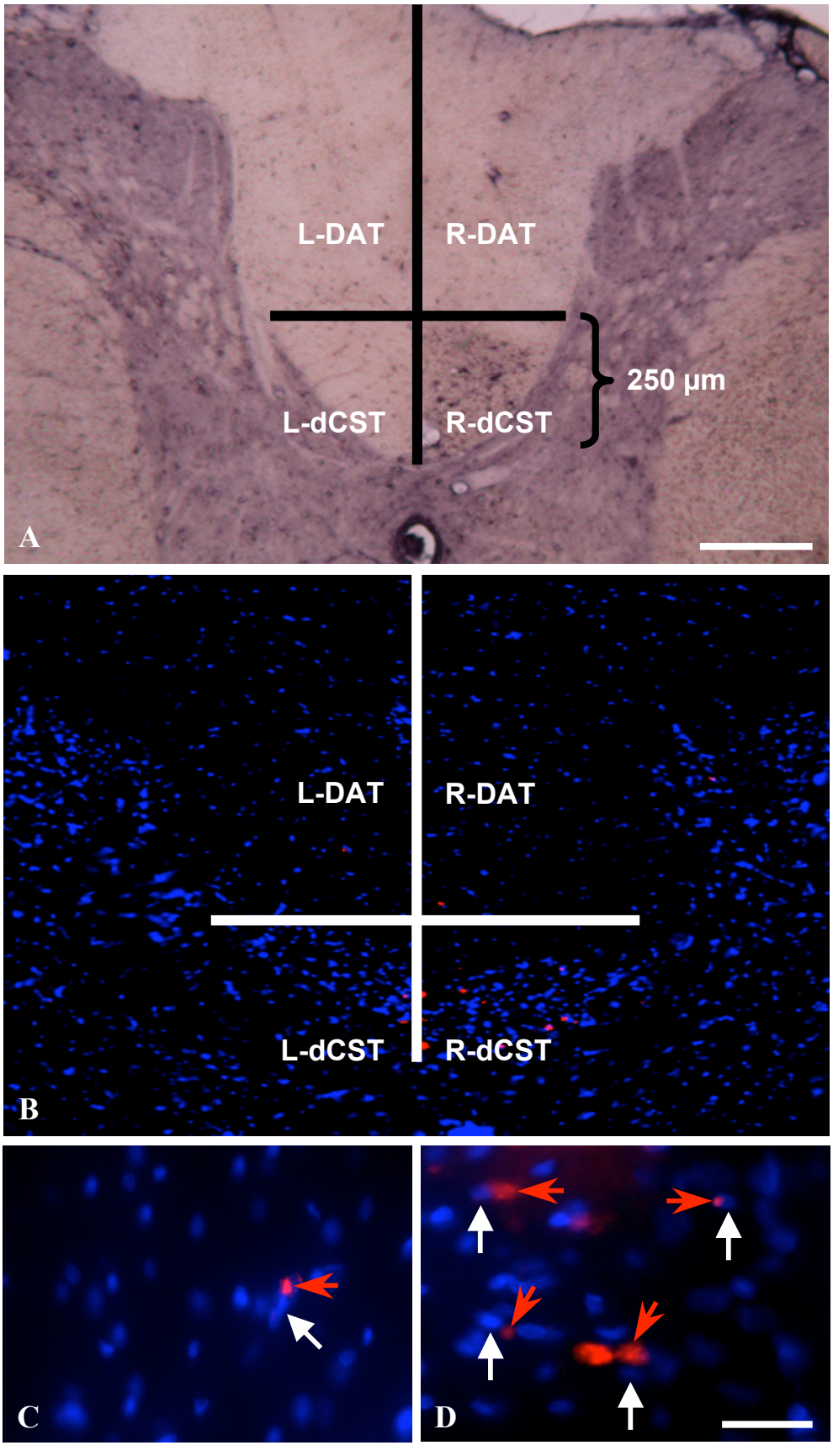
L-DAT
R-DAT
250 µm
L-dCST
R-dCST
A
L-DAT
R-DAT
L-dCST
R-dCST
B
C
D

FIGURE 4.11: Reproducibility of DiI+ve Cell Counts

Histogram depicting the mean number (+/- SEM) of DiI+ve cells (Y-axis) in the R-dCST/L-dCST (A) and in the R-DAT/L-DAT (B) of 14 tissue sections from the T11 spinal cord segment of rats in Groups 1 (n = 7 sections) and 2 (n = 7 sections). The first and second cell counts for the dCST, L-dCST, R-DAT and L-DAT were each computed 10 days apart. A t-test was applied to the data, with the data for the R-dCST (A), L-dCST (A), R-DAT (B), and L-DAT (B) being analyzed separately for statistical significance. The t-tests showed no significant differences between the first and second cell counts for any of the four fiber tracts.

A

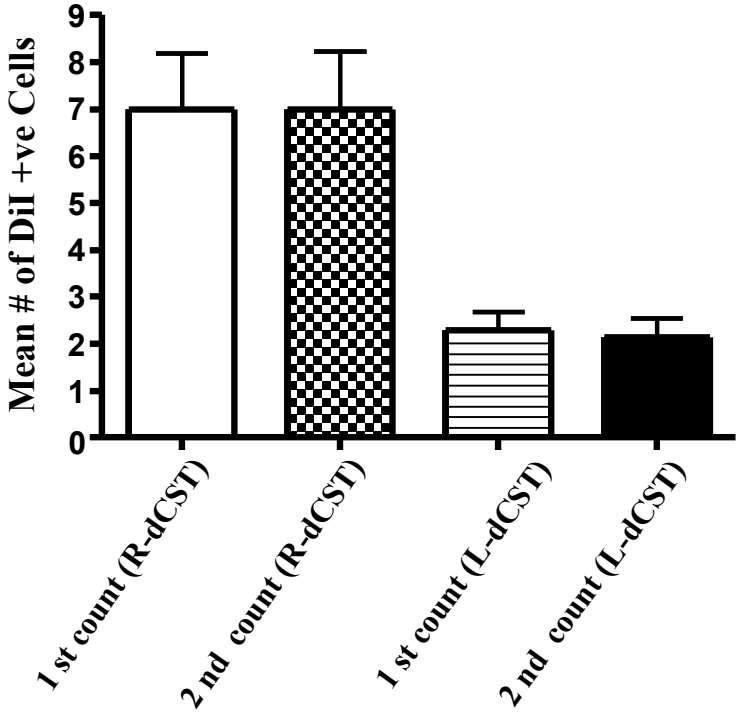
Mean # of DiI +ve Cells
0
1
2
3
4
5
6
7
8
9
1 st count (R-dCST)
2 nd count (R-dCST)
1 st count (L-dCST)
2 nd count (L-dCST)

B

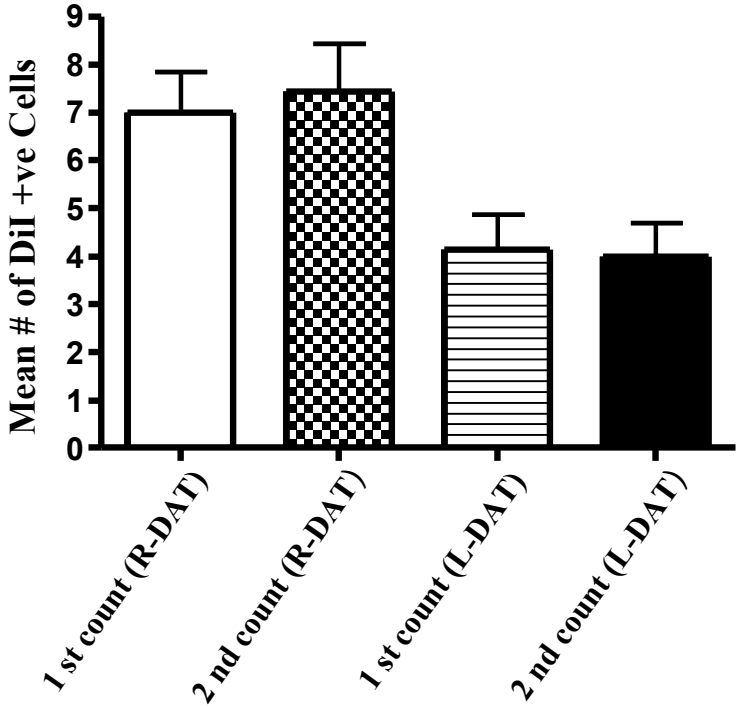
Mean # of DiI +ve Cells
0
1
2
3
4
5
6
7
8
9
1 st count (R-DAT)
2 nd count (R-DAT)
1 st count (L-DAT)
2 nd count (L-DAT)

FIGURE 4.12: Comparison of OX42 immunostained and Hoechst fluorescence defined areas of the dCST and of the DAT.

Histogram depicting the mean area (+/- SEM) in square microns (Y-axis) of the R-dCST/L-dCST (A) and of the R-DAT/L-DAT (B) as measured using fluorescence optics (Hoechst-stained sections; n = 12 tissue sections) and brightfield optics (OX42 immunostaining; n = 12 sections) on tissue sections from the T11 spinal cord segment of rats in Groups 1 (n = 3 sections) and 2 (n = 9 sections). The left sensorimotor cortex of each rat had been lesioned 16 weeks prior to perfusion, with the grafting of DiI+ve OECs into the right DF of T12 being done 8 weeks prior to perfusion. The rats received daily injections of either saline (Group 2) or minocycline (Group 1) for 6 weeks, with the daily treatments beginning 2 weeks before and ending 4 weeks after the OECs were grafted at T12. A t-test was applied to the data, with the area measurements for the R-dCST (A), L-dCST (A), R-DAT (B), and L-DAT (B) being analyzed separately for statistical significance. The t-tests showed significantly larger areas for the R-dCST and L-dCST when they were measured on the OX42 immunostained tissue sections as compared to the Hoechst-stained sections; $t(22) = 9.1$, $p<0.0001$ (single asterisk) (R-dCST); $t(22) = 6.4$, $p<0.0001$ (single asterisk) (L-dCST). Conversely, the t-tests showed significantly smaller areas for the R-DAT and L-DAT when they were measured on the OX42 immunostained tissue sections as compared to the Hoechst-stained sections; $t(22) = 5.0$, $p<0.0001$ (single asterisk) (R-DAT); $t(22) = 4.1$, $p<0.0005$ (double asterisks) (L-DAT).

A

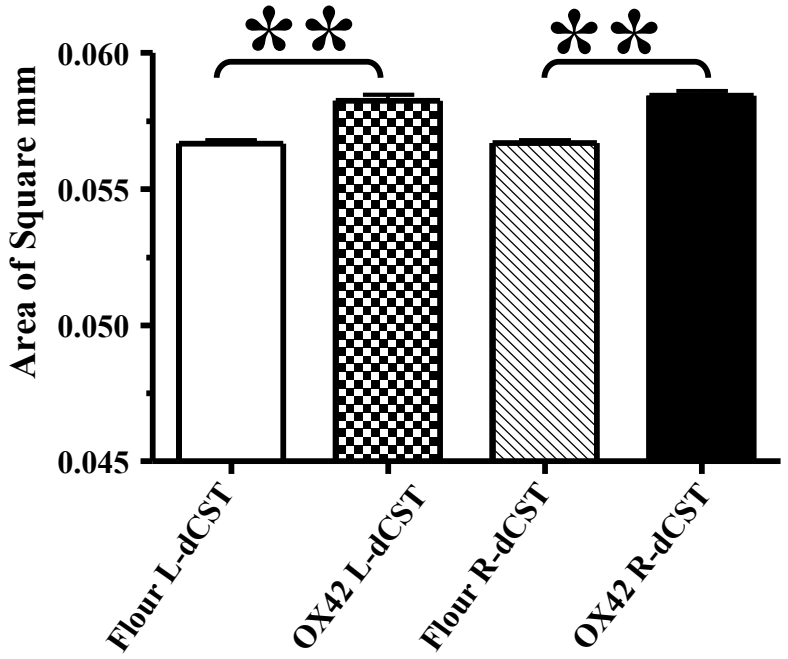
**
**
0.060
0.055
0.050
0.045
Area of Square mm
Flour L-dCST
OX42 L-dCST
Flour R-dCST
OX42 R-dCST

B

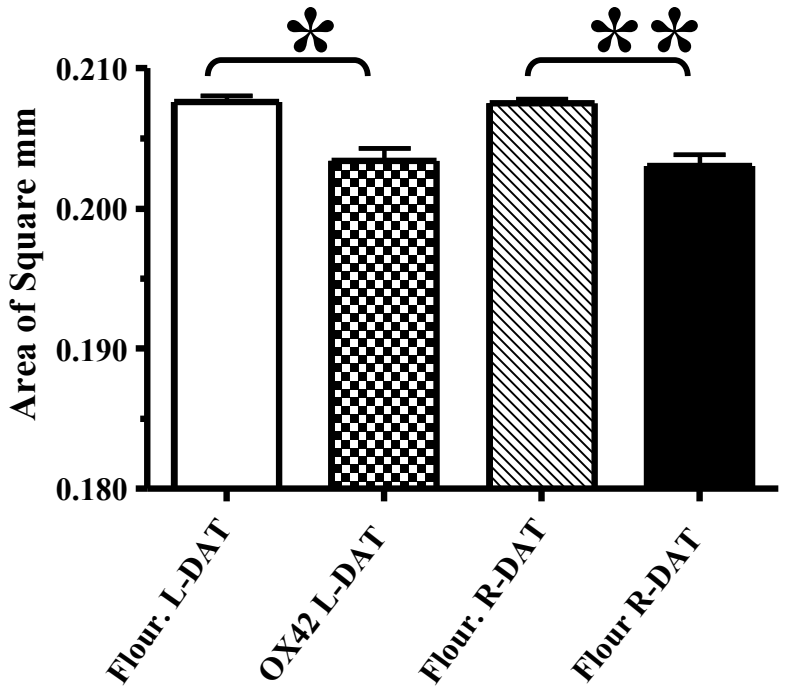
*
**
0.210
0.200
0.190
0.180
Area of Square mm
Flour. L-DAT
OX42 L-DAT
Flour. R-DAT
Flour R-DAT

FIGURE 4.13: Density of DiI+ve cells in the right dCST of T11 in Groups 1-4.

Histograms depicting the mean number (+/- SEM) of DiI+ve cells per 0.05mm^2 area in the right dCST of the rostral (A), middle (B) and caudal (C) third of the T11 spinal cord segment at 8 weeks after grafting DiI+ve OECs into the right DF of T12. The left sensorimotor cortex of rats in Groups 1 and 2 was lesioned 8 weeks prior to the cell grafting. All rats received daily injections of either saline (Groups 2 and 4) or minocycline (Groups 1 and 3) for 6 weeks, with the daily treatments beginning 2 weeks before and ending 4 weeks after the OECs were grafted at T12 (n=4 for each Group). A two-factor analysis of variance (ANOVA) was applied to the data, with the data for the rostral (A), middle (B) and caudal (C) thirds of T11 being analyzed separately for statistical significance. Multiple post hoc comparisons were performed with Bonferonni's multiple comparison post-test. Bonferonni's post-test revealed the density of DiI+ve cells in the right dCST was significantly higher ($p<0.05$; brackets) in the saline-treated cortical lesion group than in either the saline-treated no lesion group or the minocycline-treated cortical lesion group at the rostral (A), middle (B) and caudal (C) levels of T11. The post-test also revealed a significant reduction in the density of DiI+ve cells in the right dCST of the no lesion group as a consequence of the minocycline treatment ($p<0.05$; brackets), but this significant difference was only seen in the dCST of the rostral T11 (A).

A

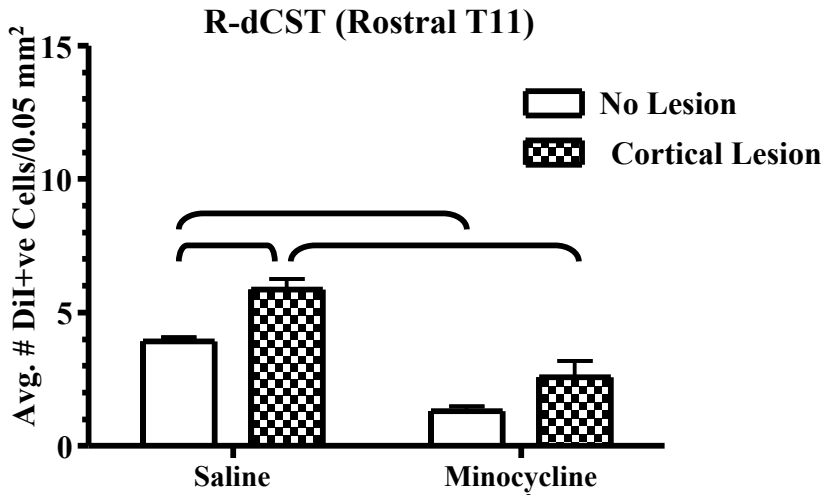
R-dCST (Rostral T11)
No Lesion
Cortical Lesion
Avg. # DiI+ve Cells/0.05 mm2
15
10
5
0
Saline
Minocycline

B

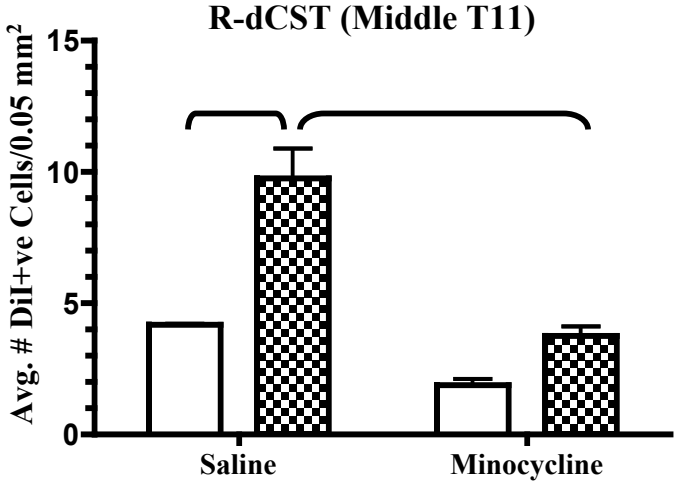
R-dCST (Middle T11)
Avg. # DiI+ve Cells/0.05 mm2
15
10
5
0
Saline
Minocycline

C

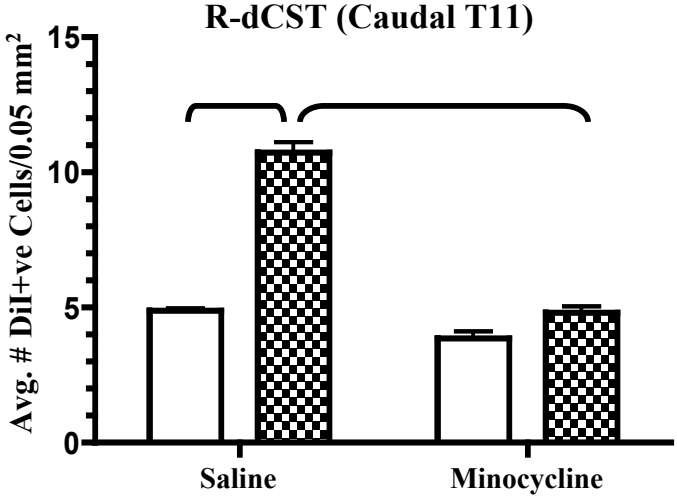
R-dCST (Caudal T11)
Avg. # DiI+ve Cells/0.05 mm2
15
10
5
0
Saline
Minocycline

FIGURE 4.14: Density of DiI+ve cells in the right DAT of T11 in Groups 1-4. Histograms depicting the mean number (+/- SEM) of DiI+ve cells per 0.05 mm^2 area in the right DF of the rostral (A), middle (B) and caudal (C) third of the T11 spinal cord segment at 8 weeks after grafting DiI+ve OECs into the right DF of T12. The left sensorimotor cortex of rats in Groups 1 and 2 was lesioned 8 weeks prior to the cell grafting. All rats received daily injections of either saline (Groups 2 and 4) or minocycline (Groups 1 and 3), with the daily treatments beginning 2 weeks before and ending 4 weeks after the OECs were grafted at T12 (n=4 for each Group). A two-factor analysis of variance (ANOVA) was applied to the data with the data for the rostral (A), middle (B) and caudal (C) thirds of T11 being analyzed separately for statistical significance. Multiple post hoc comparisons were performed with Bonferonni's multiple comparison post-test. Bonferonni's post-test revealed the density of DiI+ve cells in the right DAT was significantly higher ($p<0.05$; brackets) in the saline-treated cortical lesion group than in the minocycline-treated cortical lesion group at the rostral (A) middle (B) and caudal (C) levels of T11. The post-test also revealed a significant reduction in the density of DiI+ve cells in the right DF of the no lesion group as a consequence of the minocycline treatment ($p<0.05$; brackets), at all levels of the T11 spinal cord segment. In addition, the density of DiI +ve cells in the right DAT was significantly higher ($p<0.05$ bracket) in the saline-treated cortical lesion group than in the saline treated no lesion group only at the caudal (C) level of T11.

A

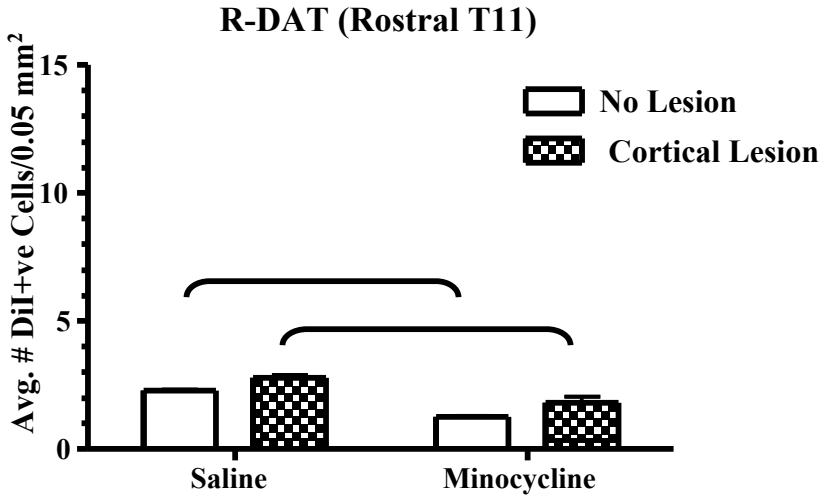
R-DAT (Rostral T11)
Avg. # DiI+ve Cells/0.05 mm2
15
10
5
0
No Lesion
Cortical Lesion
Saline
Minocycline

B

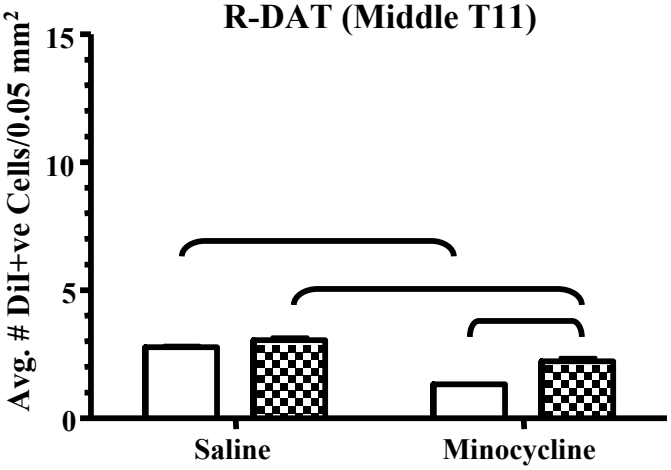
R-DAT (Middle T11)
Avg. # DiI+ve Cells/0.05 mm2
15
10
5
0
Saline
Minocycline

C

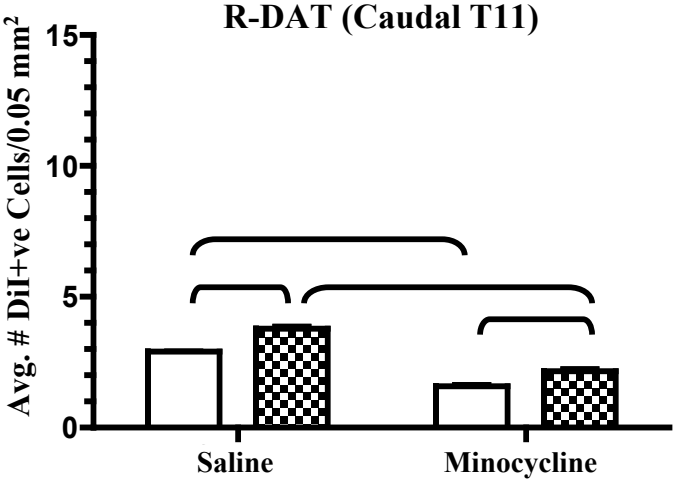
R-DAT (Caudal T11)
Avg. # DiI+ve Cells/0.05 mm2
15
10
5
0
Saline
Minocycline

FIGURE 4.15: Density of DiI+ve cells in the left dCST of T11 in Groups 1-4.

Histograms depicting the mean number (+/- SEM) of DiI+ve cells per 0.05 mm^2 area in the left dCST of the rostral (A), middle (B) and caudal (C) third of the T11 spinal cord segment at 8 weeks after grafting DiI+ve OECs into the right DF of T12. The left sensorimotor cortex of rats in Groups 1 and 2 was lesioned 8 weeks prior to the cell grafting. All rats received daily injections of either saline (Groups 2 and 4) or minocycline (Groups 1 and 3) with the daily treatments beginning 2 weeks before and ending 4 weeks after the OECs were grafted at T12 (n=4 for each Group). A two-factor analysis of variance (ANOVA) was applied to the data with the data for the rostral (A), middle (B) and caudal (C) thirds of T11 being analyzed separately for statistical significance. Multiple post hoc comparisons were performed with Bonferonni's multiple comparison post-test. Bonferonni's post-test revealed the density of DiI+ve cells in the left dCST was significantly higher ($p<0.05$; brackets) in the saline-treated cortical lesion group than in the minocycline-treated cortical lesion group at the rostral (A), middle (B) and caudal (C) levels of T11.

A

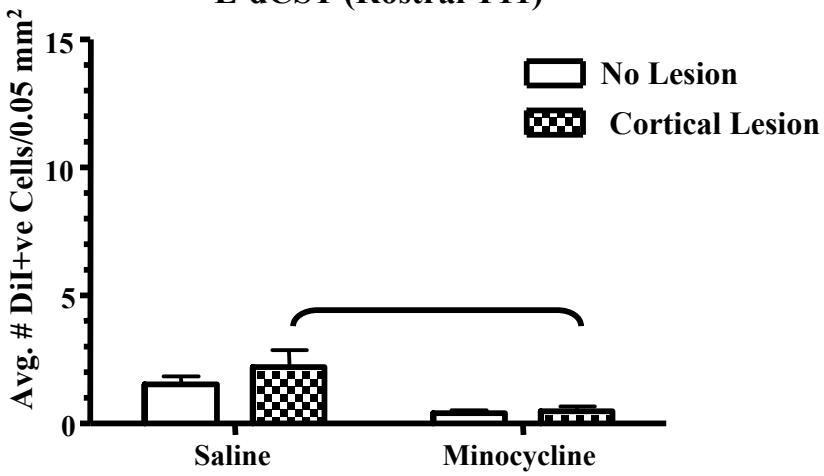
L-dCST (Rostral T11)
No Lesion
Cortical Lesion
Avg. # DiI+ve Cells/0.05 mm2
15
10
5
0
Saline
Minocycline

B

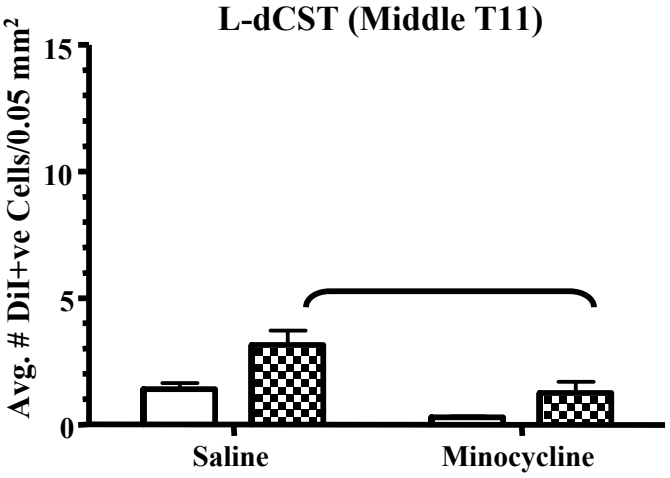
L-dCST (Middle T11)
Avg. # DiI+ve Cells/0.05 mm2
15
10
5
0
Saline
Minocycline

C

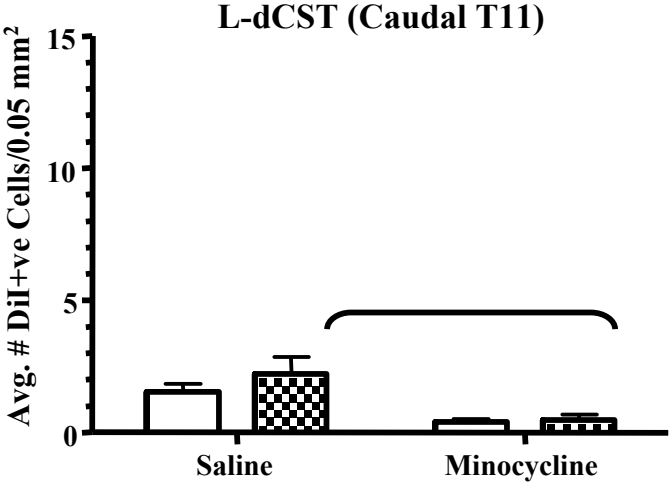
L-dCST (Caudal T11)
Avg. # DiI+ve Cells/0.05 mm2
15
10
5
0
Saline
Minocycline

FIGURE 4.16: Density of DiI+ve cells in the left DAT of T11 in Groups 1-4.

Histograms depicting the mean number (+/- SEM) of DiI+ve cells per 0.05mm^2 area in the left DAT of the rostral (A), middle (B) and caudal (C) third of the T11 spinal cord segment at 8 weeks after grafting DiI+ve OECs into the right DF of T12. The left sensorimotor cortex of rats in Groups 1 and 2 was lesioned 8 weeks prior to the cell grafting. All rats received daily injections of either saline (Groups 2 and 4) or minocycline (Groups 1 and 3), with the daily treatments beginning 2 weeks before and ending 4 weeks after the OECs were grafted at T12 (n=4 for each Group). A two-factor analysis of variance (ANOVA) was applied to the data with the data for the rostral (A), middle (B) and caudal (C) thirds of T11 being analyzed separately for statistical significance. Multiple post hoc comparisons were performed with Bonferonni's multiple comparison post-test. Bonferonni's post-test revealed the density of DiI+ve cells in the left DAT was significantly higher ($p<0.05$; brackets) in the saline-treated groups than in their respective minocycline-treated groups at the rostral (A), middle (B) and caudal (C) levels of T11. In addition, the density of DiI +ve cells in the left DAT` was significantly higher ($p<0.05$; brackets) in the minocycline-treated cortical lesion group than in the minocycline-treated no lesion groups at the middle (B) level of T11.

A

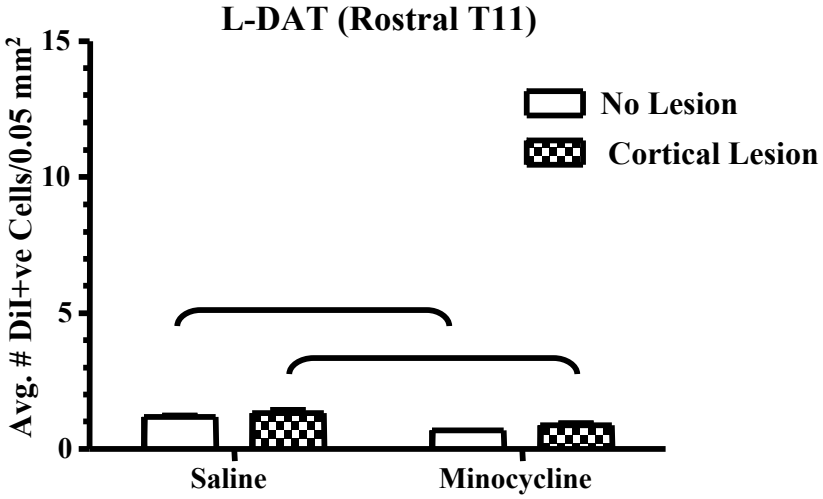
L-DAT (Rostral T11)
No Lesion
Cortical Lesion
Avg. # DiI+ve Cells/0.05 mm2
15
10
5
0
Saline
Minocycline

B

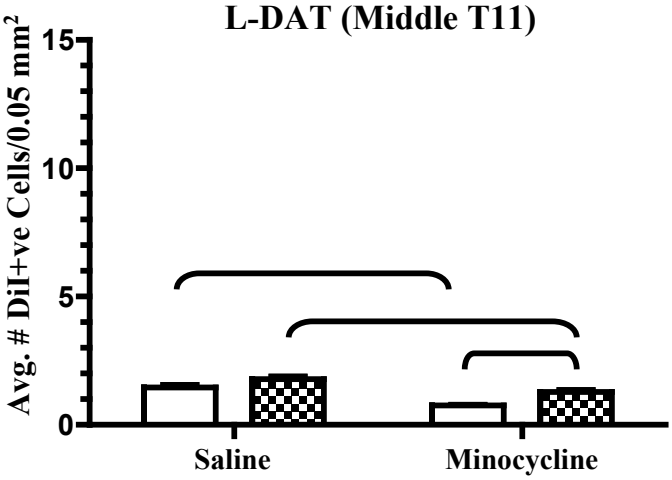
L-DAT (Middle T11)
Avg. # DiI+ve Cells/0.05 mm2
15
10
5
0
Saline
Minocycline

C

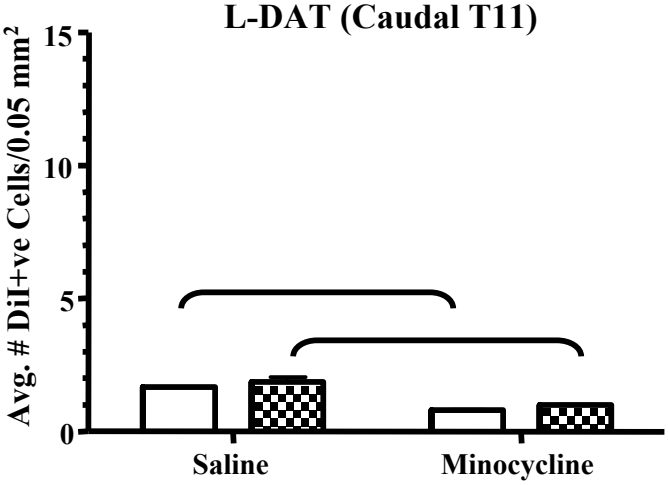
L-DAT (Caudal T11)
Avg. # DiI+ve Cells/0.05 mm2
15
10
5
0
Saline
Minocycline

4.4 Discussion

4.4.1 Sensorimotor Cortex Aspiration as a Tool for Confining Wallerian Degeneration-Induced Glial Reactivity to a Single CNS Fiber Tract

The simplest model of axon degeneration known to date is the self-destructive process observed at the distal portion of transected axons upon injury, termed "Wallerian degeneration". The Process of WD is common in a variety of degenerative disorders (Raff et al., 2002). Given that WD is an active progression, it was hypothesized (Finn et al., 2000) that this self-destructive process of injured axons might be a type of cytoskeletal reorganization. Interestingly, axons undergoing WD do not possess detectable activation of the caspase family of cysteine proteases (Finn et al., 2000), suggesting that WD in axons and programmed cell death in the neuronal perikarya may be two distinct self-destruct programs (Raff et al., 2002). Since the objective of this part of the study was to determine whether WD-induced microglial reactivity contributed to the generation of a migratory signal(s), it was important to restrict such glial reactivity to a specific CNS fiber tract. Although WD is known to occur in many types of chronic neurodegenerative diseases and after injury to axons caused by toxic, ischemic, or traumatic insults (Raff et al., 2000), the sensorimotor cortex aspiration model used in this experiment has several advantages over models used by other investigators to induce WD of CNS axons. The first advantage was that it induced glial reactivity by means of an irreversible injury; as a result of destroying the neuronal cell body of CST axons, there was no possibility of these axons regenerating into the CST at T11 and influencing the responsiveness of the microglia and astroctyes. A second advantage was the restriction of the glial reactivity in the dorsal funiculus of the spinal cord to a single fiber tract, leaving axons in the remainder of this area of white matter intact. Thirdly, it eliminated the need for toxic or direct SCI to cause WD-induced glial reactivity. Fourthly, since the BBB in the spinal cord is left intact after sensorimotor cortex aspiration, the recruitment of inflammatory-blood borne cells (e.g., monocytes, neutrophils, etc.) into the dorsal funiculus of T11 should be no greater than in normal tissue.

4.4.2 Wallerian Degeneration-Induced Glial Reactivity: Microglial Contribution to Generation of a Migratory Signal(s)

Over the last decade, there has been increasing interest in the role of reactive microglia in the process of SCI and repair (Dihne et al., 2001; Giordana et al., 1994; Kreutzberg, 1996; Stence et al., 2001). In the experiments reported in this chapter, the reactive microglia, and to a lesser extent reactive astrocytes, accumulated in the right dCST of T11 in response to the WD of axons in this fiber tract. Following CNS damage in which the BBB is broken down, the activated microglia at the site of the lesion are derived mainly from blood-borne recruited monocytes (Giulian et al., 1989). However, in CNS fiber tracts undergoing WD, reactive microglia are primarily derived from resident microglia (Lawson et al., 1994; Liu et al., 2003). Thus, in addition to contributing to the removal of axonal debris, the conversion of resting microglia into reactive microglia, and with the assistance of reactive astrocytes, might partly have functioned in filling the space created by the loss of axons in the dCST during WD.

The confinement of a significantly higher number of DiI+ve OECs to the right dCST of sensorimotor cortex lesioned rats (i.e. Group 2) and a significant reduction in the number of DiI+ve OECs in this fiber tract after minocycline treatment (i.e. Group 1) collectively point to reactive microglia as a potential source of migratory signals inducing the migration of OECs within the right dCST. This study revealed that OECs preferentially migrated along the path of microglial reactivity in the right dCST as compared to the adjoining parts of white matter in the right DAT. In fact, the presence of large and significant number of DiI+ve OECs in the right dCST (i.e Group 2) where the reactive microglia and any remnants of WD debris were located supports a potential key role of microglia in guiding OEC migration toward the lesion site. In addition, the OECs that migrated along this path of WD-induced microglial reactivity might have a potential role in neural repair, a subject that was not the focus of this research project.

Further support for the contribution of microglia to generation of a migratory signal(s) is provided by the significant reduction in numbers of DiI+ve OECs that were seen in the right dCST of minocycline-treated rats in Group 1. After peripheral nerve injury, macrophages rapidly infiltrate the distal nerve stumps and remove axonal debris

and growth inhibitory myelin debris (Bruck, 1997; Stoll et al., 1989). However, macrophages are virtually excluded from CNS fiber tracts (George and Griffin., 1994), leaving the job of phagocytic removal of the debris arising from WD to microglia (Flaris et al., 1993). The lack of spontaneous nerve regeneration in the CNS might be due to the microglia not being activated to the same extent as macrophages in the PNS (Stoll et al., 1989). In the present study, microglia expressed the complement receptor 3 (OX42), CD4 (OX35), MHC class I (OX18), and the ED1 antigenic epitope. Reactive microglia in the right dCST contralateral to the cortical lesion continued to express each of these markers up to at least 16 weeks after cortex aspiration. The prominent presence of ED1+ve cells in the right dCST of sensorimotor cortex lesioned rats (Groups 1 and 2) (Fig. 4.6) also indicated the responsiveness of the microglia to the degenerated fibers and myelin debris. Stoll et al. (2004) proposed that TGF-ß2 is a major player in the slower phagocytic response by microglia to WD. They showed, for example, that TGF-ß2 almost completely blocked the myelin phagocytosis by microglia *in vitro*. Similarly, they reported that 1`phagocytosis of myelin debris by peritoneal macrophages that were added to degenerating peripheral nerve segments *in vitro* was reduced by 50% in the presence of TGF-ß2 (Stoll et al., 2004).

The purpose of the present study was to examine the effect of reactive microglia on the migration of OECs using an irreversible injury model that involved destroying the sensorimotor cortex. The activation of microglia in the dCST at T11 as a consequence of WD of the axons in this fiber tract is slow to appear, as indicated by the use of antibodies to the OX42, OX18, OX35 and ED1 antigenic epitopes. It took at least 4-6 weeks for the first reactive microglia to be detected in the spinal cord (i.e. at both C6 and T11). This slow microglial response to axonal degeneration may have effects on the expression and secretion of chemotactic factors that may be needed to produce a favorable environment for OEC migration. The presence of reactive microglia within the right dCST may not only assist in clearance of the axonal and myelin debris but also could release various bioreactive substances that may facilitate not only OEC migration but also collateral sprouting by axons left intact due to the exclusion of their perikarya from the aspiration lesion. Although the intent was to use an irreversible injury model, due to the incompleteness of the sensorimotor cortex injury (due in large part to the vast surface

area of cerebral cortex contributing axons to the CST) it is possible there was some axonal sprouting from spared CST axons, particularly unmyelinated ones. If such sprouting occurred, then the presence of OECs within the dCST may facilitate this aspect of neural repair. At this time no study was done on the effect of reactive microglia on promoting sprouting of dCST axons.

4.4.3 Wallerian Degeneration-Induced Glial Reactivity: Potential Migratory Signal(s) Inducing OECs to Migrate

The WD-induced microglial reactivity directly and/or indirectly contributed to the generation of a migratory signal(s) inducing OECs to migrate along the dCST that contained this glial reactivity. Although much more work is required to identify the specific migratory signal(s) at the molecular level, it is possible to speculate on likely candidates for these signals, which may include cytokines, chemokines, growth factors, and MMPs. For example, since OECs express at least one type of cytokine receptor (i.e. the IL-6 receptor; Nan et al., 2001) it is possible their migration along the right dCST was chemotactically guided by this as well as other chemotactic molecules secreted as a result of the WD-induced microglial reactivity. Whether OECs express any additional cytokine receptors remain to be determined, but it is well documented that microglia are an important source of both cytokines and chemokines.

Mechanical injury to nervous tissue, ischemia, or ATP release following injury cause microglial activation that induces these cells to secrete various substances including various chemokines and cytokines (Perrin et al., 2005) as well as neurotrophic factors (Neumann et al., 2006). That might be the case in the present study as well. Reactive microglia that accumulate at a lesion site would release neurotrophins such as BDNF, NGF, and NT3 (Batchelor et al., 1999; Batchelor et al., 2002), all of which have been shown to enhance axonal growth and neuronal survival (Batchelor et al., 1999). In addition, in the rat it has been shown that damage to the lens causes macrophages to release proteins that promote regeneration of retinal ganglion cell axons (Leon et al., 2000; Yin et al., 2006). It is possible that these survival factors may also contribute to migratory signals inducing the migration of OECs along the path of microglial reactivity in the right dCST, as seen in this study.

Microglia have been shown to be in contact with axon sprouts extending into collagen gels *in vitro* (Blackshaw et al., 1997; Babington et al., 2005). In the CNS of leech, an important role for the initial accumulation of microglia in the area of injury is in the sprouting of severed axons (Ngu et al., 2007). A key observation in the study by Ngu et al. (2007) was that when microglial cell migration and accumulation at the lesion site were reduced, axon sprouting was also reduced. How microglia might enhance sprouting and possibly regeneration of axons is not completely clear. However, there is evidence that in the leech CNS, microglia can secrete laminin and other growth-promoting molecules of the extracellular matrix in a path in front of the growing axons (Von Bernhardi and Muller, 1995).

Although this study did not determine which cytokines and/or chemokines were expressed in the right dCST of left sensorimotor cortex lesioned rats, a variety of these molecules can be assumed to have been present as a result of the WD-induced microglial reaction. For example, there is a rapid increase in expression of MCP-1, MIP-1α and IL-1ß at the lesion site in the hemisected spinal cord in adult mice by day 1 after injury (Perrin et al., 2005). The increased expression of MIP-1α, MCP-1 and IL-1ß mRNA after spinal cord hemisection may correlate with the rapid influx of immune cells and to the activation of macrophages at the site of lesion (Schnell et al., 1999). Even higher levels of expression of chemokines (MCP-1, MIP-1α, CCL2, CCL3) and cytokines (TNF-α, IL-1ß, IL-6), have also been reported in the first 24-48 h at the site of a spinal cord contusion injury (Rice et al., 2007; Pan et al., 2002). Differences in the expression levels of specific cytokines and chemokines may reflect the fact that a hemisection, in comparison to a contusion injury, is a much smaller lesion. Likewise, large traumatic injuries to the cerebral cortex or to the entorhinal cortex cause a substantial increase in MCP-1 (Glabinski et al., 1996; Babcock et al., 2003), IL-1ß and TNF-α (Rostworowski et al., 1997) at the site of the lesion.

In contrast to the rapid recruitment of large numbers of macrophages at the site of a lesioned peripheral nerve (Ma et al., 2002; Popovich et al., 1999), macrophages are recruited much more slowly into areas of CNS white matter undergoing WD (Bendszus and Stoll, 2003; Buss and Schwab, 2003). However, minimal expression of MCP-1, MIP-1α and IL-1ß in these areas of white matter may account for the lack of recruitment

and activation of microglia. The injection of recombinant MCP-1 and MIP-1α into areas of spinal cord white matter undergoing WD induced a rapid increase in the number of activated microglia and rapid myelin phagocytosis (Perrin et al., 2005). The origin of these activated microglia is not known, but they are likely to be of endogenous microglial origin. It has been reported that monocyte recruitment and myelin clearance at the site of a contusion injury in the spinal cord is reduced in CCR2 chemokine receptor null mice; this receptor is a major receptor for MCP-1 (Ma et al., 2002). It has also been shown that MCP-1 and MIP-1α contribute to the recruitment of monocytes and activation of macrophages in lysophosphatidylcholine-induced demyelination in mouse spinal cord (Ousman and David, 2001). These and other studies indicate that under certain conditions, peripheral macrophages can be recruited into the CNS (Tran et al., 1998; Popovich et al., 1999). In addition to their potential beneficial effects on axon regeneration by means of clearing myelin debris, microglia/macrophages have also been shown to secrete growth factors that promote remyelination by oligodendrocyte progenitor cells (Kotter et al., 2001).

Growth factors may also have played a role in regulating OEC migration. For example, GDNF has been shown to be involved in cell migration; GDNF signaling through the Ret receptor tyrosine kinase and a glycosyl phosphatidylinositol (GPI)-linked ligand-binding subunit known as GFRα-1 was required for the migration of parasympathetic neuronal precursors during early embryonic development (Enomoto et al., 2000). In an *in vitro* and *in vivo* study, GDNF also significantly promoted OEC migration (Cao et al., 2006). In addition, GDNF has been reported to be a potent survival factor for midbrain dopaminergic neurons (Lin et al., 1993) and has been proposed as a potential therapeutic agent for the treatment of neurodegenerative diseases (Lapchak, 1996). Previous studies have shown that the transplantation of OECs genetically modified to secrete high levels of GDNF resulted in significantly improved recovery after SCI (Cao, et al., 2004). Although the underlying mechanisms are not understood, it is likely that the GDNF secreted by these genetically modified OECs had not only promoted neural repair, but also influenced the OECs themselves, given the suggested chemotactic role of this growth factor as supported by the findings of Cao et al. (2006).

Interestingly, Lai and Todd (2006) showed that minocycline had no effect on GDNF expression by microglia *in vitro*. Whether microglial expression of GDNF is similarly unaffected by minocycline treatment *in vivo* is not known at present. However, the findings of the experiments reported in this chapter demonstrated that the minocyline treatment reduced the microglia reactivity and was also accompanied by a significant decrease in the number of DiI+ve OECs in the right dCST. If GDNF is one of the migratory signals secreted by reactive microglia in the right dCST, then one can speculate that the minocycline treatment in our *in vivo* animal model must have decreased GDNF expression by the microglia in addition to having dampened their reactivity to the WD of the CST axons.

The motility of a cell depends on reorganization of the actin cytoskeleton and the development of cell polarity. Actin polymerization, extension of lamellipodia and filopodia, and the formation of new attachment to the substratum must be coordinated with contractile elements to pull the cell along the substratum and to disrupt trailing attachments (Ridley, 2001). It was found that treatment of OECs *in vitro* with GDNF induced actin filament redistribution as well as an upregulation of cytoskeleton proteins in the cytoplasmic processes of OECs. Such an effect of GDNF on the cytoskeleton of OECs is likely to influence their migration. However, further study is necessary to elucidate the underlying mechanism. A recent report has demonstrated that NCAM can act as a receptor for GDNF. GDNF binding to NCAM stimulated Schwann cell migration as well as axonal growth by hippocampal and cortical neurons (Paratcha et al., 2003). In addition, the JNK signaling pathway has been shown to play a role in regulating cell migration (Yamauchi et al., 2002). Cao and coworkers (2006) showed that Src kinase activation, which plays a role in JNK activation during cell migration, was essential for the GDNF-induced migration of OECs. Further study is necessary to clarify the details of the signaling mechanism through which JNK is involved in GDNF-mediated OEC migration. It has been reported that during development, OECs migrating toward the OB were guided by soluble factors from the OB (Liu et al., 1995). Moreover, GDNF is highly expressed in the OB neurons (Buckland and Cunningham, 1998). Therefore, it is likely that the secreted GDNF from OB might be one of the factors that promote OECs migration toward the OB during embryonic development. Whether GDNF

may have contributed towards the generation of migratory signal(s) to induce OEC migration into the right dCST in saline-treated sensorimotor cortex aspirated rats should be addreesed in future experiments.

BDNF is part of the neurotrophin family of secreted proteins, which are essential for the development and functioning of the vertebrate nervous system. BDNF can signal through two types of cell-surface receptors: the tyrosine kinase receptor TrkB and the p75 pan-neurotrophin receptor (Segal et al., 1995). Previously, several studies have shown that OECs produce BDNF *in vitro*, in addition to other neurotrophic factors (Woodhall et al., 2001 and Lipson et al., 2003). Furthermore, BDNF has been found *in vivo* in association with OEC grafts in the injured rat spinal cord (Sasaki et al., 2006). However, direct evidence implicating BDNF in the stimulation of non-olfactory CNS axon growth by grafted OECs is still lacking. BDNF is expressed in cerebellar granule cells (Rocamora et al., 1993) and the level of BDNF expression increases during development. Granule cells also express the high affinity BDNF receptor TrkB (Segal et al., 1995). It was shown that BDNF stimulates the migration of granule cells. Both *in vivo* and *in vitro* studies demonstrated that the migration of granule cells was impaired in the absence of BDNF (Borghesani et al., 2002). Interestingly the impaired migration of granule cells can be rescued by exogenous BDNF, indicating that it is a direct result of the lack of BDNF. That microglial-derived BDNF may have had a chemotactic effect on OECs is thus a possibility worth considering since the BDNF receptor (i.e. trkB) is also expressed by OECs (Bianco et al., 2004).

Matrix metalloproteases released by reactive microglia in response to the WD may also have contributed to the generation of a migratory signal(s) for OECs by creating a more favorable extracellular milieu. For example, the MMPs could break cell-matrix contacts and possibly activate cytokine precursor molecules (e.g. pre-IL-6); any of these processes would contribute to the generation of a chemotactic gradient for OEC migration. It was shown that OECs expressed the IL-6 receptor (Nan, 2001). A recent study by Pastrana et al. (2007) showed that the proportion of adult neurons that regenerate their axons was increased on OEC monolayer by adding BDNF. Combining BDNF with MMP2 further enhanced this effect. The possible release of both MMP2 and BDNF by activated microglia in our experimental animal model can be speculated. These

factors might contribute to the creation of a migratory path that supports and enhances OEC migration into the right dCST.

4.4.4 Potential Direct Effect of Minocycline Treatment on OEC Migration

It appears that minocycline offers neuroprotection via the overall down-regulation of factors produced by reactive microglial, but it is also well known that reactive microglia produce a number of neuroprotective molecules as well (Polazzi and Contestabile, 2002). Such neuroprotective molecules include neurotrophic factors that activate neuronal survival cascades and non-secreted proteins such as transporters and enzymes, which function to scavenge toxic extracellular substances. Compared to the conventional "harmful" microglial factors, these "beneficial" proteins have been relatively overlooked in the past. The minocycline-induced inhibition of the production of these beneficial proteins by reactive microglia is likely to have deleterious effects. In both *in vivo* and *in vitro* models of stroke, minocycline was found to attenuate the production of microglial mediators of inflammation, such as nitric oxide (NO), pro-inflammatory cytokines, cyclooxygenases, and prostaglandins (Yrjanheikki et al., 1998; Suk, 2004). The anti-inflammatory effects of minocycline on WD-activated microglia are unknown, but the result of the sensorimotor cortex aspiration experiment showed a dampening of microglial response to this axon degeneration as indicated by immunohistochemical staining with the ED1, OX18, OX35 and OX42 monoclonal antibodies (Fig 4.6). The six week treatment with minocycline clearly also reduced the number of OECs that migrated into the R-dCST, supportive of a link between microglial reactivity and the migration of OECs. However, we cannot rule out the possibility that the minocycline might have had a direct effect on the OECs, an effect that might have influenced their migratory ability or their responsiveness to chemotactic cues.

4.5 Conclusion

The pilot study demonstrated that glial reactivity in the dCST of the T11 segment of the spinal cord that arises as a result of WD of CST axons was very slow to appear. It was concluded that 8 weeks after the sensorimotor cortex lesion was the best time point for grafting OECs into the T12 segment of the spinal cord since at this time point both

microglia and astrocytes in the dCST were reactive at the level of T11. From the immunostaining data, it appears that the intensity of the microglial reaction to these WD of CST axons is higher than that of astrocytes, which never did express detectable levels of nestin in the R-dCST.

Two conclusions can be drawn from the cell grafting experiment reported in this chapter. Firstly, the migratory path taken by DiI+ve OECs was preferentially within areas containing reactive microglia (i.e. within the R-dCST). Thus, there appears to be something different in areas of white matter containing reactive microglia that creates a more favourable environment for OEC migration than is present in adjacent areas of white matter that contain resting microglia. Secondly, the minocycline treatment both dampened microglial reactivity and significantly reduced the number of migrating DiI+ve OECs (summarized in Fig 4.17). The findings of this study link the presence of a migratory signal(s) both spatially and temporally with the WD-induced microglial reactivity. The sensorimotor cortex aspiration model may be useful for dissecting out the migratory signal(s) driving the migration of OECs in the adult rat spinal cord.

FIGURE 4.17: Main findings of cortical lesion study

OX42 immunostained tissue sections from the middle third of the T11 segment of the spinal cord at 16 weeks after left sensorimotor cortex aspiration in rats of Groups 2 (A, D) and 4 (C, F) show the microglial reactivity is confined to the right dCST. The histograms in 'B' and 'E' are the same one's depicted in Figs 4.14B and 4.15B, respectively. These micrographs and histograms illustrate the major findings of this study: (i) there was a significantly higher density of DiI+ve OECs within the right dCST of cortical lesioned rats as compared to rats with no cortical lesion; and ii) the migratory path taken by DiI+ve OECs was preferentially within areas containing reactive microglia (i.e. the dCST).

Right dCST - Middle T11

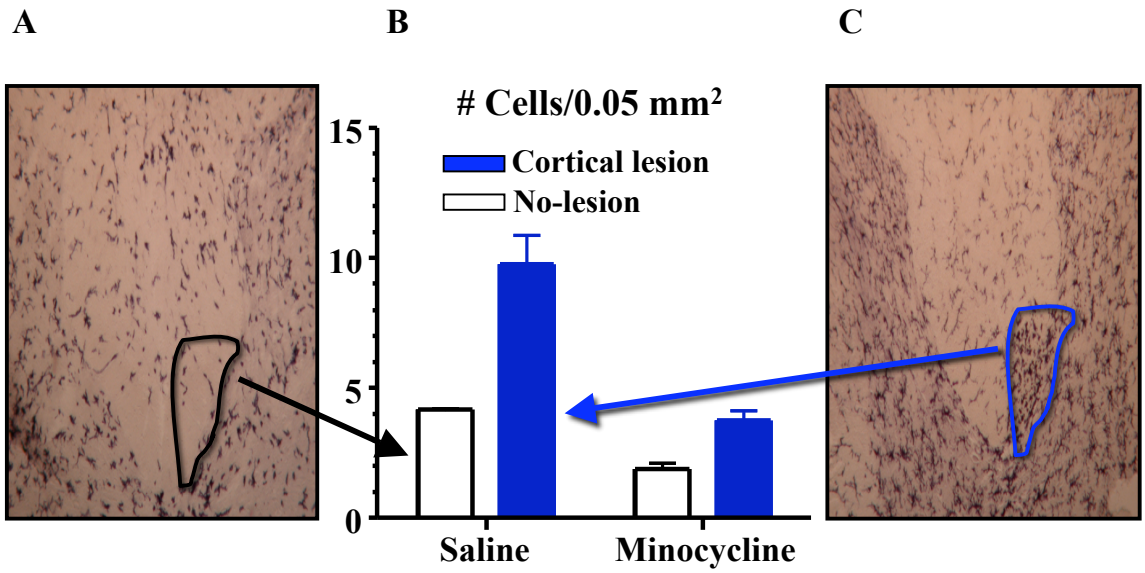

Right DAT - Middle T11

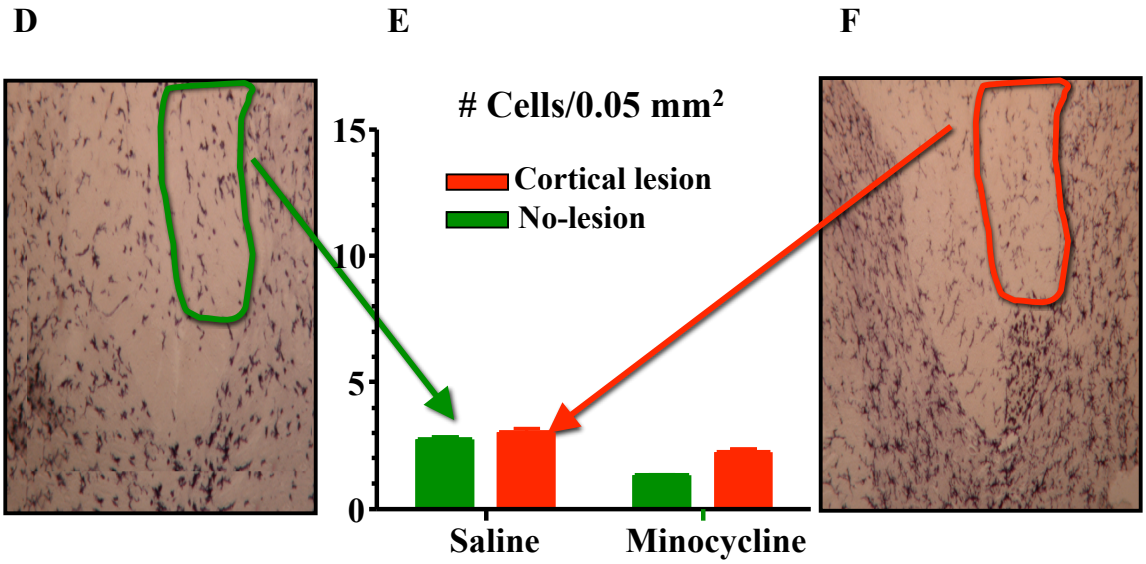

CHAPTER 5.0 OEC Migration in Response to TNF-α-Induced Glial Reactivity

5.1 Introduction

5.1.1 Tumor Necrosis Factor-α (TNF-α)

Tumor necrosis factor-α (TNF-α) is a potent, pleiotropic, proinflammatory cytokine that is produced by hematopoietic and nonhematopoietic cells, mainly macrophages, and in the CNS can be produced by activated astrocytes and microglia as well as CNS-infiltrating lymphocytes and macrophages (Palladino et al., 2003; Ware, 1995). TNF was named because of its ability to cause necrosis of tumors in experimental animal models when it was administrated in pharmocological doses (Carswell et al., 1975). TNF-α exerts its effect on cells by binding to one of two structurally related, but functionally distinct, receptors, namely the TNF-R1 (the p55 TNF receptor) and the TNF-R2 (p75 TNF receptor) receptors; these receptors are coexpressed by most cell types (Aggarwal, 2003; Peschon et al., 1998; Wallach et al., 1997), including glial, neuronal, and endothelial cells of the CNS (Dopp et al., 1997). The complexity of the action of TNF-α *in vivo* reflects factors such as the differential presence and activity of the soluble 17-kDa and cell-associated 26-kDa molecular forms of TNF-α, and to differential expression and cell signaling function of TNF-R1 and TNF-R2.

5.1.2 TNF-α signaling

Most biological activities classically attributed to TNF-α are mediated by binding to the TNF-R1 receptor. This receptor belongs to the death receptor family and can signal cell death by apoptosis (Wallach et al., 1997). In contrast, the TNF-R2 induces proliferation of thymocytes *in vitro* and possibly also plays a role in suppressing TNF-α mediated inflammatory responses *in vivo* (Peschon et al., 1998). The role of TNF-α in acute CNS pathology is complex. This may be largely due to the highly complex intracellular signaling pathways associated with the TNF-Rs, and to the fact that many ligands in addition to TNF-α can bind the TNF-Rs (reviewed in Wajant et al., 2003). The existence of two receptors contributes significantly to the diversity of cellular activities affected by the binding of TNF-α to these receptors due to their different tissue distribution and to their distinctly different intracellular signaling pathways following binding of the ligand (Aggarwal, 2003). Although TNF-R1 is constitutively expressed on

virtually all nucleated cells, expression of TNF-R2 is limited to immune cells and endothelial cells (Aggarwal, 2003). TNF-R2 does appear to have specific signaling functions in T-cells that lack the TNF-R1 receptor (Grell et al., 1998).

A big difference between the two receptors is the presence of a death domain on the cytoplasmic portion of TNF-R1 that is not found on TNF-R2. After TNF-α binding, signaling through TNF-R1 proceeds by recruitment of the TNF-receptor associated death domain (TRADD), the receptor-interacting protein (RIP), and TNF-R- associated factor 2 (TRAF2) to the cytoplasmic portion of TNF-R1. At this point, the presence in the cell of various accessory proteins determines whether signaling will lead to apoptosis or inhibition of apoptosis. Further recruitment of the Fas associated death domain (FADD) leads to the binding and activation of procaspase 8, which in turn activates caspase 3 to induce apoptosis (Ashkenazi et al., 1998). Alternatively, TRAF2 can recruit cellular inhibitors of apoptosis (cIAP-1 and cIAP-2) and activate signaling pathways leading to nuclear translocation of the anti-apoptotic NF-kB and activating protein 1 (AP-1) transcription factors, which upregulate genes necessary to increase inflammation and cell proliferation as well as block apoptosis (Baud and Karin, 2001).

Although TNF-R2 lacks the death domain and therefore cannot trigger apoptosis, it can still recruit TRAF2 and activate the NF-kB and AP-1 pathways. The path that a given cell takes is thus dependent on which receptor(s) is present as well as the gathering of other accessory proteins present in the cell. It has been reported that internalization of the TNF/TNF-R1 signaling complex is necessary for activation of apoptosis (Micheau et al., 2003; Schutze et al., 1999), whereas clustering of the TNF/TNF-R1 signaling complex in lipid rafts results in activation of the NF-kB and AP-1 pathways (Legler et al., 2003). This means of regulating the decision between cell death or cell survival could in part be controlled by the form of TNF-α encountered by the cell. The binding of soluble TNF-α is favored by TNF-R1 and therefore could signal in either direction. However, the binding of transmembrane TNF-α to TNF-R2 would result in a complex that is not internalized and is therefore unable to signal cell death.

5.1.3 Detrimental and Beneficial Proinflammatory Properties of TNF-α

TNF-α is recognized predominantly for its detrimental proinflammatory properties and their contribution to disease, but there is compelling evidence that chronic TNF-α expression *in vivo* leads to unique regulatory properties and that may be of benefit to tissue repair (Jacob et al., 1990). TNF-α can suppress the progression of autoimmune diseases *in vivo* when present systemically (Jacob et al., 1990) or expressed by target tissues (McSorley et al., 1997), and disease suppression is associated with depressed antigen-specific T-cell responses.

It would be interesting to induce EAE in transgenic mice that over express TNF-α in their glial compartments to determine whether similar beneficial effects are mediated during CNS autoimmunity induced pathology. Several mechanisms for such suppressive effects have been proposed, for example the attenuation of T-cell receptor (TCR) signaling (Cope et al., 1998). TNF-α can also directly induce apoptosis of CD8+ve and CD4+ve T cells *in vivo* (Zheng et al., 1995; Sytwu et al., 1996) and thereby may contribute to FasL/Fas-mediated signaling in the elimination of autoreactive T cells. It is particularly relevant that EAE induced in TNFR1-deficient mice results in a chronic disease with a profound increase in the number of inflammatory cells in the CNS tissue at late stages of disease progression (day 60 after immunization) and a marked reduction in T-cell apoptosis in the inflammatory infiltrates (Bachmann et al., 1999). These data indicate that TNF/TNFR1 signaling plays a major role in the removal of T cells from lesions, and therefore there may be undesirable endpoints when anti-TNF-α therapy is used during active T-cell-driven disease phases. Further evidence for regulatory effects has been obtained in TNF-deficient mice where myelin-specific T-cell reactivity fails to regress and expansion of activated/memory T cells results in an exacerbated pathology in the EAE animal model (Kassiotis and Kollias, 2001).

There is also evidence that TNF-α has an impact on the mechanisms involved in brain repair. For instance, TNF-deficient animals displayed a significant delay in remyelination, which was associated with reductions in the pool of proliferating oligodendrocyte progenitors and in the number of mature oligodendrocytes. TNF-R2, but not TNF-R1, mediated this detrimental effect on the reparative role of TNF-α (Arnett et al., 2001). TNF-R1 and TNF-R2 may also have opposing direct effects on neurons, with

the former having detrimental effects and the latter being neuroprotective (Fontaine et al., 2002). TNF-R1 has recently been shown to inhibit postnatal neurogenesis in the hippocampus (Losif et al., 2006). The exact mechanisms underlying such differential properties of these receptors have yet to be fully determined, but the dual activity of the cytokine may depend on the time and progression of the damage. In a model of traumatic brain injury, TNF-null mice exhibited less severe cognitive and motoneuron impairments than wild type mice in the acute post-traumatic period (Scherbel et al., 1999). While neurological functions following such traumatic brain injury recovered by 2–3 weeks post-injury in wild type mice, TNF-null animals still demonstrated motor deficits up to 4 weeks after injury. Brain damage at 4 weeks post-injury was also significantly more extensive in the TNF-deficient mice (Scherbel et al., 1999).

5.1.4 Major Role of TNF Signaling in CNS Inflammation and Demyelination

TNF-α released from macrophages, microglia or autoreactive T cells contribute to the pathogenesis of immune-mediated demyelination in both MS and EAE (Selmaj et al., 1991a, b; Probert and Selmaj, 1997). TNF-α has been detected within demyelinating lesions in postmortem MS brains (Hofman et al., 1989; Selmaj et al., 1991a; Woodroofe and Cuzner, 1993), and the concentration of TNF-α is elevated in the serum and cerebrospinal fluid (CSF) of patients with active MS (Hauser et al. 1990; Tsukada et al., 1991). The effects of TNF-α on cells *in vitro*, such as on astrocyte proliferation, on microglial proliferation and reactivity, and on endothelial cell activation are all consistent with an inflammatory role for this cytokine in the CNS and for a role in the induction of immune reactivity (Merrill and Benveniste, 1996). The TNF-α ligand/receptor system can trigger oligodendrocyte death, which is evidence of the role of this cytokine in demyelination. Both the TNF-R1 and the TNF-R2 receptors are selectively expressed on oligodendrocytes located at the edge of active MS lesions; TNF-α has been demonstrated to kill oligodendrocytes in primary cell cultures and to kill oligodendrocyte cell lines selectively (D'Souza et al., 1995; Selmaj and Raine, 1988).

A dominant role for the TNF-R1 in signaling both inflammation and demyelination in TNF-α transgenic mice was demonstrated by the finding that disease was completely abrogated when mice were bred onto a TNF-R1-deficient background

(Akassoglou et al., 1998). In contrast, expression of the TNF-α transgene on a TNF-R2-deficient background did not alter the disease phenotype. Further information concerning the mechanisms by which TNF-α can induce oligodendrocyte death and primary demyelination has also come from transgenic studies. In these studies, TNF-α, which can act as a soluble protein acting upon cell targets distant from its cellular source or as a transmembrane molecule that can exert its action only by cell-to-cell contact, was overexpressed in different CNS cell types (neurons, astrocytes and oligodendrocytes) using cell lineage-specific promoters. These TNF-α overexpressing cells established different cell contacts in the CNS. Among the cell types used in this study, microglia were the most appropriate source of TNF-α expression since they are immune-competent cells capable of expressing adhesion molecules and a variety of proinflammatory cytokines, including TNF-α. In addition, activated microglia/ macrophages together with astrocytes are the major source of TNF-α in MS and EAE lesions. CNS injuries are commonly damaging to neurons and oligodendrocytes, indicating that these cells are direct or indirect targets of TNF-α action (Akassoglou et al., 1997, 1999).

The relevance of results from transgenic studies has been supported by EAE studies done in mice deficient in TNF-α, or in one or both of its receptors (Frei et al., 1997; Kassiotis et al., 1999; Korner et al., 1997b; Liu et al., 1998; Suen et al., 1997). These studies demonstrated that TNF-α is not essential for CNS inflammation or demyelination because EAE can be induced in these mice and, thus, other mechanisms can compensate for TNF-α in its absence. However, TNF-α plays a critical proinflammatory role in the initiation of EAE and in the modulation of inflammatory cell trafficking into the CNS parenchyma (Kassiotis et al., 1999; Korner et al., 1997b). There is no clear consensus on the role of TNF-α in CNS acute injuries and understanding the contribution of TNF-α to brain repair and to disease progression represents a considerable challenge.

5.2 Materials and Methods

5.2.1 Anesthesia, Laminectomy, Analgesia, Wound Closure and Postoperative Care

In the experiments comprising this portion of the research project the rats underwent two surgeries, which were performed one after the other during the same surgical approach to the spinal cord. One of the surgeries was injection of vehicle (PBS) or of TNF-α (0.01ng/μl - 100 ng/μl) into the dorsal funiculus of the rostral part of T11; in the pilot study reported in Section 5.3.1 the rats were subjected to only one surgery, namely for saline or TNF-α injection. The other surgery was a laminectomy done to graft OECs into the dorsal funiculus exactly 5 mm caudal to the TNF-α/saline injection (Groups 5-10). The general surgical procedures involving anesthesia, analgesia, laminectomy, wound closure and postoperative care were as described in Sections 3.2.1, 3.2.2, and 3.2.4.

5.2.2 TNF-α Injections into Dorsal Funiculus

A pilot study was done to determine a concentration of TNF-α that would activate microglial cells in the ipsilateral dorsal funiculus over at least a 5 mm distance (the approximate rostrocaudal length of T11) and a second concentration of TNF-α for which the cytokine-induced microglial reaction would be limited to the vicinity of the injection site. A glass microcapillary was prepared using a micropipette puller (Model M1; Industrial Science Assoc., Inc, NY) and the tip was broken and polished. The microcapillary tip diameter was checked microscopically and only capillaries with a tip diameter of 15-20μm were used for the TNF-α injections. Immediately prior to use, each capillary was flushed with 70% ethanol followed by sterile 0.03 M PBS. Then the glass needle was connected to a 5 μl Hamilton syringe, which was then mounted onto a rodent stereotaxic apparatus using the syringe holder of a KD Scientific Syringe Pump (KDS 310). In the pilot study, solutions of five different concentrations of TNF-α (diluted in 0.03 M PBS) were loaded into separate microcapillaries that were attached to the 5 μl Hamilton syringe. The concentrations of TNF-α that were used included 0.01 ng/μl (n=6 rats), 0.1 ng/μl (n=6 rats), 1.0 ng/μl (n=10 rats), 10 ng/μl (n=10 rats), and 100 ng/μl (n=4

rats); 9 rats received an injection of vehicle (0.03M PBS) that were similarly loaded into separate microcapillaries, which in turn were attached to a 5 µl Hamilton syringe.

After zeroing the XYZ coordinates of the stereotaxic apparatus, the needle was slowly lowered into the right dorsal funiculus of the most rostral part of the T11 spinal cord to a depth of 1 mm; the insertion was immediately to the right of the dorsal spinal artery. All injections were made under visual control using a Nikon SMZ-1B dissecting microscope. Prior to initiating the injection of vehicle or TNF-α, the needle was first left in place in the spinal cord for 5 min, after which 2 µl of vehicle or TNF-α were injected over 10 min using the KDS 310 syringe pump. As mentioned above, separate microcapillaries were used for each concentration of TNF-α injected. No cell grafts were made in the spinal cords of rats used in this pilot study. After 1, 4, 7 and 14 days (see Tables 5.2 and 5.3) the rats were deeply anaesthetized with Somnotol and perfused intracardially as described in Section 3.3.1. For the purpose of this pilot study, a 5 mm length of spinal cord was dissected proceeding caudally from the site of injection of TNF-α or of vehicle into the right dorsal funiculus of T11, frozen, and sectioned at a thickness of 40 µm on a sliding microtome as described in Section 3.3.3. Approximately 120 sections were collected from each dissected 5 mm length of cord; with each section being collected and stored in cryoprotectant solution in 96 well plates (see Section 3.3.3).

The pilot study revealed that 1 ng/µl and 0.01ng/µl were the concentrations of TNF-α that did and did not, respectively, give rise to microglial reactivity along at least a 5 mm distance extending caudally from the site of cytokine injection (see Section 5.3.1 for the data). These two concentrations of TNF-α were chosen for use in rats that were to receive an OEC graft. Two groups of rats (n=4 per group; Groups 5 and 6) received a 2 µl injection of 1 ng/µl over a period of 10 minutes in the right dorsal funiculus of the most rostral part of the T11 spinal cord, using the procedure described above for the pilot study. An additional two groups of rats (n=4 per group; Groups 7 and 8) received an injection of 2 µl of 0.01 ng/µl TNF-α, whereas two other groups of rats (n=4 per group; Groups 9 and 10) received injections of vehicle (i.e. 0.03 M PBS). Rats in Groups 5-10 each received a cell graft of DiI-labelled OECs (1 µl volume) into the right dorsal funiculus of T12 exactly 5 mm caudal to the TNF-α (Groups 5-8) or vehicle (Groups 9-

10) injections (see Section 3.2.3). Stereotaxic coordinates were used to ensure the correct positioning of the OEC grafts exactly 5 mm caudal to the cytokine or vehicle injection.

5.2.3 Grafting DiI-Labelled OECs

For Groups 5 to 10, OECs from the cell cultures numbered K577, K594, and K56-13 (see Table 3.1) were used for the grafting of DiI-labelled OECs. A final cell concentration of 50,000 DiI-labelled OECs per µl was loaded into a 5 µl Hamilton syringe and the cells grafted into the right dorsal funiculus of T12 as described in Section 3.2.3.

5.2.4 Minocycline Treatment

In the experimental design described in Section 5.3.2, minocycline was used to dampen the TNF-α-induced microglial reactivity and thus to address the extent to which microglial reactivity contributed to the generation of a migratory signal(s). Groups 6, 8, and 10 rats received daily IP injections of minocycline (45 mg/ kg in 0.9% saline) whereas Groups 5, 7, and 9 rats received daily IP injections of an equivalent volume of vehicle (i.e. 0.9% saline). The minocycline and saline injections were begun on the day of the surgery for injecting TNF-α/saline and grafting OECs into the dorsal funiculus; the injections continued on a daily basis for a total of 4 weeks. Daily examination of each rat prior to performing the IP injection did not show any observable evidence of adverse reactions to either the minocycline or saline injections.

5.2.5 Necropsy, Tissue Sectioning and Immunohistochemistry

Rats were deeply anesthetized by administering a lethal dose (90 mg/kg body weight) of sodium pentobarbital injected IP. The timing of this perfusion in the pilot study was 1, 4, 7 and 14 days after TNF-α/saline injection; the concentrations of TNF-α that were used in the pilot study included 0.01 ng/µl (n = 6), 0.1 ng/µl (n = 6), 1.0 ng/µl (n = 10), 10 ng/µl (n = 10), and 100 ng/µl (n = 4), and 0.03M PBS (vehicle) (n=9), (See Table 5.1). The Group 5-10 rats, all of which had received an OEC graft, were killed 8 weeks after receiving the cytokine injection and cell graft. All rats were perfused through the heart with 1% sodium nitrite followed by 4% PF as described in Section 3.3.1. The

spinal cord was dissected from the vertebral column as described in Section 3.3.2. Prior to cutting free-floating frozen tissue sections on the sliding microtome, a 5 mm piece of spinal cord immediately rostral to the location of the OEC graft, which was primarily T11, as well as a corresponding 5 mm piece immediately caudal to the cell graft, which was primarily T12/13, were dissected out of the spinal cord. Each piece of spinal cord was sectioned separately on a sliding microtome; some of the tissue sections were stained with Hoechst dye and mounted in CitiFlour for cell counting (see Section 3.3.3) whereas others were mounted and immunostained with the microglial and astrocytic markers described in Section 3.4.2. The remaining tissue sections were stored in the freezer in cryoprotectant solution, as described in Section 3.3.3.

5.2.6 Data Collection and Statistical Analysis

Assessment of the presence or absence of glial reactivity in the 5 mm of the dorsal funiculus laying caudal to the TNF-α/saline injection in the rats used in the pilot study, as well as in the Group 5-10 rats that also received an OEC graft, was done subjectively. For the purpose of the experiments reported in Sections 5.3.5-5.3.6 of this chapter, tissue sections collected into the first four wells were considered to comprise the rostral one-third of T11, sections in the second four wells comprised the middle one-third, and the final four wells comprised the caudal one-third of T11.

For cell counting in Groups 5-10 rats, four sections were randomly chosen from each of the rostral, middle and caudal portions of T11 and of T12-T13 and mounted onto a microscope slide. These sections were stained with Hoechst dye (2 μg/ml) prior to mounting with CitiFluor. Each tissue section was examined to determine whether it contained any DiI+ve cells, to identify the specific location in which the cells were found (i.e. right vs. left dorsal funiculus), and to count the total number of labelled cells within the respective dorsal funiculus. The numbers of DiI-labelled cells within the dorsal funiculus on the right and left sides were computed separately. Only DiI+ve profiles that were associated with a nucleus were counted.

For statistical analysis, the mean cell count for each group of 4 sections was computed. Mean cell counts were computed for each of the rostral, middle and caudal portions of T11 and of T12-13. It is necessary to mention that because of the high density

of DiI+ve OECs at the site of cell grafting, which extended for approximately 0.4 mm in each direction (both rostrally and caudally) away from the injection site, it was not possible to visualize single DiI+ve OECs. Thus, to be more accurate in the cell counting no tissue sections were chosen for counting DiI+ve cells closer than 0.4 mm rostral and caudal to the OEC graft. The T11 cell counts collected for Groups 5-10 were statistically compared using a two-factor analysis of variance (ANOVA), with the data for the rostral, middle and caudal thirds of the right and left dorsal funiculi of this spinal cord segment being analyzed separately for statistical significance (see Section 3.5.3). Multiple post hoc comparisons were performed with Bonferonni's multiple comparison post-test. The independent variables were cytokine injection (i.e. TNF-α vs. vehicle) and treatment (i.e. minocycline vs. vehicle).

To determine whether the OECs were induced to migrate preferentially towards the TNF-α injection, ratios were computed of the number of DiI+ve OECs in the dorsal funiculus of T11 vs. T12-T13 at 8 weeks after either TNF-α (Groups 5 and 7) or vehicle (Group 9) injection into the right dorsal funiculus of the rostral part of T11. Rats in these groups had received daily IP injections of saline, with the daily treatments continuing for the first 4 weeks after the OECs were grafted. An average ratio that was higher than 1 was indicative of preferential migration towards the cytokine injection. A two-factor ANOVA was applied to these data with the data for the right and left dorsal funiculus being analyzed separately for statistical significance. Multiple post hoc comparisons were performed with Bonferonni's multiple comparison post-test. The independent variables for this two-way ANOVA were cytokine injection (i.e. TNF-α vs. vehicle) and the level of T11 (i.e. proximal, middle and distal) from which the cell counts were obtained.

5.3 Results

5.3.1 Titration of TNF-α Concentration: Focal vs. Distributed Glial Activation

Based on the immunohistochemcial examination of the spinal cord tissue between 1 and 14 days after TNF-α injection into the rostral part of T11, it was concluded that 1 ng/μl of TNF-α was sufficient to induce glial reactivity ipsilaterally along at least a 5 mm distance from the site of cytokine injection. In contrast, the lowest concentration of TNF-

α, namely 0.01 ng/µl, induced glial reactivity ipsilaterally that was restricted to the vicinity of the injection. These two concentrations were the ones chosen for use in the OEC migration experiment described in Section 5.3.2. The complete pilot study data are described in more detail in the paragraphs comprising the remainder of this section of the results, and representative immunohistochemically stained tissue sections are presented in Figures 5.1-5.7.

The vehicle injection into the rostral part of the T11 dorsal funiculus induced a focal glial reaction in the vicinity of the injection site that was detectable up to 7 days after injection. This glial reactivity included both microglial (OX42+ve, OX18+ve, OX35+ve and ED1) and astrocytic (GFAP+ve, Vim+ve and nestin+ve) components. There was no evidence of microglial or astrocytic reactivity in either the middle or the caudal parts of T11 between 1 and 14 days after vehicle injection, and by the two week time point there also was no longer any sign of glial reactivity even in the vicinity of the injection site.

In marked contrast, the two highest concentrations of TNF-α induced microglial (OX42+ve, OX18+ve, OX35+ve and ED1) and astrocytic (GFAP+ve, Vim+ve and nestin+ve) reactivity in the dorsal funiculus along the entire extent of T11 and this glial reactivity persisted for at least 14 days after injection, which was the longest survival time in the pilot study. With 100 ng /µl TNF-α this glial reactivity was bilateral along the entire T11 segment at both 1 and 14 days after cytokine injection. When a 10-fold lower concentration of TNF-α was injected (i.e. 10 ng/µl) the microglial and astrocytic reactivity was ipsilateral in the dorsal funiculus at the middle and caudal parts of T11 but was bilateral in the rostral part of T11.

The glial reactivity induced by injection of each of the three lowest concentrations of TNF-α (i.e., 0.01ng/µl, 0.1 ng/µl and 1 ng/µl) was all confined to the ipsilateral dorsal funiculus of T11. They differed, however, in how far the glial reactivity extended caudally from the TNF-α injection. After injection of 1 ng/µl TNF-α into the dorsal funiculus of T11, the microglial (OX42+ve, OX18+ve, OX35+ve and ED1) and astrocytic (GFAP+ve, Vim+ve and nestin+ve) reactivity was seen in rostral, middle and caudal levels of T11 at all survival times. A more focal, ipsilateral microglial (OX42+ve, OX18+ve, OX35+ve and ED1) and astrocytic (GFAP+ve, Vim+ve and nestin+ve)

reaction was seen with the two lowest concentrations of TNF-α (i.e., 0.01 ng/µl, 0.1 ng/µl). With the latter two concentrations, even at 14 days after cytokine injection there was no apparent spread of the glial reactivity away from the injection site, with the glial reactivity also remaining confined to the ipsilateral dorsal funiculus.

Based on the findings of the pilot study, a concentration of 1 ng/µl TNF-α was chosen for its ability to induce glial reactivity that was confined to the entire ipsilateral extent of T11. In comparison to vehicle, for which the glial reactivity was no longer seen by 14 days after injection, the 0.1 ng/µl and 0.01 ng/µl TNF-α concentrations both induced glial reactivity that was still seen in the dorsal funiculus of the rostral part of T11 even at 14 days after injection. The 0.01 ng/µl TNF-α was chosen for its ability to induce only a focal glial reaction confined to the ipsilateral dorsal funiculus in the vicinity of the injection.

Table 5.1 Pilot Study: TNF-α Induced Microglial Reactivity

		Microglial Reactivity			
Conc. of TNF-α	**Survival Time**	**Level of T11 (R, M or C)**	**Reactive (Y/N)**	**Ipsilateral only (Y/N)**	**Bilateral (Y/N)**
0.01 ng/µl	1 day (n=2)	R, M & C	Y	Y	N
	4 days (n=1)	R	Y	Y	N
		M & C	N	N/A	N/A
	7 days (n=1)	R	Y	Y	N
		M & C	N	N/A	N/A
	14 days (n=2)	R	Y	Y	N
		M & C	N	N/A	N/A
0.1 ng/µl	1 day (n=2)	R, M & C	Y	Y	N
	4 days (n=1)	R	Y	Y	N
		M & C	N	N/A	N/A
	7 days (n=1)	R	Y	Y	N
		M & C	N	N/A	N/A
	14days (n=2)	R	Y	Y	N
		M & C	N	N/A	N/A
1 ng/µl	1 day (n=3)	R, M & C	Y	Y	N
	4 days (n=2)	R, M & C	Y	Y	N
	7 days (n=2)	R, M & C	Y	Y	N
	14 days (n=3)	R, M & C	Y	Y	N
10 ng/µl	1 day (n=3)	R	Y	N	Y
		M & C	Y	Y	N
	4 days (n=2)	R	Y	N	Y
		M & C	Y	Y	N
	7 days (n=2)	R	Y	N	Y
		M & C	Y	Y	N
	14 days (n=3)	R	Y	N	Y
		M & C	Y	Y	N
100 ng/µl	1 day(n=2)	R, M & C	Y	N	Y
		R, M & C	Y	N	Y

n= number of rat
R= Rostral part of T11
M= Middle part of T11
C= Caudal part of T11
Y= Yes
N= No
N/A= Not Applicablable

Table 5.2 Pilot Study: TNF-α Induced Astrocyte Reactivity

		Astrocytes Reactivity			
Conc. of TNF-α	**Survival Time**	**Level of T11 (R, M or C)**	**Reactive (Y/N)**	**Ipsilateral only (Y/N)**	**Bilateral (Y/N)**
0.01 ng/µl	1 day (n=2)	R	Y	Y	N
		M & C	N	N/A	N/A
	4 days (n=1)	R	Y	Y	N
		M & C	N	N/A	N/A
	7 days (n=1)	R	Y	Y	N
		M & C	N	N/A	N/A
	14 days (n=2)	R, M & C	N	N/A	N/A
0.1 ng/µl	1 day (n=2)	R	Y	Y	N
		M & C	N	N/A	N/A
	4 days (n=1)	R	Y	Y	N
		M & C	N	N/A	N/A
	7 days (n=1)	R	Y	Y	N
		M & C	N	N/A	N/A
	14days (n=2)	R, M & C	N	N/A	N
1 ng/µl	1 day (n=3)	R, M & C	Y	Y	N
	4 days (n=2)	R, M & C	Y	Y	N
	7 days (n=2)	R, M & C	Y	Y	N
	14 days (n=3)	R	Y	Y	N
		M & C	N	N/A	N
10 ng/µl	1 day (n=3)	R	Y	N	Y
		M & C	Y	Y	N
	4 days (n=2)	R	Y	N	Y
		M & C	Y	Y	N
	7 days (n=2)	R	Y	N	Y
		M & C	Y	Y	N
	14 days (n=3)	R	Y	N	Y
		M & C	Y	Y	N
100 ng/µl	1 day (n=2)	R, M & C	Y	N	Y
	14 days (n=2)	R, M & C	Y	N	Y

n= number of rat
R= Rostral part of T11
M= Middle part of T11
C= Caudal part of T11
Y= Yes
N= No
N/A= Not Applicablable

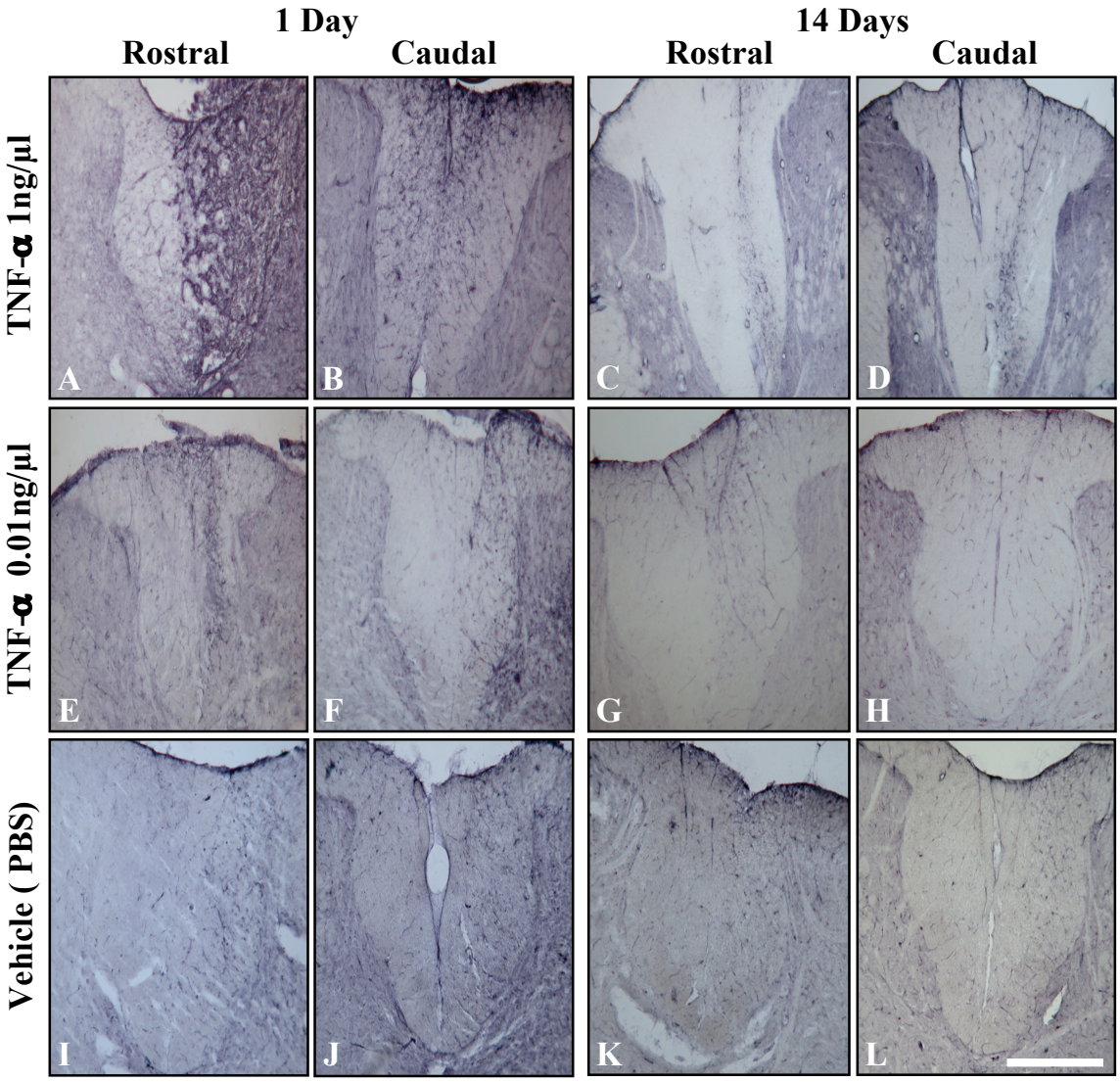

FIGURE 5.1: OX18 +ve microglia in the R-DF of T11 following TNF-α or vehicle injection into the rostral part of T11.

OX18+ve reactive microglia in the R-DF at rostral (**A**, **C**, **E**, **G**, **I**, **K**) and caudal (**B**, **D**, **F**, **H**, **J**, **L**) levels of T11 in rats receiving a 2 µl injection of either 1 ng/µl (**A-D**) or 0.01 ng/µl (**E-H**) of TNF-α or an equal volume of vehicle (**I-L**) into the most rostral part of T11. The rats were killed 1 day (**A**, **B**, **E**, **F**, **I**, **J**) or 14 days (**C**, **D**, **G**, **H**, **K**, **L**) after injection of TNF-α or vehicle. The vehicle injection induced very little microglial reactivity, as evidenced by minimal OX18 immunostaining that was confined to the rostral part of T11 at 1 day after injection (**I**). Slightly more OX18 immunostaining was seen in the 0.01 ng/µl TNF-α injected rats at the rostral part of T11 (**E**) at 1 day after injection and some reactive microglia were also seen in the caudal part of T11 (**F**) at this time point. However, by 14 days after injection of 0.01 ng/µl TNF-α the OX18 immunostaining (**G**, **H**) was virtually indistinguishable from vehicle-injected controls (**K**, **L**). In contrast, the OX18 immunostaining was quite intense in the rostral part of T11 at 1 day after 1ng/µl of TNF-α injection (**A**) and the OX18+ve reactive microglia were still present in both the rostral (**C**) and caudal (**D**) parts of T11 at 14 days after injection. Scale bar = 400 µm.

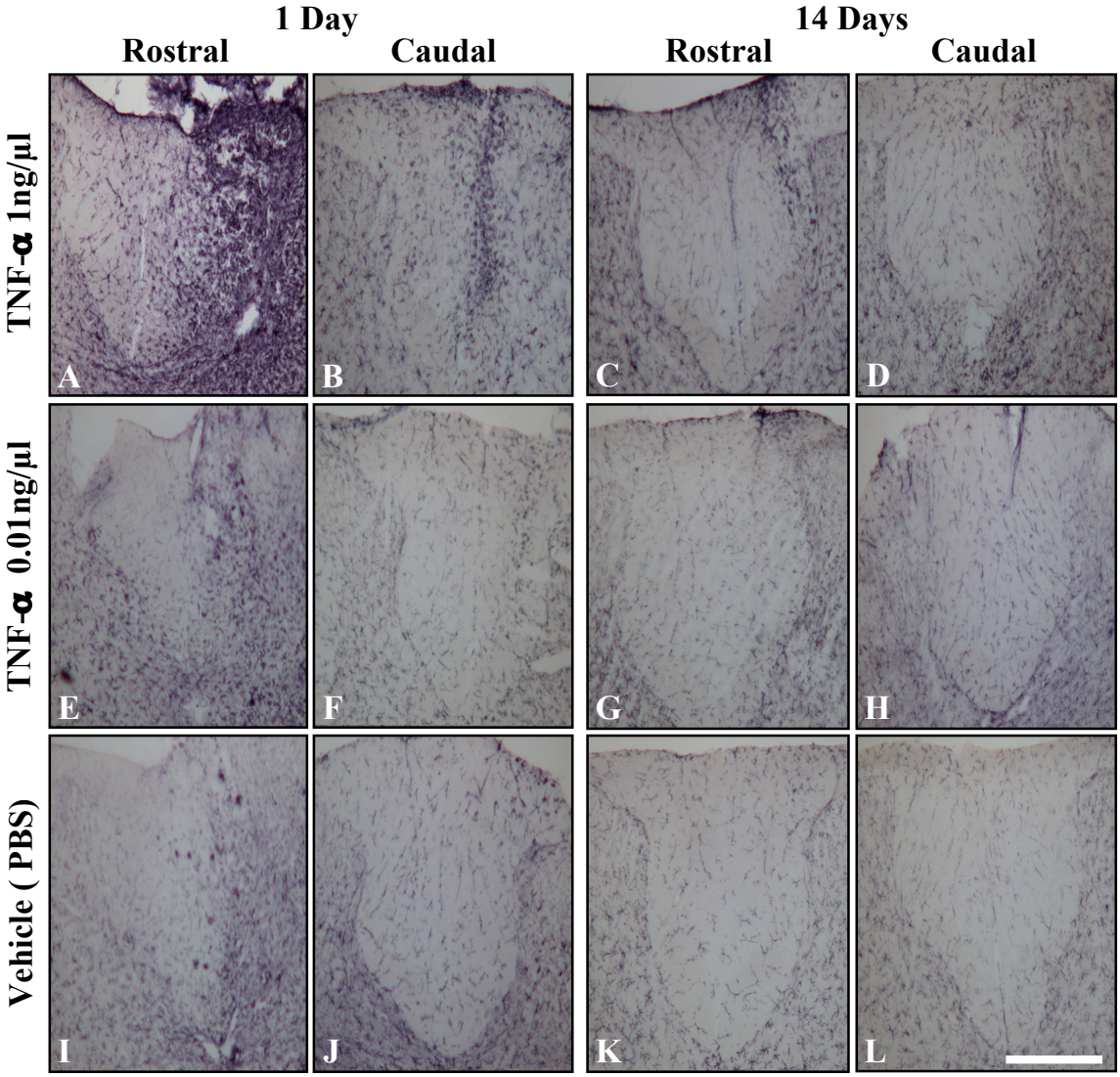

FIGURE 5.2: OX42 +ve microglia in the R-DF of T11 following TNF-α or vehicle injection into the rostral part of T11.

OX42+ve reactive microglia in the R-DF at rostral (**A**, **C**, **E**, **G**, **I**, **K**) and caudal (**B**, **D**, **F**, **H**, **J**, **L**) levels of T11 in rats receiving a 2 µl injection of either 1 ng/µl (**A-D**) or 0.01 ng/µl (**E-H**) of TNF-α or an equal volume of vehicle (**I-L**) into the most rostral part of T11. The rats were killed 1 day (**A**, **B**, **E**, **F**, **I**, **J**) or 14 days (**C**, **D**, **G**, **H**, **K**, **L**) after injection of TNF-α or vehicle. The vehicle injection induced very little microglial reactivity, as evidenced by minimal OX42 immunostaining that was confined to the rostral part of T11 at 1 day after injection (**I**). Slightly more OX42 immunostaining was seen in the 0.01 ng/µl TNF-α injected rats at the rostral part of T11 (**E**) at 1 day after injection and the OX42+ve reactive microglia were barely detectable in the caudal part of T11 (**F**) at this time point. However, by 14 days after injection of 0.01 ng/µl TNF-α the OX42 immunostaining (**G**, **H**) was indistinguishable from vehicle-injected controls (**K**, **L**). In contrast, the OX42 immunostaining was quite intense in the rostral part of T11 at 1 day after 1ng/µl of TNF-α injection (**A**) and the OX42+ve reactive microglia were still present in both the rostral (**C**) and caudal (**D**) parts of T11 at 14 days after injection. Scale bar = 400 µm.

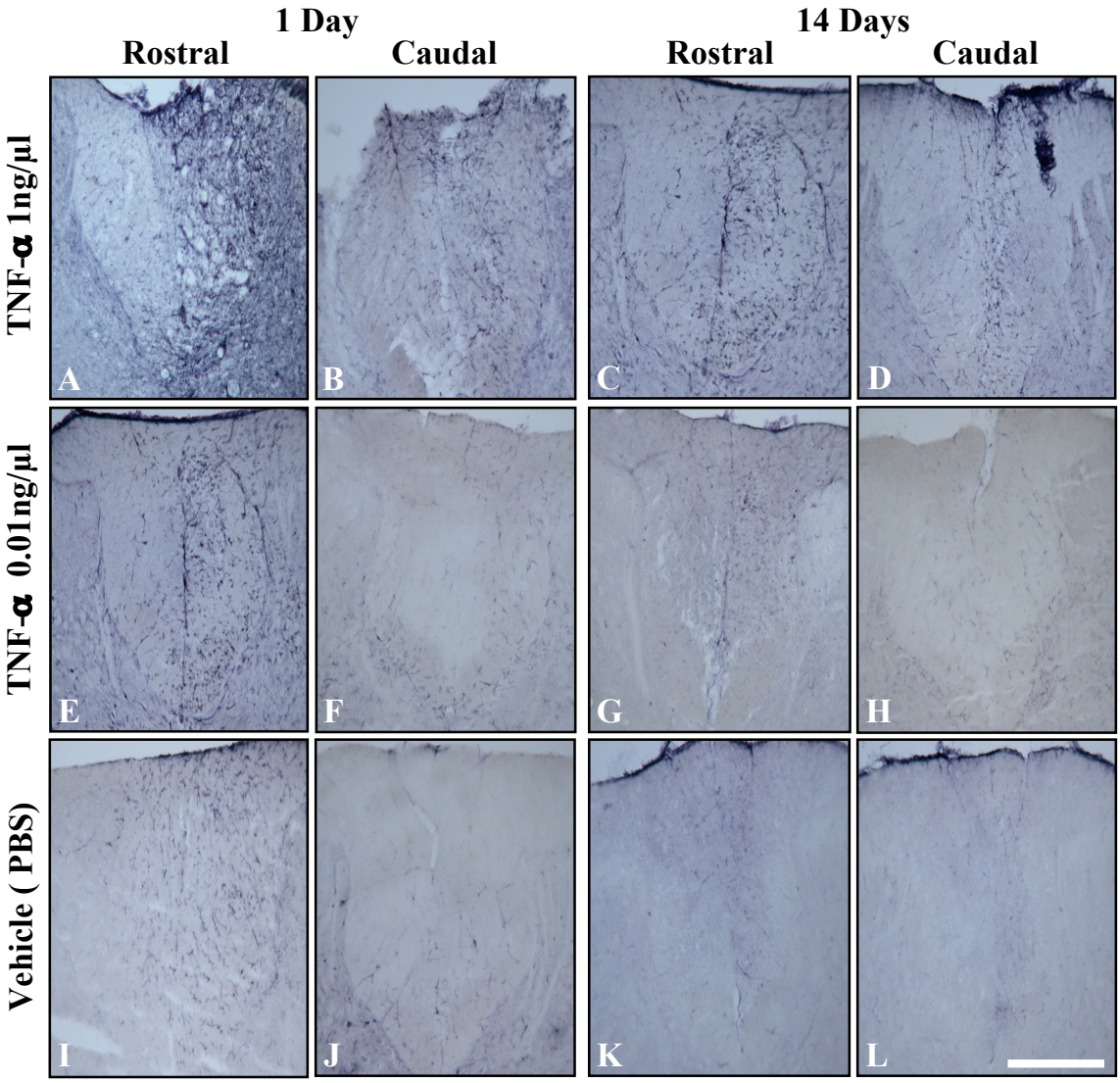

FIGURE 5.3: OX35 +ve microglia in the R-DF of T11 following TNF-α or vehicle injection into the rostral part of T11.

OX35+ve reactive microglia in the R-DF at rostral (**A**, **C**, **E**, **G**, **I**, **K**) and caudal (**B**, **D**, **F**, **H**, **J**, **L**) levels of T11 in rats receiving a 2 µl injection of either 1 ng/µl (**A-D**) or 0.01 ng/µl (**E-H**) of TNF-α or an equal volume of vehicle (**I-L**) into the most rostral part of T11. The rats were killed 1 day (**A**, **B**, **E**, **F**, **I**, **J**) or 14 days (**C**, **D**, **G**, **H**, **K**, **L**) after injection of TNF-α or vehicle. The vehicle injection induced very little microglial reactivity, as evidenced by minimal OX35 immunostaining that was confined to the rostral part of T11 at 1 day after injection (**I**). Slightly more OX35 immunostaining was seen in the 0.01 ng/µl TNF-α injected rats at the rostral part of T11 (**E**) at 1 day after injection and there were less OX35+ve microglia in the caudal part of T11 (**F**) at this time point. However, by 14 days after injection of 0.01 ng/µl TNF-α the OX35 immunostaining (**G**, **H**) was indistinguishable from vehicle-injected controls (**K**, **L**). In contrast, the OX35 immunostaining was quite intense in the rostral part of T11 at 1 day after 1ng/µl of TNF-α injection (**A**) and the OX35+ve reactive microglia were still present in both the rostral (**C**) and caudal (**D**) parts of T11 at 14 days after injection. Scale bar = 400 µm.

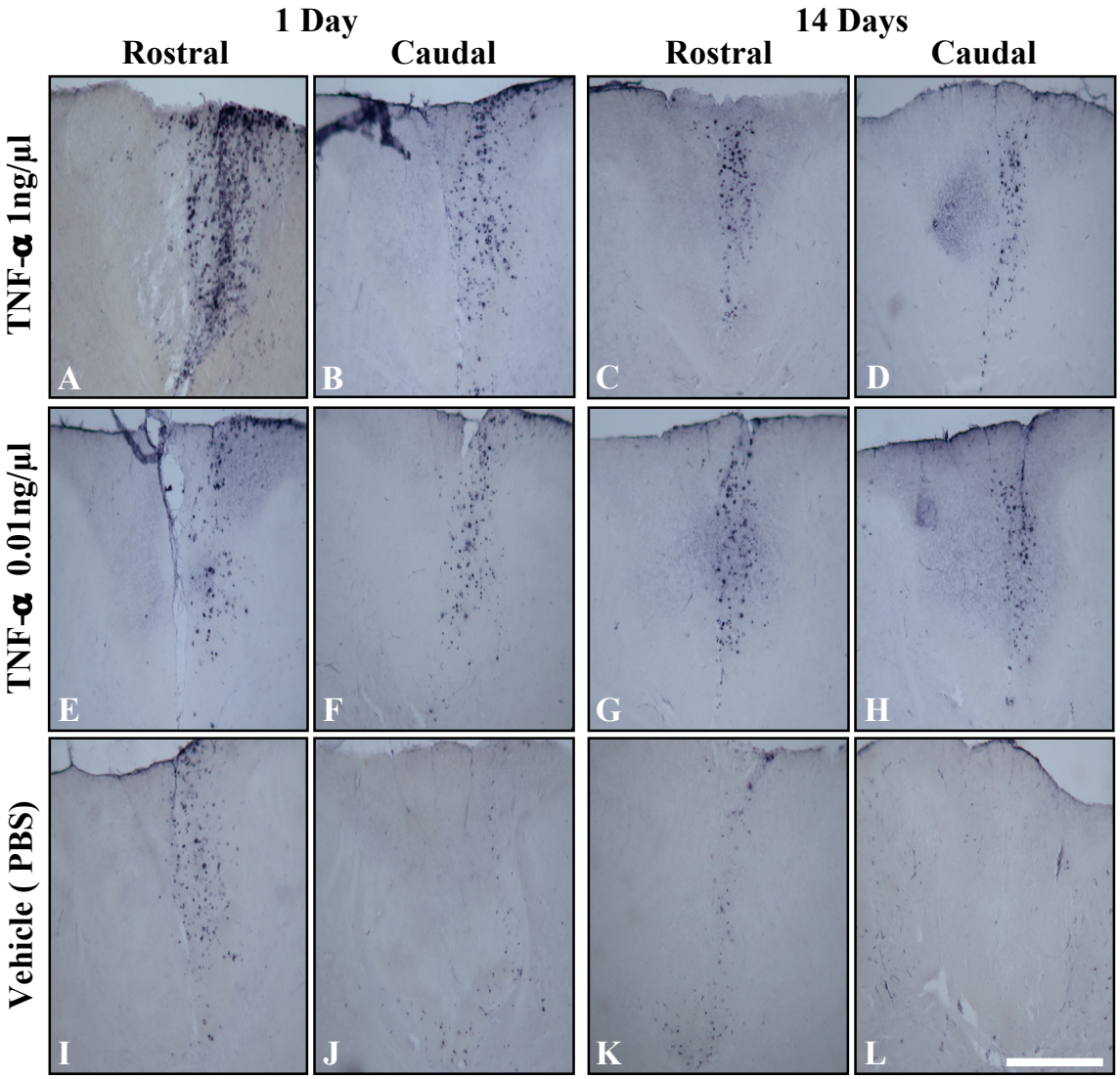

FIGURE 5.4: ED1 +ve microglia in the R-DF of T11 following TNF-α or vehicle injection into the rostral part of T11.

ED1+ve reactive microglia in the R-DF at rostral (**A**, **C**, **E**, **G**, **I**, **K**) and caudal (**B**, **D**, **F**, **H**, **J**, **L**) levels of T11 in rats receiving a 2 µl injection of either 1 ng/µl (**A-D**) or 0.01 ng/µl (E-H) of TNF-α or an equal volume of vehicle (**I-L**) into the most rostral part of T11. The rats were killed 1 day (**A**, **B**, **E**, **F**, **I**, **J**) or 14 days (**C**, **D**, **G**, **H**, **K**, **L**) after injection of TNF-α or vehicle. The vehicle injection induced very little microglial reactivity, as evidenced by minimal ED1 immunostaining that was confined to the rostral part of T11 at 1 day (**I**) and 14 days (**L**) after injection. Slightly more ED1 immunostaining was seen in the 0.01 ng/µl TNF-α injected rats at the rostral (**E**, **G**) and caudal (**F**, **H**) parts of T11 at 1 and 14 days after injection. In contrast, the ED1 immunostaining was more intense in both the rostral (**A**) and caudal (**B**) parts of T11 at 1 day after 1ng/µl of TNF-α injection (**A**) and the ED1+ve reactive microglia were still present in both the rostral (**C**) and caudal (**D**) parts of T11 at 14 days after injection. Scale bar = 400 µm.

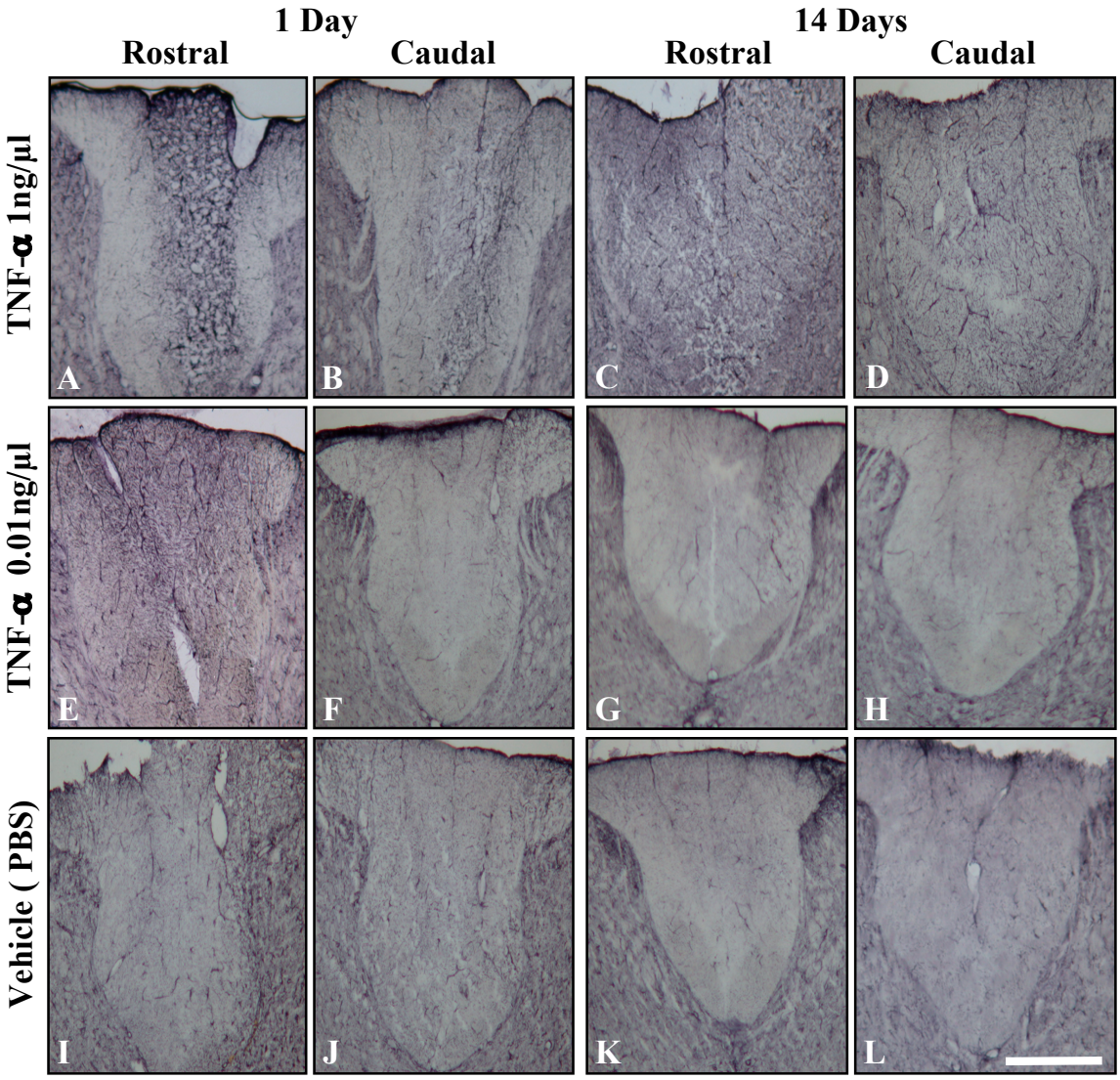

FIGURE 5.5: GFAP +ve astrocytes in the R-DF of T11 following TNF-α or vehicle injection into the rostral part of T11.

GFAP+ve astrocytes in the R-DF at rostral (**A**, **C**, **E**, **G**, **I**, **K**) and caudal (**B**, **D**, **F**, **H**, **J**, **L**) levels of T11 in rats receiving a 2 µl injection of either 1 ng/µl (**A-D**) or 0.01 ng/µl (**E-H**) of TNF-α or an equal volume of vehicle (**I-L**) into the most rostral part of T11. The rats were killed 1 day (**A**, **B**, **E**, **F**, **I**, **J**) or 14 days (**C**, **D**, **G**, **H**, **K**, **L**) after injection of TNF-α or vehicle. No detectable astrocyte reactvity was seen in the caudal parts of T11 following injection of either vehicle (**I-L**) or of 0.01 ng/µl TNF-α (**E-H**). In contrast, the GFAP immunostaining showed prominent astrocyte reactivity in the rostral (**A**) part of T11 at 1 day after 1ng/µl of TNF-α injection, but the GFAP immunostaining was indistinguishable from controls by 14 days after injection (**C**, **D**). Scale bar = 400 µm.

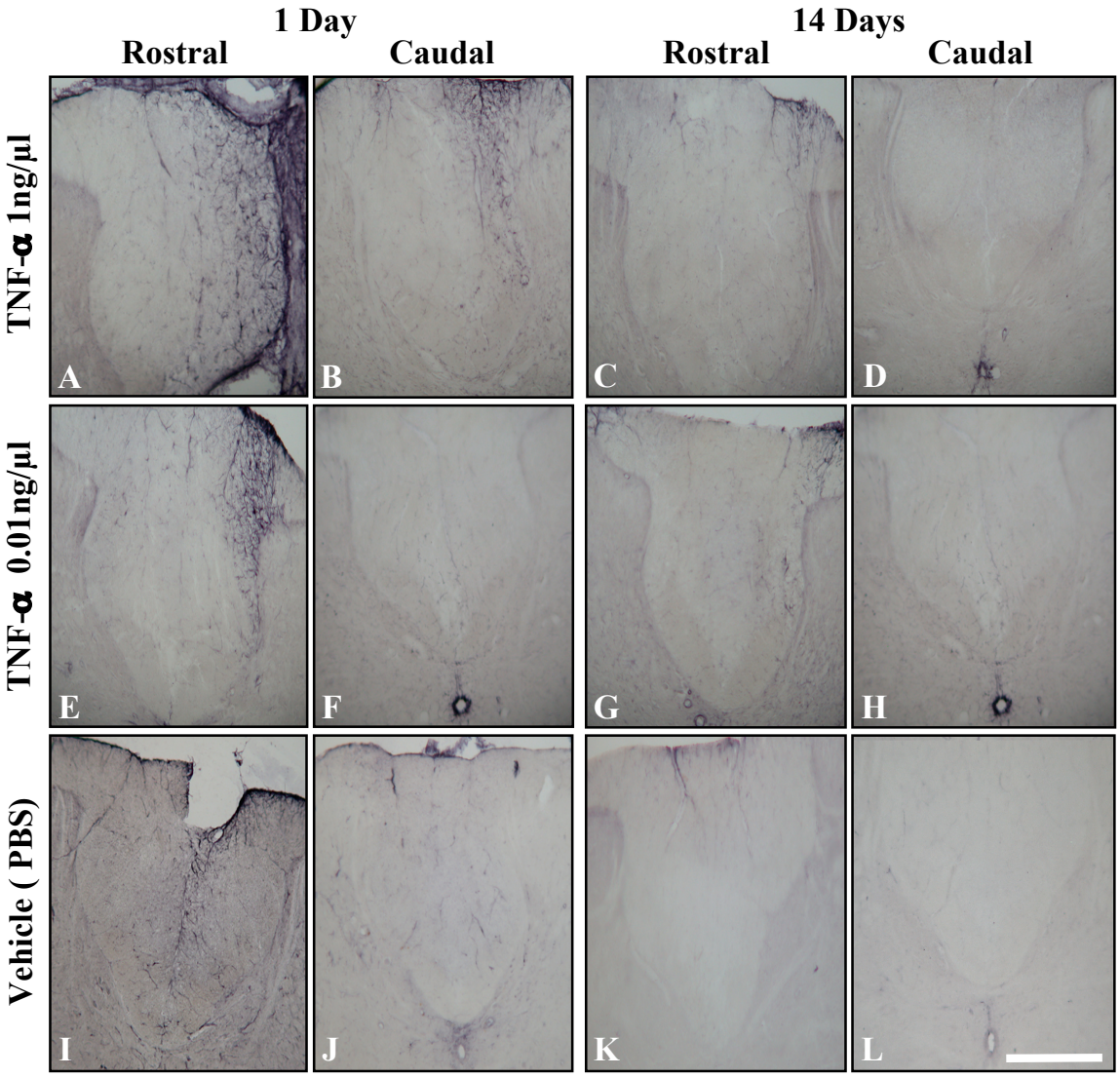

FIGURE 5.6: Vimentin+ve astrocytes in the R-DF of T11 following TNF-α or vehicle injection into the rostral part of T11.

Vimentin immunostaining of the R-DF at rostral (**A**, **C**, **E**, **G**, **I**, **K**) and caudal (**B**, **D**, **F**, **H**, **J**, **L**) levels of T11 in rats receiving a 2 µl injection of either 1 ng/µl (**A-D**) or 0.01 ng/µl (**E-H**) of TNF-α or an equal volume of vehicle (**I-L**) into the most rostral part of T11. The rats were killed 1 day (**A**, **B**, **E**, **F**, **I**, **J**) or 14 days (**C**, **D**, **G**, **H**, **K**, **L**) after injection of TNF-α or vehicle. The vehicle injection induced very little astrocyte reactivity, as evidenced by minimal vimentin immunostaining that was confined to the rostral part of T11 at 1 day (**I**) but not at 14 days (**K**) after injection. Slightly more vimentin immunostaining was seen in the 0.01 ng/µl TNF-α injected rats at the rostral part of T11 at 1 day (**E**) but not at 14 days (**G**) after injection. In contrast, the vimentin immunostaining was more intense in both the rostral (**A**) and caudal (**B**) parts of T11 at 1 day after 1ng/µl of TNF-α injection and small number of vimentin+ve reactive astrocytes were still present in the rostral (**C**) part of T11 but not in the caudal (**D**) part at 14 days after injection. Scale bar = 400 µm.

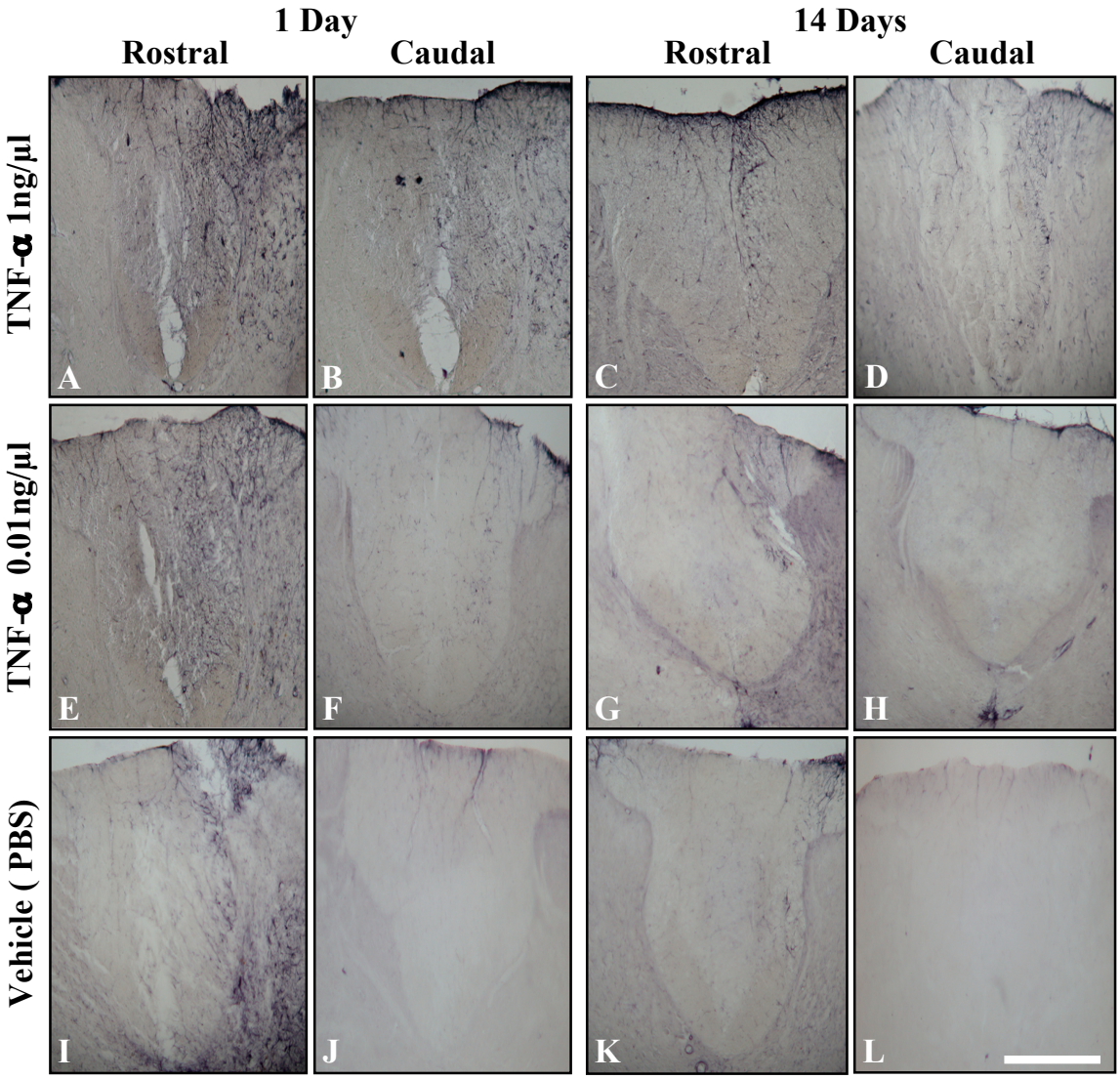

FIGURE 5.7: Nestin+ve astrocytes in the R-DF of T11 following TNF-α or vehicle injection into the rostral part of T11.

Nestin immunostaining of the R-DF at rostral (**A**, **C**, **E**, **G**, **I**, **K**) and caudal (**B**, **D**, **F**, **H**, **J**, **L**) levels of T11 in rats receiving a 2 µl injection of either 1 ng/µl (**A-D**) or 0.01 ng/µl (**E-H**) of TNF-α or an equal volume of vehicle (**I-L**) into the most rostral part of T11. The rats were killed 1 day (**A**, **B**, **E**, **F**, **I**, **J**) or 14 days (**C**, **D**, **G**, **H**, **K**, **L**) after injection of TNF-α or vehicle. The vehicle (**I**) and the 0.01 ng/µl TNF-α (**E**) injections induced some astrocyte reactivity, as evidenced by nestin immunostaining that was confined to the rostral part of T11 at 1 day after injection; no nestin immunostaining was seen in either the rostral (**G**, **K**) or caudal (**H**, **L**) parts of T11 for either group of rats by 14 days after injection. Comparable levels of nestin immunostaining was seen in the R-DF in the rostral (**A**) part of T11 at 1 day after 1ng/µl of TNF-α injection and a small number of nestin+ve reactive astrocytes were still present in the rostral (**C**) part of T11 but not in the caudal (**D**) part at 14 days after injection. Scale bar = 400 µm.

5.3.2 Experimental Design

To address Specific Aim 4 a focal injection of vehicle (0.03 M PBS), 0.01 ng/µl TNF-α, or 1 ng/µl TNF-α was made into the rostral part of the dorsal funiculus of T11. This experiment tested the hypothesis that a focal injection of TNF-α gives rise to a migratory signal inducing OECs to migrate towards the cytokine injection. Based on the pilot study, 1 ng/µl of TNF-α was determined to be a concentration that induced glial reactivity confined ipsilaterally to the entire length of the T11 spinal cord segment (~5 mm) and 0.01 ng/µl TNF-α was a concentration for which the cytokine-induced microglial and astrocytic reactivity would be confined to the vicinity of the injection site (i.e., the rostral part of T11).

A total of 24 female adult rats were assigned to one of six groups, with Group 5 and 6 rats receiving an injection of 1 ng/µl of TNF-α, Group 7 and 8 rats receiving 0.01 ng/µl TNF-α, and Group 9 and 10 rats receiving an injection of vehicle (0.03 M PBS). The injections were made stereotactically directly into the right dorsal funiculus of T11, followed immediately by a stereotactic injection of DiI+ve OECs into the ipsilateral dorsal funiculus 5 mm caudal to the TNF-α or vehicle injection. Systemically administered minocycline was used to reduce the activation of microglia both at the site of TNF-α or vehicle injection and along the 5 mm length of white matter extending caudally from this injection site (Groups 6, 8 and 10). Rats in the remaining three groups (Groups 5, 7 and 9) received systemic injections of saline. The minocycline (45 mg/kg in 0.9% saline) and vehicle (i.e. 0.9% saline) were injected IP on a daily basis for the first four weeks after the TNF-α/vehicle injections and OEC grafts into the spinal cord (Fig. 5.8). All rats were killed 8 weeks after cell grafting for quantification of the numbers of DiI+ve OECs located in the dorsal funiculus that had migrated rostral and caudal to the cell grafts.

FIGURE 5.8: Summary of experimental design

Adult female Wistar rats (230- 260 g) received a 2 µl injection of either 1 ng/µl (Groups 5 and 6) or 0.01 ng/µl (Groups 7 and 8) of TNF-α or an equal volume of vehicle (Groups 9 and 10) into the right DF in the most rostral part of T11 (n = 4 per group). Immediately after injecting the TNF-α or the vehicle into the rostral part of the DF of T11, DiI labeled OECs were grafted into the right DF exactly 5 mm caudally. All rats received daily i.p. injections of either saline (Groups 5, 7 and 9) or minocycline (Groups 6, 8 and 10), with the daily treatments continuing for the first 4 weeks after the OECs were grafted. All rats were killed 8 weeks after cell grafting.

Vehicle (Saline)	Minocycline
Group 5 TNF-α (1ng/µl) injected into T11/OEC grafted into T12	**Group 6** TNF-α (1ng/µl) injected into T11/OEC grafted into T12
Group 7 TNF-α (0.01µl) injected into T11/OEC grafted into T12	**Group 8** TNF-α (0.01µl) injected into T11/OEC grafted into T12
Group 9 PBS injected into T11/OEC grafted into T12	**Group 10** PBS injected into T11/OEC grafted into T12

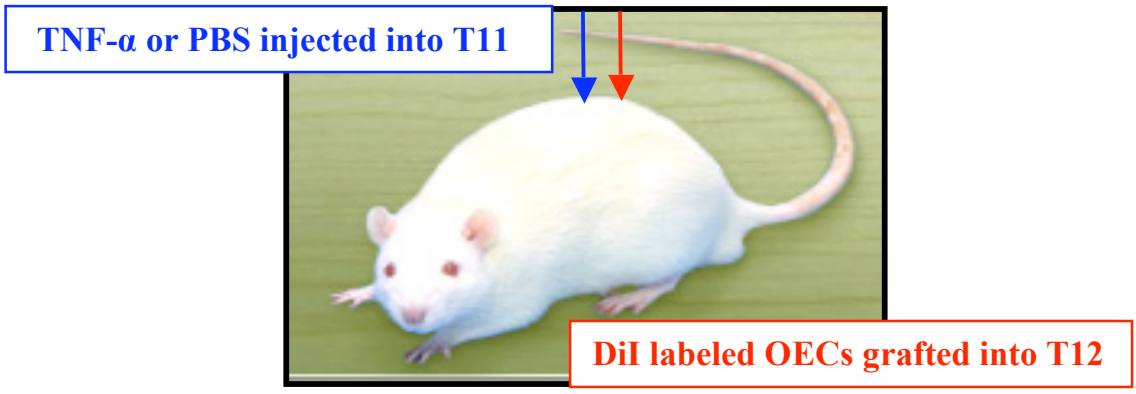

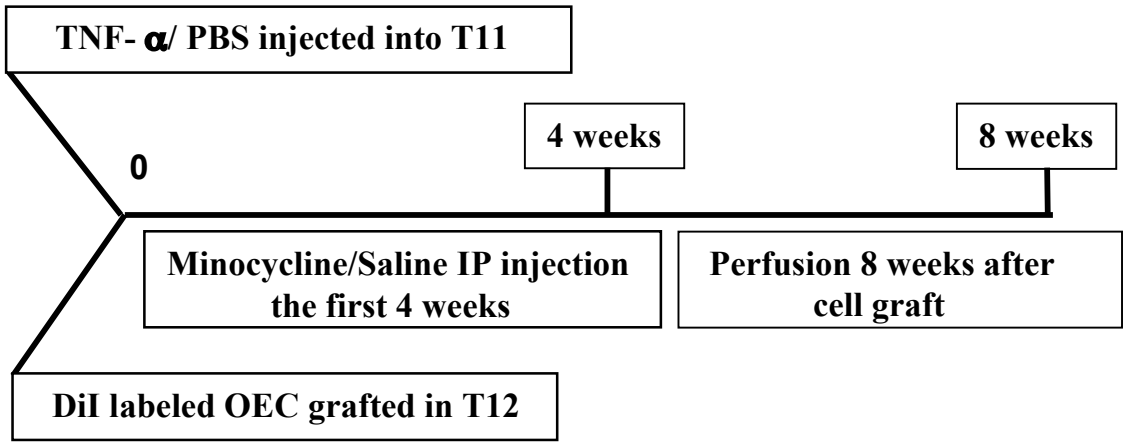

5.3.3 Microglial and astrocytic reactivity: Effectiveness of minocycline treatment

The spinal cord tissues of Groups 5-10 rats were stained with antibodies that identified reactive microglia (OX18, OX42, OX35 and ED1 monoclonal antibodies) and reactive astrocytes (GFAP, Vim and nestin monoclonal antibodies) to confirm that the minocycline treatment had been effective in preventing the activation of microglia and in assessing the treatment's effect on astrogliosis. In the saline-treated rats that had received an injection of TNF-α into the rostral part of T11 and a cell graft of DiI+ve OECs 5 mm caudally (Groups 5 and 7), OX18+ve (Fig. 5.9), OX42+ve (Fig.5.10), OX35+ve (Fig. 5.11) and ED1+ve (Fig. 5.12) reactive microglia were present in the right dorsal funiculus at the rostral and middle levels of T11 at 8 weeks after TNF-α injection and OEC grafting. Although no cell counts of microglia or other tests to determine the level of OX42, OX18, OX35 and ED1 expression were performed on spinal cord tissue of Group 5-10 rats, the immunostaining of the reactive microglia appeared to be more intense especially in the rostral part of T11 in Group 5 rats (i.e. after injection of 1 ng/µl TNF-α) than in the Group 7 rats (i.e. after injection of 0.01 ng /µl TNF-α) (Fig 5.9-5.12). In the saline-treated control rats of Group 9 (i.e. 0.03 M PBS injected into dorsal funiculus) there was no detectable OX18+ve (Fig. 5.9), OX35+ve (Fig. 5.11) or ED1+ve (Fig. 5.12) immunostaining in the right dorsal funiculus of T11. In the saline-treated rats of Groups 5, 7 and 9, GFAP+ve (Fig. 5.13), Vim+ve (Fig. 5.14) and nestin+ve (Fig. 5.15) reactive astrocytes were seen only in the rostral part of T11 and only after injection of 1 ng/µl of TNF-α (Group 5). There was no detectable astrocyte reactivity in either the rostral or middle parts of T11 following injection of vehicle (Group 9; Fig. 5.13-5.15).

In the minocycline-treated rats that had received an injection of TNF-α into the rostral part of T11 and a cell graft of DiI+ve OECs 5 mm caudally (Groups 6 and 8), OX18+ve (Fig. 5.9), OX42+ve (Fig. 5.10), OX35+ve (Fig. 5.11) and ED1+ve (Fig. 5.12) reactive microglia appeared to be less intensely immunostained in both the rostral and middle parts of T11 in the Group 6 rats (i.e. after injection of 1 ng/µl TNF-α) than in the Group 8 rats (i.e. after injection of 0.01 ng/µl TNF-α) (Fig 5.9-5.12). In the minocycline-treated control rats of Group 10 (i.e. 0.03 M PBS injected into dorsal funiculus) there was no detectable OX18+ve (Fig.5.9), OX35+ve (Fig. 5.11) or ED1+ve (Fig. 5.12) immunostaining in the right dorsal funiculus of T11. In the minocycline-treated rats of

Groups 6, 8 and 10, reactive astrocytes were seen only in Group 6 rats (i.e. after injection of 1 ng/µl of TNF-α) and only in the rostral part of T11 (Fig. 5.13-5.15).

5.3.4 Quantification of DiI+ve cells: Right dorsal funiculus (R-DF) of T11

We found that OECs migrated into the R-DF of T11 in response to TNF-α induced microglial reactivity within the R-DF following an injection of DiI+ve OECs into the R-DF exactly 5 mm caudal to an injection of TNF-α. A two-factor analysis of variance (ANOVA) was applied to the data with the data for the rostral (A), middle (B) and caudal (C) thirds of T11 being analyzed separately for statistical significance. Multiple post hoc comparisons were performed with Bonferonni's multiple comparison post-test. The two-factor ANOVA showed a significant main effect of the TNF-α injection at all levels of the T11 spinal cord segment; $F(2,18)= 681.2$, $p <0.0001$ (A), $F(2,18) = 520.6$, $p <0.0001$ (B), $F(2, 18) = 821.4$, $p <0.0001$ (C). There was also a significant main effect of the minocycline treatment at all levels of T11; $F(1,18) = 543.9$, $p<0.0001$ (A), $F(1, 18) = 465.2$, $p<0.0001$ (B), and $F(1, 18) = 235.5$, $p<0.0001$ (C). The two-factor ANOVA revealed a significant interaction between the TNF-α/vehicle and minocycline/saline variables in the right DF at all levels of T11 spinal cord segment; $F(2,18) = 208.1$, $p <0.0001$ (A), $F(2,18) = 154.8$, $p <0.0001$ (B), $F(2,18) = 47.8$, $p <0.0001$ (C). Bonferonni's post-test revealed the number of DiI+ve cells in the right DF was significantly higher ($p<0.05$; brackets) in the 1 ng/µl TNF-α than either 0.01 ng/µl TNF-α or vehicle groups at the rostral (A), middle (B) and caudal (C) levels of T11. In addition, Bonferonni's post-test revealed the number of DiI+ve cells in the right DF was significantly higher in the 0.01 ng/µl TNF-α than vehicle groups at the rostral (A), middle (B) and caudal (C) levels of T11. The post-test also revealed a significant reduction in the number of DiI+ve cells in the right DF in minocycline treated rats both in the 1 ng/µl TNF-α and the 0.01 ng/µl TNF-α groups (Groups 6 and 8) compared with the saline treated groups (Groups 5 and 7) at all levels of T11. The post-test also revealed a significant reduction in the number of DiI+ve cells in the right DF in the minocycline treated rats injected with vehicle (Group 10) compared to the saline treated rats (Group 9), but only at the rostral (A) and middle (B) levels of T11 (Fig 5.16). In the saline-treated rats that had received an injection of 1 ng/µl TNF-α into the rostral part of T11

and a cell graft of DiI+ve OECs 5 mm caudally (Group 5), the average number of DiI+ve cells in the rostral, middle and caudal portion of T11 was 29.25 +/- 0.71, 44.21 +/- 0.68 and 60.12 +/- 0.68 cells per 40 μm tissue section, respectively. In contrast, the average number of DiI+ve cells in the corresponding portions of T11 varied from 9.43 +/- 0.54 (rostral), 18.56 +/- 0.56 (middle), and 32.87 +/- 0.88 (caudal) cells for the Group 7 (0.01 ng/μl TNF-α) rats, and from 6.06 +/- 0.29 (rostral), 14.93 +/- 0.32 (middle), and 24.18 +/- 0.57 (caudal) cells in Group 9 (vehicle control) rats. In the minocycline-treated rats that had received an injection of 1 ng/μl TNF-α into the rostral part of T11 and a cell graft of DiI+ve OECs 5 mm caudally (Group 6), the average number of DiI+ve cells in the rostral, middle and caudal portion of T11 was 10.56 +/- 0.23, 19.81 +/- 0.31 and 43.43 +/-0.94 per 40 μm tissue section, respectively. In contrast, the average number of DiI+ve cells in the corresponding portions of T11 varied from 6.06 +/- 0.37 (rostral), 14.50 +/- 1.23 (middle), and 23.12 +/-0.59 (caudal) cells for the Group 8 (0.01 ng/μl TNF-α) rats, and from 3.06 +/- 0.25 (rostral), 9.12 +/- 0.29 (middle), and 22.25 +/- 0.77 (caudal) cells for the Group 9 (vehicle control) rats.

5.3.5 Quantification of DiI+ve cells: Left dorsal funiculus (L-DF) of T11

We also found that some OECs migrated into the L-DF of T11 following an injection of DiI+ve OECs into the R-DF exactly 5 mm caudal to an injection of TNF-α. A two-factor analysis of variance (ANOVA) was applied to the data with the data for the rostral (A), middle (B) and caudal (C) thirds of T11 being analyzed separately for statistical significance. Multiple post hoc comparisons were performed with Bonferonni's multiple comparison post-test (Fig. 5.17).The two-factor ANOVA showed a significant main effect of the TNF-α injection at all levels of the T11 segment; $F(2,18)= 119.6$, $p <0.0001$ (A), $F(2,18) = 148.3$, $p <0.0001$ (B), $F(2, 18)= 408.6$, $p <0.0001$ (C). There was also a significant main effect of the minocycline treatment at all levels of T11; $F(1,18) = 103.8$, $p<0.0001$ (A), $F(1, 18) = 109.1$, $p<0.0001$ (B), and $F(1,18) = 51.95$, $p<0.0001$ (C). The two-factor ANOVA revealed a significant interaction between the TNF-α/vehicle and minocycline/saline variables in the left DF only at the rostral and middle thirds of T11; $F (2, 18)= 67.04$, $p <0.0001$ (A), $F (2,18)= 37.2$, $p <0.0001$ (B). Bonferonni's post-test revealed the mean number of DiI+ve cells in the left DF was significantly higher

($p<0.05$) in the 1 ng/µl TNF-α than either 0.01 ng/µl TNF-α or vehicle groups at the rostral, middle and caudal levels of T11 (Fig. 5.17). In addition, Bonferonni's post-test revealed the mean number of DiI+ve cells in the left DF was significantly higher ($p<0.05$) in the 0.01 ng/µl TNF-α than vehicle groups at only the caudal level of the T11 segment (Fig. 5.17C). The post-test also revealed a significant reduction in the number of DiI+ve cells in the left DF ($p<0.05$) in the minocycline treated 1 ng/µl TNF-α animal group (Group 6) compared to saline treated ones (Group 5) at all levels of T11 (Fig. 5.17). However, the post-test also revealed a significant reduction in the average number of DiI+ve cells in the left DF ($p<0.05$; brackets) in minocycline treated 0.01 ng/µl TNF-α rats (Group 8) compared to saline treated ones (Group 7) only at the caudal part of T11 (Fig. 5.17C). The post-test also revealed a significant reduction in the mean number of DiI+ve cells in the left DF ($p<0.05$) in minocycline treated rats who received a vehicle injection (Group 10) compared to saline treated ones (Group 9) only at the middle and caudal part of T11 (Fig 5.17B & C). In the saline-treated rats that had received an injection of 1 ng/µl TNF-α into the rostral part of T11 and a cell graft of DiI+ve OECs 5 mm caudally (Group 5), the average number of DiI+ve cells in the rostral, middle, and caudal portion of T11 was 14.06 +/- 1.08, 20.43 +/- 0.92 and 22.68 +/- 0.63 cells per 40 µm tissue section, respectively (Fig. 5.17). In contrast, the average number of DiI+ve cells in the corresponding portions of T11 for the Group 7 (0.01 ng/µl TNF-α) and 9 (vehicle control) rats varied from 2.62 +/- 0.52, 6.87 +/- 0.92, and 12.75 +/- 0.36, and from 1.50 +/- 0.10, 5.68 +/- 0.41, 9.43 +/- 0.31, respectively (Fig. 5.17 and Fig. 5.19). In the minocycline-treated rats that had received an injection of 1 ng/µl TNF-α into the rostral part of T11 and a cell graft of DiI+ve OECs 5 mm caudally (Group 6), the average number of DiI+ve cells in the rostral, middle, and caudal portion of T11 was 2.87 +/- 0.33, 8.62 +/- 0.26, and 19.31 +/-0.44 cells per 40 µm tissue section, respectively (Fig. 5.17). In contrast, the average number of DiI+ve cells in the corresponding portions of T11 for the Group 8 (0.01 ng/µl TNF-α) and 9 (vehicle control) rats varied from 1.87 +/- 0.12 (rostral), 5.56 +/- 0.60 (middle), 10.06 +/- 0.57 (caudal), and from 0.56 +/- 0.12 (rostral), 2.31 +/-0.42 (middle), and 7.37 +/- 0.33 (caudal), respectively (Fig. 5.17).

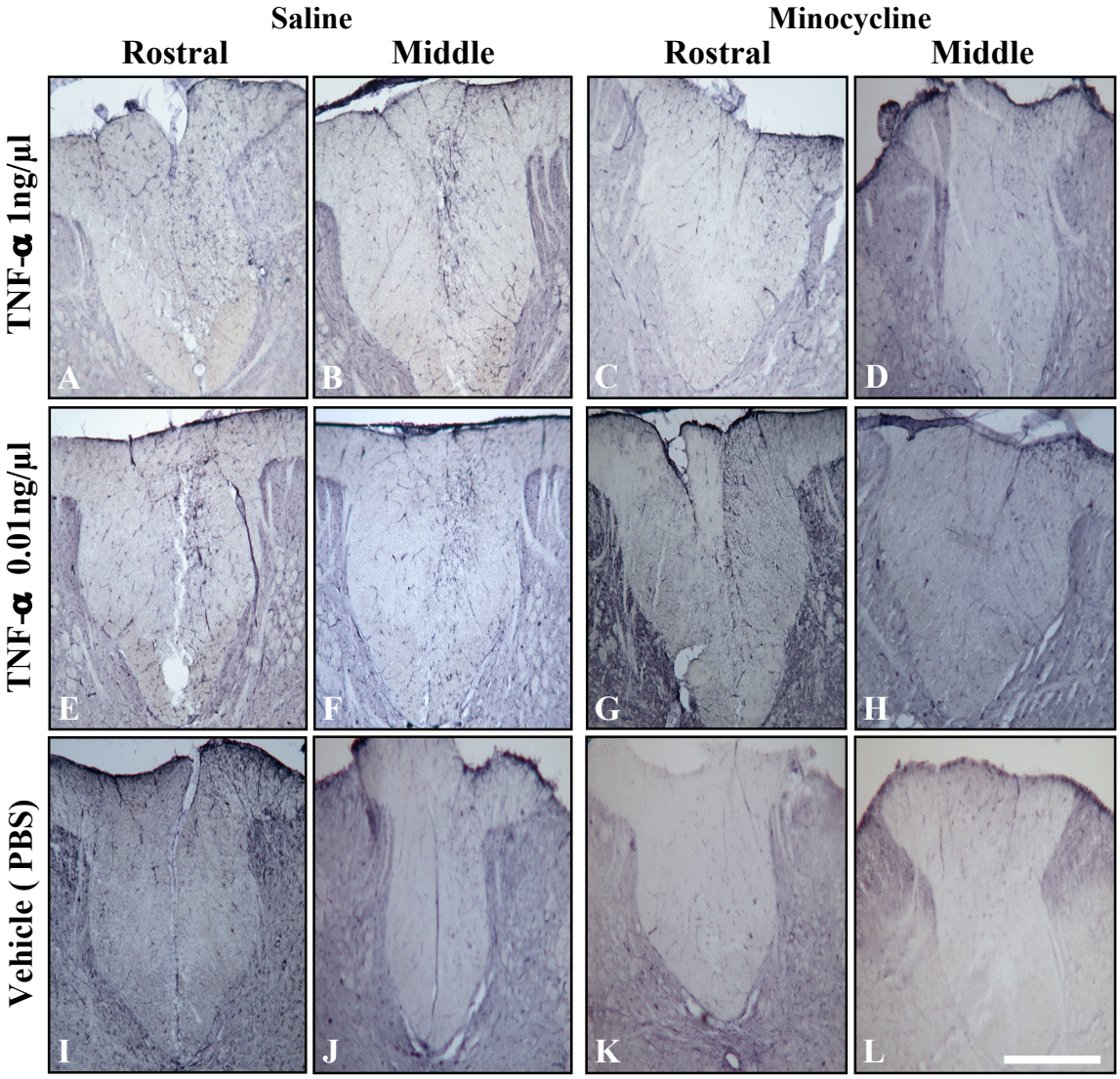

FIGURE 5.9: OX18 +ve microglia in the dorsal funiculus of T11 in Groups 5-10.

OX18+ve reactive microglia in the R-DF at rostral (**A**, **C**, **E**, **G**, **I**, **K**) and middle (**B**, **D**, **F**, **H**, **J**, **L**) levels of T11 in rats receiving a 2 µl injection of either 1 ng/µl (**A-D**) or 0.01 ng/µl (**E-H**) of TNF-α or an equal volume of vehicle (**I-L**) into the most rostral part of T11. The rats received daily i.p. injections of either saline (**A**, **B**, **E**, **F**, **I**, **J**) or minocycline (**C**, **D**, **G**, **H**, **K**, **L**), with the daily treatments continuing for the first 4 weeks after the OECs were grafted. OX18+ve reactive microglia were still present in the R-DF at the rostral and middle levels of T11 at 8 weeks after the TNF-α injections (**A**, **B**, **E**, **F**) in rats treated with saline daily for the first 4 weeks, but there was very little microglial reactivity in TNF-a injected rats treated with minocycline (**C**, **D**, **G**, **H**). No detectable OX18 immunostaining (**I-L**) was seen in the R-DF of the rats in which vehicle had been injected into the rostral part of T11 (Groups 9 and 10). Scale bar = 400 µm.

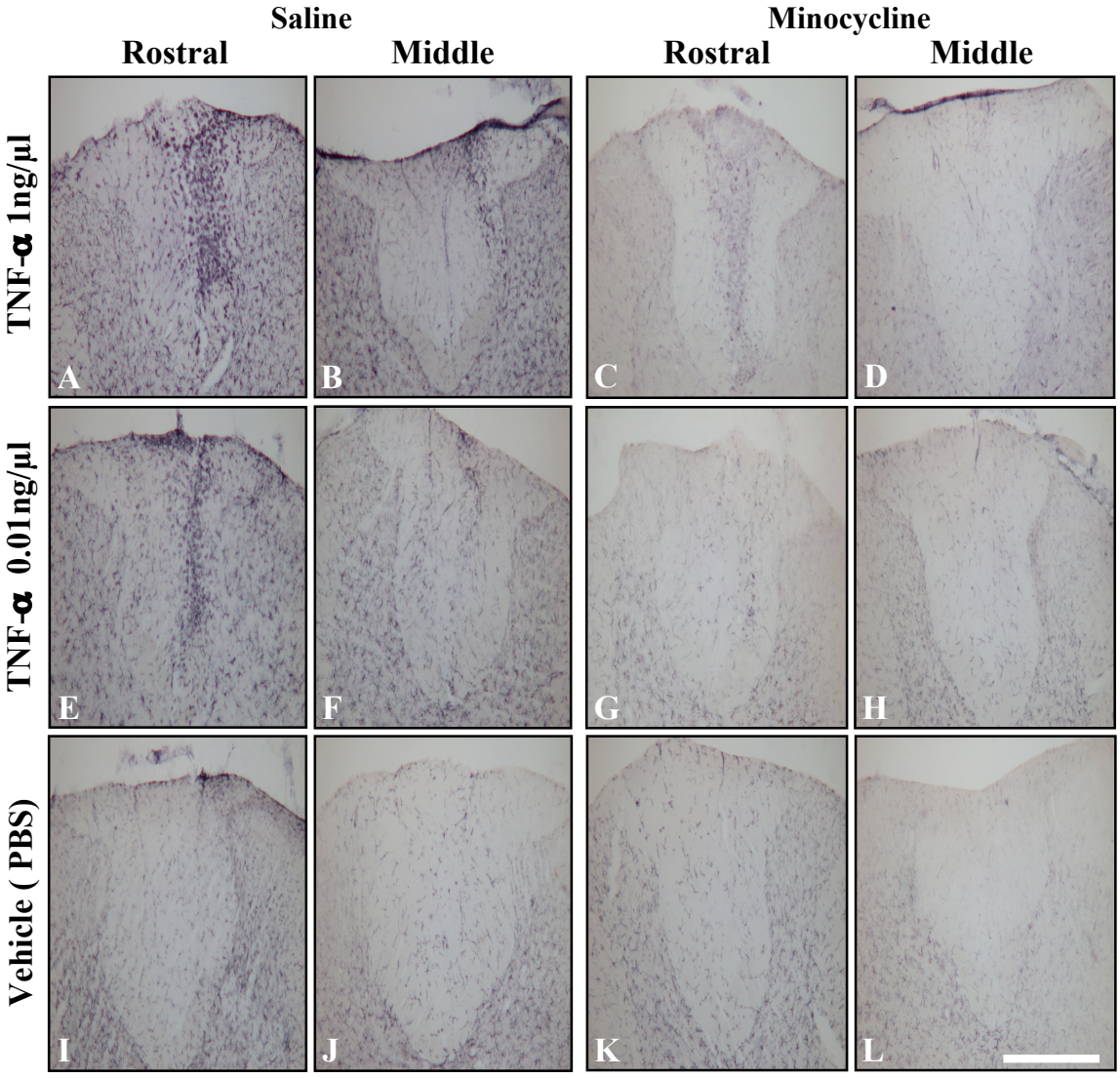

FIGURE 5.10: OX42 +ve microglia in the dorsal funiculus of T11 in Groups 5-10.

OX42+ve microglia in the R-DF at rostral (**A**, **C**, **E**, **G**, **I**, **K**) and middle (**B**, **D**, **F**, **H**, **J**, **L**) levels of T11 in rats receiving a 2 µl injection of either 1 ng/µl (**A-D**) or 0.01 ng/µl (**E-H**) of TNF-α or an equal volume of vehicle (**I-L**) into the most rostral part of T11. The rats received daily i.p. injections of either saline (**A**, **B**, **E**, **F**, **I**, **J**) or minocycline (**C**, **D**, **G**, **H**, **K**, **L**), with the daily treatments continuing for the first 4 weeks after the OECs were grafted. OX42+ve reactive microglia were still present in the R-DF at the rostral and middle levels of T11 at 8 weeks after the TNF-α injections (**A**, **B**, **E**, **F**) in rats treated with saline daily for the first 4 weeks, but there was very little OX42 immunostaining in TNF-α injected rats treated with minocycline (**C**, **D**, **G**, **H**). In the Group 9 and 10 rats (i.e. vehicle injections in rostral T11) there was a small area in the R-DF in the rostral part of T11 that contained OX42+ve reactive microglia in the saline treated rats (**I**), but otherwise the OX42 immunostaining revealed no microglial reactivity (**J-L**). Scale bar = 400 µm.

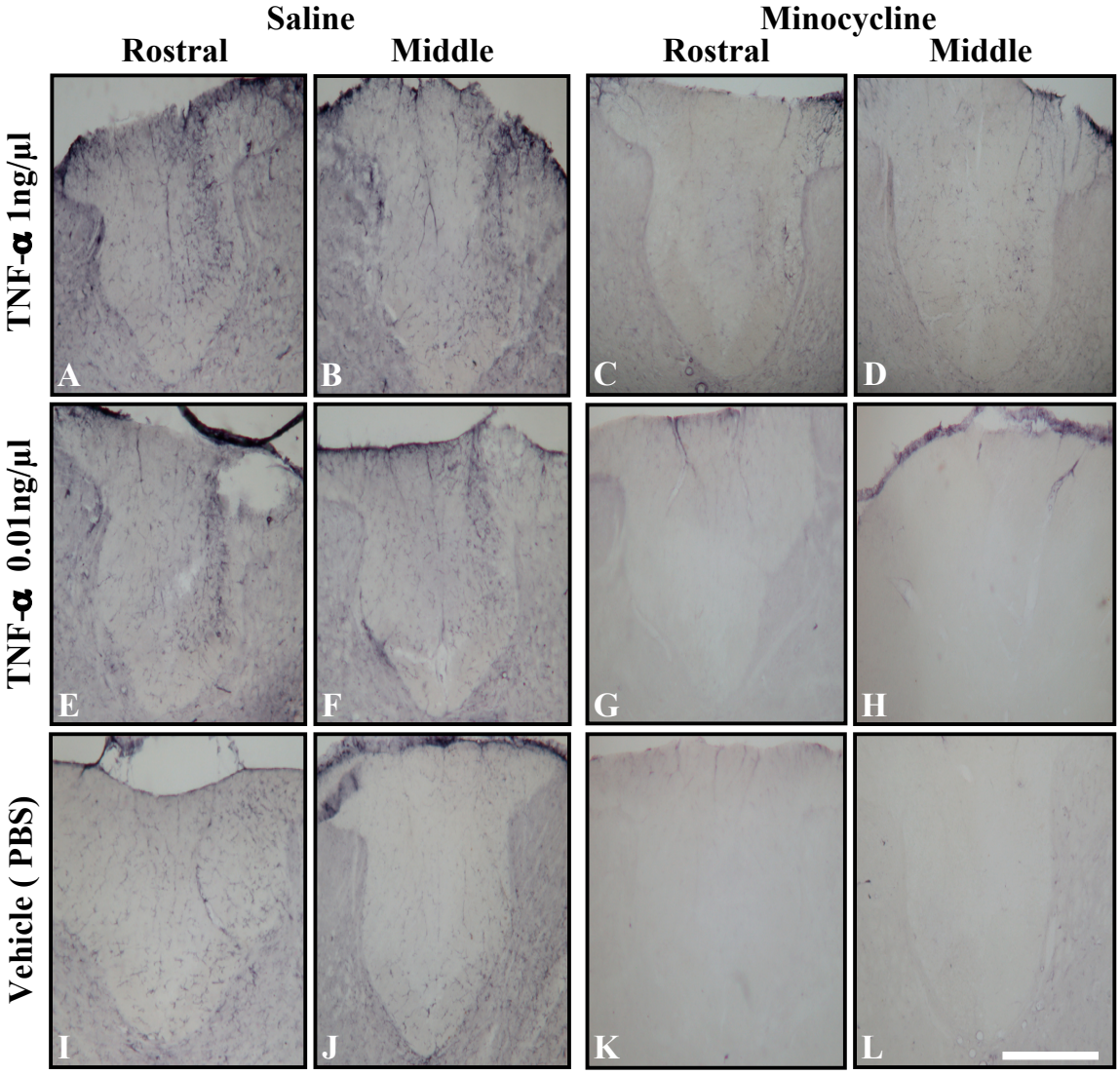

FIGURE 5.11: OX35 +ve microglia in the dorsal funiculus of T11 in Groups 5-10.

OX35+ve microglia in the R-DF at rostral (**A**, **C**, **E**, **G**, **I**, **K**) and middle (**B**, **D**, **F**, **H**, **J**, **L**) levels of T11 in rats receiving a 2 µl injection of either 1 ng/µl (**A-D**) or 0.01 ng/µl (**E-H**) of TNF-α or an equal volume of vehicle (**I-L**) into the most rostral part of T11. The rats received daily i.p. injections of either saline (**A**, **B**, **E**, **F**, **I**, **J**) or minocycline (**C**, **D**, **G**, **H**, **K**, **L**), with the daily treatments continuing for the first 4 weeks after the OECs were grafted. OX35+ve reactive microglia were still present in the R-DF at the rostral and middle levels of T11 at 8 weeks after the TNF-α injections (**A**, **B**, **E**, **F**) in rats treated with saline daily for the first 4 weeks, but there was very little OX35 immunostaining in TNF-α injected rats treated with minocycline (**C**, **D**, **G**, **H**). In the Group 9 and 10 rats (i.e. vehicle injections in rostral T11) there was no OX35 immunostaining in the T11 segment of the spinal cord (**I-L**). Scale bar = 400 µm.

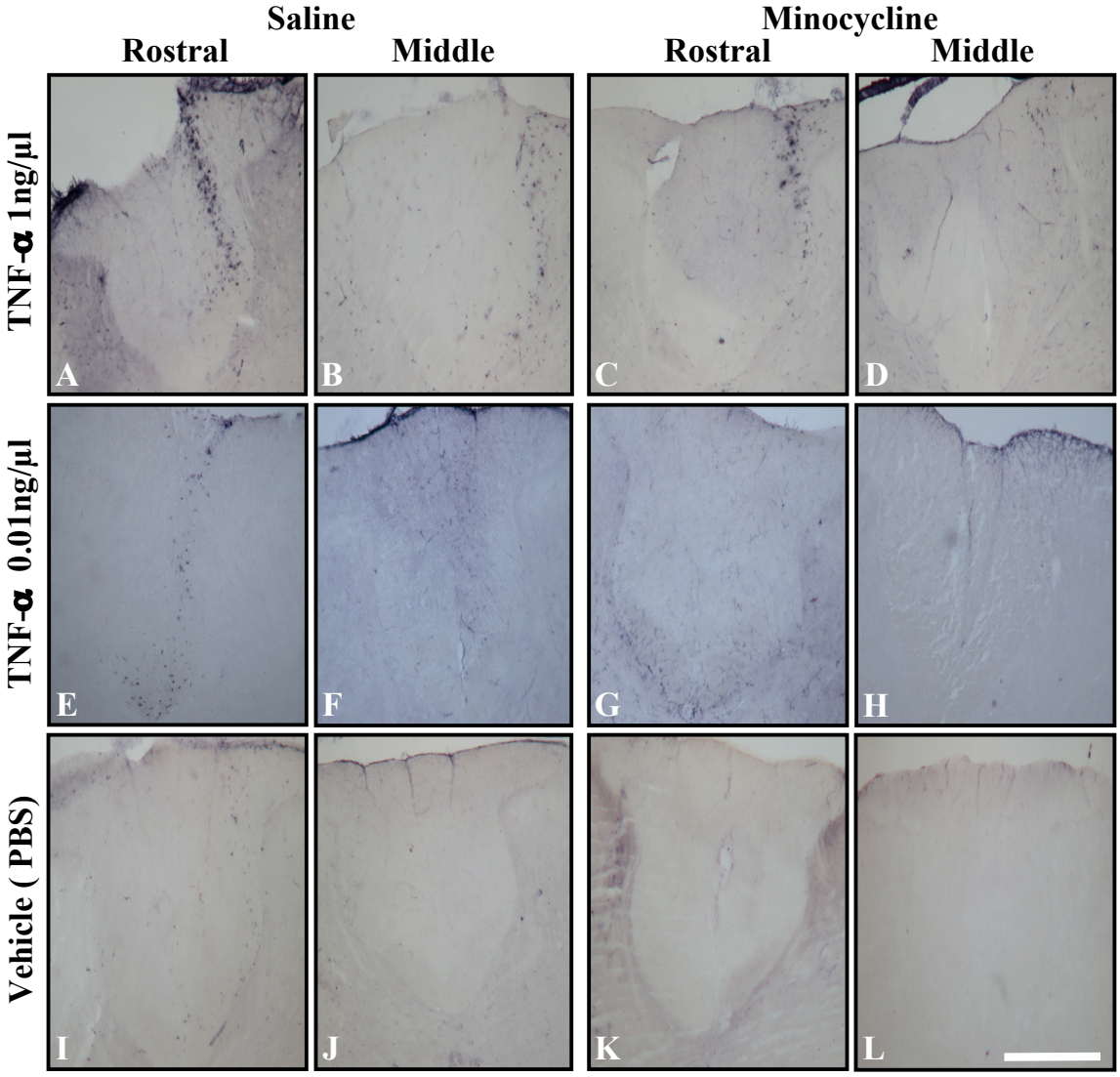

FIGURE 5.12: ED1 +ve microglia in the dorsal funiculus of T11 in Groups 5-10.

ED1+ve microglia in the R-DF at rostral (**A**, **C**, **E**, **G**, **I**, **K**) and middle (**B**, **D**, **F**, **H**, **J**, **L**) levels of T11 in rats receiving a 2 µl injection of either 1 ng/µl (**A-D**) or 0.01 ng/µl (**E-H**) of TNF-α or an equal volume of vehicle (**I-L**) into the most rostral part of T11. The rats received daily i.p. injections of either saline (**A**, **B**, **E**, **F**, **I**, **J**) or minocycline (**C**, **D**, **G**, **H**, **K**, **L**), with the daily treatments continuing for the first 4 weeks after the OECs were grafted. ED1+ve reactive microglia were still present in the R-DF at the rostral levels of T11 at 8 weeks after the TNF-α injections (**A**, **E**) in rats treated with saline daily for the first 4 weeks, and this immunostaining was most noticeably reduced in the 0.01 ng/µl TNF-α Group 8 rats that were treated with minocycline. Some ED1 immunostaining was also seen in the R-DF at the caudal level of T11 of the TNF-α injected rats treated with saline (**C**, **G**), but there were no ED1+ve microglia at the caudal level of T11 following minocycline treatment (**D**, **H**). In the Group 9 and 10 rats (i.e. vehicle injections in rostral T11) there was no ED1 immunostaining in the T11 segment of the spinal cord (**I-L**). Scale bar = 400 µm.

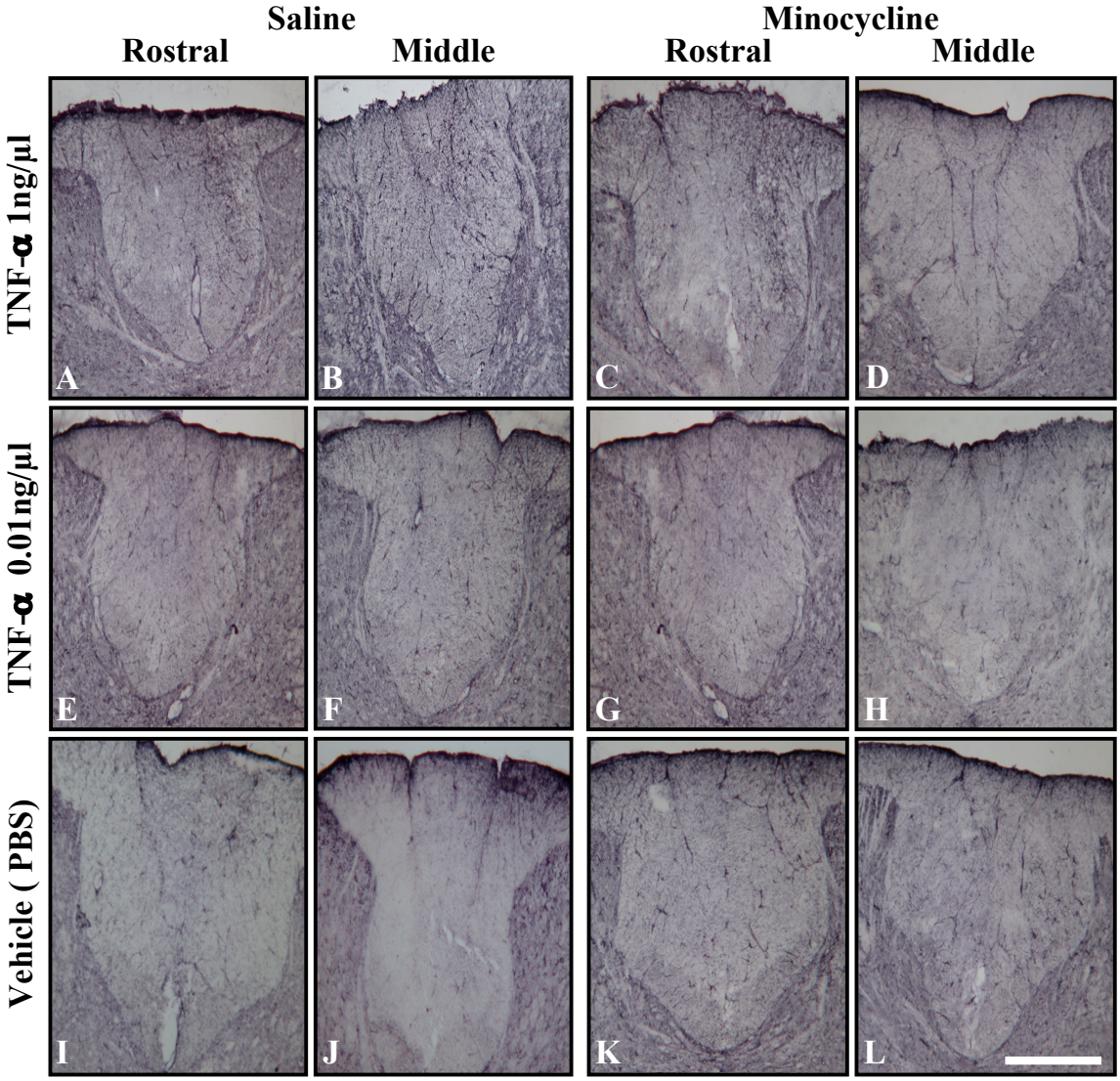

FIGURE 5.13: GFAP+ve astrocytes in the dorsal funiculus of T11 in Groups 5-10.

GFAP+ve astrocytes in the R-DF at rostral (**A**, **C**, **E**, **G**, **I**, **K**) and middle (**B**, **D**, **F**, **H**, **J**, **L**) levels of T11 in rats receiving a 2 µl injection of either 1 ng/µl (**A-D**) or 0.01 ng/µl (**E-H**) of TNF-α or an equal volume of vehicle (**I-L**) into the most rostral part of T11. The rats received daily i.p. injections of either saline (**A**, **B**, **E**, **F**, **I**, **J**) or minocycline (**C**, **D**, **G**, **H**, **K**, **L**), with the daily treatments continuing for the first 4 weeks after the OECs were grafted. No detectable astrocyte reactvity was seen in either the rostral or middle parts of T11 following injection of either vehicle (**I-L**) or of 0.01 ng/µl TNF-α (**E-H**). In contrast, the GFAP immunostaining showed a small amount of astrocyte reactivity in the rostral part of T11 after 1ng/µl of TNF-α injection in both the saline treated (**A**) and the minocycline treated (**C**) groups. Scale bar = 400 µm.

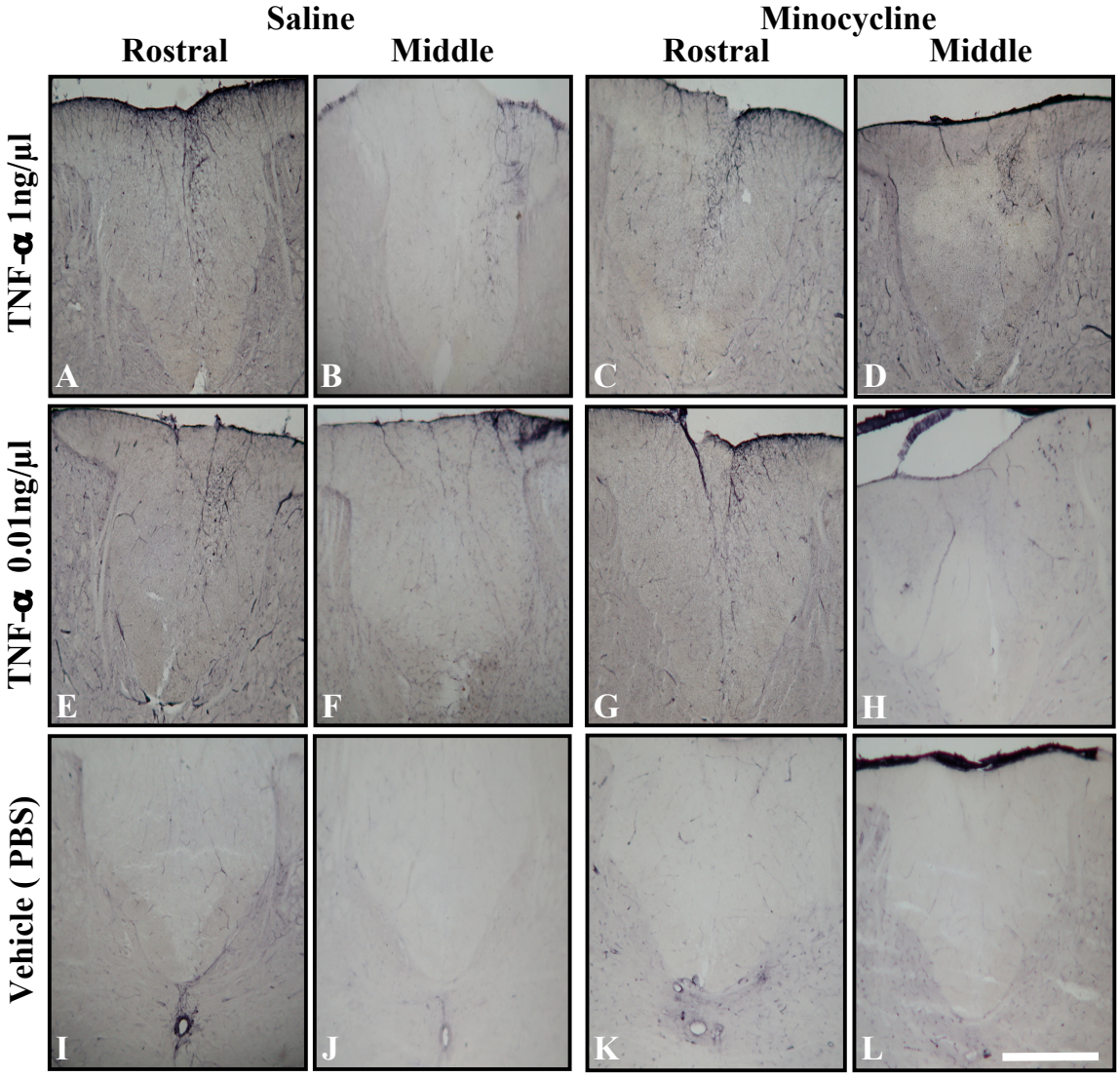

FIGURE 5.14: Vimentin +ve astrocytes in the dorsal funiculus of T11 in Groups 5-10.

Vimentin immunostaining in the R-DF at rostral (**A**, **C**, **E**, **G**, **I**, **K**) and middle (**B**, **D**, **F**, **H**, **J**, **L**) levels of T11 in rats receiving a 2 µl injection of either 1 ng/µl (**A-D**) or 0.01 ng/µl (**E-H**) of TNF-α or an equal volume of vehicle (**I-L**) into the most rostral part of T11. The rats received daily i.p. injections of either saline (**A**, **B**, **E**, **F**, **I**, **J**) or minocycline (**C**, **D**, **G**, **H**, **K**, **L**), with the daily treatments continuing for the first 4 weeks after the OECs were grafted. The only vimentin+ve reactive astrocytes seen were in the R-DF of the rostral part of T11 in the TNF-α injected rats treated with saline (**A**, **E**) or with minocycline (**C**, **G**). Scale bar = 400 µm.

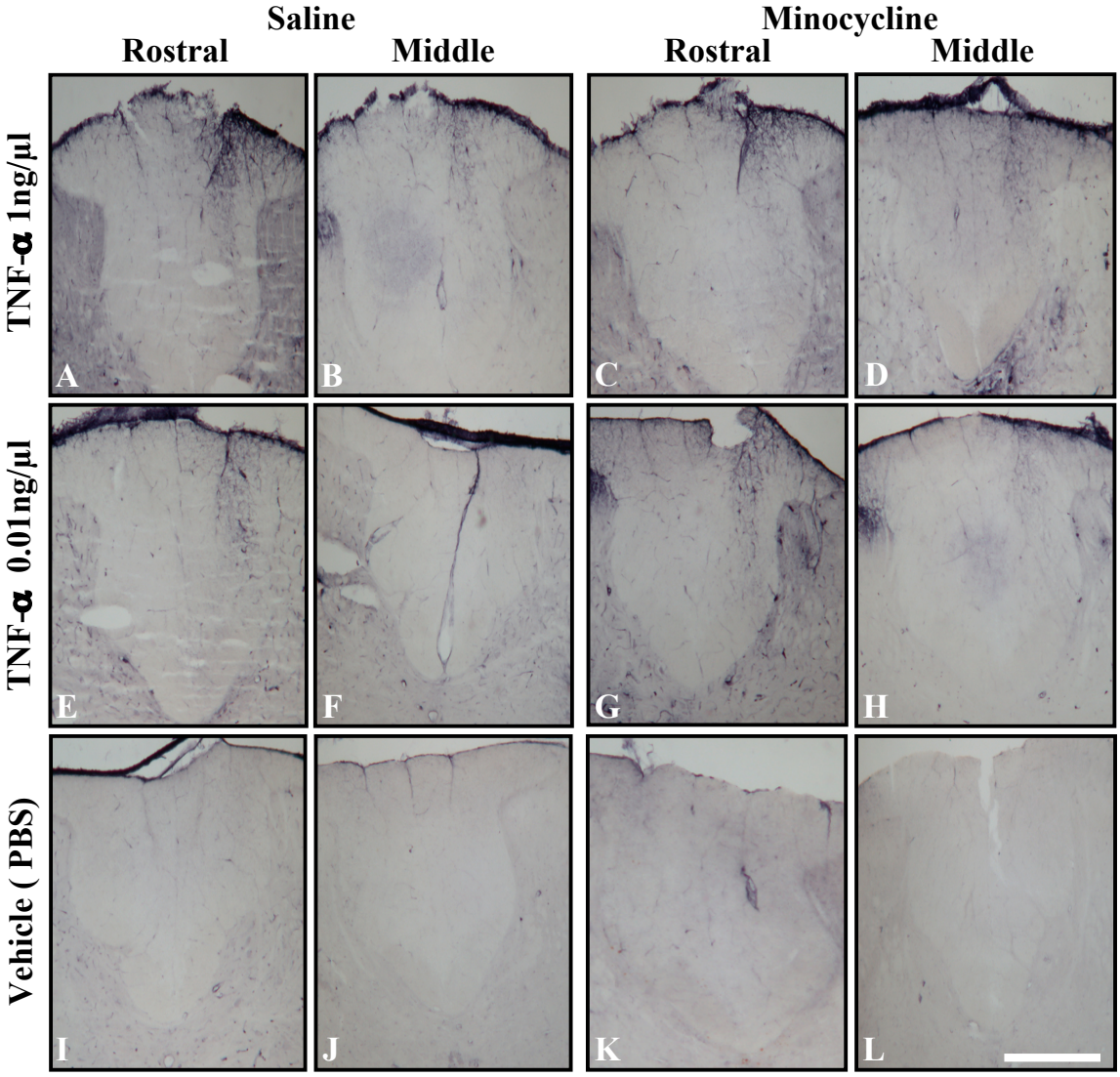

FIGURE 5.15: Nestin +ve astrocyte in the dorsal funiculus of T11 in Groups 5-10.

Nestin immunostaining in the R-DF at rostral (**A**, **C**, **E**, **G**, **I**, **K**) and middle (**B**, **D**, **F**, **H**, **J**, **L**) levels of T11 in rats receiving a 2 µl injection of either 1 ng/µl (**A-D**) or 0.01 ng/µl (**E-H**) of TNF-α or an equal volume of vehicle (**I-L**) into the most rostral part of T11. The rats received daily i.p. injections of either saline (**A**, **B**, **E**, **F**, **I**, **J**) or minocycline (**C**, **D**, **G**, **H**, **K**, **L**), with the daily treatments continuing for the first 4 weeks after the OECs were grafted. The only nestin+ve reactive astrocytes seen were in the R-DF of the rostral part of T11 in the TNF-α injected rats treated with saline (**A**, **E**) or with minocycline (**C**, **G**). Scale bar = 400 µm.

5.3.6 Preferential Migration of OECs towards T11 vs. T12-T13

We found that OECs migrated preferentially in the rostral direction towards the TNF- α injection site and through the TNF-α induced microglial reactivity in the R-DF of T11, in comparison to the corresponding part of the DF that extended caudally from the cell graft into T12 and part of T13. A two-factor analysis of variance (ANOVA) was applied to the data with the data for the right and left DF being analyzed separately for statistical significance. Multiple post hoc comparisons were performed with Bonferonni's multiple comparison post-test (Fig. 5.18). The two-factor ANOVA showed a significant main effect of TNF-α injection in both the right and left DF (Fig. 5.18 & 5.19); $F(2,18)= 60.6$, $p <0.0001$(A) (right DF), $F(2,18) = 10.7$, $p <0.0004$ (B) (left DF). There was also a significant main effect of T11 (i.e., rostral, middle and caudal) in both the right and left DF; $F(2,18) = 27.4$, $p<0.0001$ (right DF), $F(2, 18) = 20.3$, $p<0.0001$ (left DF). The two-factor ANOVA revealed a significant interaction between the TNF-α/vehicle and rostral/middle/caudal variables in the right and left DF; $F(4,18)= 8.21$, $p <0.0002$ (A) (right DF), $F(4,18)= 3.4$, $p <0.0216$ (B) (left DF). Bonferonni's post-test revealed the ratio of DiI+ve cells was significantly different ($p<0.05$) between the comparisons indicated by the brackets in Fig 5.18A and Fig. 5.18B.

FIGURE 5.16: Number of DiI+ve OECs in the right dorsal funiculus of T11 in Groups 5-10

Histograms depicting the mean number (+/- SEM) of DiI+ve OECs (Y-axis) in the right DF of the rostral (A), middle (B) and caudal (C) third of the T11 spinal cord segment at 8 weeks after either TNF-α (Groups 5-8) or vehicle (Groups 9-10) injection into the R-DF of the rostral part of T11 and OECs grafted 5 mm caudally. The rats received daily i.p. injections of either saline (Groups 5, 7 and 9) or minocycline (Groups 6, 8 and 10), with the daily treatments continuing for the first 4 weeks after the OECs were grafted. A two-factor analysis of variance (ANOVA) was applied to the data with the data for the rostral (A), middle (B) and caudal (C) thirds of T11 being analyzed separately for statistical significance (see Section 5.2.6). Multiple post hoc comparisons were performed with Bonferonni's multiple comparison post-test. Bonferonni's post-test revealed the density of DiI+ve cells in the right DF was significantly higher ($p<0.05$; brackets) in the 1 ng/µl TNF-α than either 0.01 ng/µl TNF-α or vehicle groups at the rostral (A), middle (B) and caudal (C) levels of T11. In addition, Bonferonni's post-test revealed the number of DiI+ve cells in the right DF was significantly higher ($p<0.05$; brackets) in the 0.01 ng/µl TNF-α than vehicle groups at the rostral (A), middle (B) and caudal (C) levels of T11. The post-test also revealed a significant reduction in the number of DiI+ve cells in the right DF ($p<0.05$; brackets) in minocycline treated rats both in the 1 ng/µl TNF-α and the 0.01 ng/µl TNF-α groups (Groups 6 and 8) compared with the saline treated groups (Groups 5 and 7) at all levels of T11. The post-test also revealed a significant reduction in the number of DiI+ve cells in the right DF ($p<0.05$; brackets) in the minocycline treated rats injected with vehicle (Group 10) compared to the saline treated rats (Group 9) only at the rostral (A) and middle (B) levels of T11.

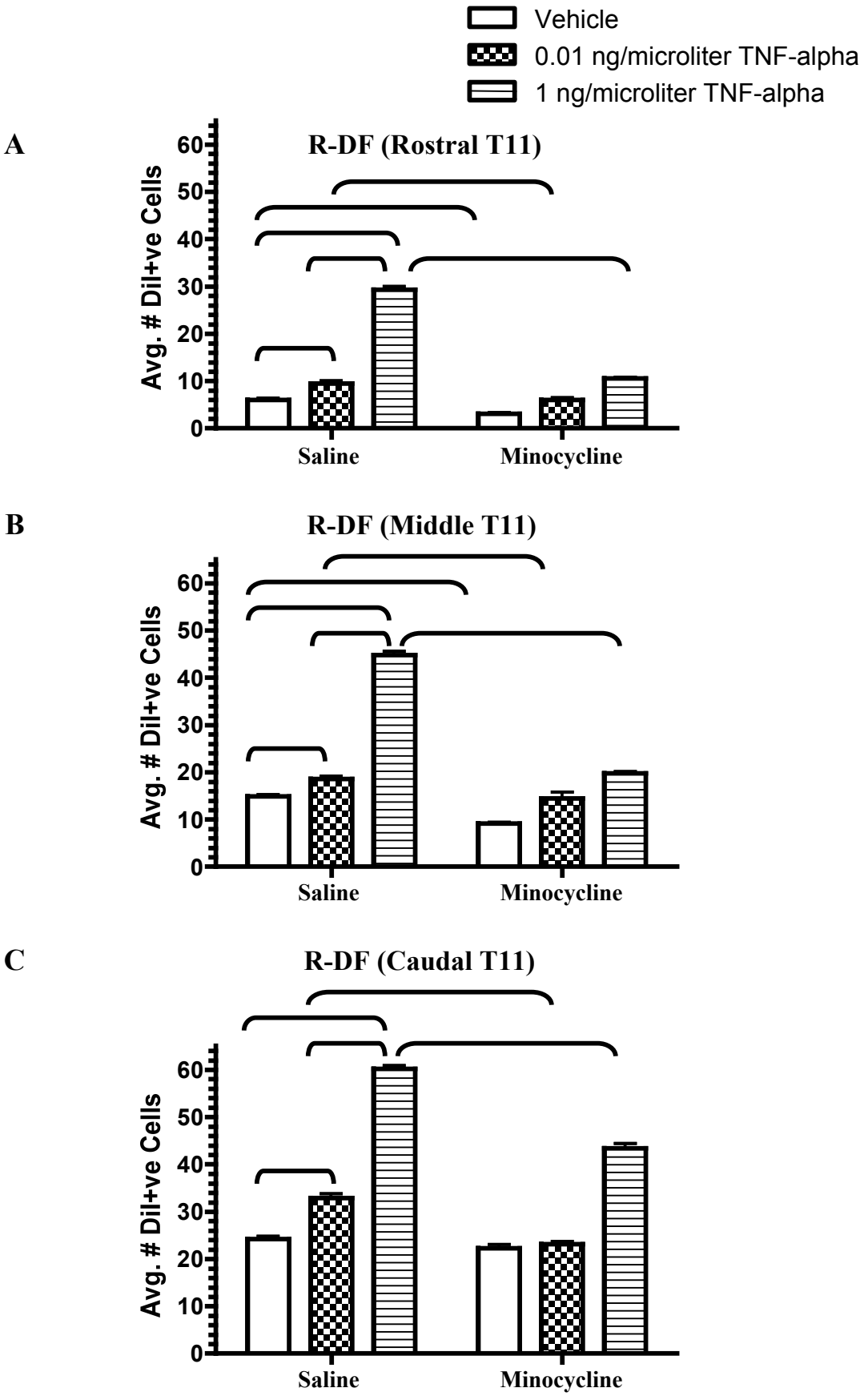
Vehicle
0.01 ng/microliter TNF-alpha
1 ng/microliter TNF-alpha
A
R-DF (Rostral T11)
Avg. # DiI+ve Cells
0
10
20
30
40
50
60
Saline
Minocycline
B
R-DF (Middle T11)
Avg. # DiI+ve Cells
0
10
20
30
40
50
60
Saline
Minocycline
C
R-DF (Caudal T11)
Avg. # DiI+ve Cells
0
10
20
30
40
50
60
Saline
Minocycline

FIGURE 5.17: Number of DiI+ve OECs in the left dorsal funiculus of T11 in Groups 5-10

Histograms depicting the mean number (+/- SEM) of DiI+ve OECs (Y-axis) in the left DF of the rostral (A), middle (B) and caudal (C) third of the T11 spinal cord segment at 8 weeks after either TNF-α (Groups 5-8) or vehicle (Groups 9-10) injection into the R-DF of the rostral part of T11 and OECs grafted 5 mm caudally. The rats received daily i.p. injections of either saline (Groups 5, 7 and 9) or minocycline (Groups 6, 8 and 10), with the daily treatments continuing for the first 4 weeks after the OECs were grafted. A two-factor analysis of variance (ANOVA) was applied to the data with the data for the rostral (A), middle (B) and caudal (C) thirds of T11 being analyzed separately for statistical significance. Multiple post hoc comparisons were performed with Bonferonni's multiple comparison post-test. Bonferonni's post-test revealed the number of DiI+ve cells in the left DF was significantly higher ($p<0.05$; brackets) in the 1 ng/µl TNF-α than either 0.01 ng/µl TNF-α or vehicle groups at the rostral (A), middle (B) and caudal (C) levels of T11. In addition, Bonferonni's post-test revealed the number of DiI+ve cells in the left DF was significantly higher ($p<0.05$; brackets) in the 0.01 ng/µl TNF-α than vehicle groups at only the caudal (C) level of the T11 segment. The post-test also revealed a significant reduction in the number of DiI+ve cells in the left DF ($p<0.05$; brackets) in the minocycline treated 1 ng/µl TNF-α animal group (Group 6) compared to saline treated ones (Group 5) at all levels of T11. However, the post-test also revealed a significant reduction in the number of DiI+ve cells in the left DF ($p<0.05$; brackets) in minocycline treated 0.01 ng/µl TNF-α rats (Group 8) compared to saline treated ones (Group 7) only at the caudal (C) part of T11. The post-test also revealed a significant reduction in the number of DiI+ve cells in the left DF ($p<0.05$; brackets) in minocycline treated rats who received a vehicle injection (Group 10) compared to saline treated ones (Group 9) only at the middle and caudal (C) part of T11.

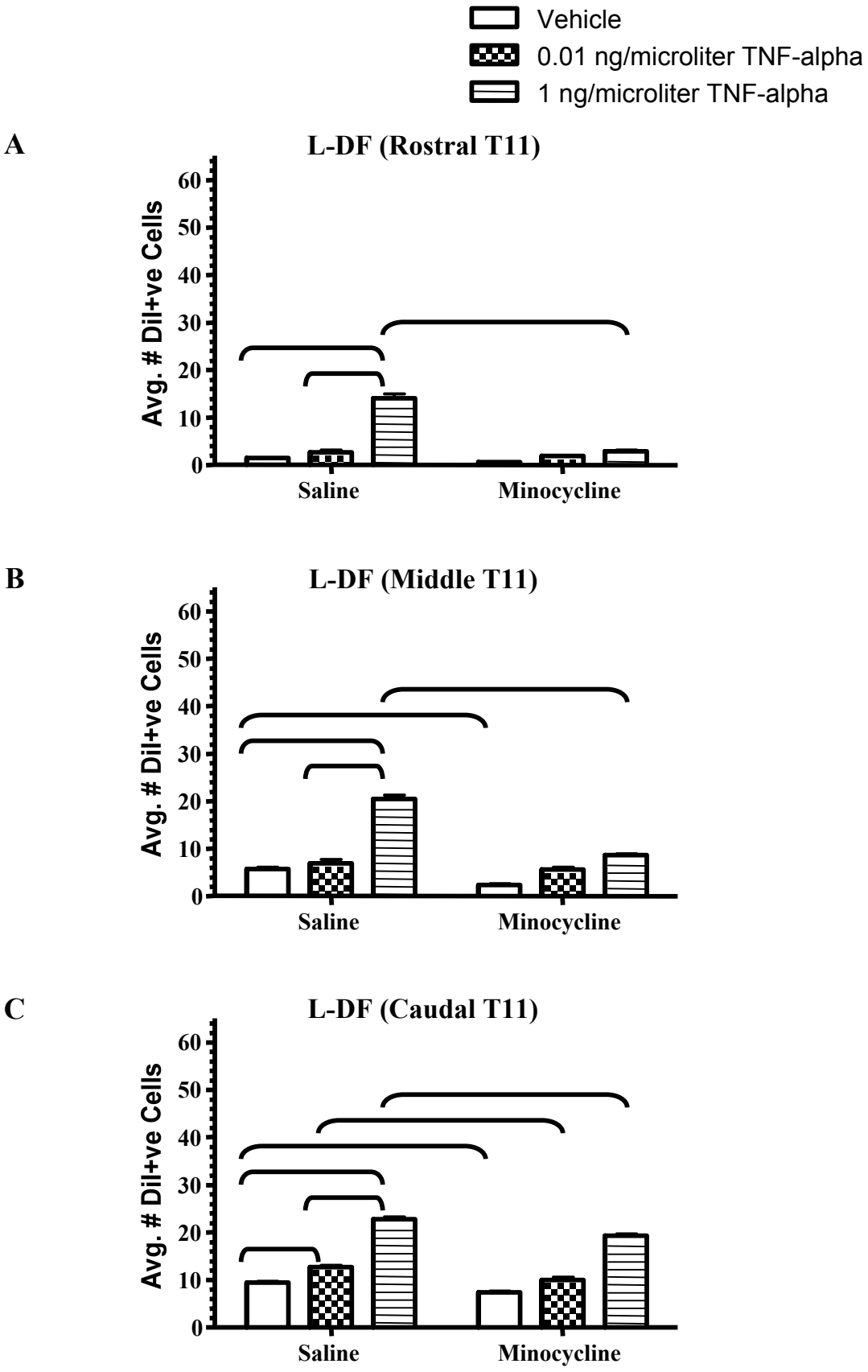
Vehicle
0.01 ng/microliter TNF-alpha
1 ng/microliter TNF-alpha
A
L-DF (Rostral T11)
Avg. # DiI+ve Cells
60
50
40
30
20
10
0
Saline
Minocycline
B
L-DF (Middle T11)
Avg. # DiI+ve Cells
60
50
40
30
20
10
0
Saline
Minocycline
C
L-DF (Caudal T11)
Avg. # DiI+ve Cells
60
50
40
30
20
10
0
Saline
Minocycline

FIGURE 5.18: **Ratio of DiI+ve OECs in the dorsal funiculus of T11 vs. T12/13 in Groups 5-10**

Histograms depicting the mean ratio (+/- SEM) of DiI+ve OECs (Y-axis) in the right (A) and left (B) DF of the rostral, middle and caudal third of the T11 spinal cord segment at 8 weeks after either TNF-α (Groups 5 and 7) or vehicle (Group 9) injection into the R-DF of the rostral part of T11 and OECs grafted 5 mm caudally. All rats received daily i.p. injections of saline, with the daily treatments continuing for the first 4 weeks after the OECs were grafted. A two-factor analysis of variance (ANOVA) was applied to the data with the data for the right (A) and left (B) DF being analyzed separately for statistical significance. Multiple post hoc comparisons were performed with Bonferonni's multiple comparison post-test. Bonferonni's post-test revealed the ratio of DiI+ve cells was significantly different ($p<0.05$) between the comparisons indicated by the brackets in 'A' and 'B'.

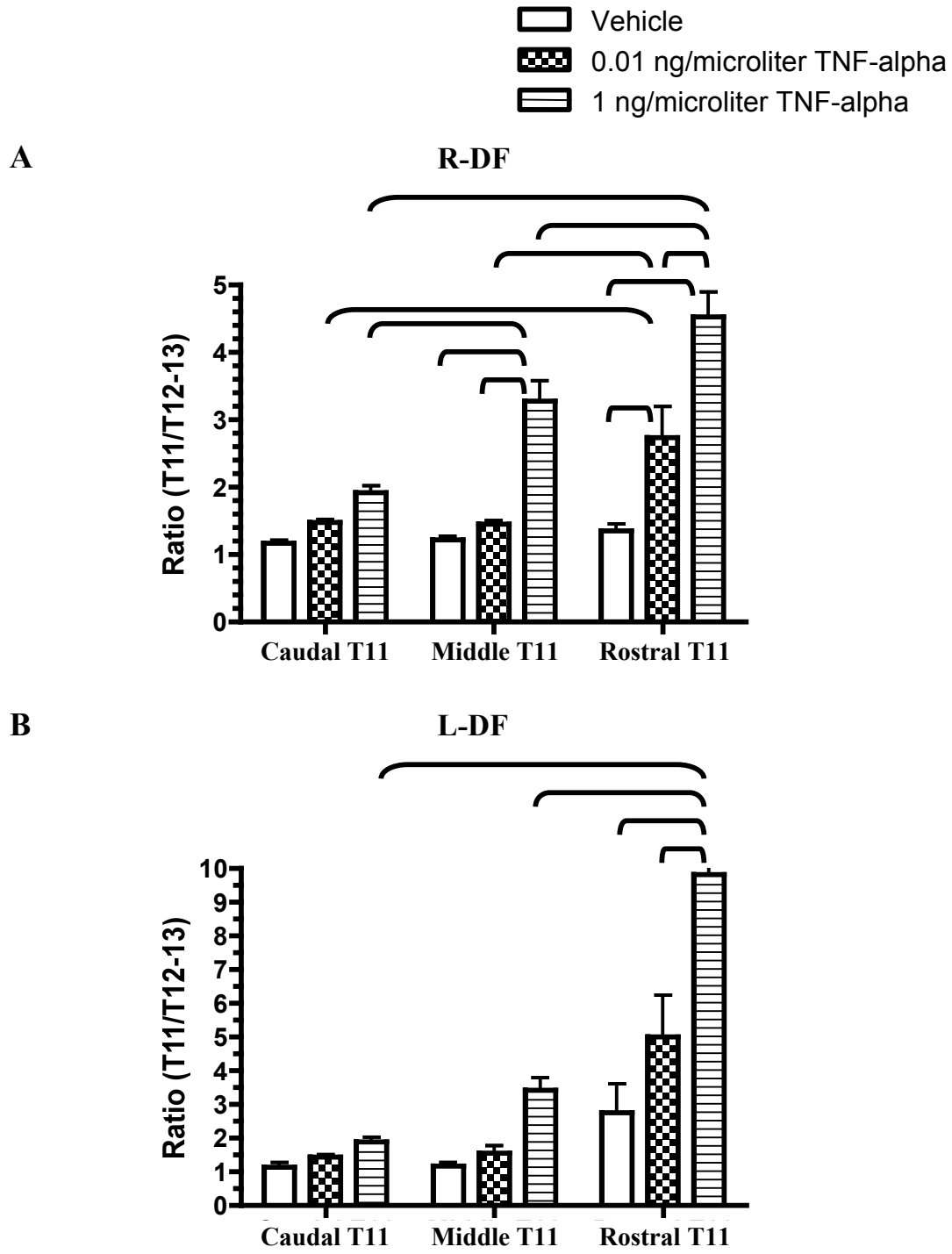
Vehicle
0.01 ng/microliter TNF-alpha
1 ng/microliter TNF-alpha
A
R-DF
Ratio (T11/T12-13)
0
1
2
3
4
5
Caudal T11
Middle T11
Rostral T11
B
L-DF
Ratio (T11/T12-13)
0
1
2
3
4
5
6
7
8
9
10
Caudal T11
Middle T11
Rostral T11

FIGURE 5.19: DiI+ve cells in the dorsal funiculus of T11 in Group 5, 7 and 9
A, C, E show low power fluorescent image of the DF of the T11 spinal cord segment of a rat from Group 5, 7, and 9 respectively that were injected with a 2 µl volume of 1 ng/µl of TNF-α (group 5), 0.01 ng/µl of TNF-α (group 7), vehicle 0.03M PBS (group 9) in the R-DF of the rostral part of T11 and received an OEC graft 5 mm caudally. The part of the R-DF enclosed in the white rectangle is shown at higher power in 'B,D,F'; Higher power view of part of the R-DF showing a single DiI+ve cell (red arrowhead) (B) and its blue Hoechst-stained nucleus (white arrow), three DiI+ve cells (red arrowheads) and their blue Hoechst-stained nuclei (white arrows) (D), four DiI+ve cells (red arrowheads) and their blue Hoechst-stained nuclei (white arrows) (F).
Scale `Bar = 400 µm for 'A,C, and E '
Scale Bar= 20 µm for 'B,D, and F

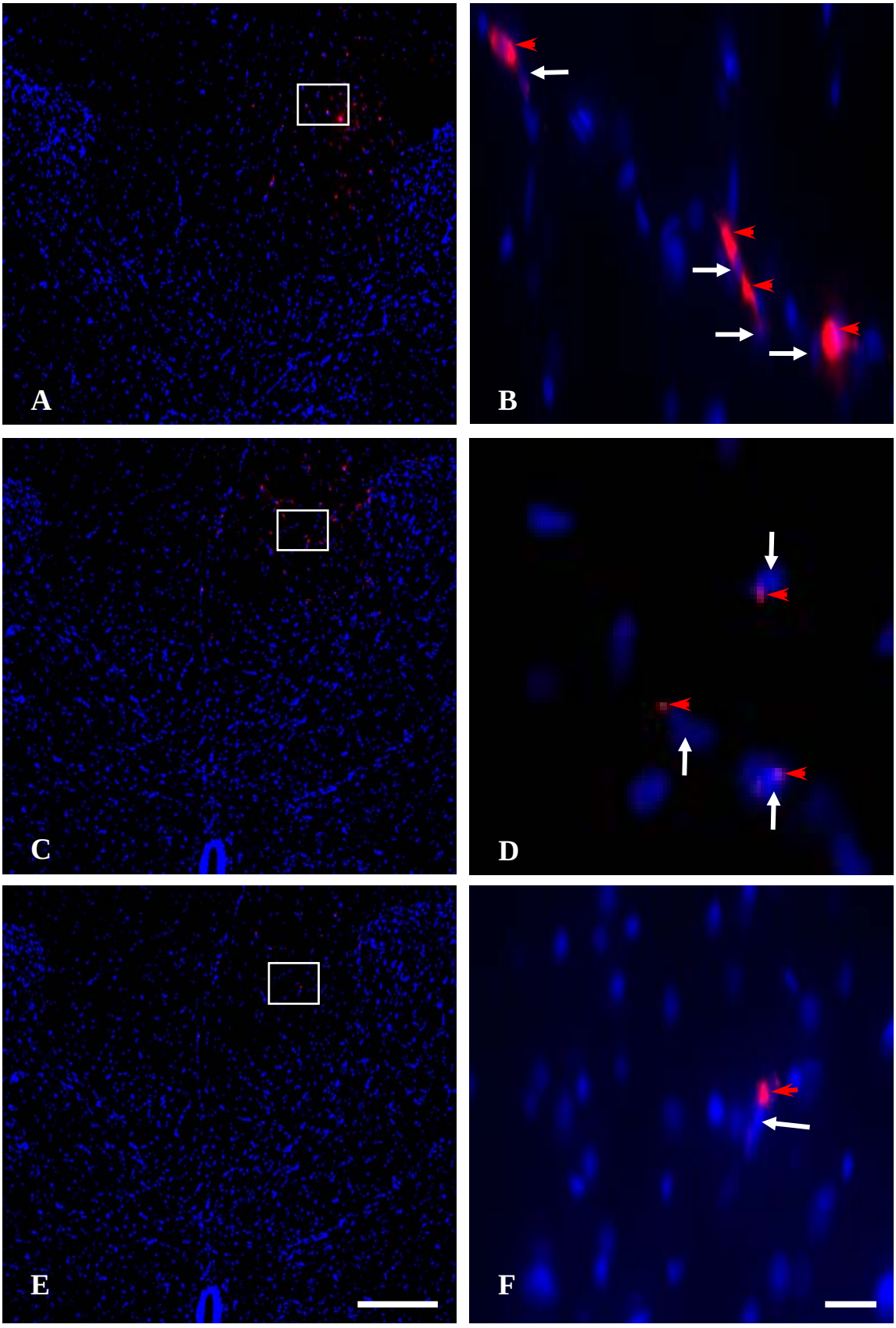
A
B
C
D
E
F

5.4 Discussion

5.4.1 Focal Injection of TNF-α as a Tool for Restricting Cytokine-Induced Glial Reactivity to Specific Parts of Spinal Cord White Matter

The findings of the experiment reported in Chapter 4 linked the presence of a migratory signal(s) both spatially and temporally with WD-induced microglial reactivity. The purpose of the experiment reported in Chapter 5 was to determine whether cytokine-induced microglial reactivity would also be associated with the presence of migratory signal(s) and whether this microglial reactivity must extend at least as far as the OEC graft for any migratory signal(s) to be effective. TNF-α was chosen for use in this experiment because it is one of the proinflammatory cytokines for which both microglia and astrocytes have receptors on the cell surface (see Section 1.5.1). Injections of small quantities of a proinflammatory cytokine into neural tissue to induce inflammation has been used by other scientists (Claudio et al., 1994; Schnell et al., 1999; Simmon and Willenborg, 1990), but this is the first instance in which such an injection was used for the specific purpose of studying the contribution of reactive microglia to the generation of a migratory signal(s).

For example, intracerebral injections of TNF-α have been shown to induce inflammatory reactions in murine brain as indicated by immunohistochemical analysis for mononuclear infiltrated cells. However, ultrastructural examinations 2 months after TNF-α injection showed no apparent pathological changes in glial and endothelial cells (Yamasaki et al., 1992). Claudio et al. (1994) studied the role of inflammatory cytokines (TNF-α and Il-1ß) in induction of inflammation, with the retina system having been used as a model for the cytokine injections. Their study showed the inflammatory response is characterized by the presence of polymorphonuclear and mononuclear cells. In the CNS the effect of cytokine injection appears to be site specific. For reasons that are poorly understood, significantly different inflammatory responses occur in brain and spinal cord following cytokine injections. Schnell et al. (1990) demonstrated that the injection of TNF-α into the striatum of Wistar rats failed to break down the BBB or to recruit leukocytes, whereas in the spinal cord injection of TNF-α resulted in marked BBB breakdown and leukocyte recruitment. It was also reported that there was an inflammatory response similar in pattern to that observed during EAE following a single

injection of TNF-α into the lumbosacral spinal cord of rats, with the appearance of mononuclear cuffs within the spinal cord (Simmons and Willenborg, 1990).

The TNF-α Pilot Study (see Section 5.3.1) determined that a concentration of 1 ng/µl TNF-α injected into the dorsal funiculus of the T11 spinal cord segment induced glial reactivity that extended the entire 5 mm distance between T11 and T12 whereas 0.01 ng/µl TNF-α only induced a localized glial response confined to the vicinity of the injection site. Whether this cytokine-induced glial reactivity as a result of a focal injection of TNF-α was due to diffusion of the cytokine over this 5 mm distance cannot be ruled out, though it seems unlikely. In support of this idea, Felts et al. (1997, 2005) found that a lesion induced by an intraspinal injection of 1-2 µl of ethidium bromide or lipopolysaccharide (LPS) is typically only a few millimeters (1-2 mm) in longitudinal extent, indicating limited spread of the cytotoxin within the spinal cord white matter. It is more likely that microglia situated close to the injection site were activated as a consequence of the TNF-α injection. These cytokine-activated microglia, through the secretion of proinflammatory cytokines that include TNF-α, may result in the sequential activation of additional microglia in a paracrine manner that could extend as far away as 5 mm from the TNF-α injection site.

The results of the pilot study are summarized in Tables 5.1 and 5.2. These data showed that a single injection of TNF-α (either 1 ng/µl or 0.01 ng/µl) into the dorsal funiculus of the spinal cord was well tolerated in adult rats. These doses of TNF-α triggered a pronounced microglial reactivity, based on immunostaining with the OX18, OX35, OX42 and ED1 monoclonoal antibodies, as well as astrocyte reactivity, based on immunostaining with antibodies to GFAP, Vim and nestin. These results support a key role for TNF-α as a mediator of the microglial and astrocytic responses within the white matter of the adult rat spinal cord. Based on the results of the pilot study the concentrations of 1 ng/µl and 0.01 ng/µl of TNF-α were identified as optimal concentrations to test our hypothesis.

5.4.2 TNF-α Induced Glial Reactivity: Microglial Contribution to Generation of a Migratory Signal

The early release of TNF-α after CNS injury is essential for a proper microglial response that can effectively resolve and phagocytose the initial damage and act to prevent, or at least limit, subsequent secondary damage (Blais and Rivest, 2004); the absence of TNF-α delays activation of microglial cells, which leads subsequently to an exaggerated activation of microglia in response to the accumulation of necrotic debris (Blais and Rivest, 2004). Interestingly, the priming of microglial cells by innate immunity is TNF-α specific because these effects do not extend to other proinflammatory cytokines such as IL-1ß (Blais and Rivest, 2004). The results of the experiments reported in this chapter support the presence of a rapid, well regulated microglial reaction in response to direct TNF-α injection into the dorsal funiculus of the spinal cord.

In the current study, a focal injection of TNF-α into the dorsal funiculus of T11 was used as a tool to induce microglial reactivity; the concentrations of TNF-α used were pharmacological doses (Anderson et al., 1992; Glabinski et al., 1998). Thus, a possible gliotoxic effect of TNF-α injection might lead to cell apoptosis, particularly of oligodendrocytes. Although no test was employed to verify this possible gliotoxic effect, phagocytic microglia (paricularly OX42+ve microglia) (see Section 5.3.3) were detected in the rostral part of T11 close to the site of TNF-α injection in Groups 5 and 7 rats, which had received a focal injection of TNF-α. A less intense immunostaining of microglia with the OX42 antibody in tissue sections from Group 7 rats (i.e. focal injection of 0.01 ng /µl of TNF-α) as compared to Group 5 rats (i.e. focal injection of 1 ng/µl of TNF-α) (see Section 5.3.3) suggests a dose-dependent effect of TNF-α on the expression of CR3 (the receptor that binds the OX42 antibody). Furthermore, there was no phagocytic phenotype of microglia seen in the vicinity of the vehicle injection (Groups 9 and 10).

Due to the large number of factors, which include cytokines, chemokines, and enzymes, that will be released by activated microglia (Kim and Vellis, 2005; Kreutzberg, 1996; Thomas et al., 2006), it is hard to judge microglial functions by assessment of the effects of only a few isolated microglial factors while neglecting many others. Based on microarray data, the upregulation or downregulation of such factors produced by LPS-

activated microglia ranges from two to at least a thousand fold change in expression levels (Thomas et al., 2006), suggesting that the amounts of the corresponding proteins may change accordingly. The current study used several selected markers known to be upregulated during microglial activation and confirmed that the TNF-α activated microglia upregulated their expression of complement receptor 3 (OX42), MHC class I (OX18), CD4 (OX35), and the lysosomal antigenic epitope recognized by the ED1 monoclonal antibody. This microglial reactivity extended the entire length of the T11 segment (approximately 5 mm) in response to a focal injection of 1 ng/µl of TNF-α, whereas the reactive microglia were confined mostly to the rostral part of T11 in response to an injection of 0.01 ng/µl TNF-α.

In many injury and disease models microglial activation gradually increases from mild to intense. For instance, CR3 expression (OX42 monoclonal antibody), which is the most commonly used microglial marker, has been reported to be only slightly upregulated on day 1 but drastically upregulated on day 5 in the vicinity of axotomized motor neurons (He et al., 1997). In the pilot study, the intensity of immunostaining of microglia with the OX42 monoclonal antibody was most intense in the rostral portion of T11 at 1 and 4 days after TNF-α injection; the intensity of OX42 immunostaining was reduced dramatically by 14 days after cytokine injection, irrespective of the concentration of TNF-α which had been used. However, in rats that had received both a focal injection of TNF-α and an OEC graft and were treated with daily IP injections of vehicle (i.e. Group 5 rats) there was intense OX42 immunostaining of the microglia suggestive of their reactivation or of the microglial reaction being prolonged when the cytokine injection at T11 was coupled with an OEC graft 5 mm caudally. The reason for such fluctuation in microglia reactivity will require more study.

Minocycline is a tetracycline derivative that exerts anti-inflammatory effects and inhibits microglial activation by decreasing IL-1β (Vincet and Mohr, 2007), nitric oxide release (Tikka and Koistinaho, 2001) and TNF-α secretion (Fan et al., 2007)**.** The data presented in this chapter demonstrate that daily treatment of adult rats with minocycline over a 4 week time period after a focal injection of TNF-α into the dorsal funiculus of the spinal cord resulted in a marked reduction in the cytokine-induced microglial reactivity in comparison to vehicle-treated controls. This reduction in microglial activation in

response to minocycline treatment occurred in the absence of any demonstrable change in the immunophenotype or morphology of reactive astrocytes since the immunostaining intensity for GFAP, Vim, and nestin and the morphology of the astrocytyes was not noticeably different from the vehicle controls (see Section 5.3.3). Furthermore, the reduction in microglial activation was accompanied by a significant reduction in the number of DiI+ve OECs that were seen in the dorsal funiculus of T11. In other words, the decreased cell number of migrated OECs in the minocycline-treated rats was associated with a dampening of the microglial reactivity as indicated by immunostaining the microglia with the OX42, OX18, OX35 and ED1 monoclonal antibodies (see Sections 5.3.3 and 5.3.4). These findings support the hypothesis that microglial reactivity plays a role in the generation of a migratory signal(s) inducing OECs to migrate towards the source of a focal injection of TNF-α.

5.4.3 TNF-α Induced Glial Reactivity: Potential Migratory Signals Inducing OECs to Migrate

TNF-α by itself activates microglia (John et al., 2003) and activated microglia release numerous neuroinflammatory substances, which include prostanoids, proteases, nitric oxide (NO), superoxide, and the proinflammatory cytokines TNF-α and IL-1β, that potentially can break down the BBB (Dringen, 2005; Tsao et al., 2001; and Yenari et al., 2006). Could some of these factors play a role either directly or indirectly in the migration of OECs? TNF-α certainly could since it causes a redistribution of cadherin and of the junctional adhesion molecule (JAM) leading to a rearrangement of microfilaments and a down-regulation of occludin expression in endothelial cells, increases BBB permeability, and allows the infiltration of immune cells giving rise to a more complex cellular environment in the area containing elevated levels of TNF-α (Petrache et al., 2003; Mankertz et al., 2000). We cannot at this time, however, verify or reject a direct role for TNF-α in the generation of a migratory signal(s) and it remains to be determined whether OECs even express the TNF-α receptor. However, the data do indicate OECs preferentially migrated towards the source of the TNF-α injection, and that this migration occurred only when the TNF-α induced microglial reactivity extended the full distance between the cell graft and the cytokine injection (see Section 5.3.4).

Microinjection of the chemokines MCP-1 and MIP-1α into the normal, unlesioned spinal cord induced slightly increased expression of IL-1ß, TNF-α, IL-10 and RANTES and injection of IL-1ß induced a marked increase in MCP-1 and MIP-1α expression as well as that of other cytokines (Perrin et al., 2005). Furthermore, MCP-1, MIP-1α and IL-1ß also induced expression of the anti-inflammatory cytokines IL-10 and TGF-ß (Perrin et al., 2005). The latter response may in part underlie the protective effects noted after injection of proinflammatory cytokines, including IL-1ß, into spinal cord lesions (Klusman and Schwab, 1997). There is also likely a dynamic interaction between various chemokines and cytokines in which the expression of one regulates the expression of others and vice versa. The expression profile of members of this cytokine/chemokine network may be crucial for the effective recruitment and activation of microglia/macrophages and also for shutting down the immune response to prevent abnormal inflammation and tissue damage.

Whether this expression profile also contributes to the migratory signal(s) that induces OECs to migrate along the path of microglial reactivity towards the source of the TNF-α injection is a question to be addressed by future studies. However, it is possible to speculate based on the findings of other studies that support chemotactic roles for some of these factors. Previous studies have shown that microglia release a large number of bioactive factors and each individual factor could exert protective/trophic or destructive/toxic effects on cells within the area of microglial reactivity (Giulian and Robertson, 1990). The goal of the present study was not to show the type and amounts of potential chemotactic factors released from activated microglia, although the data do suggest that the strength of the migratory signal(s) might be determined, in part, by the intensity of the microglial reactivity and its distribution in the dorsal funiculus of T11 with respect to the OEC graft.

The fact that activated microglia resemble peripheral macrophages (Raivich and Banati, 2004) is the reason why the exact role that microglia play in immunologic functions in the CNS has been difficult to study. It was long believed that the CNS had a poor ability to tolerate activity of intrinsic immune cells like microglia. According to this view, activation of these cells would always be detrimental to the CNS, causing death of neurons and oligodendrocytes, and interfering with repair processes. However, more

recent studies showed that a local immune response that is properly controlled can support survival, promote remyelination, and facilitate recovery (Schwartz et al., 2003). When microglia are activated, they start secreting a broad range of cytokines, trophic factors and toxic mediators that could mediate a protective or damaging effect on surrounding cells. One of the most remarkable properties of microglia is their ability to respond to internal signals (e.g., from cells of the body that are damaged or stressed) or to signals that arise from outside the body (e.g. from pathogens); the microglial response is directed for purposes of tissue repair or induction of an immune response (Aloisi, 2001). When activated *in vitro*, microglia undergo morphological changes including shortening of cellular processes and enlargement of their soma and become phenotypically and morphologically similar to peripheral macrophages. Reactive microglia upregulate the expression of several molecules, which include CD4, MHC-I, CR3 and ED1 antigenic epitope. The opposite can also happen; when macrophages from the blood stream enter the CNS environment, they will gradually transform into ramified microglia (Raivich and banati, 2004). Microglia have also been shown to differentiate *in vitro* into cells that resemble dendritic cells. As stated before, microglia upregulate a number of molecules when they are activated, including CD11b, which is a dendritic cell marker (Fischer and Reichmann, 2001). Microglia can express a large array of receptors, which are either constitutively expressed or induced by certain signals. This variety of receptors enables microglia to response differently to various signals (Aloisi, 2001). Both activated microglia and macrophages express all of the markers that were used in the experiments described in this thesis; therefore, it would be impossible to distinguish microglia from infiltrated macrophages in the inflamed environment of spinal cord created through the TNF-α injection.

A common problem encountered with cell-based therapy is exposure of transplanted cells to host cytokines such as TNF-α which results in donor cell damage. The initial damage may then trigger a secondary phase of damage causing substantial destruction of the spinal cord. OEC grafting has been introduced as one of the prominent candidates to assist CNS axon regeneration and remyelination in several animal models of SCI (Li et al., 1997; Ramon-Cueto et al., 2000). Since OECs are able to modify the behavior of host glial cells (Lakatos et al., 2000) they are candidates for cell-based

therapy, and initial experimental studies in rats demonstrated neuroprotection by reducing astrocystic gliosis and cystic cavitation (Verdu et al., 2001). We used an *in vivo* animal model in which OECs were grafted into the right dorsal funiculus of T12 in adult rats; in one group of rats, the cells were injected into an area of white matter containing activated microglia that were participating in an inflammatory response due to the focal injection of 1 ng/µl TNF-α exactly 5 mm rostral to the graft. Several immunohistochemical markers, including immunstaining with the antibodies recognizing CR3, MHC-I, CD4, and ED1 (CD68) antigenic epitopes confirmed that the focal injection of TNF-α resulted in the activation of microglia (Fig 5.1, 5.2, 5.3, 5.4), and a lesser activation of astrocytes (Fig 5.5, 5.6, 5.7). Significant more OECs migrated towards the TNF injection site in the rostral portion of T11 when reactive microglia were present than in their absence, which demonstrated the ability of OECs to enter areas undergoing an inflammatory reaction (5.10, 5.17 and 5.18).

It was reported that microglia-derived TNF-α acts in an autocrine manner to regulate the secretion of inflammatory mediators including TNF-α (Kuno et al., 2005). It was proposed that microglial autocrine responses contribute to the persistent activation of microglia in chronic inflammatory diseases (Kuno et al., 2005). Production of TNF-α within the CNS is induced after injury (Fan et al., 1996). The limited entry of TNF-α from the periphery to regions distant from the site of injury might not only provide a feedback signal to restrict local production but may also serve as a mediator for neuroregeneration. An adequate concentration of TNF-α seems to be essential for homeostasis in the CNS. TNF-α also induces the secretion of nerve trophic factors including NGF and GDNF (Appel et al., 1997; Brodie, 1996; Hattori et al., 1996) that might contribute to OEC migration. Indeed, it was shown that GDNF significantly promoted OEC migration *in vitro* and *in vivo* (Cao et al., 2006). GDNF has raised great expectations as a potential therapeutic agent for the treatment of neurodegenerative diseases (Lapchak, 1996). The transplantation of OECs genetically modified to secrete high levels of GDNF significantly improved neural repair after SCI (Cao, et al., 2004). The underlying mechanisms are not fully understood. It was likely that the OEC-secreted GDNF had not only promoted neural repair, but also had some effects on OECs themselves such that GDNF might be a an important regulator of OEC migration during

nerve regeneration after SCI in a paracrine and/or autocrine fashion (Cao et al., 2006). Interestingly, an *in vitro* study (Lai and Todd, 2006) showed that minocycline has no effect on GDNF expression by microglia; whether minocycline's effect on microglia is the same *in vivo* remains to be determined. Our data showed that minocyline treatment substantially reduced microglial reactivity after TNF-α injection and to a significant decrease in the number of OECs that had migrated along the right DF of T11. If GDNF is a potent migratory signal for OECs, then the minocycline treatment in our *in vivo* animal model must act differently from that reported previously by Lai and Todd (2006) in their *in vitro* study.

Exogenous microglia directly applied to hippocampal slice cultures could save more neurons after deprivation of oxygen and glucose (Neumann et al., 2006). Transplanted microglial cells were found to facilitate neuronal growth in the injured site in the CNS (Kitamura et al., 2004). Activated microglia could also secrete some neurotrophic factors such as NGF, NT-3, GDNF and BNDF, which have been demonstrated to be neuroprotective (Nakajima et al., 2001). On the other hand, TNF-α released from LPS-activated microglia could not only lead to a significant loss of motoneurons *in vitro* (He et al., 2002), but also be directly cytotoxic to oligodendrocytes *in vitro* and induce significant demyelination *in vivo* (Probert et al., 1995). Therefore, the inhibition of microglial activation may possibly attenuate neuronal degeneration induced either by ischemia (Giulian and Robertson, 1990) or by excitatory neurotoxin (Coffey et al., 1990). However, it is difficult to predict which function activated microglia would predominantly execute in various pathological conditions of the CNS. The balance between co- and counter-effects of various microglial factors might determine the role of microglia after neural injury or in neurodegeneation diseases.

In most neurodegenerative diseases, post-mortem analysis found the clustering of activated microglia in and around the brain regions affected by the pathology (Dickson et al., 1993). The increased numbers of microglia in such regions has been claimed to be a result of microglial proliferation and migration. An increase in the number of activated microglia may correspondingly increase the concentration of factors released from reactive microglia and these factors may play a role in inducing OEC migration. In fact the results of this research project demonstrated that the higher concentration of TNF-α,

in comparison to the lower concentration of TNF-α, induced a more intense microglial activation that spatially extended for at least 5 mm away from the injection site. This 5 mm length extent of microglial reactivity may create an environment containing migratory signals that induce OEC migration towards the rostral part of T11. Whether direct contact between activated microglia and OECs was required for OEC migration cannot be answered at present, but as shown in the experiments in Chapter 4 the OECs preferentially migrated along a pathway containing reactive microglia.

Merrill et al. (1993) showed that direct contact between activated microglia and oligodendrocytes induced cell death of the latter cells (Merrill et al., 1993). Although this microglial toxicity through direct cell–cell contact may involve special molecules, a possible immediate effect on OECs from the cell-to-cell proximity of the glial cells migrating through areas containing microglial reactivity would be an increase in concentrations of migratory signal(s) directly or indirectly released as a consequence of the activation of the microglia. Therefore, the duration and spatial effects of microglial activation in injured areas of the CNS may indicate dual microglial functions. The type of microglia reactivity as induced in the experiments reported in Chapters 4 and 5 of this thesis, may contribute to the formation of more inducible environment for OEC migration.

All together, the present results indicate that direct injection of TNF-α into the dorsal funiculus of the spinal cord of adult rats is an appropriate animal model with which to investigate at the molecular level the mechanisms through which microglial activation induce OEC migration. Another substantial result of this experiment is the capacity of OECs to intermingle with microglia and astrocytes within an area of white matter undergoing an inflammatory reaction. Presumably, some of components of this inflammatory response could contribute to the migratory signal(s) that drove the OEC migration in these TNF-α experiments.

5.4.4 Conclusion

The data from this experiment demonstrated that a focal injection of 1 ng/µl of TNF-α created a path of reactive microglia that extended caudally as far as the OEC graft, gave rise to a migratory signal(s) that induced OECs to migrate, and dampening the

microglial reactivity with minocycline also decreased the number of OECs that migrated towards the cytokine injection. Therefore, the hypothesis of microglial reactivity contributing to the generation of a migratory signal(s) for the OECs was supported. In addition, the OEC migration toward the site of the TNF-α injection in the animal model used in this chapter should be considered as an important subject of therapeutic relevance to any treatment of SCI or demyelination disorders that involves glial cell transplantation. The TNF-α model used in this research project induced less glial reactivity and inflammation compared to animal models using chemotoxins such as EtBr. Nevertheless, the ultimate effect of the TNF-α induced microglial activation still generated migratory signal(s) that were strong enough to induce OECs to migrate.

It was noted that the expression of all microglial markers used in this experiment fluctuated such that there was a remarkable downregulation of expression by 14 days after TNF-α injection as compared to 1 day after injection. However, in the rats who received an OEC graft 5 mm caudal to the TNF-α injection then these markers, particularly CR3 expression (OX42+ve microglia) (Fig 5.10), appeared to be upregulated at the 8 week time point after cell grafting. The OEC grafting might be the reason for what appeared to be microglial reactivation, as opposed to a *de novo* activation of the microglia. Firstly, the OECs were grafted at T12 some 5 mm away from the TNF-α injection site but the most intense microglial reaction was detected in the rostral part of T11 far removed from the site of the cell graft. Secondly, if the microglial reaction at 8 weeks after injury was due mainly to the cell grafting, then a similar microglial response should have been seen in all animal groups, including those receiving the lowest concentration of TNF-α or vehicle. However, the immunohistochemical staining showed clear differences in the intensituy of microglial reactivity in different animal groups (Fig. 5.9, 5.10).

However, the mechanism of microglia re-activation and how such activation might induce OEC migration are two challenging questions that need to be addressed in future studies. It seems that the mechanism of microglia activation is dependent on the type of signal(s) inducing their reactivity. This re-activation of microglia may create an appropriate environment containing robust migratory signals that facilitate the migration

of OECs. What microglia do to manipulate the environment to maximize OEC migration is another challenging question that needs to be investigated.

CHAPTER 6.0 GENERAL CONCLUSION

Following OEC transplantation into the host parenchyma it is important that the grafted cells survive if they are to exert their regenerative effects and to be fully functional. The extracellular environment of the injured spinal cord contains some toxic and apoptotic factors that can affect glial cell survival (Beatti et al., 2000). Hence, it stands to reason that OECs have a better chance of surviving the cell grafting process if they are transplanted into intact spinal cord tissue some millimeters away from the lesion site. In fact, when grafted into such areas adjacent to tissue injury, OECs were reported to have integrated successfully into the host spinal cord (Ramon-Cueto and Avila, 1998; Ramon-Cueto et al., 2000; Ramon-Cueto and Nieto Sampedro, 1994). Several studies have demonstrated that OECs were able to migrate from the injection sites following transplantation into tissue near a spinal cord transection. They crossed the injury region and reached the tissue on the opposite side of the transection (Boruch et al., 2001, Ramon-Cueto et al., 1998, Ramon-Cueto, and Nieto Sampedro 1994).

When OECs were grafted into tissue adjacent to a spinal cord transection in combination with Schwann cell-filled PAN/PVC guidance channels (Ramon-Cueto et al., 1998), the OECs freely moved through the glial scar at the border between CNS tissue and guidance channel and crossed the astrocyte-Schwann cell interface. Interestingly, OECs entered the guidance channel containing Schwann cells and exited the channel at the distal end to once again enter the CNS tissue. In contrast, Schwann cells remained inside the bridges and did not migrate through spinal cord tissue (Xu, et al., 1997). In the presence of astrocytes, Schwann cells have a poor ability to migrate (Franklin and Blakemore, 1993; Iwashita, et al., 2000; Lakatos et al., 2000), and this could be related to the morphological and biochemical changes induced in astrocytes by Schwann cells (Qiu et al., 2000). In contrast, OECs are able to intermingle with astrocytes after transplantation into injured spinal cord, with no separate territories being formed (Boruch et al., 2001; Li, et al., 1998; Ramon-Cueto et al., 2000; Ramon-Cueto and Nieto Sampedro, 1994). Both *in vivo* and *in vitro* observations have demonstrated this interaction between OECs and astrocytes (Lakatos et al., 2000). Furthermore, OECs do not induce astrocyte hypertrophy or their expression of neurite-inhibitory CSPGs and OECs are less adhesive to astrocytic surfaces than other cells used for transplantation.

OECs were also reported to migrate through connective tissue and peripheral nerves (Ramon-Cueto et al., 2000, Ramon-Cueto et al., 1998).

The capacity of OECs to migrate within the CNS environment can be at least partially explained by the ability of OECs to interact with astrocytes. However, more studies are needed to fully understand the molecular mechanisms responsible for facilitating OEC migration within the CNS. Some recent data suggest that neuregulins might be involved in OEC migration (Boruch, et al., 2001; Meintanis et al., 2001; Pollock et al., 1999; Thompson et al., 2000). In addition, OECs produce a number of different growth associated factors, and if needed they change their morphology, intermingle with reactive CNS glia, and migrate within the CNS. OECs are able to properly integrate within the host parenchyma and cross the PNS/CNS boundary.

The signals responsible for promoting OEC migration toward the site of a SCI are unknown. A limited migration of GFP^+ OECs was observed by Pearse et al. (2007) after a contusion injury of the spinal cord. In the study by Pearse et al. (2007), GFP^+ OECs were not observed within regions of normal appearing white or gray matter. Furthermore, even when the OECs were grafted rostral and caudal to the contusion injury, where the OECs exhibited higher cell survival, they failed to migrate from the site of grafting into surrounding host tissue. However, Ramon-Cueto et al. (2000) reported that OECs did migrate away from a complete spinal cord transection in adult rats. OEC migration over an approximately 20 mm distance towards the site of injury was demonstrated by Skihar (2004) using ethidium bromide to induce a focal demyelination in the adult rat spinal cord. These discrepancies of whether or not OECs will or will not migrate away from the site of grafting may be due either to the different injury paradigms that were used or to the different sources or cell culture techniques that were used. For example, differences in the presence or absence of migration might be due to the use of cells from different passages (e.g. primary vs. secondary cell cultures) or from different tissue sources (e.g. OB vs. lamina propria). The timing of implantation also may play a significant role in the ability of grafted OECs to migrate from their original site of deposition. The implantation of cells immediately after injury, before the formation of a glial scar around the lesion site (Silver and Miller, 2004), may enable the cells to migrate out from the injection site (Li et al., 2003; Ramon-Cueto et al., 1998, 2000; Richter et al., 2005). At later times,

such as after a delay of some days or weeks the formation of the glial boundary within the injured spinal cord may restrict the ability of implanted glia to migrate into normal host cord tissue (Barakat et al., 2005; Pearse et al., 2004) due to the presence of various inhibitory components of the ECM (Faissner, 1997; Kapfhammer and Schwab, 1992), such as CSPG and tenascin, to soluble chemorepellant molecules (Barallobre et al., 2005), or even to physical interactions with the astrocytic-meningeal fibroblast network (Fawcett, 1997). A study by Plant et al. (2003), however, showed there was little migration of OECs into the surrounding host cord tissue after transplantation into a spinal contusion injury in rats at two different time points after injury, namely at 0 and 7 days. Additionally, the lesion environment may play a role in altering the ability of implanted glia to migrate outward into the host cord as OECs have been reported to exhibit an extensive migratory capacity in models of spinal cord hemisection (Deng et al., 2006; Li et al., 2003) but not after contusion injury (Barakat et al., 2005; Collazos-Castro et al., 2005; Pearse et al., 2004; Plant et al., 2003). Besides, when OECs are transplanted directly into the lesion site the cells may be induced to stay in place within the lesion to assist host cells in neural repair, rather than migrate away from the site of injury.

Microglia rapidly respond to microenvironmental changes within the CNS (Streit, 2004). They are thus one of the most important cells in directing the repair of the CNS. Despite the clear association between reactive microglia and disease processes, the precise consequence of microglia activation on OEC survival and migration *in vivo* remain uncertain. *In vitro*, activated microglia produce cytotoxins such as free radicals, excitory amino acids, and inflammatory cytokines, as well as trophic factors, suggesting that activated microglia play dual roles (Streit, 2004). The outcome is likely the combined effect of both detrimental and beneficial effects. The experiments reported in Chapters 4 and 5 of this thesis demonstrate that OEC migration is enhanced when it occurs in the presence of micoglial reactivity. The two different animal models used in this study implicate microglia as playing an important role in generating migratory signal(s) that induce OECs to migrate. Thus, defining the role of reactive microglia and identifying ways to modulate activated microglia *in vivo* will be instrumental to the design of treatments that permit the beneficial effects of microglial reactivity to occur without dampening its contribution to generation of migratory signal(s).

The potential advantages of OEC transplantation for neural repair are several. Firstly, is the ability of the OECs to integrate properly within the CNS after transplantation (Ramon-Cueto and Nieto-sampedro, 1994). Secondly, although the glial scar, which is formed predominantly by reactive astrocytes and microglia, is a major obstacle to the migration of myelin-forming glia in the CNS after damage (Fernaud-Espinosa et al., 1993; Hatten et al., 1991), OECs allow the regenerating axons to grow through known growth inhibitory substrates such as this gliotic tissue (Ramon-Cueto and Nieto-sampedro, 1994). Thus, the OECs might also be able to navigate glial scars and remyelinate axons in the damaged CNS (Ramon-Cueto and Nieto-sampedro, 1994). Thirdly, OECs are a source of neurotrophic factors, such as nerve growth factor (NGF), platelet-derived growth factor (PDGF) and neuropeptide Y (Knott et al., 1994; Ubink et al., 1994; Williams and Rush 1988). Thus, trophic factor production by OECs might enhance the survival of neurons whose axons have been damaged. Fourthly, OECs may also remyelinate demyelinated CNS axons based on reports that have appeared of their remyelination of CNS axons *in vivo* after transplantation of either rodent or human OECs (Barnett et al., 2000; Kato et al., 2000) (Barnett et al., 2000; Imaizumi et al., 1998 ; Kato et al., 2000). A fifth advantage is that OECs respond to migratory signals arising as a result of WD and migrate towards the area containing the degenerating axons (e.g. the right dCST), as described in this research project. Finally, OECs can respond to migratory signals arising as a result of a single direct injection of TNF-α into the spinal cord. This latter finding suggests that the more prolonged production of proinflammatory cytokines that occurs after SCI or in areas of white matter undergoing demyelination is likely to provide, directly and/or indirectly, a more constant source of migratory signals than would arise from a single intraparenchymal injection.

CHAPTER 7.0 FUTURE DIRECTIONS

Identifying migratory signals is an important issue in the design of any therapeutic approach that involves glial cell transplantation. Scattered lesions in the CNS white matter, as occurs for example in MS, presents the challenge of delivering the myelinating glia directly to multiple plaques containing the demyelinated axons. Thus, understanding the endogenous host glial cell response to the exogenous grafted OECs as well as the molecular interactions among these cells that create a migratory path for the OECs is a new avenue for future studies that involve cell transplantation into areas of CNS adjacent to or remote from areas of injury.

Microglia respond to microenvironment changes within the CNS rapidly. Therefore, they are one of the most essential cells in directing neural repair in the CNS. The precise consequence of microglial activation on OEC migration *in vivo* remains uncertain. *In vitro*, stimulated microglia produce cytotoxins such as free radicals, excitatory amino acids, and proinflammatory cytokines as well as trophic factors, which collectively suggests that activated microglia play dual roles. The outcome is likely the combined effect of both detrimental and beneficial effects. Thus defining the role of reactive microglia and identifying ways to modulate activated microglia *in vivo* will be instrumental to the design of therapeutic approaches to treating neurological disorders.

Two different animal models used in my thesis research have provided some important insights into the key role of reactive microglia in the generation of migratory signals that induce OECs to migrate. All of my experiments were performed *in vivo*, leaving plenty of opportunity now to use an *in vitro* approach to see whether molecules directly released by activated microglia are chemotactic for OECs. Thus, in spite of several benefits of using *in vivo* animal models to study OEC migration, due to the complexity of these *in vivo* models it is a huge challenge to determine the underlying molecular mechanisms. The *in vitro* approach would allow for the identification of putative chemotactic molecules, which could then be tested using, for example, the animal model used in Chapter 5.

I demonstrated that OEC migration occurred along a migratory path containing reactive microglia and that minocycline treatment for 4-6 weeks not only dampened the microglia reactivity but also resulted in a significant reduction in the number of OECs

that migrated into the T11 segment. It was shown by Kotter et al. (2001) that an early treatment of animals with clodronate caused depletion of microglia in lysolecithin-induced demyelinated areas in the CNS of adult rats and also resulted in a decreased remylination by oligodendrocytes. However, late treatment with clodronate had no effect on this neural repair although it was still effective in reducing the number of reactive microglia (Kotter et al., 2001). Preliminary data from our lab also showed that early minocycline treatment (i.e. during the first 2 weeks after injury) caused a remarkable reduction in microglial reactivity and a significant decrease in the number of OECs that migrated towards an EtBr-induced demyelination in the adult rat spinal. To work out the timing of the relationship between the micoglial reaction and the generation of a migratory signal(s) it is important to know whether delaying the minocycline treatment until, for example, weeks 3-4 after TNF-α injection, would have any impact on OEC migration. A similar delayed treatment with minocycline could also be used with the WD animal model I used in Chapter 4. Knowing the critical time frame is important for designing experiments to identify the molecules comprising the migratory signals. Indeed, once the time frame over which the microglial response contributes to the generation of the migratory signal(s), it may be possible to predict whether early vs. late proinflammatory cytokines contribute to migratory signal(s).

In my second animal model, TNF-α was used as a tool to activate microglia and I have not tested whether TNF-α itself is a migratory factor that induced OECs to migrate. In addition, whether other proinflammatory cytokines (e.g., IL-6) will have the same effect on microglial activation should also be addressed in future studies. The next step then would be to determine whether OECs migrate in response to such microglial cell activation. It can be also hypothesized that anti-inflammatory cytokines will attenuate microglial activation and thus should not induce OEC migration. Thus, an additional set of experiments should test the effect of anti-inflammatory cytokines on microglial reactivity and on OEC migration.

CHAPTER 8.0 REFRENCES

Aarli, J.A. 2003. Role of cytokines in neurological disorders. *Curr Med Chem*. 10:1931-7.

Acarin, L., B. Gonzalez, and B. Castellano. 2000. Neuronal, astroglial and microglial cytokine expression after an excitotoxic lesion in the immature rat brain. *Eur J Neurosci*. 12:3505-20.

Aggarwal, B.B. 2003. Signalling pathways of the TNF superfamily: a double-edged sword. *Nat Rev Immunol*. 3:745-56.

Ahlemeyer, B., S. Kolker, Y. Zhu, G.F. Hoffmann, and J. Krieglstein. 2002. Increase in glutamate-induced neurotoxicity by activated astrocytes involves stimulation of protein kinase C. *J Neurochem*. 82:504-15.

Akassoglou, K., J. Bauer, G. Kassiotis, H. Lassmann, G. Kollias, and L. Probert. 1999. Transgenic models of TNF induced demyelination. *Adv Exp Med Biol*. 468:245-59.

Akassoglou, K., J. Bauer, G. Kassiotis, M. Pasparakis, H. Lassmann, G. Kollias, and L. Probert. 1998. Oligodendrocyte apoptosis and primary demyelination induced by local TNF/p55TNF receptor signaling in the central nervous system of transgenic mice: models for multiple sclerosis with primary oligodendrogliopathy. *Am J Pathol*. 153:801-13.

Akassoglou, K., L. Probert, G. Kontogeorgos, and G. Kollias. 1997. Astrocyte-specific but not neuron-specific transmembrane TNF triggers inflammation and degeneration in the central nervous system of transgenic mice. *J Immunol*. 158:438-45.

Akiyama, Y., O. Honmou, T. Kato, T. Uede, K. Hashi, and J.D. Kocsis. 2001. Transplantation of clonal neural precursor cells derived from adult human brain establishes functional peripheral myelin in the rat spinal cord. *Exp Neurol*. 167:27-39.

Akiyama, Y., K. Lankford, C. Radtke, C.A. Greer, and J.D. Kocsis. 2004. Remyelination of spinal cord axons by olfactory ensheathing cells and Schwann cells derived from a transgenic rat expressing alkaline phosphatase marker gene. *Neuron Glia Biol*. 1:47-55.

Akiyama, Y., C. Radtke, and J.D. Kocsis. 2002. Remyelination of the rat spinal cord by transplantation of identified bone marrow stromal cells. *J Neurosci*. 22:6623-30.

Alcazar, A., I. Regidor, J. Masjuan, M. Salinas, and J.C. Alvarez-Cermeno. 2000. Axonal damage induced by cerebrospinal fluid from patients with relapsing-remitting multiple sclerosis. *J Neuroimmunol*. 104:58-67.

Aldskogius, H. 1974. Direct Wallerian degeneration in intramedullary root fibres of the kitten hypoglossal nerve light and electron microscopical observations on silver impregnated sections. *Neurobiology*. 4:151-66.

Aldskogius, H., and E.N. Kozlova. 1998. Central neuron-glial and glial-glial interactions following axon injury. *Prog Neurobiol*. 55:1-26.

Allan, S.M., and N.J. Rothwell. 2003. Inflammation in central nervous system injury. *Philos Trans R Soc Lond B Biol Sci*. 358:1669-77.

Aloisi, F. 2001. Immune function of microglia. *Glia*. 36:165-79.

Armand, J. 1982. The origin, course and terminations of corticospinal fibers in various mammals. *Prog Brain Res*. 57:329-60.
Aronica, E., J.A. Gorter, H. Ijlst-Keizers, A.J. Rozemuller, B. Yankaya, S. Leenstra, and D. Troost. 2003. Expression and functional role of mGluR3 and mGluR5 in human astrocytes and glioma cells: opposite regulation of glutamate transporter proteins. *Eur J Neurosci*. 17:2106-18.
Aronson, A.L. 1980. Pharmacotherapeutics of the newer tetracyclines. *J Am Vet Med Assoc*. 176:1061-8.
Ashkenazi, A., and V.M. Dixit. 1998. Death receptors: signaling and modulation. *Science*. 281:1305-8.
Ashwell, K. 1990. Microglia and cell death in the developing mouse cerebellum. *Brain Res Dev Brain Res*. 55:219-30.
Astic, L., V. Pellier-Monnin, and F. Godinot. 1998. Spatio-temporal patterns of ensheathing cell differentiation in the rat olfactory system during development. *Neuroscience*. 84:295-307.
Au, E., and A.J. Roskams. 2003. Olfactory ensheathing cells of the lamina propria in vivo and in vitro. *Glia*. 41:224-36.
Babcock, A.A., W.A. Kuziel, S. Rivest, and T. Owens. 2003. Chemokine expression by glial cells directs leukocytes to sites of axonal injury in the CNS. *J Neurosci*. 23:7922-30.
Babington, E.J., J. Vatanparast, J. Verrall, and S.E. Blackshaw. 2005. Three-dimensional culture of leech and snail ganglia for studies of neural repair. *Invert Neurosci*. 5:173-82.
Bachmann, R., H.P. Eugster, K. Frei, A. Fontana, and H. Lassmann. 1999. Impairment of TNF-receptor-1 signaling but not fas signaling diminishes T-cell apoptosis in myelin oligodendrocyte glycoprotein peptide-induced chronic demyelinating autoimmune encephalomyelitis in mice. *Am J Pathol*. 154:1417-22.
Baldwin, S.A., and S.W. Scheff. 1996. Intermediate filament change in astrocytes following mild cortical contusion. *Glia*. 16:266-75.
Banati, R.B. 2002. Brain plasticity and microglia: is transsynaptic glial activation in the thalamus after limb denervation linked to cortical plasticity and central sensitisation? *J Physiol Paris*. 96:289-99.
Banati, R.B. 2003. Neuropathological imaging: in vivo detection of glial activation as a measure of disease and adaptive change in the brain. *Br Med Bull*. 65:121-31.
Barber, P.C., and R.M. Lindsay. 1982. Schwann cells of the olfactory nerves contain glial fibrillary acidic protein and resemble astrocytes. *Neuroscience*. 7:3077-90.
Barnett, M.H., and J.W. Prineas. 2004. Relapsing and remitting multiple sclerosis: pathology of the newly forming lesion. *Ann Neurol*. 55:458-68.
Barnett, S.C., C.L. Alexander, Y. Iwashita, J.M. Gilson, J. Crowther, L. Clark, L.T. Dunn, V. Papanastassiou, P.G. Kennedy, and R.J. Franklin. 2000. Identification of a human olfactory ensheathing cell that can effect transplant-mediated remyelination of demyelinated CNS axons. *Brain*. 123 (Pt 8):1581-8.
Barnett, S.C., and L. Chang. 2004. Olfactory ensheathing cells and CNS repair: going solo or in need of a friend? *Trends Neurosci*. 27:54-60.
Barnett, S.C., A.M. Hutchins, and M. Noble. 1993. Purification of olfactory nerve ensheathing cells from the olfactory bulb. *Dev Biol*. 155:337-50.

Basiri,M and Doucette, R. 2007 OECs migration in response to wallerian degeneration - induced glial reactivity, 1st Annual Meeting ; The Canadian association for Neuroscience,

Batchelor, P.E., G.T. Liberatore, J.Y. Wong, M.J. Porritt, F. Frerichs, G.A. Donnan, and D.W. Howells. 1999. Activated macrophages and microglia induce dopaminergic sprouting in the injured striatum and express brain-derived neurotrophic factor and glial cell line-derived neurotrophic factor. *J Neurosci*. 19:1708-16.

Batchelor, P.E., M.J. Porritt, P. Martinello, C.L. Parish, G.T. Liberatore, G.A. Donnan, and D.W. Howells. 2002. Macrophages and Microglia Produce Local Trophic Gradients That Stimulate Axonal Sprouting Toward but Not beyond the Wound Edge. *Mol Cell Neurosci*. 21:436-53.

Baud, V., and M. Karin. 2001. Signal transduction by tumor necrosis factor and its relatives. *Trends Cell Biol*. 11:372-7.

Bauer, J., T. Sminia, F.G. Wouterlood, and C.D. Dijkstra. 1994. Phagocytic activity of macrophages and microglial cells during the course of acute and chronic relapsing experimental autoimmune encephalomyelitis. *J Neurosci Res*. 38:365-75.

Bechmann, I., S. Lossau, B. Steiner, G. Mor, U. Gimsa, and R. Nitsch. 2000. Reactive astrocytes upregulate Fas (CD95) and Fas ligand (CD95L) expression but do not undergo programmed cell death during the course of anterograde degeneration. *Glia*. 32:25-41.

Beiter, T., M.R. Artelt, K. Trautmann, and H.J. Schluesener. 2005. Experimental autoimmune neuritis induces differential microglia activation in the rat spinal cord. *J Neuroimmunol*. 160:25-31.

Bendszus, M., and G. Stoll. 2003. Caught in the act: in vivo mapping of macrophage infiltration in nerve injury by magnetic resonance imaging. *J Neurosci*. 23:10892-6.

Benveniste, E.N. 1994. Cytokine circuits in brain. Implications for AIDS dementia complex. *Res Publ Assoc Res Nerv Ment Dis*. 72:71-88.

Benveniste, E.N., V.T. Nguyen, and G.M. O'Keefe. 2001. Immunological aspects of microglia: relevance to Alzheimer's disease. *Neurochem Int*. 39:381-91.

Benveniste, E.N., S.M. Sparacio, J.G. Norris, H.E. Grenett, and G.M. Fuller. 1990. Induction and regulation of interleukin-6 gene expression in rat astrocytes. *J Neuroimmunol*. 30:201-12.

Besedovsky, H.O., and A. del Rey. 1996. Immune-neuro-endocrine interactions: facts and hypotheses. *Endocr Rev*. 17:64-102.

Bethea, J.R. 2000. Spinal cord injury-induced inflammation: a dual-edged sword. *Prog Brain Res*. 128:33-42.

Bethea, J.R., M. Castro, R.W. Keane, T.T. Lee, W.D. Dietrich, and R.P. Yezierski. 1998. Traumatic spinal cord injury induces nuclear factor-kappaB activation. *J Neurosci*. 18:3251-60.

Bethea, J.R., H. Nagashima, M.C. Acosta, C. Briceno, F. Gomez, A.E. Marcillo, K. Loor, J. Green, and W.D. Dietrich. 1999. Systemically administered interleukin-10 reduces tumor necrosis factor-alpha production and significantly improves functional recovery following traumatic spinal cord injury in rats. *J Neurotrauma*. 16:851-63.

Bianco, J.I., C. Perry, D.G. Harkin, A. Mackay-Sim, and F. Feron. 2004. Neurotrophin 3 promotes purification and proliferation of olfactory ensheathing cells from human nose. *Glia*. 45:111-23.

Bignami, A., D. Dahl, B.T. Nguyen, and C.J. Crosby. 1981. The fate of axonal debris in Wallerian degeneration of rat optic and sciatic nerves. Electron microscopy and immunofluorescence studies with neurofilament antisera. *J Neuropathol Exp Neurol*. 40:537-50.

Bignami, A., and L.F. Eng. 1973. Biochemical studies of myelin in Wallerian degeneration of rat optic nerve. *J Neurochem*. 20:165-73.

Bignami, A., L.F. Eng, D. Dahl, and C.T. Uyeda. 1972. Localization of the glial fibrillary acidic protein in astrocytes by immunofluorescence. *Brain Res*. 43:429-35.

Bjorklund, L.M., R. Sanchez-Pernaute, S. Chung, T. Andersson, I.Y. Chen, K.S. McNaught, A.L. Brownell, B.G. Jenkins, C. Wahlestedt, K.S. Kim, and O. Isacson. 2002. Embryonic stem cells develop into functional dopaminergic neurons after transplantation in a Parkinson rat model. *Proc Natl Acad Sci U S A*. 99:2344-9.

Blackshaw, S.E., S. Arkison, C. Cameron, and J.A. Davies. 1997. Promotion of regeneration and axon growth following injury in an invertebrate nervous system by the use of three-dimensional collagen gels. *Proc Biol Sci*. 264:657-61.

Blais, V., and S. Rivest. 2004. Effects of TNF-alpha and IFN-gamma on nitric oxide-induced neurotoxicity in the mouse brain. *J Immunol*. 172:7043-52.

Booth, P.L., and W.E. Thomas. 1991. Evidence for motility and pinocytosis in ramified microglia in tissue culture. *Brain Res*. 548:163-71.

Borghesani, P.R., J.M. Peyrin, R. Klein, J. Rubin, A.R. Carter, P.M. Schwartz, A. Luster, G. Corfas, and R.A. Segal. 2002. BDNF stimulates migration of cerebellar granule cells. *Development*. 129:1435-42.

Boruch, A.V., J.J. Conners, M. Pipitone, G. Deadwyler, P.D. Storer, G.H. Devries, and K.J. Jones. 2001. Neurotrophic and migratory properties of an olfactory ensheathing cell line. *Glia*. 33:225-9.

Bouldin, T.W., T.S. Earnhardt, and N.D. Goines. 1990. Sequential changes in the permeability of the blood-nerve barrier over the course of ricin neuronopathy in the rat. *Neurotoxicology*. 11:23-34.

Boyd, J.G., R. Doucette, and M.D. Kawaja. 2005. Defining the role of olfactory ensheathing cells in facilitating axon remyelination following damage to the spinal cord. *Faseb J*. 19:694-703.

Boyd, J.G., J. Lee, V. Skihar, R. Doucette, and M.D. Kawaja. 2004. LacZ-expressing olfactory ensheathing cells do not associate with myelinated axons after implantation into the compressed spinal cord. *Proc Natl Acad Sci U S A*. 101:2162-6.

Bregman, B.S., J.V. Coumans, H.N. Dai, P.L. Kuhn, J. Lynskey, M. McAtee, and F. Sandhu. 2002. Transplants and neurotrophic factors increase regeneration and recovery of function after spinal cord injury. *Prog Brain Res*. 137:257-73.

Bregman, B.S., P.S. Diener, M. McAtee, H.N. Dai, and C. James. 1997. Intervention strategies to enhance anatomical plasticity and recovery of function after spinal cord injury. *Adv Neurol*. 72:257-75.

Bresnahan, J.C., M.S. Beattie, F.D. Todd, 3rd, and D.H. Noyes. 1987. A behavioral and anatomical analysis of spinal cord injury produced by a feedback-controlled impaction device. *Exp Neurol*. 95:548-70.

Brodie, C. 1996. Differential effects of Th1 and Th2 derived cytokines on NGF synthesis by mouse astrocytes. *FEBS Lett*. 394:117-20.

Brook, G.A., A. Perez-Bouza, J. Noth, and W. Nacimiento. 1999. Astrocytes re-express nestin in deafferented target territories of the adult rat hippocampus. *Neuroreport*. 10:1007-11.

Brosamle, C., and M.E. Schwab. 1997. Cells of origin, course, and termination patterns of the ventral, uncrossed component of the mature rat corticospinal tract. *J Comp Neurol*. 386:293-303.

Brostoff, S.W., and T.M. White. 1986. Treatment of clinical experimental allergic encephalomyelitis in the rat with monoclonal antibodies. *J Neuroimmunol*. 13:233-40.

Bruck, W. 1997. The role of macrophages in Wallerian degeneration. *Brain Pathol*. 7:741-52.

Brustle, O., K.N. Jones, R.D. Learish, K. Karram, K. Choudhary, O.D. Wiestler, I.D. Duncan, and R.D. McKay. 1999. Embryonic stem cell-derived glial precursors: a source of myelinating transplants. *Science*. 285:754-6.

Brustle, O., U. Maskos, and R.D. McKay. 1995. Host-guided migration allows targeted introduction of neurons into the embryonic brain. *Neuron*. 15:1275-85.

Buckland, M.E., and A.M. Cunningham. 1998. Alterations in the neurotrophic factors BDNF, GDNF and CNTF in the regenerating olfactory system. *Ann N Y Acad Sci*. 855:260-5.

Buss, A., G.A. Brook, B. Kakulas, D. Martin, R. Franzen, J. Schoenen, J. Noth, and A.B. Schmitt. 2004. Gradual loss of myelin and formation of an astrocytic scar during Wallerian degeneration in the human spinal cord. *Brain*. 127:34-44.

Buss, A., and M.E. Schwab. 2003. Sequential loss of myelin proteins during Wallerian degeneration in the rat spinal cord. *Glia*. 42:424-32.

Butt, A.M., and S. Kirvell. 1996. Glial cells in transected optic nerves of immature rats. II. An immunohistochemical study. *J Neurocytol*. 25:381-92.

Calof, A.L., and D.M. Chikaraishi. 1989. Analysis of neurogenesis in a mammalian neuroepithelium: proliferation and differentiation of an olfactory neuron precursor in vitro. *Neuron*. 3:115-27.

Calvo, C.F., E. Amigou, M. Tence, T. Yoshimura, and J. Glowinski. 2005. Albumin stimulates monocyte chemotactic protein-1 expression in rat embryonic mixed brain cells. *J Neurosci Res*. 80:707-14.

Camussi, G., E. Albano, C. Tetta, and F. Bussolino. 1991. The molecular action of tumor necrosis factor-alpha. *Eur J Biochem*. 202:3-14.

Cao, L., L. Liu, Z.Y. Chen, L.M. Wang, J.L. Ye, H.Y. Qiu, C.L. Lu, and C. He. 2004. Olfactory ensheathing cells genetically modified to secrete GDNF to promote spinal cord repair. *Brain*. 127:535-49.

Cao, L., Z. Su, Q. Zhou, B. Lv, X. Liu, L. Jiao, Z. Li, Y. Zhu, Z. Huang, A. Huang, and C. He. 2006. Glial cell line-derived neurotrophic factor promotes olfactory ensheathing cells migration. *Glia*. 54:536-44.

Carswell, E.A., L.J. Old, R.L. Kassel, S. Green, N. Fiore, and B. Williamson. 1975. An endotoxin-induced serum factor that causes necrosis of tumors. *Proc Natl Acad Sci U S A*. 72:3666-70.

Casha, S., W.R. Yu, and M.G. Fehlings. 2001. Oligodendroglial apoptosis occurs along degenerating axons and is associated with FAS and p75 expression following spinal cord injury in the rat. *Neuroscience*. 103:203-18.

Chamak, B., V. Morandi, and M. Mallat. 1994. Brain macrophages stimulate neurite growth and regeneration by secreting thrombospondin. *J Neurosci Res*. 38:221-33.

Chang, Y.P., K.M. Fang, T.I. Lee, and S.F. Tzeng. 2006. Regulation of microglial activities by glial cell line derived neurotrophic factor. *J Cell Biochem*. 97:501-11.

Chiarugi, A., and M.A. Moskowitz. 2003. Poly(ADP-ribose) polymerase-1 activity promotes NF-kappaB-driven transcription and microglial activation: implication for neurodegenerative disorders. *J Neurochem*. 85:306-17.

Chuah, M.I., D. Choi-Lundberg, S. Weston, A.J. Vincent, R.S. Chung, J.C. Vickers, and A.K. West. 2004. Olfactory ensheathing cells promote collateral axonal branching in the injured adult rat spinal cord. *Exp Neurol*. 185:15-25.

Chung, I.Y., and E.N. Benveniste. 1990. Tumor necrosis factor-alpha production by astrocytes. Induction by lipopolysaccharide, IFN-gamma, and IL-1 beta. *J Immunol*. 144:2999-3007.

Ciccarelli, R., F.X. Sureda, G. Casabona, P. Di Iorio, A. Caruso, F. Spinella, D.F. Condorelli, F. Nicoletti, and F. Caciagli. 1997. Opposite influence of the metabotropic glutamate receptor subtypes mGlu3 and -5 on astrocyte proliferation in culture. *Glia*. 21:390-8.

Claudio, L., J.A. Martiney, and C.F. Brosnan. 1994. Ultrastructural studies of the blood-retina barrier after exposure to interleukin-1 beta or tumor necrosis factor-alpha. *Lab Invest*. 70:850-61.

Coffey, P.J., V.H. Perry, and J.N. Rawlins. 1990. An investigation into the early stages of the inflammatory response following ibotenic acid-induced neuronal degeneration. *Neuroscience*. 35:121-32.

Coleman, M.P., and V.H. Perry. 2002. Axon pathology in neurological disease: a neglected therapeutic target. *Trends Neurosci*. 25:532-7.

Collins, G.H., and N.R. West. 1989. Prospects for axonal regrowth in spinal cord injury. *Brain Res Bull*. 22:89-92.

Cope, A.P. 1998. Regulation of autoimmunity by proinflammatory cytokines. *Curr Opin Immunol*. 10:669-76.

Costanzo, R.M., and P.P. Graziadei. 1983. A quantitative analysis of changes in the olfactory epithelium following bulbectomy in hamster. *J Comp Neurol*. 215:370-81.

Coumans, J.V., T.T. Lin, H.N. Dai, L. MacArthur, M. McAtee, C. Nash, and B.S. Bregman. 2001. Axonal regeneration and functional recovery after complete spinal cord transection in rats by delayed treatment with transplants and neurotrophins. *J Neurosci*. 21:9334-44.

Dado, R.J., and G.J. Giesler, Jr. 1990. Afferent input to nucleus submedius in rats: retrograde labeling of neurons in the spinal cord and caudal medulla. *J Neurosci*. 10:2672-86.

Dalmau, I., B. Finsen, N. Tonder, J. Zimmer, B. Gonzalez, and B. Castellano. 1997. Development of microglia in the prenatal rat hippocampus. *J Comp Neurol*. 377:70-84.

David, S., C. Bouchard, O. Tsatas, and N. Giftochristos. 1990. Macrophages can modify the nonpermissive nature of the adult mammalian central nervous system. *Neuron*. 5:463-9.

Deehan, D.J., S.D. Heys, W. Simpson, J. Broom, D.N. McMillan, and O. Eremin. 1995. Modulation of the cytokine and acute-phase response to major surgery by recombinant interleukin-2. *Br J Surg*. 82:86-90.

Devon, R., and R. Doucette. 1992. Olfactory ensheathing cells myelinate dorsal root ganglion neurites. *Brain Res*. 589:175-9.

Devon, R., and R. Doucette. 1995. Olfactory ensheathing cells do not require L-ascorbic acid in vitro to assemble a basal lamina or to myelinate dorsal root ganglion neurites. *Brain Res*. 688:223-9.

Dickson, D.W., S.C. Lee, L.A. Mattiace, S.H. Yen, and C. Brosnan. 1993. Microglia and cytokines in neurological disease, with special reference to AIDS and Alzheimer's disease. *Glia*. 7:75-83.

Dihne, M., F. Block, H. Korr, and R. Topper. 2001. Time course of glial proliferation and glial apoptosis following excitotoxic CNS injury. *Brain Res*. 902:178-89.

Dinarello, C.A. 2000. Proinflammatory cytokines. *Chest*. 118:503-8.

Dopp, J.M., A. Mackenzie-Graham, G.C. Otero, and J.E. Merrill. 1997. Differential expression, cytokine modulation, and specific functions of type-1 and type-2 tumor necrosis factor receptors in rat glia. *J Neuroimmunol*. 75:104-12.

Doucette, J.R. 1984. The glial cells in the nerve fiber layer of the rat olfactory bulb. *Anat Rec*. 210:385-91.

Doucette, J.R., J.A. Kiernan, and B.A. Flumerfelt. 1983. The re-innervation of olfactory glomeruli following transection of primary olfactory axons in the central or peripheral nervous system. *J Anat*. 137 (Pt 1):1-19.

Doucette, R. 1989. Development of the nerve fiber layer in the olfactory bulb of mouse embryos. *J Comp Neurol*. 285:514-27.

Doucette, R. 1990. Glial influences on axonal growth in the primary olfactory system. *Glia*. 3:433-49.

Doucette, R. 1991. PNS-CNS transitional zone of the first cranial nerve. *J Comp Neurol*. 312:451-66.

Doucette, R. 1993a. Glial cells in the nerve fiber layer of the main olfactory bulb of embryonic and adult mammals. *Microsc Res Tech*. 24:113-30.

Doucette, R. 1993b. Glial progenitor cells of the nerve fiber layer of the olfactory bulb: effect of astrocyte growth media. *J Neurosci Res*. 35:274-87.

Doucette, R. 1995. Olfactory ensheathing cells: potential for glial cell transplantation into areas of CNS injury. *Histol Histopathol*. 10:503-7.

Doucette, R., and R. Devon. 1994. Media that support the growth and differentiation of oligodendrocytes do not induce olfactory ensheathing cells to express a myelinating phenotype. *Glia*. 10:296-310.

Doucette, R., and R. Devon. 1995. Elevated intracellular levels of cAMP induce olfactory ensheathing cells to express GAL-C and GFAP but not MBP. *Glia*. 13:130-40.

D'Souza, S., K. Alinauskas, E. McCrea, C. Goodyer, and J.P. Antel. 1995. Differential susceptibility of human CNS-derived cell populations to TNF-dependent and independent immune-mediated injury. *J Neurosci*. 15:7293-300.

Duan, S., C.M. Anderson, B.A. Stein, and R.A. Swanson. 1999. Glutamate induces rapid upregulation of astrocyte glutamate transport and cell-surface expression of GLAST. *J Neurosci*. 19:10193-200.

Duncan, I.D., J.P. Hammang, K.F. Jackson, P.M. Wood, R.P. Bunge, and L. Langford. 1988. Transplantation of oligodendrocytes and Schwann cells into the spinal cord of the myelin-deficient rat. *J Neurocytol*. 17:351-60.

Elkabes, S., E.M. DiCicco-Bloom, and I.B. Black. 1996. Brain microglia/macrophages express neurotrophins that selectively regulate microglial proliferation and function. *J Neurosci*. 16:2508-21.

Eng, D.L., Y.L. Lee, and P.G. Lal. 1997. Expression of glutamate uptake transporters after dibutyryl cyclic AMP differentiation and traumatic injury in cultured astrocytes. *Brain Res*. 778:215-21.

Enomoto, H., R.O. Heuckeroth, J.P. Golden, E.M. Johnson, and J. Milbrandt. 2000. Development of cranial parasympathetic ganglia requires sequential actions of GDNF and neurturin. *Development*. 127:4877-89.

Ernst, C., and B.R. Christie. 2006. The putative neural stem cell marker, nestin, is expressed in heterogeneous cell types in the adult rat neocortex. *Neuroscience*. 138:183-8.

Fabry, Z., K.M. Fitzsimmons, J.A. Herlein, T.O. Moninger, M.B. Dobbs, and M.N. Hart. 1993. Production of the cytokines interleukin 1 and 6 by murine brain microvessel endothelium and smooth muscle pericytes. *J Neuroimmunol*. 47:23-34.

Fadok, V.A., and P.M. Henson. 2003. Apoptosis: giving phosphatidylserine recognition an assist--with a twist. *Curr Biol*. 13:R655-7.

Fan, L., P.R. Young, F.C. Barone, G.Z. Feuerstein, D.H. Smith, and T.K. McIntosh. 1996. Experimental brain injury induces differential expression of tumor necrosis factor-alpha mRNA in the CNS. *Brain Res Mol Brain Res*. 36:287-91.

Fan, R., F. Xu, M.L. Previti, J. Davis, A.M. Grande, J.K. Robinson, and W.E. Van Nostrand. 2007. Minocycline reduces microglial activation and improves behavioral deficits in a transgenic model of cerebral microvascular amyloid. *J Neurosci*. 27:3057-63.

Farbman, A.I. 1990. Olfactory neurogenesis: genetic or environmental controls? *Trends Neurosci*. 13:362-5.

Farbman, A.I., and L.M. Squinto. 1985. Early development of olfactory receptor cell axons. *Brain Res*. 351:205-13.

Farina, L., and C. Winkelman. 2005. A review of the role of proinflammatory cytokines in labor and noninfectious preterm labor. *Biol Res Nurs*. 6:230-8.

Farooque, M., T. Badonic, Y. Olsson, and A. Holtz. 1995. Astrocytic reaction after graded spinal cord compression in rats: immunohistochemical studies on glial fibrillary acidic protein and vimentin. *J Neurotrauma*. 12:41-52.

Fawcett, J.W. 1997. Astrocytic and neuronal factors affecting axon regeneration in the damaged central nervous system. *Cell Tissue Res*. 290:371-7.

Fawcett, J.W., and R.A. Asher. 1999. The glial scar and central nervous system repair. *Brain Res Bull*. 49:377-91.

Felts, P.A., T.A. Baker, and K.J. Smith. 1997. Conduction in segmentally demyelinated mammalian central axons. *J Neurosci*. 17:7267-77.

Felts, P.A., A.M. Woolston, H.B. Fernando, S. Asquith, N.A. Gregson, O.J. Mizzi, and K.J. Smith. 2005. Inflammation and primary demyelination induced by the intraspinal injection of lipopolysaccharide. *Brain*. 128:1649-66.

Fernaud-Espinosa, I., M. Nieto-Sampedro, and P. Bovolenta. 1993. Differential activation of microglia and astrocytes in aniso- and isomorphic gliotic tissue. *Glia*. 8:277-91.

Fetler, L., and S. Amigorena. 2005. Neuroscience. Brain under surveillance: the microglia patrol. *Science*. 309:392-3.

Feuerstein, G.Z., T. Liu, and F.C. Barone. 1994. Cytokines, inflammation, and brain injury: role of tumor necrosis factor-alpha. *Cerebrovasc Brain Metab Rev*. 6:341-60.

Finn, J.T., M. Weil, F. Archer, R. Siman, A. Srinivasan, and M.C. Raff. 2000. Evidence that Wallerian degeneration and localized axon degeneration induced by local neurotrophin deprivation do not involve caspases. *J Neurosci*. 20:1333-41.

Finsen, B.R., N. Tonder, G.F. Xavier, J.C. Sorensen, and J. Zimmer. 1993. Induction of microglial immunomolecules by anterogradely degenerating mossy fibres in the rat hippocampal formation. *J Chem Neuroanat*. 6:267-75.

Fischer, H.G., and G. Reichmann. 2001. Brain dendritic cells and macrophages/microglia in central nervous system inflammation. *J Immunol*. 166:2717-26.

Flaris, N.A., T.L. Densmore, M.C. Molleston, and W.F. Hickey. 1993. Characterization of microglia and macrophages in the central nervous system of rats: definition of the differential expression of molecules using standard and novel monoclonal antibodies in normal CNS and in four models of parenchymal reaction. *Glia*. 7:34-40.

Flugel, A., G. Hager, A. Horvat, C. Spitzer, G.M. Singer, M.B. Graeber, G.W. Kreutzberg, and F.W. Schwaiger. 2001. Neuronal MCP-1 expression in response to remote nerve injury. *J Cereb Blood Flow Metab*. 21:69-76.

Fontaine, V., S. Mohand-Said, N. Hanoteau, C. Fuchs, K. Pfizenmaier, and U. Eisel. 2002. Neurodegenerative and neuroprotective effects of tumor Necrosis factor (TNF) in retinal ischemia: opposite roles of TNF receptor 1 and TNF receptor 2. *J Neurosci*. 22:RC216.

Ford, A.L., A.L. Goodsall, W.F. Hickey, and J.D. Sedgwick. 1995. Normal adult ramified microglia separated from other central nervous system macrophages by flow cytometric sorting. Phenotypic differences defined and direct ex vivo antigen presentation to myelin basic protein-reactive CD4+ T cells compared. *J Immunol*. 154:4309-21.

Fordyce, C.B., R. Jagasia, X. Zhu, and L.C. Schlichter. 2005. Microglia Kv1.3 channels contribute to their ability to kill neurons. *J Neurosci*. 25:7139-49.

Fraher, J.P. 1992. The CNS-PNS transitional zone of the rat. Morphometric studies at cranial and spinal levels. *Prog Neurobiol*. 38:261-316.

Franceschini, I.A., and S.C. Barnett. 1996. Low-affinity NGF-receptor and E-N-CAM expression define two types of olfactory nerve ensheathing cells that share a common lineage. *Dev Biol*. 173:327-43.

Franklin, R.J. 2003. Remyelination by transplanted olfactory ensheathing cells. *Anat Rec B New Anat*. 271:71-6.
Franklin, R.J., and S.C. Barnett. 1997. Do olfactory glia have advantages over Schwann cells for CNS repair? *J Neurosci Res*. 50:665-72.
Franklin, R.J., and S.C. Barnett. 2000. Olfactory ensheathing cells and CNS regeneration: the sweet smell of success? *Neuron*. 28:15-8.
Franklin, R.J., S.A. Bayley, and W.F. Blakemore. 1996a. Transplanted CG4 cells (an oligodendrocyte progenitor cell line) survive, migrate, and contribute to repair of areas of demyelination in X-irradiated and damaged spinal cord but not in normal spinal cord. *Exp Neurol*. 137:263-76.
Franklin, R.J., and W.F. Blakemore. 1993. Requirements for Schwann cell migration within CNS environments: a viewpoint. *Int J Dev Neurosci*. 11:641-9.
Franklin, R.J., and W.F. Blakemore. 1995. Glial-cell transplantation and plasticity in the O-2A lineage--implications for CNS repair. *Trends Neurosci*. 18:151-6.
Franklin, R.J., J.M. Gilson, I.A. Franceschini, and S.C. Barnett. 1996b. Schwann cell-like myelination following transplantation of an olfactory bulb-ensheathing cell line into areas of demyelination in the adult CNS. *Glia*. 17:217-24.
Franson, P., and L.O. Ronnevi. 1984. Myelin breakdown and elimination in the posterior funiculus of the adult cat after dorsal rhizotomy: a light and electron microscopic qualitative and quantitative study. *J Comp Neurol*. 223:138-51.
Franzen, R., J. Schoenen, P. Leprince, E. Joosten, G. Moonen, and D. Martin. 1998. Effects of macrophage transplantation in the injured adult rat spinal cord: a combined immunocytochemical and biochemical study. *J Neurosci Res*. 51:316-27.
Frei, K., H.P. Eugster, M. Bopst, C.S. Constantinescu, E. Lavi, and A. Fontana. 1997. Tumor necrosis factor alpha and lymphotoxin alpha are not required for induction of acute experimental autoimmune encephalomyelitis. *J Exp Med*. 185:2177-82.
Geisert, E.E., Jr., H.G. Johnson, and L.I. Binder. 1990. Expression of microtubule-associated protein 2 by reactive astrocytes. *Proc Natl Acad Sci U S A*. 87:3967-71.
George, E.B., J.D. Glass, and J.W. Griffin. 1995. Axotomy-induced axonal degeneration is mediated by calcium influx through ion-specific channels. *J Neurosci*. 15:6445-52.
George, R., and J.W. Griffin. 1994a. Delayed macrophage responses and myelin clearance during Wallerian degeneration in the central nervous system: the dorsal radiculotomy model. *Exp Neurol*. 129:225-36.
George, R., and J.W. Griffin. 1994b. The proximo-distal spread of axonal degeneration in the dorsal columns of the rat. *J Neurocytol*. 23:657-67.
Giaume, C., and K.D. McCarthy. 1996. Control of gap-junctional communication in astrocytic networks. *Trends Neurosci*. 19:319-25.
Gilbert, M., J. Smith, A.J. Roskams, and V.J. Auld. 2001. Neuroligin 3 is a vertebrate gliotactin expressed in the olfactory ensheathing glia, a growth-promoting class of macroglia. *Glia*. 34:151-64.
Giordana, M.T., A. Attanasio, P. Cavalla, A. Migheli, M.C. Vigliani, and D. Schiffer. 1994. Reactive cell proliferation and microglia following injury to the rat brain. *Neuropathol Appl Neurobiol*. 20:163-74.

Giulian, D., and T.J. Baker. 1986. Characterization of ameboid microglia isolated from developing mammalian brain. *J Neurosci*. 6:2163-78.

Giulian, D., J. Chen, J.E. Ingeman, J.K. George, and M. Noponen. 1989. The role of mononuclear phagocytes in wound healing after traumatic injury to adult mammalian brain. *J Neurosci*. 9:4416-29.

Giulian, D., and C. Robertson. 1990. Inhibition of mononuclear phagocytes reduces ischemic injury in the spinal cord. *Ann Neurol*. 27:33-42.

Glabinski, A.R., V. Balasingam, M. Tani, S.L. Kunkel, R.M. Strieter, V.W. Yong, and R.M. Ransohoff. 1996. Chemokine monocyte chemoattractant protein-1 is expressed by astrocytes after mechanical injury to the brain. *J Immunol*. 156:4363-8.

Gong, Q., M.S. Bailey, S.K. Pixley, M. Ennis, W. Liu, and M.T. Shipley. 1994. Localization and regulation of low affinity nerve growth factor receptor expression in the rat olfactory system during development and regeneration. *J Comp Neurol*. 344:336-48.

Gonzalez, R., J. Glaser, M.T. Liu, T.E. Lane, and H.S. Keirstead. 2003. Reducing inflammation decreases secondary degeneration and functional deficit after spinal cord injury. *Exp Neurol*. 184:456-63.

Goodman, M.N., J. Silver, and J.W. Jacobberger. 1993. Establishment and neurite outgrowth properties of neonatal and adult rat olfactory bulb glial cell lines. *Brain Res*. 619:199-213.

Gorgels, T.G. 1990. A quantitative analysis of axon outgrowth, axon loss, and myelination in the rat pyramidal tract. *Brain Res Dev Brain Res*. 54:51-61.

Gorgels, T.G., E.J. De Kort, H.T. Van Aanholt, and R. Nieuwenhuys. 1989. A quantitative analysis of the development of the pyramidal tract in the cervical spinal cord in the rat. *Anat Embryol (Berl)*. 179:377-85.

Graeber, M.B., and G.W. Kreutzberg. 1986. Astrocytes increase in glial fibrillary acidic protein during retrograde changes of facial motor neurons. *J Neurocytol*. 15:363-73.

Graeber, M.B., F. Lopez-Redondo, E. Ikoma, M. Ishikawa, Y. Imai, K. Nakajima, G.W. Kreutzberg, and S. Kohsaka. 1998. The microglia/macrophage response in the neonatal rat facial nucleus following axotomy. *Brain Res*. 813:241-53.

Graeber, M.B., W.J. Streit, D. Buringer, D.L. Sparks, and G.W. Kreutzberg. 1992. Ultrastructural location of major histocompatibility complex (MHC) class II positive perivascular cells in histologically normal human brain. *J Neuropathol Exp Neurol*. 51:303-11.

Graeber, M.B., W.J. Streit, and G.W. Kreutzberg. 1988. Axotomy of the rat facial nerve leads to increased CR3 complement receptor expression by activated microglial cells. *J Neurosci Res*. 21:18-24.

Graeber, M.B., W.J. Streit, and G.W. Kreutzberg. 1990. The third glial cell type, the microglia: cellular markers of activation in situ. *Acta Histochem Suppl*. 38:157-60.

Graziadei, P.P., and G.A. Monti Graziadei. 1980. Neurogenesis and neuron regeneration in the olfactory system of mammals. III. Deafferentation and reinnervation of the olfactory bulb following section of the fila olfactoria in rat. *J Neurocytol*. 9:145-62.

Grell, M., F.M. Becke, H. Wajant, D.N. Mannel, and P. Scheurich. 1998. TNF receptor type 2 mediates thymocyte proliferation independently of TNF receptor type 1. *Eur J Immunol*. 28:257-63.

Griffin, J.W., R. George, C. Lobato, W.R. Tyor, L.C. Yan, and J.D. Glass. 1992. Macrophage responses and myelin clearance during Wallerian degeneration: relevance to immune-mediated demyelination. *J Neuroimmunol*. 40:153-65.

Groves, A.K., S.C. Barnett, R.J. Franklin, A.J. Crang, M. Mayer, W.F. Blakemore, and M. Noble. 1993. Repair of demyelinated lesions by transplantation of purified O-2A progenitor cells. *Nature*. 362:453-5.

Guillemin, G.J., and B.J. Brew. 2004. Microglia, macrophages, perivascular macrophages, and pericytes: a review of function and identification. *J Leukoc Biol*. 75:388-97.

Gumpel, M., O. Gout, C. Lubetzki, A. Gansmuller, and N. Baumann. 1989. Myelination and remyelination in the central nervous system by transplanted oligodendrocytes using the shiverer model. Discussion on the remyelinating cell population in adult mammals. *Dev Neurosci*. 11:132-9.

Guo, L.H., K. Trautmann, and H.J. Schluesener. 2005. Expression of P2X4 receptor by lesional activated microglia during formalin-induced inflammatory pain. *J Neuroimmunol*. 163:120-7.

Haddad, J.J. 2002. Antioxidant and prooxidant mechanisms in the regulation of redox(y)-sensitive transcription factors. *Cell Signal*. 14:879-97.

Hailer, N.P., A. Grampp, and R. Nitsch. 1999. Proliferation of microglia and astrocytes in the dentate gyrus following entorhinal cortex lesion: a quantitative bromodeoxyuridine-labelling study. *Eur J Neurosci*. 11:3359-64.

Hajos, F., B. Gerics, and E. Turai. 1993. Astroglial reaction following Wallerian degeneration in the rat visual cortex: proliferation or hypertrophy? *Neurobiology (Bp)*. 1:123-31.

Hallpike, J.F., and C.W. Adams. 1969. Proteolysis and myelin breakdown: a review of recent histochemical and biochemical studies. *Histochem J*. 1:559-78.

Hashizume, H., J.A. DeLeo, R.W. Colburn, and J.N. Weinstein. 2000. Spinal glial activation and cytokine expression after lumbar root injury in the rat. *Spine*. 25:1206-17.

Hatten, M.E., R.K. Liem, M.L. Shelanski, and C.A. Mason. 1991. Astroglia in CNS injury. *Glia*. 4:233-43.

Hattori, A., K. Hayashi, and M. Kohno. 1996. Tumor necrosis factor (TNF) stimulates the production of nerve growth factor in fibroblasts via the 55-kDa type 1 TNF receptor. *FEBS Lett*. 379:157-60.

Hauser, S.L., T.H. Doolittle, R. Lincoln, R.H. Brown, and C.A. Dinarello. 1990. Cytokine accumulations in CSF of multiple sclerosis patients: frequent detection of interleukin-1 and tumor necrosis factor but not interleukin-6. *Neurology*. 40:1735-9.

He, B.P., S.S. Tay, and S.K. Leong. 1997. Microglia responses in the CNS following sciatic nerve transection in C57BL/Wld(s) and BALB/c mice. *Exp Neurol*. 146:587-95.

He, B.P., W. Wen, and M.J. Strong. 2002. Activated microglia (BV-2) facilitation of TNF-alpha-mediated motor neuron death in vitro. *J Neuroimmunol*. 128:31-8.

Hermanson, M., T. Olsson, B. Westermark, and K. Funa. 1995. PDGF and its receptors following facial nerve axotomy in rats: expression in neurons and surrounding glia. *Exp Brain Res*. 102:415-22.

Hoek, R.M., S.R. Ruuls, C.A. Murphy, G.J. Wright, R. Goddard, S.M. Zurawski, B. Blom, M.E. Homola, W.J. Streit, M.H. Brown, A.N. Barclay, and J.D. Sedgwick. 2000. Down-regulation of the macrophage lineage through interaction with OX2 (CD200). *Science*. 290:1768-71.

Hofman, F.M., D.R. Hinton, K. Johnson, and J.E. Merrill. 1989. Tumor necrosis factor identified in multiple sclerosis brain. *J Exp Med*. 170:607-12.

Honmou, O., P.A. Felts, S.G. Waxman, and J.D. Kocsis. 1996. Restoration of normal conduction properties in demyelinated spinal cord axons in the adult rat by transplantation of exogenous Schwann cells. *J Neurosci*. 16:3199-208.

Hopkins, S.J., and N.J. Rothwell. 1995. Cytokines and the nervous system. I: Expression and recognition. *Trends Neurosci*. 18:83-8.

Hosoi, T., Y. Okuma, and Y. Nomura. 2002. The mechanisms of immune-to-brain communication in inflammation as a drug target. *Curr Drug Targets Inflamm Allergy*. 1:257-62.

Hughes, P.M., G.M. Wells, J.M. Clements, A.J. Gearing, E.J. Redford, M. Davies, K.J. Smith, R.A. Hughes, M.C. Brown, and K.M. Miller. 1998. Matrix metalloproteinase expression during experimental autoimmune neuritis. *Brain*. 121 (Pt 3):481-94.

Imaizumi, T., K.L. Lankford, J.D. Kocsis, M. Sasaki, Y. Akiyama, and K. Hashi. 2000. [Comparison of myelin-forming cells as candidates for therapeutic transplantation in demyelinated CNS axons]. *No To Shinkei*. 52:609-15.

Imaizumi, T., K.L. Lankford, S.G. Waxman, C.A. Greer, and J.D. Kocsis. 1998. Transplanted olfactory ensheathing cells remyelinate and enhance axonal conduction in the demyelinated dorsal columns of the rat spinal cord. *J Neurosci*. 18:6176-85.

Innocenti, G.M., S. Clarke, and H. Koppel. 1983. Transitory macrophages in the white matter of the developing visual cortex. II. Development and relations with axonal pathways. *Brain Res*. 313:55-66.

Isaksson, J., M. Farooque, A. Holtz, L. Hillered, and Y. Olsson. 1999. Expression of ICAM-1 and CD11b after experimental spinal cord injury in rats. *J Neurotrauma*. 16:165-73.

Jacob, C.O., S. Aiso, S.A. Michie, H.O. McDevitt, and H. Acha-Orbea. 1990. Prevention of diabetes in nonobese diabetic mice by tumor necrosis factor (TNF): similarities between TNF-alpha and interleukin 1. *Proc Natl Acad Sci U S A*. 87:968-72.

Jahed, A., J.W. Rowland, T. McDonald, J.G. Boyd, R. Doucette, and M.D. Kawaja. 2007. Olfactory ensheathing cells express smooth muscle alpha-actin in vitro and in vivo. *J Comp Neurol*. 503:209-23.

Jakeman, L.B., and P.J. Reier. 1991. Axonal projections between fetal spinal cord transplants and the adult rat spinal cord: a neuroanatomical tracing study of local interactions. *J Comp Neurol*. 307:311-34.

Jensen, M.B., B. Finsen, and J. Zimmer. 1997. Morphological and immunophenotypic microglial changes in the denervated fascia dentata of adult rats: correlation with blood-brain barrier damage and astroglial reactions. *Exp Neurol*. 143:103-16.

Jensen, M.B., B. Gonzalez, B. Castellano, and J. Zimmer. 1994. Microglial and astroglial reactions to anterograde axonal degeneration: a histochemical and immunocytochemical study of the adult rat fascia dentata after entorhinal perforant path lesions. *Exp Brain Res*. 98:245-60.

Jensen, M.B., I.V. Hegelund, F.R. Poulsen, T. Owens, J. Zimmer, and B. Finsen. 1999. Microglial reactivity correlates to the density and the myelination of the anterogradely degenerating axons and terminals following perforant path denervation of the mouse fascia dentata. *Neuroscience*. 93:507-18.

John, G.R., S.C. Lee, and C.F. Brosnan. 2003. Cytokines: powerful regulators of glial cell activation. *Neuroscientist*. 9:10-22.

Jones, L.L., G.W. Kreutzberg, and G. Raivich. 1998. Transforming growth factor beta's 1, 2 and 3 inhibit proliferation of ramified microglia on an astrocyte monolayer. *Brain Res*. 795:301-6.

Jones, T.B., R.P. Hart, and P.G. Popovich. 2005. Molecular control of physiological and pathological T-cell recruitment after mouse spinal cord injury. *J Neurosci*. 25:6576-83.

Joosten, E.A., and D.P. Bar. 1999. Axon guidance of outgrowing corticospinal fibres in the rat. *J Anat*. 194 (Pt 1):15-32.

Joosten, E.A., and A.A. Gribnau. 1988. Unmyelinated corticospinal axons in adult rat pyramidal tract. An electron microscopic tracer study. *Brain Res*. 459:173-7.

Kafitz, K.W., and C.A. Greer. 1998. The influence of ensheathing cells on olfactory receptor cell neurite outgrowth in vitro. *Ann N Y Acad Sci*. 855:266-9.

Karimi-Abdolrezaee, S., V.M. Verge, and D.J. Schreyer. 2002. Developmental down-regulation of GAP-43 expression and timing of target contact in rat corticospinal neurons. *Exp Neurol*. 176:390-401.

Kassiotis, G., K. Kranidioti, and G. Kollias. 2001. Defective CD4T cell priming and resistance to experimental autoimmune encephalomyelitis in TNF-deficient mice due to innate immune hypo-responsiveness. *J Neuroimmunol*. 119:239-47.

Kassiotis, G., M. Pasparakis, G. Kollias, and L. Probert. 1999. TNF accelerates the onset but does not alter the incidence and severity of myelin basic protein-induced experimental autoimmune encephalomyelitis. *Eur J Immunol*. 29:774-80.

Kato, T., O. Honmou, T. Uede, K. Hashi, and J.D. Kocsis. 2000. Transplantation of human olfactory ensheathing cells elicits remyelination of demyelinated rat spinal cord. *Glia*. 30:209-18.

Kaur, C., A.J. Hao, C.H. Wu, and E.A. Ling. 2001. Origin of microglia. *Microsc Res Tech*. 54:2-9.

Kaur, C., and E.A. Ling. 1991. Study of the transformation of amoeboid microglial cells into microglia labelled with the isolectin Griffonia simplicifolia in postnatal rats. *Acta Anat (Basel)*. 142:118-25.

Kaur, C., and E.A. Ling. 1992. Activation and re-expression of surface antigen in microglia following an epidural application of kainic acid in the rat brain. *J Anat*. 180 (Pt 2):333-42.

Keirstead, H.S., G. Nistor, G. Bernal, M. Totoiu, F. Cloutier, K. Sharp, and O. Steward. 2005. Human embryonic stem cell-derived oligodendrocyte progenitor cell transplants remyelinate and restore locomotion after spinal cord injury. *J Neurosci*. 25:4694-705.

Keyvan-Fouladi, N., G. Raisman, and Y. Li. 2003. Functional repair of the corticospinal tract by delayed transplantation of olfactory ensheathing cells in adult rats. *J Neurosci*. 23:9428-34.
Kielian, T. 2006. Toll-like receptors in central nervous system glial inflammation and homeostasis. *J Neurosci Res*. 83:711-30.
Killackey, H.P., K.A. Koralek, N.L. Chiaia, and R.W. Rhodes. 1989. Laminar and areal differences in the origin of the subcortical projection neurons of the rat somatosensory cortex. *J Comp Neurol*. 282:428-45.
Kim, M.O., Q. Si, J.N. Zhou, R.G. Pestell, C.F. Brosnan, J. Locker, and S.C. Lee. 2002. Interferon-beta activates multiple signaling cascades in primary human microglia. *J Neurochem*. 81:1361-71.
Kim, S.U., and J. de Vellis. 2005. Microglia in health and disease. *J Neurosci Res*. 81:302-13.
Kimelberg, H.K. 1995. Receptors on astrocytes--what possible functions? *Neurochem Int*. 26:27-40.
Kitamura, T., T. Miyake, and S. Fujita. 1984. Genesis of resting microglia in the gray matter of mouse hippocampus. *J Comp Neurol*. 226:421-33.
Kitamura, Y., K. Takata, M. Inden, D. Tsuchiya, D. Yanagisawa, J. Nakata, and T. Taniguchi. 2004. Intracerebroventricular injection of microglia protects against focal brain ischemia. *J Pharmacol Sci*. 94:203-6.
Klein, M.A., J.C. Moller, L.L. Jones, H. Bluethmann, G.W. Kreutzberg, and G. Raivich. 1997. Impaired neuroglial activation in interleukin-6 deficient mice. *Glia*. 19:227-33.
Kloss, C.U., G.W. Kreutzberg, and G. Raivich. 1997. Proliferation of ramified microglia on an astrocyte monolayer: characterization of stimulatory and inhibitory cytokines. *J Neurosci Res*. 49:248-54.
Klusman, I., and M.E. Schwab. 1997. Effects of pro-inflammatory cytokines in experimental spinal cord injury. *Brain Res*. 762:173-84.
Kobbert, C., and S. Thanos. 2000. Topographic representation of the sciatic nerve motor neurons in the spinal cord of the adult rat correlates to region-specific activation patterns of microglia. *J Neurocytol*. 29:271-83.
Kocsis, J.D. 1999. Restoration of function by glial cell transplantation into demyelinated spinal cord. *J Neurotrauma*. 16:695-703.
Koopmans, G.C., R. Deumens, W.M. Honig, F.P. Hamers, H.W. Steinbusch, and E.A. Joosten. 2005. The assessment of locomotor function in spinal cord injured rats: the importance of objective analysis of coordination. *J Neurotrauma*. 22:214-25.
Koshinaga, M., and S.R. Whittemore. 1995. The temporal and spatial activation of microglia in fiber tracts undergoing anterograde and retrograde degeneration following spinal cord lesion. *J Neurotrauma*. 12:209-22.
Kott, J.N., L.E. Westrum, E.W. Raines, M. Sasahara, and R. Ross. 1994. Olfactory ensheathing glia and platelet-derived growth factor B-chain reactivity in the transplanted rat olfactory bulb. *Int J Dev Neurosci*. 12:315-23.
Kotter, M.R., A. Setzu, F.J. Sim, N. Van Rooijen, and R.J. Franklin. 2001. Macrophage depletion impairs oligodendrocyte remyelination following lysolecithin-induced demyelination. *Glia*. 35:204-12.

Kreutzberg, G.W. 1996. Microglia: a sensor for pathological events in the CNS. *Trends Neurosci*. 19:312-8.

Krum, J.M., T.M. Phillips, and J.M. Rosenstein. 2002. Changes in astroglial GLT-1 expression after neural transplantation or stab wounds. *Exp Neurol*. 174:137-49.

Kuhlmann, T., U. Wendling, C. Nolte, F. Zipp, B. Maruschak, C. Stadelmann, H. Siebert, and W. Bruck. 2002. Differential regulation of myelin phagocytosis by macrophages/microglia, involvement of target myelin, Fc receptors and activation by intravenous immunoglobulins. *J Neurosci Res*. 67:185-90.

Kunkel-Bagden, E., and B.S. Bregman. 1990. Spinal cord transplants enhance the recovery of locomotor function after spinal cord injury at birth. *Exp Brain Res*. 81:25-34.

Kuno, R., J. Wang, J. Kawanokuchi, H. Takeuchi, T. Mizuno, and A. Suzumura. 2005. Autocrine activation of microglia by tumor necrosis factor-alpha. *J Neuroimmunol*. 162:89-96.

Lachapelle, F., M. Gumpel, M. Baulac, C. Jacque, P. Duc, and N. Baumann. 1983. Transplantation of CNS fragments into the brain of shiverer mutant mice: extensive myelination by implanted oligodendrocytes. I. Immunohistochemical studies. *Dev Neurosci*. 6:325-34.

Ladeby, R., M. Wirenfeldt, D. Garcia-Ovejero, C. Fenger, L. Dissing-Olesen, I. Dalmau, and B. Finsen. 2005. Microglial cell population dynamics in the injured adult central nervous system. *Brain Res Brain Res Rev*. 48:196-206.

Lai, A.Y., and K.G. Todd. 2006. Hypoxia-activated microglial mediators of neuronal survival are differentially regulated by tetracyclines. *Glia*. 53:809-16.

Lakatos, A., S.C. Barnett, and R.J. Franklin. 2003a. Olfactory ensheathing cells induce less host astrocyte response and chondroitin sulphate proteoglycan expression than Schwann cells following transplantation into adult CNS white matter. *Exp Neurol*. 184:237-46.

Lakatos, A., R.J. Franklin, and S.C. Barnett. 2000a. Olfactory ensheathing cells and Schwann cells differ in their in vitro interactions with astrocytes. *Glia*. 32:214-25.

Lakatos, A., P.M. Smith, S.C. Barnett, and R.J. Franklin. 2003b. Meningeal cells enhance limited CNS remyelination by transplanted olfactory ensheathing cells. *Brain*. 126:598-609.

Lakatos, P., J. Foldes, Z. Nagy, I. Takacs, G. Speer, C. Horvath, S. Mohan, D.J. Baylink, and P.H. Stern. 2000b. Serum insulin-like growth factor-I, insulin-like growth factor binding proteins, and bone mineral content in hyperthyroidism. *Thyroid*. 10:417-23.

Lawson, L.J., L. Frost, J. Risbridger, S. Fearn, and V.H. Perry. 1994. Quantification of the mononuclear phagocyte response to Wallerian degeneration of the optic nerve. *J Neurocytol*. 23:729-44.

Lechan, R.M., R. Toni, B.D. Clark, J.G. Cannon, A.R. Shaw, C.A. Dinarello, and S. Reichlin. 1990. Immunoreactive interleukin-1 beta localization in the rat forebrain. *Brain Res*. 514:135-40.

Lee, J.C., G.S. Cho, J.H. Kwon, M.H. Shin, J.H. Lim, and W.K. Kim. 2006. Macrophageal/microglial cell activation and cerebral injury induced by excretory-secretory products secreted by Paragonimus westermani. *Neurosci Res*. 54:133-9.

Leenen, L.P., J. Meek, P.R. Posthuma, and R. Nieuwenuys. 1989. Differences in the fiber composition of the pyramidal tract in two- and 14-month-old rats. *Neuroscience*. 28:635-43.

Legler, D.F., O. Micheau, M.A. Doucey, J. Tschopp, and C. Bron. 2003. Recruitment of TNF receptor 1 to lipid rafts is essential for TNFalpha-mediated NF-kappaB activation. *Immunity*. 18:655-64.

Lendahl, U., L.B. Zimmerman, and R.D. McKay. 1990. CNS stem cells express a new class of intermediate filament protein. *Cell*. 60:585-95.

Leon, S., Y. Yin, J. Nguyen, N. Irwin, and L.I. Benowitz. 2000. Lens injury stimulates axon regeneration in the mature rat optic nerve. *J Neurosci*. 20:4615-26.

Li, S., and S.M. Strittmatter. 2003. Delayed systemic Nogo-66 receptor antagonist promotes recovery from spinal cord injury. *J Neurosci*. 23:4219-27.

Li, X.G., S.L. Florence, and J.H. Kaas. 1990. Areal distributions of cortical neurons projecting to different levels of the caudal brain stem and spinal cord in rats. *Somatosens Mot Res*. 7:315-35.

Li, Y., P.M. Field, and G. Raisman. 1997. Repair of adult rat corticospinal tract by transplants of olfactory ensheathing cells. *Science*. 277:2000-2.

Li, Y., P.M. Field, and G. Raisman. 1998. Regeneration of adult rat corticospinal axons induced by transplanted olfactory ensheathing cells. *J Neurosci*. 18:10514-24.

Li, Y., D. Li, and G. Raisman. 2005. Interaction of olfactory ensheathing cells with astrocytes may be the key to repair of tract injuries in the spinal cord: the 'pathway hypothesis'. *J Neurocytol*. 34:343-51.

Liberto, C.M., P.J. Albrecht, L.M. Herx, V.W. Yong, and S.W. Levison. 2004. Pro-regenerative properties of cytokine-activated astrocytes. *J Neurochem*. 89:1092-100.

Licinio, J., and P. Frost. 2000. The neuroimmune-endocrine axis: pathophysiological implications for the central nervous system cytokines and hypothalamus-pituitary-adrenal hormone dynamics. *Braz J Med Biol Res*. 33:1141-8.

Lin, L.F., D.H. Doherty, J.D. Lile, S. Bektesh, and F. Collins. 1993. GDNF: a glial cell line-derived neurotrophic factor for midbrain dopaminergic neurons. *Science*. 260:1130-2.

Lindholm, D., E. Castren, R. Kiefer, F. Zafra, and H. Thoenen. 1992. Transforming growth factor-beta 1 in the rat brain: increase after injury and inhibition of astrocyte proliferation. *J Cell Biol*. 117:395-400.

Lindholm, D., R. Heumann, M. Meyer, and H. Thoenen. 1987. Interleukin-1 regulates synthesis of nerve growth factor in non-neuronal cells of rat sciatic nerve. *Nature*. 330:658-9.

Ling, E.A. 1979. Transformation of monocytes into amoeboid microglia in the corpus callosum of postnatal rats, as shown by labelling monocytes by carbon particles. *J Anat*. 128:847-58.

Ling, E.A., A. Dahlstrom, R.J. Polinsky, L.E. Nee, and A. McRae. 1992. Studies of activated microglial cells and macrophages using Alzheimer's disease cerebrospinal fluid in adult rats with experimentally induced lesions. *Neuroscience*. 51:815-25.

Ling, E.A., C. Kaur, and W.C. Wong. 1991. Expression of major histocompatibility complex and leukocyte common antigens in amoeboid microglia in postnatal rats. *J Anat*. 177:117-26.

Ling, E.A., and W.C. Wong. 1993. The origin and nature of ramified and amoeboid microglia: a historical review and current concepts. *Glia*. 7:9-18.

Lipson, A.C., J. Widenfalk, E. Lindqvist, T. Ebendal, and L. Olson. 2003. Neurotrophic properties of olfactory ensheathing glia. *Exp Neurol*. 180:167-71.

Liu, B., and J.S. Hong. 2003. Role of microglia in inflammation-mediated neurodegenerative diseases: mechanisms and strategies for therapeutic intervention. *J Pharmacol Exp Ther*. 304:1-7.

Liu, J., M.W. Marino, G. Wong, D. Grail, A. Dunn, J. Bettadapura, A.J. Slavin, L. Old, and C.C. Bernard. 1998a. TNF is a potent anti-inflammatory cytokine in autoimmune-mediated demyelination. *Nat Med*. 4:78-83.

Liu, K.L., M.I. Chuah, and K.K. Lee. 1995. Soluble factors from the olfactory bulb attract olfactory Schwann cells. *J Neurosci*. 15:990-1000.

Liu, L., J.K. Persson, M. Svensson, and H. Aldskogius. 1998b. Glial cell responses, complement, and clusterin in the central nervous system following dorsal root transection. *Glia*. 23:221-38.

Liu, P.H., Y.J. Wang, and G.F. Tseng. 2003. Close axonal injury of rubrospinal neurons induced transient perineuronal astrocytic and microglial reaction that coincided with their massive degeneration. *Exp Neurol*. 179:111-26.

Lopez-Redondo, F., K. Nakajima, S. Honda, and S. Kohsaka. 2000. Glutamate transporter GLT-1 is highly expressed in activated microglia following facial nerve axotomy. *Brain Res Mol Brain Res*. 76:429-35.

Lotan, M., and M. Schwartz. 1994. Cross talk between the immune system and the nervous system in response to injury: implications for regeneration. *Faseb J*. 8:1026-33.

Lu, J., F. Feron, A. Mackay-Sim, and P.M. Waite. 2002. Olfactory ensheathing cells promote locomotor recovery after delayed transplantation into transected spinal cord. *Brain*. 125:14-21.

Lu, P., L.L. Jones, E.Y. Snyder, and M.H. Tuszynski. 2003. Neural stem cells constitutively secrete neurotrophic factors and promote extensive host axonal growth after spinal cord injury. *Exp Neurol*. 181:115-29.

Lucchinetti, C., W. Bruck, and J. Noseworthy. 2001. Multiple sclerosis: recent developments in neuropathology, pathogenesis, magnetic resonance imaging studies and treatment. *Curr Opin Neurol*. 14:259-69.

Ludwin, S.K., and M.A. Bisby. 1992. Delayed wallerian degeneration in the central nervous system of Ola mice: an ultrastructural study. *J Neurol Sci*. 109:140-7.

Lundberg, C., and A. Bjorklund. 1996. Host regulation of glial markers in intrastriatal grafts of conditionally immortalized neural stem cell lines. *Neuroreport*. 7:847-52.

Ma, M., T. Wei, L. Boring, I.F. Charo, R.M. Ransohoff, and L.B. Jakeman. 2002. Monocyte recruitment and myelin removal are delayed following spinal cord injury in mice with CCR2 chemokine receptor deletion. *J Neurosci Res*. 68:691-702.

Mander, T.H., and J.F. Morris. 1995. Immunophenotypic evidence for distinct populations of microglia in the rat hypothalamo-neurohypophysial system. *Cell Tissue Res*. 280:665-73.
Mansour, H., A. Bignami, B. Labkovsky, and D. Dahl. 1989. Neurofilament phosphorylation in neuronal perikarya following axotomy: a study of rat spinal cord with ventral and dorsal root transection. *J Comp Neurol*. 283:481-5.
Markiewicz, I., and B. Lukomska. 2006. The role of astrocytes in the physiology and pathology of the central nervous system. *Acta Neurobiol Exp (Wars)*. 66:343-58.
Martinez, G., M.L. Carnazza, C. Di Giacomo, V. Sorrenti, M. Avitabile, and A. Vanella. 1998. GFAP, S-100 and vimentin proteins in rat after cerebral post-ischemic reperfusion. *Int J Dev Neurosci*. 16:519-26.
Matthews, M.A., and D. Duncan. 1971. A quantitative study of morphological changes accompanying the initiation and progress of myelin production in the dorsal funiculus of the rat spinal cord. *J Comp Neurol*. 142:1-22.
Mazzanti, M., J.Y. Sul, and P.G. Haydon. 2001. Glutamate on demand: astrocytes as a ready source. *Neuroscientist*. 7:396-405.
McGraw, J., G.W. Hiebert, and J.D. Steeves. 2001. Modulating astrogliosis after neurotrauma. *J Neurosci Res*. 63:109-15.
McKay, S.M., D.J. Brooks, P. Hu, and E.M. McLachlan. 2007. Distinct types of microglial activation in white and grey matter of rat lumbosacral cord after mid-thoracic spinal transection. *J Neuropathol Exp Neurol*. 66:698-710.
McSorley, S.J., S. Soldera, L. Malherbe, C. Carnaud, R.M. Locksley, R.A. Flavell, and N. Glaichenhaus. 1997. Immunological tolerance to a pancreatic antigen as a result of local expression of TNFalpha by islet beta cells. *Immunity*. 7:401-9.
McTigue, D.M., P.J. Horner, B.T. Stokes, and F.H. Gage. 1998. Neurotrophin-3 and brain-derived neurotrophic factor induce oligodendrocyte proliferation and myelination of regenerating axons in the contused adult rat spinal cord. *J Neurosci*. 18:5354-65.
Mehler, M.F., and J.A. Kessler. 1997. Hematolymphopoietic and inflammatory cytokines in neural development. *Trends Neurosci*. 20:357-65.
Menei, P., C. Montero-Menei, S.R. Whittemore, R.P. Bunge, and M.B. Bunge. 1998. Schwann cells genetically modified to secrete human BDNF promote enhanced axonal regrowth across transected adult rat spinal cord. *Eur J Neurosci*. 10:607-21.
Merrill, J.E., and E.N. Benveniste. 1996. Cytokines in inflammatory brain lesions: helpful and harmful. *Trends Neurosci*. 19:331-8.
Merrill, J.E., L.J. Ignarro, M.P. Sherman, J. Melinek, and T.E. Lane. 1993. Microglial cell cytotoxicity of oligodendrocytes is mediated through nitric oxide. *J Immunol*. 151:2132-41.
Merrill, J.E., and R.P. Zimmerman. 1991. Natural and induced cytotoxicity of oligodendrocytes by microglia is inhibitable by TGF beta. *Glia*. 4:327-31.
Messier, W., and C.B. Stewart. 1997. Episodic adaptive evolution of primate lysozymes. *Nature*. 385:151-4.
Meyer, M., I. Matsuoka, C. Wetmore, L. Olson, and H. Thoenen. 1992. Enhanced synthesis of brain-derived neurotrophic factor in the lesioned peripheral nerve:

different mechanisms are responsible for the regulation of BDNF and NGF mRNA. *J Cell Biol*. 119:45-54.
Miller, D.C., M.L. Goodman, B.Z. Pilch, S.R. Shi, G.R. Dickersin, H. Halpern, and C.M. Norris, Jr. 1984. Mixed olfactory neuroblastoma and carcinoma. A report of two cases. *Cancer*. 54:2019-28.
Miller, M.W. 1987. The origin of corticospinal projection neurons in rat. *Exp Brain Res*. 67:339-51.
Milward, E.A., S.C. Zhang, M. Zhao, C. Lundberg, B. Ge, B.D. Goetz, and I.D. Duncan. 2000. Enhanced proliferation and directed migration of oligodendroglial progenitors co-grafted with growth factor-secreting cells. *Glia*. 32:264-70.
Minoshima, T., and S. Nakanishi. 1999. Structural organization of the mouse metabotropic glutamate receptor subtype 3 gene and its regulation by growth factors in cultured cortical astrocytes. *J Biochem (Tokyo)*. 126:889-96.
Miragall, F., G. Kadmon, M. Husmann, and M. Schachner. 1988. Expression of cell adhesion molecules in the olfactory system of the adult mouse: presence of the embryonic form of N-CAM. *Dev Biol*. 129:516-31.
Montgomery, D.L. 1994. Astrocytes: form, functions, and roles in disease. *Vet Pathol*. 31:145-67.
Morioka, T., A.N. Kalehua, and W.J. Streit. 1991. The microglial reaction in the rat dorsal hippocampus following transient forebrain ischemia. *J Cereb Blood Flow Metab*. 11:966-73.
Muir, G.D., and I.Q. Whishaw. 1999. Complete locomotor recovery following corticospinal tract lesions: measurement of ground reaction forces during overground locomotion in rats. *Behav Brain Res*. 103:45-53.
Munoz-Fernandez, M.A., and M. Fresno. 1998. The role of tumour necrosis factor, interleukin 6, interferon-gamma and inducible nitric oxide synthase in the development and pathology of the nervous system. *Prog Neurobiol*. 56:307-40.
Murphy, G.M., Jr., L. Yang, and B. Cordell. 1998. Macrophage colony-stimulating factor augments beta-amyloid-induced interleukin-1, interleukin-6, and nitric oxide production by microglial cells. *J Biol Chem*. 273:20967-71.
Murray, M., S.D. Wang, M.E. Goldberger, and P. Levitt. 1990. Modification of astrocytes in the spinal cord following dorsal root or peripheral nerve lesions. *Exp Neurol*. 110:248-57.
Nagai, A., E. Nakagawa, K. Hatori, H.B. Choi, J.G. McLarnon, M.A. Lee, and S.U. Kim. 2001. Generation and characterization of immortalized human microglial cell lines: expression of cytokines and chemokines. *Neurobiol Dis*. 8:1057-68.
Nakajima, K., S. Honda, Y. Nakamura, F. Lopez-Redondo, S. Kohsaka, M. Yamato, A. Kikuchi, and T. Okano. 2001. Intact microglia are cultured and non-invasively harvested without pathological activation using a novel cultured cell recovery method. *Biomaterials*. 22:1213-23.
Nakamura, Y. 2002. Regulating factors for microglial activation. *Biol Pharm Bull*. 25:945-53.
Nan, B., M.L. Getchell, J.V. Partin, and T.V. Getchell. 2001. Leukemia inhibitory factor, interleukin-6, and their receptors are expressed transiently in the olfactory mucosa after target ablation. *J Comp Neurol*. 435:60-77.

Nash, H.H., R.C. Borke, and J.J. Anders. 2002. Ensheathing cells and methylprednisolone promote axonal regeneration and functional recovery in the lesioned adult rat spinal cord. *J Neurosci*. 22:7111-20.

Natarajan, C., S. Sriram, G. Muthian, and J.J. Bright. 2004. Signaling through JAK2-STAT5 pathway is essential for IL-3-induced activation of microglia. *Glia*. 45:188-96.

Neary, J.T., Y. Kang, Y. Bu, E. Yu, K. Akong, and C.M. Peters. 1999. Mitogenic signaling by ATP/P2Y purinergic receptors in astrocytes: involvement of a calcium-independent protein kinase C, extracellular signal-regulated protein kinase pathway distinct from the phosphatidylinositol-specific phospholipase C/calcium pathway. *J Neurosci*. 19:4211-20.

Neary, J.T., Y. Kang, Y.F. Shi, M.D. Tran, and I.B. Wanner. 2006. P2 receptor signalling, proliferation of astrocytes, and expression of molecules involved in cell-cell interactions. *Novartis Found Symp*. 276:131-43; discussion 143-7, 233-7, 275-81.

Neumann, J., M. Gunzer, H.O. Gutzeit, O. Ullrich, K.G. Reymann, and K. Dinkel. 2006. Microglia provide neuroprotection after ischemia. *Faseb J*. 20:714-6.

Ngu, E.M., C.L. Sahley, and K.J. Muller. 2007. Reduced axon sprouting after treatment that diminishes microglia accumulation at lesions in the leech CNS. *J Comp Neurol*. 503:101-9.

Nimmerjahn, A., F. Kirchhoff, and F. Helmchen. 2005. Resting microglial cells are highly dynamic surveillants of brain parenchyma in vivo. *Science*. 308:1314-8.

Nistor, G.I., M.O. Totoiu, N. Haque, M.K. Carpenter, and H.S. Keirstead. 2005. Human embryonic stem cells differentiate into oligodendrocytes in high purity and myelinate after spinal cord transplantation. *Glia*. 49:385-96.

Noble, L.J., and J.R. Wrathall. 1985. Spinal cord contusion in the rat: morphometric analyses of alterations in the spinal cord. *Exp Neurol*. 88:135-49.

Norenberg, M.D. 1994. Astrocyte responses to CNS injury. *J Neuropathol Exp Neurol*. 53:213-20.

Norenberg, U., M. Hubert, and F.G. Rathjen. 1996. Structural and functional characterization of tenascin-R (restrictin), an extracellular matrix glycoprotein of glial cells and neurons. *Int J Dev Neurosci*. 14:217-31.

Norris, J.G., L.P. Tang, S.M. Sparacio, and E.N. Benveniste. 1994. Signal transduction pathways mediating astrocyte IL-6 induction by IL-1 beta and tumor necrosis factor-alpha. *J Immunol*. 152:841-50.

Oberheim, N.A., X. Wang, S. Goldman, and M. Nedergaard. 2006. Astrocytic complexity distinguishes the human brain. *Trends Neurosci*. 29:547-53.

Ousman, S.S., and S. David. 2001. MIP-1alpha, MCP-1, GM-CSF, and TNF-alpha control the immune cell response that mediates rapid phagocytosis of myelin from the adult mouse spinal cord. *J Neurosci*. 21:4649-56.

Palladino, M.A., F.R. Bahjat, E.A. Theodorakis, and L.L. Moldawer. 2003. Anti-TNF-alpha therapies: the next generation. *Nat Rev Drug Discov*. 2:736-46.

Pan, J.Z., L. Ni, A. Sodhi, A. Aguanno, W. Young, and R.P. Hart. 2002. Cytokine activity contributes to induction of inflammatory cytokine mRNAs in spinal cord following contusion. *J Neurosci Res*. 68:315-22.

Paratcha, G., F. Ledda, and C.F. Ibanez. 2003. The neural cell adhesion molecule NCAM is an alternative signaling receptor for GDNF family ligands. *Cell*. 113:867-79.
Pascual, J.I., G. Gudino-Cabrera, R. Insausti, and M. Nieto-Sampedro. 2002. Spinal implants of olfactory ensheathing cells promote axon regeneration and bladder activity after bilateral lumbosacral dorsal rhizotomy in the adult rat. *J Urol*. 167:1522-6.
Pasterkamp, R.J., F. De Winter, A.J. Holtmaat, and J. Verhaagen. 1998. Evidence for a role of the chemorepellent semaphorin III and its receptor neuropilin-1 in the regeneration of primary olfactory axons. *J Neurosci*. 18:9962-76.
Pastrana, E., M.T. Moreno-Flores, J. Avila, F. Wandosell, L. Minichiello, and J. Diaz-Nido. 2007. BDNF production by olfactory ensheathing cells contributes to axonal regeneration of cultured adult CNS neurons. *Neurochem Int*. 50:491-8.
Paxions and Watson. 1998. The rat brain in stereotaxic coordinates. San Diego : Academic Press
Pearse, D.D., A.E. Marcillo, M. Oudega, M.P. Lynch, P.M. Wood, and M.B. Bunge. 2004. Transplantation of Schwann cells and olfactory ensheathing glia after spinal cord injury: does pretreatment with methylprednisolone and interleukin-10 enhance recovery? *J Neurotrauma*. 21:1223-39.
Pearse, D.D., A.R. Sanchez, F.C. Pereira, C.M. Andrade, R. Puzis, Y. Pressman, K. Golden, B.M. Kitay, B. Blits, P.M. Wood, and M.B. Bunge. 2007. Transplantation of Schwann cells and/or olfactory ensheathing glia into the contused spinal cord: Survival, migration, axon association, and functional recovery. *Glia*. 55:976-1000.
Pekny, M., and M. Pekna. 2004. Astrocyte intermediate filaments in CNS pathologies and regeneration. *J Pathol*. 204:428-37.
Perrin, F.E., S. Lacroix, M. Aviles-Trigueros, and S. David. 2005. Involvement of monocyte chemoattractant protein-1, macrophage inflammatory protein-1alpha and interleukin-1beta in Wallerian degeneration. *Brain*. 128:854-66.
Perry, V.H., M.K. Matyszak, and S. Fearn. 1993. Altered antigen expression of microglia in the aged rodent CNS. *Glia*. 7:60-7.
Perry, V.H., J.W. Tsao, S. Fearn, and M.C. Brown. 1995. Radiation-induced reductions in macrophage recruitment have only slight effects on myelin degeneration in sectioned peripheral nerves of mice. *Eur J Neurosci*. 7:271-80.
Persson, M., M. Brantefjord, E. Hansson, and L. Ronnback. 2005. Lipopolysaccharide increases microglial GLT-1 expression and glutamate uptake capacity in vitro by a mechanism dependent on TNF-alpha. *Glia*. 51:111-20.
Peschon, J.J., D.S. Torrance, K.L. Stocking, M.B. Glaccum, C. Otten, C.R. Willis, K. Charrier, P.J. Morrissey, C.B. Ware, and K.M. Mohler. 1998. TNF receptor-deficient mice reveal divergent roles for p55 and p75 in several models of inflammation. *J Immunol*. 160:943-52.
Petrache, I., A. Birukova, S.I. Ramirez, J.G. Garcia, and A.D. Verin. 2003. The role of the microtubules in tumor necrosis factor-alpha-induced endothelial cell permeability. *Am J Respir Cell Mol Biol*. 28:574-81.
Pineau, I., and S. Lacroix. 2007. Proinflammatory cytokine synthesis in the injured mouse spinal cord: multiphasic expression pattern and identification of the cell types involved. *J Comp Neurol*. 500:267-85.

Pinzon, A., B. Calancie, M. Oudega, and B.R. Noga. 2001. Conduction of impulses by axons regenerated in a Schwann cell graft in the transected adult rat thoracic spinal cord. *J Neurosci Res*. 64:533-41.

Pixley, S.K. 1992. The olfactory nerve contains two populations of glia, identified both in vivo and in vitro. *Glia*. 5:269-84.

Pixley, S.K. 1996. Characterization of olfactory receptor neurons and other cell types in dissociated rat olfactory cell cultures. *Int J Dev Neurosci*. 14:823-39.

Pixley, S.K., and J. de Vellis. 1984. Transition between immature radial glia and mature astrocytes studied with a monoclonal antibody to vimentin. *Brain Res*. 317:201-9.

Plant, G.W., C.L. Christensen, M. Oudega, and M.B. Bunge. 2003. Delayed transplantation of olfactory ensheathing glia promotes sparing/regeneration of supraspinal axons in the contused adult rat spinal cord. *J Neurotrauma*. 20:1-16.

Plant, G.W., P.F. Currier, E.P. Cuervo, M.L. Bates, Y. Pressman, M.B. Bunge, and P.M. Wood. 2002. Purified adult ensheathing glia fail to myelinate axons under culture conditions that enable Schwann cells to form myelin. *J Neurosci*. 22:6083-91.

Pluchino, S., A. Quattrini, E. Brambilla, A. Gritti, G. Salani, G. Dina, R. Galli, U. Del Carro, S. Amadio, A. Bergami, R. Furlan, G. Comi, A.L. Vescovi, and G. Martino. 2003. Injection of adult neurospheres induces recovery in a chronic model of multiple sclerosis. *Nature*. 422:688-94.

Polazzi, E., and A. Contestabile. 2002. Reciprocal interactions between microglia and neurons: from survival to neuropathology. *Rev Neurosci*. 13:221-42.

Popovic, N., A. Schubart, B.D. Goetz, S.C. Zhang, C. Linington, and I.D. Duncan. 2002. Inhibition of autoimmune encephalomyelitis by a tetracycline. *Ann Neurol*. 51:215-23.

Popovich, P.G., Z. Guan, P. Wei, I. Huitinga, N. van Rooijen, and B.T. Stokes. 1999. Depletion of hematogenous macrophages promotes partial hindlimb recovery and neuroanatomical repair after experimental spinal cord injury. *Exp Neurol*. 158:351-65.

Popovich, P.G., and W.F. Hickey. 2001. Bone marrow chimeric rats reveal the unique distribution of resident and recruited macrophages in the contused rat spinal cord. *J Neuropathol Exp Neurol*. 60:676-85.

Popovich, P.G., P. Wei, and B.T. Stokes. 1997. Cellular inflammatory response after spinal cord injury in Sprague-Dawley and Lewis rats. *J Comp Neurol*. 377:443-64.

Prewitt, C.M., I.R. Niesman, C.J. Kane, and J.D. Houle. 1997. Activated macrophage/microglial cells can promote the regeneration of sensory axons into the injured spinal cord. *Exp Neurol*. 148:433-43.

Privat, A., J. Valat, and J. Fulcrand. 1981. Proliferation of neuroglial cell lines in the degenerating optic nerve of young rats. A radioautographic study. *J Neuropathol Exp Neurol*. 40:46-60.

Probert, L., K. Akassoglou, M. Pasparakis, G. Kontogeorgos, and G. Kollias. 1995. Spontaneous inflammatory demyelinating disease in transgenic mice showing central nervous system-specific expression of tumor necrosis factor alpha. *Proc Natl Acad Sci U S A*. 92:11294-8.

Probert, L., and K. Selmaj. 1997. TNF and related molecules: trends in neuroscience and clinical applications. *J Neuroimmunol*. 72:113-7.

Puliti, M., R. Mazzolla, A. Brozzetti, R. Neglia, D. Radzioch, F. Bistoni, and E. Blasi. 1999. Differential effector and secretory functions of microglial cell lines derived from BCG-resistant and -susceptible congenic mouse strains. *J Neuroimmunol*. 101:27-33.

Raff, M.C., A.V. Whitmore, and J.T. Finn. 2002. Axonal self-destruction and neurodegeneration. *Science*. 296:868-71.

Raisman, G. 2000. Repair of corticospinal axons by transplantation of olfactory ensheathing cells. *Novartis Found Symp*. 231:94-7; discussion 97-109.

Raivich, G., and R. Banati. 2004. Brain microglia and blood-derived macrophages: molecular profiles and functional roles in multiple sclerosis and animal models of autoimmune demyelinating disease. *Brain Res Brain Res Rev*. 46:261-81.

Raivich, G., M. Bohatschek, C.U. Kloss, A. Werner, L.L. Jones, and G.W. Kreutzberg. 1999a. Neuroglial activation repertoire in the injured brain: graded response, molecular mechanisms and cues to physiological function. *Brain Res Brain Res Rev*. 30:77-105.

Raivich, G., L.L. Jones, C.U. Kloss, A. Werner, H. Neumann, and G.W. Kreutzberg. 1998. Immune surveillance in the injured nervous system: T-lymphocytes invade the axotomized mouse facial motor nucleus and aggregate around sites of neuronal degeneration. *J Neurosci*. 18:5804-16.

Raivich, G., L.L. Jones, A. Werner, H. Bluthmann, T. Doetschmann, and G.W. Kreutzberg. 1999b. Molecular signals for glial activation: pro- and anti-inflammatory cytokines in the injured brain. *Acta Neurochir Suppl*. 73:21-30.

Raivich, G., and G.W. Kreutzberg. 1994. Pathophysiology of glial growth factor receptors. *Glia*. 11:129-46.

Ralston, D.D., A.M. Milroy, and H.J. Ralston, 3rd. 1987. Non-myelinated axons are rare in the medullary pyramids of the macaque monkey. *Neurosci Lett*. 73:215-9.

Ramer, M.S., I. Duraisingam, J.V. Priestley, and S.B. McMahon. 2001. Two-tiered inhibition of axon regeneration at the dorsal root entry zone. *J Neurosci*. 21:2651-60.

Ramon-Cueto, A., and J. Avila. 1998. Olfactory ensheathing glia: properties and function. *Brain Res Bull*. 46:175-87.

Ramon-Cueto, A., M.I. Cordero, F.F. Santos-Benito, and J. Avila. 2000. Functional recovery of paraplegic rats and motor axon regeneration in their spinal cords by olfactory ensheathing glia. *Neuron*. 25:425-35.

Ramon-Cueto, A., and M. Nieto-Sampedro. 1992. Glial cells from adult rat olfactory bulb: immunocytochemical properties of pure cultures of ensheathing cells. *Neuroscience*. 47:213-20.

Ramon-Cueto, A., and M. Nieto-Sampedro. 1994. Regeneration into the spinal cord of transected dorsal root axons is promoted by ensheathing glia transplants. *Exp Neurol*. 127:232-44.

Ramon-Cueto, A., J. Perez, and M. Nieto-Sampedro. 1993. In vitro enfolding of olfactory neurites by p75 NGF receptor positive ensheathing cells from adult rat olfactory bulb. *Eur J Neurosci*. 5:1172-80.

Ramon-Cueto, A., G.W. Plant, J. Avila, and M.B. Bunge. 1998. Long-distance axonal regeneration in the transected adult rat spinal cord is promoted by olfactory ensheathing glia transplants. *J Neurosci*. 18:3803-15.

Rapalino, O., O. Lazarov-Spiegler, E. Agranov, G.J. Velan, E. Yoles, M. Fraidakis, A. Solomon, R. Gepstein, A. Katz, M. Belkin, M. Hadani, and M. Schwartz. 1998. Implantation of stimulated homologous macrophages results in partial recovery of paraplegic rats. *Nat Med*. 4:814-21.

Reier, P.J., D.K. Anderson, W. Young, M.E. Michel, and R. Fessler. 1994. Workshop on intraspinal transplantation and clinical application. *J Neurotrauma*. 11:369-77.

Reier, P.J., M.J. Perlow, and L. Guth. 1983. Development of embryonic spinal cord transplants in the rat. *Brain Res*. 312:201-19.

Reier, P.J., B.T. Stokes, F.J. Thompson, and D.K. Anderson. 1992. Fetal cell grafts into resection and contusion/compression injuries of the rat and cat spinal cord. *Exp Neurol*. 115:177-88.

Rezaie, P., and D. Male. 2002. Mesoglia & microglia--a historical review of the concept of mononuclear phagocytes within the central nervous system. *J Hist Neurosci*. 11:325-74.

Rice, T., J. Larsen, S. Rivest, and V.W. Yong. 2007. Characterization of the early neuroinflammation after spinal cord injury in mice. *J Neuropathol Exp Neurol*. 66:184-95.

Ridet, J.L., S.K. Malhotra, A. Privat, and F.H. Gage. 1997. Reactive astrocytes: cellular and molecular cues to biological function. *Trends Neurosci*. 20:570-7.

Ridley, A.J. 2001. Rho GTPases and cell migration. *J Cell Sci*. 114:2713-22.

Rocamora, N., F.J. Garcia-Ladona, J.M. Palacios, and G. Mengod. 1993. Differential expression of brain-derived neurotrophic factor, neurotrophin-3, and low-affinity nerve growth factor receptor during the postnatal development of the rat cerebellar system. *Brain Res Mol Brain Res*. 17:1-8.

Rogers, S.D., E. Demaster, M. Catton, J.R. Ghilardi, L.A. Levin, J.E. Maggio, and P.W. Mantyh. 1997. Expression of endothelin-B receptors by glia in vivo is increased after CNS injury in rats, rabbits, and humans. *Exp Neurol*. 145:180-95.

Rohlmann, A., R. Laskawi, A. Hofer, R. Dermietzel, and J.R. Wolff. 1994. Astrocytes as rapid sensors of peripheral axotomy in the facial nucleus of rats. *Neuroreport*. 5:409-12.

Rosenberg, M.E., and J. Silkensen. 1995. Clusterin: physiologic and pathophysiologic considerations. *Int J Biochem Cell Biol*. 27:633-45.

Rostworowski, M., V. Balasingam, S. Chabot, T. Owens, and V.W. Yong. 1997. Astrogliosis in the neonatal and adult murine brain post-trauma: elevation of inflammatory cytokines and the lack of requirement for endogenous interferon-gamma. *J Neurosci*. 17:3664-74.

Rothstein, J.D., L. Martin, A.I. Levey, M. Dykes-Hoberg, L. Jin, D. Wu, N. Nash, and R.W. Kuncl. 1994. Localization of neuronal and glial glutamate transporters. *Neuron*. 13:713-25.

Ruan, R.S., S.K. Leong, and K.H. Yeoh. 1994. Glial reaction after facial nerve compression in the facial canal of the albino rat. *Acta Otolaryngol*. 114:271-7.

Rubin, L.L., and J.M. Staddon. 1999. The cell biology of the blood-brain barrier. *Annu Rev Neurosci*. 22:11-28.

Rudge, J.S., Y. Li, E.M. Pasnikowski, K. Mattsson, L. Pan, G.D. Yancopoulos, S.J. Wiegand, R.M. Lindsay, and N.Y. Ip. 1994. Neurotrophic factor receptors and their signal transduction capabilities in rat astrocytes. *Eur J Neurosci*. 6:693-705.

Ruitenberg, M.J., D.B. Levison, S.V. Lee, J. Verhaagen, A.R. Harvey, and G.W. Plant. 2005. NT-3 expression from engineered olfactory ensheathing glia promotes spinal sparing and regeneration. *Brain*. 128:839-53.

Ruitenberg, M.J., G.W. Plant, C.L. Christensen, B. Blits, S.P. Niclou, A.R. Harvey, G.J. Boer, and J. Verhaagen. 2002. Viral vector-mediated gene expression in olfactory ensheathing glia implants in the lesioned rat spinal cord. *Gene Ther*. 9:135-46.

Ruitenberg, M.J., G.W. Plant, F.P. Hamers, J. Wortel, B. Blits, P.A. Dijkhuizen, W.H. Gispen, G.J. Boer, and J. Verhaagen. 2003. Ex vivo adenoviral vector-mediated neurotrophin gene transfer to olfactory ensheathing glia: effects on rubrospinal tract regeneration, lesion size, and functional recovery after implantation in the injured rat spinal cord. *J Neurosci*. 23:7045-58.

Sasaki, A., H. Yokoo, M. Naito, C. Kaizu, L.D. Shultz, and Y. Nakazato. 2000. Effects of macrophage-colony-stimulating factor deficiency on the maturation of microglia and brain macrophages and on their expression of scavenger receptor. *Neuropathology*. 20:134-42.

Sasaki, M., B.C. Hains, K.L. Lankford, S.G. Waxman, and J.D. Kocsis. 2006. Protection of corticospinal tract neurons after dorsal spinal cord transection and engraftment of olfactory ensheathing cells. *Glia*. 53:352-9.

Sasaki, M., K.L. Lankford, M. Zemedkun, and J.D. Kocsis. 2004. Identified olfactory ensheathing cells transplanted into the transected dorsal funiculus bridge the lesion and form myelin. *J Neurosci*. 24:8485-93.

Sawada, M., N. Kondo, A. Suzumura, and T. Marunouchi. 1989. Production of tumor necrosis factor-alpha by microglia and astrocytes in culture. *Brain Res*. 491:394-7.

Scherbel, U., R. Raghupathi, M. Nakamura, K.E. Saatman, J.Q. Trojanowski, E. Neugebauer, M.W. Marino, and T.K. McIntosh. 1999. Differential acute and chronic responses of tumor necrosis factor-deficient mice to experimental brain injury. *Proc Natl Acad Sci U S A*. 96:8721-6.

Schiffer, D., M.T. Giordana, A. Migheli, G. Giaccone, S. Pezzotta, and A. Mauro. 1986. Glial fibrillary acidic protein and vimentin in the experimental glial reaction of the rat brain. *Brain Res*. 374:110-8.

Schlaepfer, W.W. 1974. Calcium-induced degeneration of axoplasm in isolated segments of rat peripheral nerve. *Brain Res*. 69:203-15.

Schnell, L., S. Fearn, M.E. Schwab, V.H. Perry, and D.C. Anthony. 1999. Cytokine-induced acute inflammation in the brain and spinal cord. *J Neuropathol Exp Neurol*. 58:245-54.

Schnitzer, J., W.W. Franke, and M. Schachner. 1981. Immunocytochemical demonstration of vimentin in astrocytes and ependymal cells of developing and adult mouse nervous system. *J Cell Biol*. 90:435-47.

Schreyer, D.J., and E.G. Jones. 1982. Growth and target finding by axons of the corticospinal tract in prenatal and postnatal rats. *Neuroscience*. 7:1837-53.

Schreyer, D.J., and E.H. Jones. 1988. Topographic sequence of outgrowth of corticospinal axons in the rat: a study using retrograde axonal labeling with Fast blue. *Brain Res*. 466:89-101.

Schwab, M.E., and L. Schnell. 1989. Region-specific appearance of myelin constituents in the developing rat spinal cord. *J Neurocytol*. 18:161-9.

Schwartz, M., O. Butovsky, W. Bruck, and U.K. Hanisch. 2006. Microglial phenotype: is the commitment reversible? *Trends Neurosci*. 29:68-74.
Schwartz, M., I. Shaked, J. Fisher, T. Mizrahi, and H. Schori. 2003. Protective autoimmunity against the enemy within: fighting glutamate toxicity. *Trends Neurosci*. 26:297-302.
Schwartz, M., and E. Yoles. 2006. Immune-based therapy for spinal cord repair: autologous macrophages and beyond. *J Neurotrauma*. 23:360-70.
Segal, B.M. 2005. CNS chemokines, cytokines, and dendritic cells in autoimmune demyelination. *J Neurol Sci*. 228:210-4.
Segal, R.A., S.L. Pomeroy, and C.D. Stiles. 1995. Axonal growth and fasciculation linked to differential expression of BDNF and NT3 receptors in developing cerebellar granule cells. *J Neurosci*. 15:4970-81.
Selmaj, K., C.S. Raine, and A.H. Cross. 1991a. Anti-tumor necrosis factor therapy abrogates autoimmune demyelination. *Ann Neurol*. 30:694-700.
Selmaj, K., C.S. Raine, M. Farooq, W.T. Norton, and C.F. Brosnan. 1991b. Cytokine cytotoxicity against oligodendrocytes. Apoptosis induced by lymphotoxin. *J Immunol*. 147:1522-9.
Selmaj, K.W., and C.S. Raine. 1988. Tumor necrosis factor mediates myelin and oligodendrocyte damage in vitro. *Ann Neurol*. 23:339-46.
Shamash, S., F. Reichert, and S. Rotshenker. 2002. The cytokine network of Wallerian degeneration: tumor necrosis factor-alpha, interleukin-1alpha, and interleukin-1beta. *J Neurosci*. 22:3052-60.
Shrikant, P., and E.N. Benveniste. 1996. The central nervous system as an immunocompetent organ: role of glial cells in antigen presentation. *J Immunol*. 157:1819-22.
Skihar, V. 2004. Migration of Olfactory Ensheathing Cells Grafted Into Adult Rat Spinal Cord. Unpublished doctoral dissertation, University of Saskatchewan, Saskatoon, Saskatchewan, Canada
Smale, K.A., R. Doucette, and M.D. Kawaja. 1996. Implantation of olfactory ensheathing cells in the adult rat brain following fimbria-fornix transection. *Exp Neurol*. 137:225-33.
Small, R.K., P. Riddle, and M. Noble. 1987. Evidence for migration of oligodendrocyte--type-2 astrocyte progenitor cells into the developing rat optic nerve. *Nature*. 328:155-7.
Sminia, T., C.J. de Groot, C.D. Dijkstra, J.C. Koetsier, and C.H. Polman. 1987. Macrophages in the central nervous system of the rat. *Immunobiology*. 174:43-50.
Smith, G.M., R.H. Miller, and J. Silver. 1986. Changing role of forebrain astrocytes during development, regenerative failure, and induced regeneration upon transplantation. *J Comp Neurol*. 251:23-43.
Song, X., S. Tanaka, D. Cox, and S.C. Lee. 2004. Fcgamma receptor signaling in primary human microglia: differential roles of PI-3K and Ras/ERK MAPK pathways in phagocytosis and chemokine induction. *J Leukoc Biol*. 75:1147-55.
Sonigra, R.J., P.C. Brighton, J. Jacoby, S. Hall, and C.B. Wigley. 1999. Adult rat olfactory nerve ensheathing cells are effective promoters of adult central nervous system neurite outgrowth in coculture. *Glia*. 25:256-69.

Sorensen, J.C., I. Dalmau, J. Zimmer, and B. Finsen. 1996. Microglial reactions to retrograde degeneration of tracer-identified thalamic neurons after frontal sensorimotor cortex lesions in adult rats. *Exp Brain Res*. 112:203-12.

Spranger, M., D. Lindholm, C. Bandtlow, R. Heumann, H. Gnahn, M. Naher-Noe, and H. Thoenen. 1990. Regulation of Nerve Growth Factor (NGF) Synthesis in the Rat Central Nervous System: Comparison between the Effects of Interleukin-1 and Various Growth Factors in Astrocyte Cultures and in vivo. *Eur J Neurosci*. 2:69-76.

Steinmetz, M.P., K.P. Horn, V.J. Tom, J.H. Miller, S.A. Busch, D. Nair, D.J. Silver, and J. Silver. 2005. Chronic enhancement of the intrinsic growth capacity of sensory neurons combined with the degradation of inhibitory proteoglycans allows functional regeneration of sensory axons through the dorsal root entry zone in the mammalian spinal cord. *J Neurosci*. 25:8066-76.

Stella, N., A. Estelles, J. Siciliano, M. Tence, S. Desagher, D. Piomelli, J. Glowinski, and J. Premont. 1997. Interleukin-1 enhances the ATP-evoked release of arachidonic acid from mouse astrocytes. *J Neurosci*. 17:2939-46.

Stemple, D.L., and D.J. Anderson. 1992. Isolation of a stem cell for neurons and glia from the mammalian neural crest. *Cell*. 71:973-85.

Stence, N., M. Waite, and M.E. Dailey. 2001. Dynamics of microglial activation: a confocal time-lapse analysis in hippocampal slices. *Glia*. 33:256-66.

Stoll, G., J.W. Griffin, C.Y. Li, and B.D. Trapp. 1989. Wallerian degeneration in the peripheral nervous system: participation of both Schwann cells and macrophages in myelin degradation. *J Neurocytol*. 18:671-83.

Stoll, G., and S. Jander. 1999. The role of microglia and macrophages in the pathophysiology of the CNS. *Prog Neurobiol*. 58:233-47.

Stoll, G., and H.W. Muller. 1999. Nerve injury, axonal degeneration and neural regeneration: basic insights. *Brain Pathol*. 9:313-25.

Stoll, G., M. Schroeter, S. Jander, H. Siebert, A. Wollrath, C. Kleinschnitz, and W. Bruck. 2004. Lesion-associated expression of transforming growth factor-beta-2 in the rat nervous system: evidence for down-regulating the phagocytic activity of microglia and macrophages. *Brain Pathol*. 14:51-8.

Streit, W.J. 2004. Microglia and Alzheimer's disease pathogenesis. *J Neurosci Res*. 77:1-8.

Streit, W.J., M.B. Graeber, and G.W. Kreutzberg. 1989. Expression of Ia antigen on perivascular and microglial cells after sublethal and lethal motor neuron injury. *Exp Neurol*. 105:115-26.

Streit, W.J., N.W. Sammons, A.J. Kuhns, and D.L. Sparks. 2004. Dystrophic microglia in the aging human brain. *Glia*. 45:208-12.

Streit, W.J., S.A. Walter, and N.A. Pennell. 1999. Reactive microgliosis. *Prog Neurobiol*. 57:563-81.

Suen, W.E., C.M. Bergman, P. Hjelmstrom, and N.H. Ruddle. 1997. A critical role for lymphotoxin in experimental allergic encephalomyelitis. *J Exp Med*. 186:1233-40.

Suk, K. 2004. Minocycline suppresses hypoxic activation of rodent microglia in culture. *Neurosci Lett*. 366:167-71.

Suzuki, K., Y. Ikegaya, S. Matsuura, Y. Kanai, H. Endou, and N. Matsuki. 2001. Transient upregulation of the glial glutamate transporter GLAST in response to fibroblast growth factor, insulin-like growth factor and epidermal growth factor in cultured astrocytes. *J Cell Sci*. 114:3717-25.

Svensson, M., L. Liu, P. Mattsson, B.P. Morgan, and H. Aldskogius. 1995. Evidence for activation of the terminal pathway of complement and upregulation of sulfated glycoprotein (SGP)-2 in the hypoglossal nucleus following peripheral nerve injury. *Mol Chem Neuropathol*. 24:53-68.

Sytwu, H.K., R.S. Liblau, and H.O. McDevitt. 1996. The roles of Fas/APO-1 (CD95) and TNF in antigen-induced programmed cell death in T cell receptor transgenic mice. *Immunity*. 5:17-30.

Takami, T., M. Oudega, M.L. Bates, P.M. Wood, N. Kleitman, and M.B. Bunge. 2002. Schwann cell but not olfactory ensheathing glia transplants improve hindlimb locomotor performance in the moderately contused adult rat thoracic spinal cord. *J Neurosci*. 22:6670-81.

Takamiya, Y., S. Kohsaka, S. Toya, M. Otani, and Y. Tsukada. 1988. Immunohistochemical studies on the proliferation of reactive astrocytes and the expression of cytoskeletal proteins following brain injury in rats. *Brain Res*. 466:201-10.

Takehana, K., M. Abe, M. Yamaguchi, T. Uchida, M. Inagaki, K. Yamamoto, J. Masty, A. Winnard, H. Ueda, and H. Miyata. 1992. Cytoplasmic filaments in the endothelial cells of the sheathed capillary: an ultrastructural and immunocytochemical study in the pig spleen. *Acta Anat (Basel)*. 143:294-300.

Tanaka, H., T. Yamashita, K. Yachi, T. Fujiwara, H. Yoshikawa, and M. Tohyama. 2004. Cytoplasmic p21(Cip1/WAF1) enhances axonal regeneration and functional recovery after spinal cord injury in rats. *Neuroscience*. 127:155-64.

Tateishi, N., T. Shimoda, N. Yada, R. Shinagawa, and Y. Kagamiishi. 2006. [S100B: astrocyte specific protein]. *Nihon Shinkei Seishin Yakurigaku Zasshi*. 26:11-6.

Taylor, D.L., F. Jones, E.S. Kubota, and J.M. Pocock. 2005. Stimulation of microglial metabotropic glutamate receptor mGlu2 triggers tumor necrosis factor alpha-induced neurotoxicity in concert with microglial-derived Fas ligand. *J Neurosci*. 25:2952-64.

Tennent, R., and M.I. Chuah. 1996. Ultrastructural study of ensheathing cells in early development of olfactory axons. *Brain Res Dev Brain Res*. 95:135-9.

Tetzlaff, W., M.B. Graeber, M.A. Bisby, and G.W. Kreutzberg. 1988. Increased glial fibrillary acidic protein synthesis in astrocytes during retrograde reaction of the rat facial nucleus. *Glia*. 1:90-5.

Thomas, D.M., D.M. Francescutti-Verbeem, and D.M. Kuhn. 2006. Gene expression profile of activated microglia under conditions associated with dopamine neuronal damage. *Faseb J*. 20:515-7.

Tikka, T.M., and J.E. Koistinaho. 2001. Minocycline provides neuroprotection against N-methyl-D-aspartate neurotoxicity by inhibiting microglia. *J Immunol*. 166:7527-33.

Tomozawa, Y., T. Inoue, M. Takahashi, M. Adachi, and M. Satoh. 1996. Apoptosis of cultured microglia by the deprivation of macrophage colony-stimulating factor. *Neurosci Res*. 25:7-15.

Tran, E.H., K. Hoekstra, N. van Rooijen, C.D. Dijkstra, and T. Owens. 1998. Immune invasion of the central nervous system parenchyma and experimental allergic encephalomyelitis, but not leukocyte extravasation from blood, are prevented in macrophage-depleted mice. *J Immunol*. 161:3767-75.

Tsacopoulos, M., and P.J. Magistretti. 1996. Metabolic coupling between glia and neurons. *J Neurosci*. 16:877-85.

Tsao, N., H.P. Hsu, C.M. Wu, C.C. Liu, and H.Y. Lei. 2001. Tumour necrosis factor-alpha causes an increase in blood-brain barrier permeability during sepsis. *J Med Microbiol*. 50:812-21.

Tsukada, N., K. Miyagi, M. Matsuda, N. Yanagisawa, and K. Yone. 1991. Tumor necrosis factor and interleukin-1 in the CSF and sera of patients with multiple sclerosis. *J Neurol Sci*. 104:230-4.

Ubink, R., and T. Hokfelt. 2000. Expression of neuropeptide Y in olfactory ensheathing cells during prenatal development. *J Comp Neurol*. 423:13-25.

Ullian, E.M., S.K. Sapperstein, K.S. Christopherson, and B.A. Barres. 2001. Control of synapse number by glia. *Science*. 291:657-61.

Valverde, F., and L. Lopez-Mascaraque. 1991. Neuroglial arrangements in the olfactory glomeruli of the hedgehog. *J Comp Neurol*. 307:658-74.

Valverde, F., M. Santacana, and M. Heredia. 1992. Formation of an olfactory glomerulus: morphological aspects of development and organization. *Neuroscience*. 49:255-75.

Verdu, E., G. Garcia-Alias, J. Fores, G. Gudino-Cabrera, V.C. Muneton, M. Nieto-Sampedro, and X. Navarro. 2001. Effects of ensheathing cells transplanted into photochemically damaged spinal cord. *Neuroreport*. 12:2303-9.

Vilcek, J., and M. Feldmann. 2004. Historical review: Cytokines as therapeutics and targets of therapeutics. *Trends Pharmacol Sci*. 25:201-9.

von Bernhardi, R., and K.J. Muller. 1995. Repair of the central nervous system: lessons from lesions in leeches. *J Neurobiol*. 27:353-66.

Wagner, A.P., G. Reck, and D. Platt. 1993. Evidence that V+ fibronectin, GFAP and S100 beta mRNAs are increased in the hippocampus of aged rats. *Exp Gerontol*. 28:135-43.

Wajant, H., K. Pfizenmaier, and P. Scheurich. 2003. Tumor necrosis factor signaling. *Cell Death Differ*. 10:45-65.

Wallach, D., M. Boldin, E. Varfolomeev, R. Beyaert, P. Vandenabeele, and W. Fiers. 1997. Cell death induction by receptors of the TNF family: towards a molecular understanding. *FEBS Lett*. 410:96-106.

Wang, C.C., C.H. Wu, J.Y. Shieh, C.Y. Wen, and E.A. Ling. 1996. Immunohistochemical study of amoeboid microglial cells in fetal rat brain. *J Anat*. 189 (Pt 3):567-74.

Warden, P., N.I. Bamber, H. Li, A. Esposito, K.A. Ahmad, C.Y. Hsu, and X.M. Xu. 2001. Delayed glial cell death following wallerian degeneration in white matter tracts after spinal cord dorsal column cordotomy in adult rats. *Exp Neurol*. 168:213-24.

Weaver, L.C., A.K. Cassam, A.V. Krassioukov, and I.J. Llewellyn-Smith. 1997. Changes in immunoreactivity for growth associated protein-43 suggest reorganization of

synapses on spinal sympathetic neurons after cord transection. *Neuroscience*. 81:535-51.

Whishaw, I.Q., B. Gorny, and J. Sarna. 1998. Paw and limb use in skilled and spontaneous reaching after pyramidal tract, red nucleus and combined lesions in the rat: behavioral and anatomical dissociations. *Behav Brain Res*. 93:167-83.

Wolburg, H., J. Neuhaus, U. Kniesel, B. Krauss, E.M. Schmid, M. Ocalan, C. Farrell, and W. Risau. 1994. Modulation of tight junction structure in blood-brain barrier endothelial cells. Effects of tissue culture, second messengers and cocultured astrocytes. *J Cell Sci*. 107 (Pt 5):1347-57.

Wolswijk, G., and M. Noble. 1989. Identification of an adult-specific glial progenitor cell. *Development*. 105:387-400.

Woodhall, E., A.K. West, and M.I. Chuah. 2001. Cultured olfactory ensheathing cells express nerve growth factor, brain-derived neurotrophic factor, glia cell line-derived neurotrophic factor and their receptors. *Brain Res Mol Brain Res*. 88:203-13.

Woodhouse, A., A.J. Vincent, M.A. Kozel, R.S. Chung, P.M. Waite, J.C. Vickers, A.K. West, and M.I. Chuah. 2005. Spinal cord tissue affects ensheathing cell proliferation and apoptosis. *Neuroreport*. 16:737-40.

Woodroofe, M.N., and M.L. Cuzner. 1993. Cytokine mRNA expression in inflammatory multiple sclerosis lesions: detection by non-radioactive in situ hybridization. *Cytokine*. 5:583-8.

Woodruff, R.H., and R.J. Franklin. 1999. Demyelination and remyelination of the caudal cerebellar peduncle of adult rats following stereotaxic injections of lysolecithin, ethidium bromide, and complement/anti-galactocerebroside: a comparative study. *Glia*. 25:216-28.

Wu, C.H., H.J. Wang, C.Y. Wen, K.C. Lien, and E.A. Ling. 1997. Response of amoeboid and ramified microglial cells to lipopolysaccharide injections in postnatal rats--a lectin and ultrastructural study. *Neurosci Res*. 27:133-41.

Wu, Y.P., and E.A. Ling. 1998. Transsynaptic changes of neurons and associated microglial reaction in the spinal cord of rats following middle cerebral artery occlusion. *Neurosci Lett*. 256:41-4.

Wujek, J.R., C. Bjartmar, E. Richer, R.M. Ransohoff, M. Yu, V.K. Tuohy, and B.D. Trapp. 2002. Axon loss in the spinal cord determines permanent neurological disability in an animal model of multiple sclerosis. *J Neuropathol Exp Neurol*. 61:23-32.

Xu, X.M., V. Guenard, N. Kleitman, and M.B. Bunge. 1995. Axonal regeneration into Schwann cell-seeded guidance channels grafted into transected adult rat spinal cord. *J Comp Neurol*. 351:145-60.

Yamagishi, S., M. Fujitani, K. Hata, K. Kitajo, F. Mimura, H. Abe, and T. Yamashita. 2005. Wallerian degeneration involves Rho/Rho-kinase signaling. *J Biol Chem*. 280:20384-8.

Yamasaki, T., H. Kikuchi, K. Moritake, S. Nagao, K. Iwasaki, J.T. Paine, T. Kagawa, and Y. Namba. 1992. A morphological and ultrastructural investigation of normal mouse brain tissue after intracerebral injection of tumor necrosis factor. *J Neurosurg*. 77:279-87.

Yamauchi, J., Y. Miyamoto, H. Kokubu, H. Nishii, M. Okamoto, Y. Sugawara, A. Hirasawa, G. Tsujimoto, and H. Itoh. 2002. Endothelin suppresses cell migration via the JNK signaling pathway in a manner dependent upon Src kinase, Rac1, and Cdc42. *FEBS Lett*. 527:284-8.

Yandava, B.D., L.L. Billinghurst, and E.Y. Snyder. 1999. "Global" cell replacement is feasible via neural stem cell transplantation: evidence from the dysmyelinated shiverer mouse brain. *Proc Natl Acad Sci U S A*. 96:7029-34.

Yenari, M.A., L. Xu, X.N. Tang, Y. Qiao, and R.G. Giffard. 2006. Microglia potentiate damage to blood-brain barrier constituents: improvement by minocycline in vivo and in vitro. *Stroke*. 37:1087-93.

Yin, Y., M.T. Henzl, B. Lorber, T. Nakazawa, T.T. Thomas, F. Jiang, R. Langer, and L.I. Benowitz. 2006. Oncomodulin is a macrophage-derived signal for axon regeneration in retinal ganglion cells. *Nat Neurosci*. 9:843-52.

Yokoyama, A., L. Yang, S. Itoh, K. Mori, and J. Tanaka. 2004. Microglia, a potential source of neurons, astrocytes, and oligodendrocytes. *Glia*. 45:96-104.

Yrjanheikki, J., R. Keinanen, M. Pellikka, T. Hokfelt, and J. Koistinaho. 1998. Tetracyclines inhibit microglial activation and are neuroprotective in global brain ischemia. *Proc Natl Acad Sci U S A*. 95:15769-74.

Zelenaia, O., B.D. Schlag, G.E. Gochenauer, R. Ganel, W. Song, J.S. Beesley, J.B. Grinspan, J.D. Rothstein, and M.B. Robinson. 2000. Epidermal growth factor receptor agonists increase expression of glutamate transporter GLT-1 in astrocytes through pathways dependent on phosphatidylinositol 3-kinase and transcription factor NF-kappaB. *Mol Pharmacol*. 57:667-78.

Zhai, Q., J. Wang, A. Kim, Q. Liu, R. Watts, E. Hoopfer, T. Mitchison, L. Luo, and Z. He. 2003. Involvement of the ubiquitin-proteasome system in the early stages of wallerian degeneration. *Neuron*. 39:217-25.

Zheng, L., G. Fisher, R.E. Miller, J. Peschon, D.H. Lynch, and M.J. Lenardo. 1995. Induction of apoptosis in mature T cells by tumour necrosis factor. *Nature*. 377:348-51.

Zimmermann, H. 1994. Signalling via ATP in the nervous system. *Trends Neurosci*. 17:420-6.

Zipp, F., and O. Aktas. 2006. The brain as a target of inflammation: common pathways link inflammatory and neurodegenerative diseases. *Trends Neurosci*. 29:518-27.